NONLINEAR FINITE ELEMENT MODELING AND CHARACTERIZATION OF GUYED TOWERS UNDER SEVERE LOADING

A Dissertation

presented to

the Faculty of the Graduate School

University of Missouri-Columbia

In Partial Fulfillment

of the Requirements for the Degree

Doctor of Philosophy

---

by

HAIJIAN SHI

Dr. Hani Salim, Dissertation Supervisor

Dr. P. Frank Pai, Co-Advisor

DECEMBER 2007

The undersigned, appointed by the dean of the Graduate School, have examined the dissertation entitled

NONLINEAR FINITE ELEMENT MODELING AND CHARACTERIZATION OF GUYED TOWERS UNDER SEVERE LOADING

presented by Haijian Shi,

a candidate for the degree of doctor of philosophy

and hereby certify that, in their opinion, it is worthy of acceptance.

Hani Salim

Frank Pai

Sam Kiger

Glenn Washer

Sherif EI-Gizawy

ACKNOWLEDGEMENTS

First, I would like to thank my dissertation advisor, Dr. Hani Salim, for his invaluable guidance, insightful advices, and continuous encouragement. It is his direction and support that motivates me to overcome various challenges, improve and excel. He is not only a remarkable advisor but also a good friend.

I would also like thank my co-advisor, Dr. Frank Pai, for his generous support and patient correction of my dissertation. His amazing expertise in finite element method provides essential help in this dissertation. My gratitude is extended to Dr. Sam Kiger, Dr. Glenn Washer and Dr. Sherif EI-Gizawy for their suggestions and serving on my committee.

I also greatly appreciate Dr. Guowei Ma for his initiative guidance during my early PhD study. Many thanks go to Professor George Wagner for his timely proofreading of the dissertation.

My parents, sister and my friend Jing Xiong deserve my most special thanks. I am forever indebted to their love and support.

TABLE OF CONTENTS

LIST OF FIGURES

LIST OF TABLES

ABSTRACT

Guyed towers have been widely employed in the telecommunication industry. However, in current building codes, there is still no comprehensive specification for their nonlinear response under severe loads, which includes large static loads, seismic loads and impulsive loads. This study thus intends to improve the understanding and analysis of guyed towers that undergo not only large deformation, but also large strain. Impulsive loads are potential threat to the safety of guyed towers besides wind load, earthquake, and ice storm. No methodology or related research has been conducted in this area so far. This research explores the area using an already developed P-I diagram method and nonlinear finite element modeling to provide an efficient and effective way for structural integrity evaluation for guyed towers.

The mechanical characteristics of basic components of guyed towers are investigated first. Geometric nonlinearity is of the main concern for the impact of large deflection. The modified Riks scheme has been applied in nonlinear static analysis and the Newmark beta method for dynamic analysis. To investigate the efficiency and effectiveness of linear analysis methods, several corresponding examples are studied. It is found that linear static analysis works only when the deformation is small. The equivalent inertia force method and the large additional stiffness method for guyed towers under seismic loads are compared and validated. Their results are very similar.

Because guyed towers with large defection also have large strain in some parts, material nonlinearity is introduced by improving the existing FEM codes for trusses and cables. Isotropic hardening is employed in nonlinear static analysis. Dynamic

hardening is used in dynamic analysis. Some specific examples have been conducted to verify the improvements. It is found that the improved methodology can well predict the performance of structures and tremendous difference exists between elastic analysis and inelastic analysis. Under seismic loading condition, inelasticity in material can help dissipate the inputted seismic energy and reduce the intensity of structural response.

The combined application of nonlinear finite elements and algorithm enables the nonlinear analysis for guyed towers. A 50 ft guyed tower with taut cables and a 100 m guyed tower with sagged cables were studied for their response under large static loads and seismic loads. The nonlinear static and dynamic response was accurately traced. It is found that equivalent static analysis works well when deflection is small. In sagged guyed tower, the structure is relatively soft at the beginning of static loading. With the increase of deflection, the structure is gradually stiffened. The consideration of inelasticity greatly improves the accuracy of analysis.

To evaluate the guyed tower's safety under impulsive loads, relative P-I formulas have been derived based on existing transverse velocity profiles of rigid plastic beams under impulsive loads. Two failure modes (shear failure and bending failure) were differentiated. The impact of boundary condition and load types on the response is investigated. It is found under certain conditions only one failure mode is possible. But shear failure and bending failure can coexist under very severe impulsive loads. One specific example has been used to demonstrate the combined application of the P-I diagram method and FEM. Most guyed towers are expected to survive light or medium impulsive loads due to their high redundancy and small loading area.

Chapter 1 Introduction

1.1 Background

Towers are one of the most efficient structures. With a small amount of materials they can sustain considerable loads and behave favorably. They are ideal for most communication needs, including transmission, wireless internet, cellular, and antenna radio towers. Though satellite technology tends to supersede the communication towers, the economical and easily accessible characteristics still make many contractors prefer towers.

There are two common types of towers: self supporting and guyed towers. Self supporting towers (Fig 1.1) usually have rectangular cross sections. The major components are legs, braces and attached antennas. The bracing has various patterns as cross bracing, portal bracing, cranked K type bracing (TIA/EIA-222-G.5, 2006). Fig 1.1 illustrates a self supporting tower with K-type bracing. The disadvantage for self supporting towers is low height limit. Generally, the height can not exceed 300 ft (Madugula, 2002). For towers that exceed this height limit, guyed towers should be employed.

Figure 1.1 A self supporting telecommunication tower.

Guyed tower (Fig 1.2) has been widely used in North America. The attached guys provide additional lateral support to the tower, which greatly increases the structure's stability. The guy clusters are located at different heights along the mast and can form up to nine layers. The mast base can be pinned to the ground through bolts and steel plates. Unlike the self supporting towers, the cross section is triangular as shown in Fig 1.3. To anchor the guys, wide space around the mast is needed. Thus, guyed towers are most common in rural areas. In highly urbanized areas, self supporting towers are preferred due to space restriction.

Figure 1.2 A guyed tower with four guyed layers.

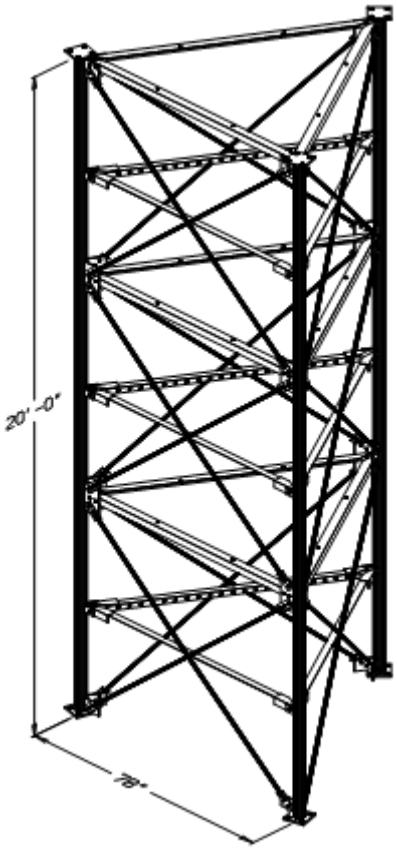

Figure 1.3 Cross section of masts.

1.2 Problem statement

Various literatures and building codes, such as TIA/EIA-222-G.5 (TIA/EIA, 2006), CSA S37-94 (CSA, 1994), BS 8100 Part 4 (BSI, 1994), and European Standard EC3 (CEN, 1997), have already explored the analysis and design of towers in detail. Some quick but efficient way to assess the towers' response have been proposed and proved in the literatures (Galvez, 1995; Sackmann, 1996; Amiri, 1997; Wahba, 1999). But compared to the state-of-art analysis and design technique existing in buildings and bridges, the corresponding technique for towers is still lagging.

For static analysis of towers, it is relatively simple. But for dynamic response of guyed towers, it is very complicated and hard to be simplified. The cables can behave highly nonlinearly and be hard to predict by linear cable theories. The mast and cluster of cables also exhibit dynamic interaction, which further increases the complexity. The most efficient and recommended way by authority so far is to conduct real time history analysis, which is usually aided by Finite Element Analysis (FEA).

Commercial softwares such as ABAQUS, ANSYS, and ADINA can handle most cases with considerable accuracy. But the real deformation mechanism requires cable elements, which is usually simulated by tension-only rods or link elements in FEA softwares. This simulation technique has some problems because incompressible truss elements are not exactly the same as cable elements.

Besides, few researches have been done on towers' performance under seismic excitation (Madugula, 2002). The existing code EIA 222-G addresses the importance of seismic analysis and proposed four equivalent static methods. But the discrepancy between equivalent static analysis and dynamic analysis can be considerable,

especially when large deformation causes geometric nonlinearity. Wahba (1999) and Hussam (2005) did modal analysis for dynamic response of guyed tower by ABAQUS. But this approach usually targets a specific case and needs familiarity with commercial FEA software. Nabil (1993) researched geometric nonlinearity of guyed towers and developed NSDAGT by including nonlinearity factors in modeling basic structural elements (trusses, cables and beams). But he simplified all the components in the mast as truss elements, which result in loss of accuracy.

Impulsive load on large scale tower structures is another design consideration that needs attention. Since an impulsive load has a very short duration and a high peak pressure, the structural response is very different from conventional dynamic response. However, there is very little literature on the impulsive response and failure mechanism of tower systems.

In a word, the understanding of guyed towers' response under severe loads, especial nonlinear response, is still very limited.

1.3 Objective

The objectives of this research are to improve the understanding of static and dynamic responses of guyed tower systems under multi-hazard load conditions by using fully nonlinear finite element modeling and analysis. The considered load conditions include large static loads, uniform load, severe earthquakes, wind loads and impulsive loads. The influence of geometric and material nonlinearities on the response will be investigated. The impulsive response and damage mechanism for tower systems will be explored as well.

To achieve the objectives of this dissertation, the following tasks were realized:

1. Apply geometrically nonlinear analysis for pure truss, cable and beam

structures to prepare for the global analysis of guyed towers.

2. Implement material nonlinearity in truss and cable elements to enable them for inelastic analysis.
3. Perform geometrically nonlinear analysis of guyed towers.
4. Perform nonlinear analysis of guyed towers with geometric and material nonlinearities.
5. Develop P-I threshold curves for safety assessment of individual members of guyed towers.
6. Conduct global stability analysis of guyed towers under impulsive loads.

1.4 Scope

The structural analysis and design of towers apparently include many aspects that can hardly be covered by any single reference, including this dissertation. The scope will cover the major concern of structural engineers when facing similar problems. It includes nonlinear static and dynamic finite element analysis of truss, cable and beam elements. All three nonlinear elements will be implemented in the analysis of guyed towers. Geometric nonlinearity as well as material nonlinearity will be included to develop more accurate models for analysis. Quasi static analysis is discussed and examined to check the efficiency and accuracy. Methods for simulating the impulsive response of tower members will also be developed for the overall evaluation of the structural safety.

Chapter 2 Background Review

Nonlinearity in structural analysis comes from three common sources: geometric nonlinearity, material nonlinearity, and boundary condition nonlinearity. Since this research will focus on nonlinear behaviors of towers under severe loading, a series of reviews have been conducted. Research about geometric nonlinearity in the structural members (truss, cable and beam) will be presented first. General material nonlinearity will be introduced afterwards. The algorithms that implement static analysis and dynamic analysis will be briefly reviewed as well. Finally, the evaluation method for beams under impulsive loading will be introduced.

2.1 Basic elements used in FEM: truss, cable and beam

Literature (Bhatti, 2005; Madenci, 2006; Zienkiewicz *et al*, 2005) has explored the formulations of basic elements in FEM. But most of them only discussed about linear elements, which do not adjust element stiffness matrix according to deformation. Because in a large deformation scenario the influence of changing geometry is considerable and can not be neglected, the fully nonlinear elements developed by Pai (2007) are introduced herein.

2.1.1 Fully nonlinear truss element

From Fig. 2.1, it can be seen that the undeformed length of the truss element (Pai, 2007) is

$$l = \sqrt{(x_2 - x_1)^2 + (y_2 - y_1)^2 + (z_2 - z_1)^2} \tag{2.1}$$

Where (x_1, y_1, z_1) and (x_2, y_2, z_2) are position coordinates of points P_1 and P_2.

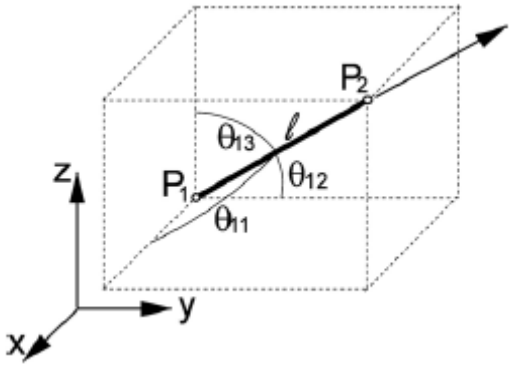

Figure 2.1 Undeformed geometry of a truss element.

Assume the position vectors of points P_1 and P_2 after deformation is

$$\mathbf{R}_1 = (x_1 + u_1)\mathbf{i} + (y_1 + v_1)\mathbf{j} + (z_1 + w_1)\mathbf{k} \tag{2.2a}$$

$$\mathbf{R}_2 = (x_2 + u_2)\mathbf{i} + (y_2 + v_2)\mathbf{j} + (z_2 + w_2)\mathbf{k} \tag{2.2b}$$

The Jaumann strain B_{11} along the deformed axis is

$$\begin{aligned} B_{11} &= \frac{|\mathbf{R}_2 - \mathbf{R}_1| - l}{l} \\ &= \frac{\sqrt{(u_2 - u_1 + x_2 - x_1)^2 + (v_2 - v_1 + y_2 - y_1)^2 + (w_2 - w_1 + z_2 - z_1)^2} - l}{l} \end{aligned} \tag{2.3}$$

Thus, the variation of B_{11} is

$$\begin{aligned} \delta B_{11} &= \{\delta u_1, \delta v_1, \delta w_1, \delta u_2, \delta v_2, \delta w_2\} \left\{ \frac{\partial B_{11}}{\partial u_1}, \frac{\partial B_{11}}{\partial v_1}, \frac{\partial B_{11}}{\partial w_1}, \frac{\partial B_{11}}{\partial u_2}, \frac{\partial B_{11}}{\partial v_2}, \frac{\partial B_{11}}{\partial w_2} \right\}^T \\ &= \{\delta u\}^T \{\phi\} \end{aligned} \tag{2.4}$$

If the initial strain caused by prestress in the bar is B_0, then the variation of elastic

energy is given by

$$\begin{aligned}\delta\Pi &= \sum_{1}^{ne}\int_0^l\int_A E\left(B_{11}-B_0\right)\delta B_{11}\,dA\,ds \\ &= \sum_{1}^{ne}\{\delta u\}^T\left([k]\{u\}-\{Q\}\right)\end{aligned} \tag{2.5}$$

where $[k]\{u\} = EAlB_{11}\{\phi\}$, $\{Q\} = EAlB_0\{\phi\}$.

The tangent stiffness matrix is

$$\begin{aligned}[\breve{k}] &= \frac{\partial([k]\{u\})}{\partial\{u\}} \\ &= EAl\{\phi\}\frac{\partial B_{11}}{\partial\{u\}} + EAlB_{11}\frac{\partial\{\phi\}}{\partial\{u\}} \\ &= EAl\{\phi\}\{\phi\}^T + EAlB_{11}\frac{\partial^2 B_{11}}{\partial\{u\}^2}\end{aligned} \tag{2.6}$$

The mass matrix is the same as that of the linear truss element:

$$[m] = \frac{\rho Al}{6}\begin{bmatrix}2&0&0&1&0&0\\0&2&0&0&1&0\\0&0&2&0&0&1\\1&0&0&2&0&0\\0&1&0&0&2&0\\0&0&1&0&0&2\end{bmatrix} \tag{2.7}$$

2.1.2 Fully nonlinear cable element

The static load is assumed to be applied before the dynamic loads in Fig. 2.2(a). $\hat{P}$ is the position of P_0 under static loads and P is the position under static and dynamic loads. If the displacement vector of P is $\{x_1, x_2, x_3\}$ and the one of $\hat{P}$ is $\{\alpha_1, \alpha_2, \alpha_3\}$, then

$$x_i = \alpha_i + u_i \qquad i = 1,2,3 \tag{2.8}$$

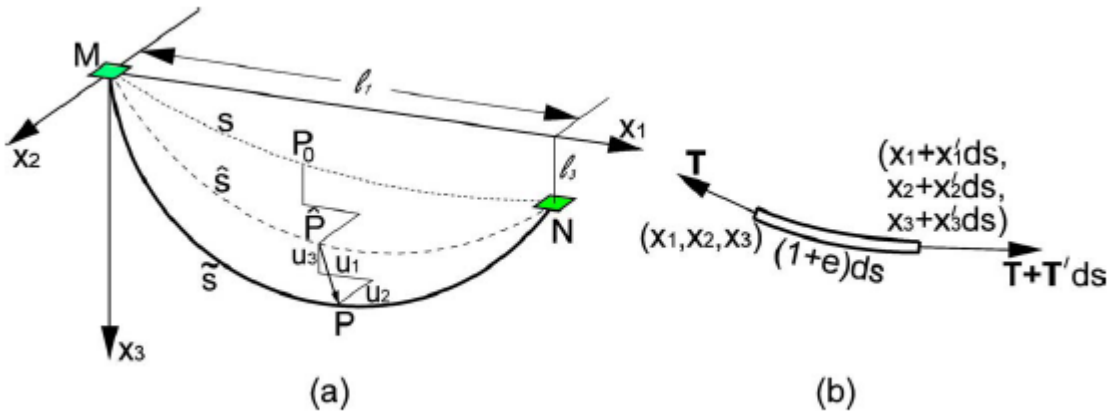

Figure 2.2 Deformed geometry of a cable element.

It follows from Fig. 2.2(b) that the axial strain (Pai, 2007) is

$$\begin{aligned} e &= \frac{\sqrt{\left(x_1' ds\right)^2 + \left(x_2' ds\right)^2 + \left(x_3' ds\right)^2} - ds}{ds} \\ &= \sqrt{\left(\alpha_1' + u_1'\right)^2 + \left(\alpha_2' + u_2'\right)^2 + \left(\alpha_3' + u_3'\right)^2} - 1 \end{aligned} \tag{2.9}$$

where $(\ )' = \dfrac{\partial(\ )}{\partial s}$.

The internal tension force is

$$\tilde{T} = EA_0\left[1 - \upsilon e\right]^2 e \tag{2.10}$$

where initial strain caused by prestress in the bar is e_0, υ is the poisson's ratio, A_0 is the original cross section area, and E is the young's modulus.

The variation of elastic energy is

$$\delta\Pi = \sum_{1}^{ne}\int_0^l EA_0\left[1-\upsilon e\right]^2 e\,\delta e\,ds$$

$$= \sum_{1}^{ne}\int_0^l EA_0\left[1-\upsilon e\right]^2 e\left[\frac{\alpha_1{}' + u_1{}'}{1+e}\delta\left(\alpha_1{}' + u_1{}'\right) + \frac{\alpha_2{}' + u_2{}'}{1+e}\delta\left(\alpha_2{}' + u_2{}'\right) + \frac{\alpha_3{}' + u_3{}'}{1+e}\delta\left(\alpha_3{}' + u_3{}'\right)\right]ds$$

$$= \sum_{1}^{ne}\int_0^l EA_0\left[1-\upsilon e\right]^2 e\left[\frac{\alpha_1{}' + u_1{}'}{1+e}\delta u_1{}' + \frac{\alpha_2{}' + u_2{}'}{1+e}\delta u_2{}' + \frac{\alpha_3{}' + u_3{}'}{1+e}\delta u_3{}'\right]ds$$

$$= \sum_{1}^{ne}\int_0^l EA_0\left[1-\upsilon e\right]^2 e\left\{\delta u_1{}', \delta u_2{}', \delta u_3{}'\right\}\left\{\frac{\alpha_1{}' + u_1{}'}{1+e}, \frac{\alpha_2{}' + u_2{}'}{1+e}, \frac{\alpha_3{}' + u_3{}'}{1+e}\right\}^T ds$$

in which, $\left\{\delta u_1{}', \delta u_2{}', \delta u_3{}'\right\}^T = \dfrac{d\left[N\right]}{ds}\left\{\delta u\right\}$

$$\left\{u\right\} = \left\{u_1^{[j]}, u_2^{[j]}, u_3^{[j]}, u_1^{[j+1]}, u_2^{[j+1]}, u_3^{[j+1]}\right\}^T$$

$$\left[N\right] = \begin{bmatrix} 1-\dfrac{s}{l_j} & 0 & 0 & \dfrac{s}{l_j} & 0 & 0 \\ 0 & 1-\dfrac{s}{l_j} & 0 & 0 & \dfrac{s}{l_j} & 0 \\ 0 & 0 & 1-\dfrac{s}{l_j} & 0 & 0 & \dfrac{s}{l_j} \end{bmatrix}$$

where l_j is the undeformed length of the *j*th element and s is the local physical coordinate. Assume $\left\{\phi\right\} = \left\{\dfrac{\alpha_1{}' + u_1{}'}{1+e}, \dfrac{\alpha_2{}' + u_2{}'}{1+e}, \dfrac{\alpha_3{}' + u_3{}'}{1+e}\right\} = \left\{\dfrac{\partial e}{\partial x_i{}'}\right\}$, and $\left[D\right] = \dfrac{d\left[N\right]}{ds}$.

Thus,

$$\begin{aligned}\delta\Pi &= \sum_{1}^{ne}\int_0^l \left\{\delta u\right\}^T EA_0\left[1-\upsilon e\right]^2 e\left[D\right]^T\left\{\phi\right\}ds \\ &= \sum_{1}^{ne}\left\{\delta u\right\}^T\left[k\right]\left\{u\right\}\end{aligned} \tag{2.11}$$

where $\left[k\right]\left\{u\right\} = \int_0^l EA_0\left[1-\upsilon e\right]^2 e\left[D\right]^T\left\{\phi\right\}ds$

And the tangent stiffness matrix becomes

$$
\begin{aligned}
\left[\breve{k}\right] &= \frac{\partial\left(\left[k\right]\cdot\left\{u\right\}\right)}{\partial\left\{u\right\}} \\
&= \int_0^l EA_0\left[\left[1-4\upsilon e+3\upsilon^2 e^2\right]\frac{\partial e}{\partial\left\{u\right\}}\left[D\right]^T\left\{\phi\right\}+\left[1-\upsilon e\right]^2 e\left[D\right]^T\frac{\partial\left\{\phi\right\}}{\partial\left\{u\right\}}\right]ds \\
&= \int_0^l EA_0\left[\left[1-4\upsilon e+3\upsilon^2 e^2\right]\left[D\right]^T\left\{\phi\right\}\left\{\phi\right\}^T\left[D\right]+\left[1-\upsilon e\right]^2 e\left[D\right]^T\frac{\partial^2 e}{\partial\left\{x'\right\}^2}\left[D\right]\right]ds
\end{aligned}
\tag{2.12}
$$

The mass matrix is the same as Eq. (2.7).

2.1.3 Beam element with von karman nonlinearity

The two well known beam theories are Euler-Bernouli and Timoshenko beam theories. The first one assumes the cross section remains plane and normal to the reference line after bending, which a rigidity higher than the actual one. Timosheko's beam theory overcomes this problem by including the shear deformation in the modeling. This improvement produces reasonable results for thick beams. But for thin beams, shear locking appears also due to the introduction of shear deformation. It is because of the domination of shear deformation over the bending deformation. Because structural members of guyed towers are usually slender, shear deformation is negligible. Therefore, nonlinear Euler-Bernouli beam with von karman nonlinearity can be employed for the modeling and analysis of guyed towers. Besides the bending effect, torsion and stretch effect is considered as well in the beam element (Pai, 2007).

The strains in the element can be expressed as

$$\varepsilon_{11} = e + z\rho_2 - y\rho_3 \tag{2.13}$$

$$\varepsilon_{12} = -z\rho_1 \tag{2.14}$$

$$\varepsilon_{13} = y\rho_1 \tag{2.15}$$

$$e = u' + v'^2/2 + w'^2/2 \tag{2.16}$$

$$\rho_1 = \phi' \tag{2.17}$$

$$\rho_2 = -w''\left(1 - w'^2\right) \tag{2.18}$$

$$\rho_3 = v''\left(1 - v'^2\right) \tag{2.19}$$

$$\{U\} = \{u', v', w', \phi', v'', w''\}^T = [B]\{d^{(i)}\} \tag{2.20}$$

where ε_{ij} is the tensorial engineering strain, e is the axial strain, y and z are coordinates in the cross section, ρ_i is the deformed curvatures with respect to the axes x, y and z. u, v and w are the displacements on the cross section, and $\{d^{(i)}\} = \{u_1, v_1, w_1, \phi_1, -w_1', v_1', \ldots, u_n, v_n, w_n, \phi_n, -w_n', v_n'\}$. The strain vector then be expressed as

$$\{\varepsilon\} = \begin{Bmatrix} \varepsilon_{11} \\ \varepsilon_{12} \\ \varepsilon_{13} \end{Bmatrix} = \begin{bmatrix} 1 & 0 & z & -y \\ 0 & -z & 0 & 0 \\ 0 & y & 0 & 0 \end{bmatrix} \begin{Bmatrix} e \\ \rho_1 \\ \rho_2 \\ \rho_3 \end{Bmatrix} = [Z]\{\psi\} \tag{2.21}$$

The variation is

$$\{\delta\varepsilon\} = \begin{bmatrix} 1 & 0 & z & -y \\ 0 & -z & 0 & 0 \\ 0 & y & 0 & 0 \end{bmatrix} \begin{Bmatrix} \delta e \\ \delta\rho_1 \\ \delta\rho_2 \\ \delta\rho_3 \end{Bmatrix} \tag{2.22}$$

$$= \begin{bmatrix} 1 & 0 & z & -y \\ 0 & -z & 0 & 0 \\ 0 & y & 0 & 0 \end{bmatrix} \begin{Bmatrix} \frac{\partial e}{\partial U_j}\delta U_j \\ \frac{\partial \rho_1}{\partial U_j}\delta U_j \\ \frac{\partial \rho_2}{\partial U_j}\delta U_j \\ \frac{\partial \rho_3}{\partial U_j}\delta U_j \end{Bmatrix} \tag{2.22}$$

$$= [Z][\Psi]\{\delta U\}$$

where $[\Psi] = \begin{bmatrix} \frac{\partial e}{\partial U_1} & \frac{\partial e}{\partial U_2} & \frac{\partial e}{\partial U_3} & \frac{\partial e}{\partial U_4} & \frac{\partial e}{\partial U_5} & \frac{\partial e}{\partial U_6} \\ \frac{\partial \rho_1}{\partial U_1} & \frac{\partial \rho_1}{\partial U_2} & \frac{\partial \rho_1}{\partial U_3} & \frac{\partial \rho_1}{\partial U_4} & \frac{\partial \rho_1}{\partial U_5} & \frac{\partial \rho_1}{\partial U_6} \\ \frac{\partial \rho_2}{\partial U_1} & \frac{\partial \rho_2}{\partial U_2} & \frac{\partial \rho_2}{\partial U_3} & \frac{\partial \rho_2}{\partial U_4} & \frac{\partial \rho_2}{\partial U_5} & \frac{\partial \rho_2}{\partial U_6} \\ \frac{\partial \rho_3}{\partial U_1} & \frac{\partial \rho_3}{\partial U_2} & \frac{\partial \rho_3}{\partial U_3} & \frac{\partial \rho_3}{\partial U_4} & \frac{\partial \rho_3}{\partial U_5} & \frac{\partial \rho_3}{\partial U_6} \end{bmatrix}$

$$= \begin{bmatrix} 1 & v' & w' & 0 & 0 & 0 \\ 0 & 0 & 0 & 1 & 0 & 0 \\ 0 & 0 & 2w''w' & 0 & 0 & -\left(1-w'^2\right) \\ 0 & -2v''v' & 0 & 0 & 1-v'^2 & 0 \end{bmatrix}$$

For stress tensor, it is

$$\{\sigma\} = \begin{bmatrix} E & 0 & 0 \\ 0 & G & 0 \\ 0 & 0 & G \end{bmatrix} \{\varepsilon\} = [\overline{Q}]\{\varepsilon\} \tag{2.23}$$

The potential energy is

$$
\begin{aligned}
\delta V &= \sum_{i=1}^{N_e} \int_0^l \int_A \{\delta\varepsilon\}^T \{\sigma\} dA dx \\
&= \sum_{i=1}^{N_e} \int_0^l \int_A \{\delta\psi\}^T [Z]^T [\overline{Q}][Z]\{\psi\} dA dx \\
&= \sum_{i=1}^{N_e} \int_0^l \int_A \{\delta U\}^T [\Psi]^T [Z]^T [\overline{Q}][Z]\{\psi\} dA dx \\
&= \sum_{i=1}^{N_e} \int_0^l \int_A \{\delta d^{(i)}\}^T [B]^T [\Psi]^T [Z]^T [\overline{Q}][Z]\{\psi\} dA dx \\
&= \sum_{i=1}^{N_e} \{\delta d^{(i)}\}^T [k^{(i)}]\{d^{(i)}\}
\end{aligned}
\tag{2.24}
$$

where

$$
[k^{(i)}]\{d^{(i)}\} = \int_{l_i} [B]^T [\Psi]^T \int_A [Z]^T [\overline{Q}][Z] dA \{\psi\} dx = \int_{l_i} [B]^T [\Psi]^T [\Phi]\{\psi\} dx
$$

$$
\begin{aligned}
[\Phi] &= \int_A [Z]^T [\overline{Q}][Z] dA \\
&= \begin{bmatrix} EA & 0 & 0 & 0 \\ 0 & GI_{11} & 0 & 0 \\ 0 & 0 & EI_{22} & 0 \\ 0 & 0 & 0 & EI_{33} \end{bmatrix}
\end{aligned}
$$

Assume $\{d^{(i)}\} = \{\overline{d}\} + \{\Delta d^{(i)}\}$ and $\{U\} = \{\overline{U}\} + \{\Delta U\}$, then

$$
\{\psi\} = \{\overline{\psi}\} + [\overline{\Psi}]\{\Delta U\} \tag{2.25}
$$

$$
\{\Psi\} = \{\overline{\Psi}\} + [\Theta] \tag{2.26}
$$

Where $[\Theta]_{ij} = \dfrac{\partial \Psi_{ij}}{\partial U_k} \Delta U_k$

Applying Taylor expansion and neglect high order terms,

$$
\begin{aligned}
[k^{(i)}]\{d^{(i)}\} &= \int_{l_i} [B]^T [\Psi]^T [\Phi]\{\psi\} dx \\
&= \int_{l_i} \left([B]^T [\overline{\Psi}]^T [\Phi]\{\overline{\psi}\} + [B]^T [\overline{\Psi}]^T [\Phi][\Psi]\{\Delta U\} + [B]^T [\Theta]^T [\Phi]\{\overline{\psi}\} \right) dx
\end{aligned}
$$

$$[\Theta]^T[\Phi]\{\overline{\psi}\} = \{\Theta_{mj}\Phi_{mn}\overline{\psi}_n\} = \left\{\frac{\partial\Psi_{mi}}{\partial U_j}\Delta U_j\Phi_{mn}\overline{\psi}_n\right\} = \left\{\frac{\partial^2\psi_m}{\partial U_i\partial U_j}\Phi_{mn}\overline{\psi}_n\Delta U_j\right\} = [\Gamma]\{\Delta U\}$$

Because the nonzero terms in $\dfrac{\partial^2\psi_m}{\partial U_i\partial U_j}$ are

$$\frac{\partial^2\psi_1}{\partial U_2\partial U_2} = 1;\ \frac{\partial^2\psi_1}{\partial U_3\partial U_3} = 1$$

$$\frac{\partial^2\psi_3}{\partial U_3\partial U_3} = 2w'';\ \frac{\partial^2\psi_3}{\partial U_3\partial U_6} = 2w';$$

$$\frac{\partial^2\psi_4}{\partial U_2\partial U_2} = -2v'';\ \frac{\partial^2\psi_4}{\partial U_2\partial U_5} = -2v'$$

The nonzero terms in $[\Gamma]$ are

$$\Gamma_{22} = \{1,0,0,-2v''\}[\Phi]\{\psi\} = EAe - 2EI_{33}v''\rho_3$$

$$\Gamma_{33} = \{1,0,2w'',0\}[\Phi]\{\psi\} = EAe + 2EI_{22}w''\rho_2$$

$$\Gamma_{25} = \{0,0,0,-2v'\}[\Phi]\{\psi\} = -2EI_{33}v'\rho_3$$

$$\Gamma_{36} = \{0,0,2w',0\}[\Phi]\{\psi\} = 2EI_{22}w'\rho_2$$

Thus,

$$[\Gamma] = \left[\frac{\partial^2\psi_m}{\partial U_i\partial U_j}\Phi_{mn}\overline{\psi}_n\right]$$

$$= \begin{bmatrix} 0 & 0 & 0 & 0 & 0 & 0 \\ 0 & EAe - 2EI_{33}v''\rho_3 & 0 & 0 & -2EI_{33}v'\rho_3 & 0 \\ 0 & 0 & EAe + 2EI_{22}w''\rho_2 & 0 & 0 & 2EI_{22}w'\rho_2 \\ 0 & 0 & 0 & 0 & 0 & 0 \\ 0 & 0 & 0 & 0 & 0 & 0 \\ 0 & 0 & 0 & 0 & 0 & 0 \end{bmatrix} \quad (2.27)$$

The product of stiffness matrix and displacement vector becomes

$$\begin{aligned}\left[\tilde{k}^{(i)}\right]\left\{\Delta d^{(i)}\right\} &= \int_{l_i}\left(\left[B\right]^T\left[\overline{\Psi}\right]^T\left[\Phi\right]\left[\Psi\right]\left\{\Delta U^{(i)}\right\}+\left[B\right]^T\left[\Theta\right]^T\left[\Phi\right]\left\{\overline{\psi}\right\}\right)dx \\ &= \int_{l_i}\left[B\right]^T\left(\left[\overline{\Psi}\right]^T\left[\Phi\right]\left[\Psi\right]+\left[\Gamma\right]\right)\left\{\Delta U^{(i)}\right\}dx \\ &= \int_{l_i}\left[B\right]^T\left(\left[\overline{\Psi}\right]^T\left[\Phi\right]\left[\Psi\right]+\left[\Gamma\right]\right)\left[B\right]\left\{\Delta d^{(i)}\right\}dx\end{aligned} \tag{2.28}$$

Thus, the tangent stiffness matrix is

$$\left[\tilde{k}^{(i)}\right] = \int_{l_i}\left[B\right]^T\left(\left[\overline{\Psi}\right]^T\left[\Phi\right]\left[\Psi\right]+\left[\Gamma\right]\right)\left[B\right]dx \tag{2.29}$$

2.2 Material Nonlinearity

Plasticity is fairly common in engineering practice. Once the material enters plastic range, material modulus decreases if it is strain softening or increases if strain hardening, which would finally change the global stiffness of a structure. Thus, the response is greatly affected by material nonlinearity if it has a potential to reach inelastic stage.

Material nonlinearities can be categorized as isotropic hardening, kinetic hardening. In elastic range, incremental stresses can be expressed as the product of an elastic constitutive matrix $\left[C\right]$ and incremental strains $\left\{d\varepsilon\right\}$ as

$$\left\{d\sigma\right\} = \left[C\right]\left\{d\varepsilon\right\} \tag{2.30}$$

The general form of yield function (Bhatti, 2006) is

$$\overline{F}\left(\left\{\sigma\right\}, w^p, \left\{\alpha\right\}\right) = 0$$

where w^p is a scalar denoting the plastic work done, and $\left\{\alpha\right\}$ is a vector denoting the translation of the yield surface. Once the deformation reaches the yield surface, it can have two possibilities: (a) loading continues on the yield surface (b) unload and retrieve back into the elastic range. If there is no hardening effect, the yield surface remains fixed

and never expand. With hardening effect, the yield surface or plane can expand according to the hardening rule. To determine the strain flow on the yield surface, the following flow rule is needed.

$$\{d\varepsilon^p\} = \lambda \cdot \frac{\partial Q}{\partial \{\sigma\}} \tag{2.31}$$

where λ is a constant of proportionality that relates the plastic strains to the plastic potential, and Q is the plastic potential function. If Q is chosen to be equal to the yield function F, the flow rule is associated. The total strain increment in a plastic state can be expressed by

$$\{d\varepsilon\} = \{d\varepsilon^e\} + \{d\varepsilon^p\} \tag{2.32}$$

After manipulation (Bhatti, 2006), the constitutive stress-strain relation for plastic phase is

$$\{d\sigma\} = ([C] - [C_p])\{d\varepsilon\} \tag{2.33}$$

where $[C_p] = \frac{1}{a}[C]\frac{\partial Q}{\partial \{\sigma\}}\left(\frac{\partial \overline{F}}{\partial \{\sigma\}}\right)^T [C]$,

$$a = \left(\frac{\partial \overline{F}}{\partial \{\sigma\}}\right)^T [C]\frac{\partial Q}{\partial \{\sigma\}} - \frac{\partial \overline{F}}{\partial w^p}\{\sigma\}^T \frac{\partial Q}{\partial \{\sigma\}} - c\left(\frac{\partial \overline{F}}{\partial \{\sigma\}}\right)^T [L]\frac{\partial Q}{\partial \{\sigma\}},$$

$$[L] = \begin{bmatrix} 1 & 0 & 0 & 0 & 0 & 0 \\ 0 & 1 & 0 & 0 & 0 & 0 \\ 0 & 0 & 1 & 0 & 0 & 0 \\ 0 & 0 & 0 & \frac{1}{2} & 0 & 0 \\ 0 & 0 & 0 & 0 & \frac{1}{2} & 0 \\ 0 & 0 & 0 & 0 & 0 & \frac{1}{2} \end{bmatrix}$$

2.2.1 Isotropic hardening and dynamic hardening

Isotropic hardening assumes that the yield stress for reversed loading is equal to previous yield stress (Bhatti, 2006). Thus, the elastic range for isotropic hardening (Fig 2.3 (a)) is increased in consecutive loading and unloading cycles. For the dynamic hardening (Fig 2.3 (b)), the elastic range is fixed and the yield stress in opposite direction varies in loading and unloading.

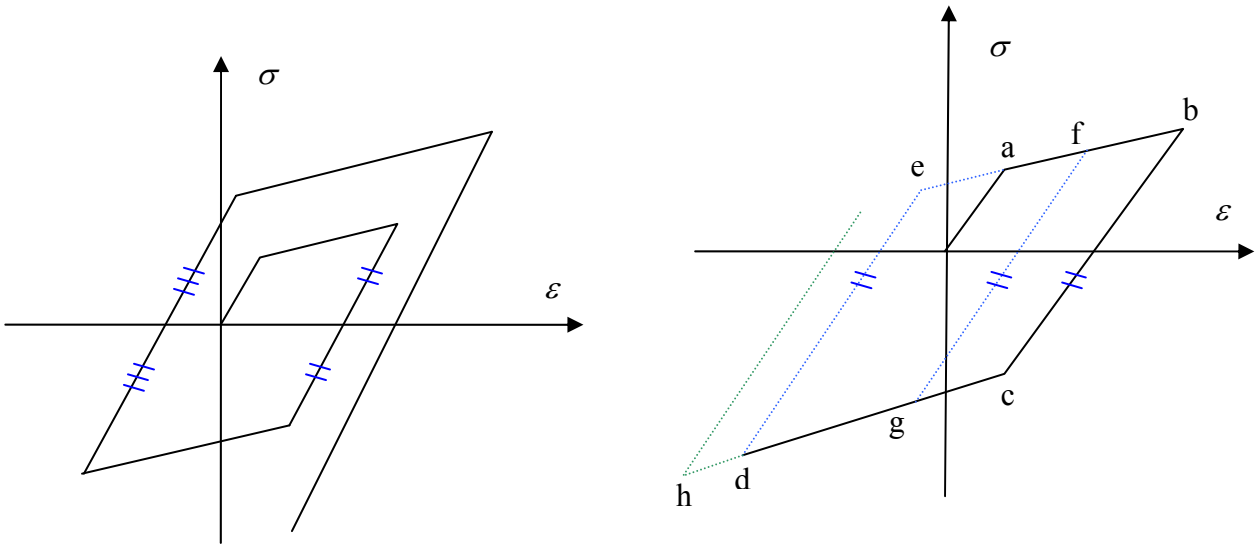

(a) (b)

Figure 2.3 (a) Isotropic hardening, and (b) dynamic hardening.

For an elastic state, the incensement of stress $d\sigma$ is proportional to the change of strain $d\varepsilon$.

$$d\{\sigma\} = Ed\{\varepsilon\} \tag{2.34}$$

For an inelastic state, the change of stress can be expressed in three ways:

$$d\{\sigma\} = Ed\{\varepsilon^e\};\ \ d\{\sigma\} = Hd\{\varepsilon^p\};\ \ d\{\sigma\} = E_t d\{\varepsilon\}$$

where $d\{\varepsilon^e\}$ is the elastic strain increment;

$d\{\varepsilon^p\}$ is plastic strain increment;

$d\{\varepsilon\} = d\{\varepsilon^e\} + d\{\varepsilon^p\}$ is the total strain increment,

H is the plastic modulus,

$E_t = \dfrac{EH}{E+H}$ is the tangent modulus

The yield stress state for isotropic hardening can be updated by

$$\{\overline{\sigma}_y\} = \{\sigma_y\} + H\{\varepsilon^p\} \tag{2.35}$$

The state for dynamic hardening can be updated by

$$\overline{F} = \left|\sigma - H\varepsilon^p\right| - \sigma_y \tag{2.36}$$

2.2.2 Algorithm implementing material nonlinearity

Reddy (2004) introduced an algorithm that checks and adjusts the stress state every step. If the force equilibrium is resumed in the following iteration, then the solution converges at that step and can move forward. For one dimensional problem, the adjustment to achieve force equilibrium is obtained by imposing an additional deformation to the inelastic element by

$$\Delta u_i = \frac{\Delta F L_i}{E_t A_i} \tag{2.37}$$

where Δu_i is the additional displacement adjustment

L_i is the length of the element

A_i is the cross section area of the element

The other elements remain unaffected if they are not yielded.

Bhatti (2006) used the Newton-Raphson approach to achieve the equilibrium. Basically, it runs iteration until the internal forces and external forces have been balanced. The other steps are essentially same as the Reddy's approach.

2.3 Algorithm for nonlinear static analysis

After the global stiffness matrix has been obtained, the solution of the nonlinear equations is not easy because the stiffness of each element can be affected by its displacement. Thus, some algorithms are needed to achieve the solutions. The most commonly used methods are: Newton-Raphson's method, the modified Newton-Raphson method, Riks' method and the modified Riks method (Crisfiled's method). Detailed explanation can be found in literatures (Davis and Thomson, 2000; Bathe, 1996).

$$[K]\{U\} = \{F\} \tag{2.38}$$

where $[K]$ is global stiffness matrix, $\{U\}$ is the displacement vector, and $\{F\}$ is global force vector.

2.3.1 Newton-Raphson method and Modified Newton-Raphson method

The scheme is illustrated in Fig 2.4. Assume the imbalance force at the beginning of $i-1$ step is

$$R\left(\{U\}^{i-1}\right) = [K]\{U\}^{i-1} - \{F\} \tag{2.39}$$

If the imbalance force at the beginning of i th step $R\left(\{U\}^{i}\right)$ is expanded to a low-order Taylor series, then

$$R\left(\{U\}^i\right) = R\left(\{U\}^{i-1}\right) + \left.\frac{\partial R}{\partial \{U\}}\right|_{\{U\}^{i-1}} \delta\{U\}$$
$$= R\left(\{U\}^{i-1}\right) + \left[K_T\right]\Big|_{\{U\}^{i-1}} \delta\{U\} \tag{2.40}$$

Where $\{U\}^i$ is the displacement vector in i th step,

$\{U\}^{i-1}$ is the displacement vector in $i-1$ th step ,

the tangent stiffness matrix is $\left(\left[K_T\right]\Big|_{\{U\}^{i-1}}\right)_{ij} = \frac{\partial [K]_{ik} \{U\}^{i-1}{}_k}{\partial \{U\}^{i-1}{}_j}$.

Set $R\left(\{U\}^i\right) = 0$, then $\delta\{U\} = -\left(\left[K_T\right]\Big|_{\{U\}^{i-1}}\right)^{-1}\left([K]\{U\}^{i-1} - \{F\}\right)$. Update $\{U\}^i = \{U\}^{i-1} + \delta\{U\}$ and repeat the above steps until the convergence criteria (the ratio of the magnitude of displacement increment vector to the previous displacement vector) is met.

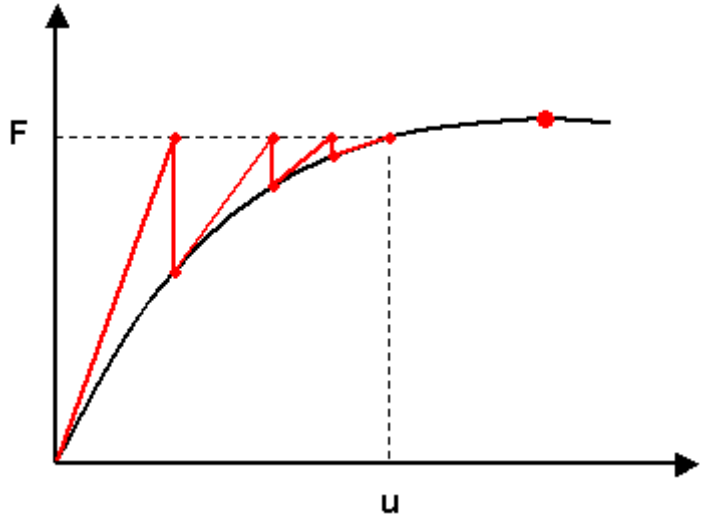

Figure 2.4 Modified Newton-Raphson method.

Since the tangent stiffness matrix is updated in each iteration, it may need large computational effort. Modified Newton-Raphson method either keep $\left[K_T\right]$ fixed or only

updating it at preselected steps (Reddy, 2004).

2.3.2 Modified Riks method (Crisfield's method)

The drawback of the Newton-Raphson method is that it can not capture some special phenomena like snap through of trusses. It is because that the tangent stiffness matrix $[K_T]$ becomes singular at some special points, which makes the solution of Eq. (2.40) inaccessible. To overcome this problem, Riks suggested a procedure that traces the intersection of the normal to tangent line with the equilibrium path as shown in Fig 2.5. Similarly, Crisfiled's method uses an arc (or circular plane in multi-dimension) instead of a perpendicular line (or perpendicular plane in multi-dimension) for solution searching. The increment of load factor becomes an unknown that needs be solved during the iteration.

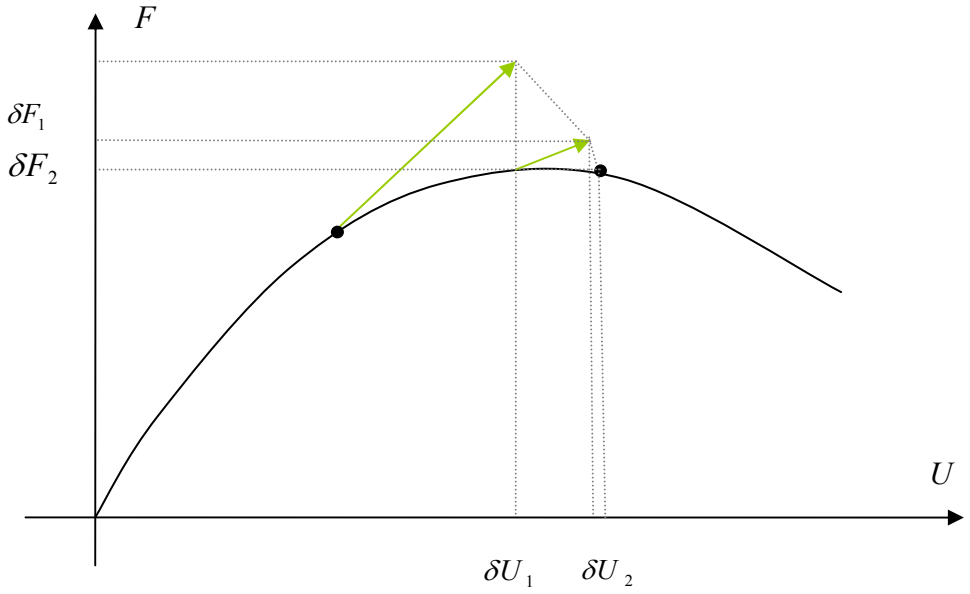

Figure 2.5 Crisfield's method.

Assume $\{F\} = \lambda\{\hat{F}\}$, where λ is a load parameter and $\{\hat{F}\}$ is a preselected load vector,

$$R\left(\{U\}^i, \lambda^i\right) = R\left(\{U\}^{i-1}, \lambda^{i-1}\right) + \left.\frac{\partial R}{\partial \{U\}}\right|_{\{U\}^{i-1}, \lambda^{i-1}} \delta\{U\}_1^i + \left.\frac{\partial R}{\partial \lambda}\right|_{\{U\}^{i-1}, \lambda^{i-1}} \delta\lambda_1^i \tag{2.41}$$

Set $R\left(\{U\}^i, \lambda^i\right) = 0$,

$$\{0\} = [K]\{U\}\Big|_{\{U\}^{i-1}, \lambda^{i-1}} - \lambda^{i-1}\{\hat{F}\} + [K_T]\Big|_{\{U\}^{i-1}, \lambda^{i-1}} \delta\{U\}_1^i + \{\hat{F}\}\delta\lambda_1^i \tag{2.42}$$

where $\delta\{U\}_1^i$ is the first increment of displacement vector and $\delta\lambda_1^i$ is the first increment of load parameter. If $\delta\lambda_1^i$ is specified, $\delta\{U\}_1^i$ can be solved. Update the displacement vector and load parameter by $\{U\}_1^i = \{U\}^{i-1} + \delta\{U\}_1^i$ and $\lambda_1^i = \lambda^{i-1} + \delta\lambda_1^i$. Obviously, the first guess usually will not be the exact solution. Therefore, following iterations are needed. With updated $\{U\}_1^i$ and λ_1^i, Eq. (2.42) turns into

$$\{0\} = [K]\{U\}\Big|_{\{U\}_1^i, \lambda_1^i} - \lambda_1^i\{\hat{F}\} + [K_T]\Big|_{\{U\}_1^i, \lambda_1^i} \delta\{U\}_2^i + \{\hat{F}\}\delta\lambda_2^i \tag{2.43}$$

By setting the following incremental searching path perpendicular to the normal of the first incremental path,

$$\{0\} = \delta\{U\}_1^i \delta\{U\}_2^i + \{\hat{F}\}\delta\lambda_1^i\{\hat{F}\}\delta\lambda_2^i \tag{2.44}$$

Solving Eq. (2.43) and Eq. (2.44) for $\delta\{U\}_2^i$ and $\delta\lambda_2^i$ yields

$$\delta\{U\}_2^i = -\left([K_T]\Big|_{\{U\}_1^i, \lambda_1^i}\right)^{-1}\left([K]\{U\}\Big|_{\{U\}_1^i, \lambda_1^i} - \lambda_1^i\{\hat{F}\} + \{\hat{F}\}\delta\lambda_2^i\right) \tag{2.45}$$

$$\delta\lambda_2^i = \frac{\delta\{U\}_1^i\left([K_T]\Big|_{\{U\}_1^i, \lambda_1^i}\right)^{-1}\left([K]\{U\}\Big|_{\{U\}_1^i, \lambda_1^i} - \lambda_1^i\{\hat{F}\}\right)}{\left(\{\hat{F}\}\delta\lambda_1^i\{\hat{F}\} - \delta U_1^i\left([K_T]\Big|_{\{U\}_1^i, \lambda_1^i}\right)^{-1}\{\hat{F}\}\right)} \tag{2.46}$$

The above steps are repeated until convergence. The converged displacement vector

and the converged load parameter are $\{U\}^i = \{U\}^{i-1} + \delta\{U\}_1^i + \delta\{U\}_2^i + \delta\{U\}_3^i + \cdots$ and $\lambda^i = \lambda^{i-1} + \delta\lambda_1^i + \delta\lambda_2^i + \delta\lambda_3^i + \cdots$.

Some limits should be set to avoid divergence, such as maximum and minimum step length and a maximum iteration number. Details can be found in Pai (2007) and Reddy (2004).

2.4 Algorithm for dynamic response

There are two approaches for the analysis of dynamic response of complex structures. The first one is an indirect method by modal analysis, which uses the superposition principle to combine the response of modal vibrations of basic modes. The second one is numerical integration methods, which is conducted by numerous time steps. The solution of next step is always based on previous converged solution. The accuracy is usually affected by the selection of proper time increases.

2.4.1 Modal analysis

Modal analysis is not only computationally efficient but also of high accuracy in a linear system. It is widely applied in vibration analysis. Extensive research already has been done on Single Degree Of Freedom (SDOF), Multiple Degree Of Freedom (MDOF) systems, and continuous systems, such as strings, bars, beams, membranes, plates and shells. If structural members or structures are simplified into SDOF or MDOF by equivalent mass and stiffness matrix, the modal analysis can be implemented by rigorous solution or numerical solution (Biggs, 1964). For structural members, the real time

response of structures or a structural element can also be assumed to be the product of the primary response spectrums and the modal participation factors. The response spectrum can be solved with the consideration of boundary conditions. After the decomposition of response functions, each modal coordinate function can be extracted by solving independent equations (Inman, 2001). As for the damping ratio, observations indicate that typical structures have between 5 and 10 percent of critical damping (Biggs, 1964).

2.4.2 General integration methods

Mode shapes do not have fixed magnitude. So they are in fact not affected by the global displacement vector. But this is only true for linear or elastic systems. In nonlinear systems, the stiffness and damping changes with the deformation of the system. So in reality, there are no fixed mode shapes for nonlinear systems. Or in other words, the mode shapes vary with the magnitude of deformation. General integration methods account for the change of system properties by the integration using small time steps. Thus, they are the only way to solve the nonlinear dynamic problems. The commonly used methods are the constant average acceleration method (or Euler-Gauss procedure) and Newmark Beta methods. Since the first one is just a special case of the second method, only Newmark Beta methods will be reviewed here. The basic integration formulas (Reddy, 2004) for the velocity and displacement of the ith step are expressed as

$$\{\dot{U}\}^i = \{\dot{U}\}^{i-1} + (1-\gamma)dt\{\ddot{U}\}^{i-1} + \gamma dt\{\ddot{U}\}^i \tag{2.47a}$$

$$\{U\}^i = \{U\}^{i-1} + dt\{\dot{U}\}^{i-1} + \left(\frac{1}{2} - \beta\right)dt^2\{\ddot{U}\}^{i-1} + \beta dt^2\{\ddot{U}\}^i \tag{2.47b}$$

where $\{U\}^i$, $\{\dot{U}\}^i$ and $\{\ddot{U}\}^i$ are the displacement vector, velocity vector and acceleration vector of i th step.

Assume the expansion of displacement vector, velocity vector and acceleration vector to be

$$\{U\}^i = \{U\}^{i-1} + \Delta\{U\}^{i-1} \tag{2.48a}$$

$$\{\dot{U}\}^i = \{\dot{U}\}^{i-1} + \Delta\{\dot{U}\}^{i-1} \tag{2.48b}$$

$$\{\ddot{U}\}^i = \{\ddot{U}\}^{i-1} + \Delta\{\ddot{U}\}^{i-1} \tag{2.48c}$$

Substituting Eq. (2.48a)-(2.48c) into the global differential equation,

$$[M]\{\ddot{U}\}+[C]\{\dot{U}\}+[K]\{U\}=\{F\} \tag{2.49}$$

Eq. (2.49) can be further transformed into

$$[M]\Delta\{\ddot{U}\}^{i-1}+[C]\Delta\{\dot{U}\}^{i-1}+[K]\Delta\{U\}^{i-1}=\{F\}-\left([M]\{\ddot{U}\}^{i-1}+[C]\{\dot{U}\}^{i-1}+[K]\{U\}^{i-1}\right) \tag{2.50}$$

Substituting Eq. (2.48a) and Eq. (2.48b) into Eq.(2.47a) and Eq. (2.47b) yields

$$\Delta\{\dot{U}\}^{i-1} = \left(1-\frac{\gamma}{2\beta}\right)dt\{\ddot{U}\}^{i-1}+\frac{\gamma}{\beta dt}\Delta\{U\}^{i-1}-\frac{\gamma}{\beta}\{\dot{U}\}^{i-1} \tag{2.51a}$$

$$\Delta\{\ddot{U}\}^{i-1} = \frac{1}{\beta dt^2}\Delta\{U\}^{i-1}-\frac{1}{\beta dt}\{\dot{U}\}^{i-1}-\frac{1}{2\beta}\{\ddot{U}\}^{i-1} \tag{2.51b}$$

Substituting Eq.(2.51 a) and Eq. (2.51 b) into Eq. (2.50) yields

$$[\tilde{K}]\Delta\{U\}^{i-1} = \{\tilde{F}\} \tag{2. 52}$$

where

$$[\tilde{K}]=[K]+\frac{1}{\beta dt^2}[M]+\frac{\alpha}{\beta dt}[C]$$

$$\{\widetilde{F}\}=\{F\}-\left([M]\{\ddot{U}\}^{i-1}+[C]\{\dot{U}\}^{i-1}+[K]\{U\}^{i-1}\right)+[M]\left(\frac{1}{2\beta}\{\ddot{U}\}^{i-1}+\frac{1}{\beta dt}\{\dot{U}\}^{i-1}\right)$$
$$+[C]\left(\left(\frac{\alpha}{2\beta}-1\right)dt\{\ddot{U}\}^{i-1}+\frac{\alpha}{\beta}\{\dot{U}\}^{i-1}\right)$$

The solution of Eq. (2.52) gives the first estimation of $\Delta\{U\}_1^{i-1}$. Since the tangent stiffness and damping matrix are computed at the beginning of each time step, it may be not right for the whole time step. So Newton-Raphson's iteration is again used to obtain the exact solution (Pai, 2007). The algorithm is as follows:

Assume

$$\Delta\{U\}^{i-1}=\Delta\{U\}_1^{i-1}+\delta\{U\}_1^{i-1} \tag{2.53a}$$

$$\Delta\{\dot{U}\}^{i-1}=\Delta\{\dot{U}\}_1^{i-1}+\delta\{\dot{U}\}_1^{i-1} \tag{2.53b}$$

$$\Delta\{\ddot{U}\}^{i-1}=\Delta\{\ddot{U}\}_1^{i-1}+\delta\{\ddot{U}\}_1^{i-1} \tag{2.53c}$$

Where $\delta\{U\}_1^{i-1}$, $\delta\{\dot{U}\}_1^{i-1}$ and $\delta\{\ddot{U}\}_1^{i-1}$ are the incremental of displacement, velocity and acceleration of the $i-1$ step. Since the solution of Eq. (2.47a) and Eq. (2.47b) gives

$$\{\dot{U}\}^{i}=\left(1-\frac{\alpha}{2\beta}\right)dt\{\ddot{U}\}^{i-1}+\left(1-\frac{\alpha}{\beta}\right)\{\dot{U}\}^{i-1}+\frac{\alpha}{\beta dt}\left(\{U\}^{i}-\{U\}^{i-1}\right) \tag{2.54a}$$

$$\{\ddot{U}\}^{i}=\left(1-\frac{1}{2\beta}\right)\{\ddot{U}\}^{i-1}-\frac{1}{\beta dt}\{\dot{U}\}^{i-1}+\frac{1}{\beta dt^2}\left(\{U\}^{i}-\{U\}^{i-1}\right) \tag{2.54b}$$

It can be derived therefore that

$$\delta\{\dot{U}\}^{i-1}=\frac{\alpha}{\beta dt}\delta\{U\}^{i-1} \tag{2.55a}$$

$$\delta\{\ddot{U}\}^{i-1}=\frac{1}{\beta dt^2}\delta\{U\}^{i-1} \tag{2.55b}$$

Substituting Eqs. (2.53a) - (2.53c), Eq. (2.55a) and Eq. (2.55b) into Eq. (2.50) yields

$$[M]\delta\{\ddot{U}\}^{i-1}+[C]\delta\{\dot{U}\}^{i-1}+[K]\delta\{U\}^{i-1}=\{F\}-\left([M]\{\ddot{U}\}^{i-1}+[C]\{\dot{U}\}^{i-1}+[K]\{U\}^{i-1}\right)$$
$$-\left([M]\Delta\{\ddot{U}\}_1^{i-1}+[C]\Delta\{\dot{U}\}_1^{i-1}+[K]\Delta\{U\}_1^{i-1}\right)$$

$$\left[\breve{K}\right]\delta\{U\}^{i-1}=\left\{\breve{F}\right\} \tag{2.56}$$

Where

$$\left[\widetilde{K}\right]=[K]+\frac{1}{\beta dt^2}[M]+\frac{\alpha}{\beta dt}[C]$$

$$\left\{\widetilde{F}\right\}=\{F\}-\left([M]\{\ddot{U}\}^{i-1}+[C]\{\dot{U}\}^{i-1}+[K]\{U\}^{i-1}\right)-\left([M]\Delta\{\ddot{U}\}_1^{i-1}+[C]\Delta\{\dot{U}\}_1^{i-1}+[K]\Delta\{U\}_1^{i-1}\right)$$

Once Eq.(2.56) is solved, $\delta\{\dot{U}\}^{i-1}$ and $\delta\{\ddot{U}\}^{i-1}$ can be obtained by Eq.(2.55a) and Eq.(2.55b). The iterations should be terminated when the convergence criteria is met. The displacement, velocity and acceleration vectors will be updated until the desired time limit is achieved. The Newmark method is unconditionally stable when $\alpha \geq \frac{1}{2}$ and $\beta \geq \frac{1}{4}\left(\alpha+\frac{1}{2}\right)^2$ (Bathe and Wilson, 1976).

2.5 Evaluation of impulsive response

Since under an impulsive loading, the members of a tower will behave like beams. The Pressure-impulse (P-I) method is introduced to evaluate the response and damage of members of a tower.

Pressure-impulse (P-I) diagram is used to evaluate the critical status of beams in bending failure because it has a straightforward expression form. This method was first used to assess the damage extent of structural elements and buildings in the World War II

(Smith and Hetherington, 1995). Stanford Research Institute used P-I diagram to evaluate the effects of blast on aircraft structures in 1951 (Abrahamson and Lindberg, 1976). The critical load curves for simple rigid-plastic systems were calculated using the P-I diagram method (Mortion, 1954). Velocity and acceleration were used as the coordinates, which are equivalent to the peak load and impulse system, to derive the curves for different structures (Kornhauser, 1954). It was identified that the peak load is very important for impulsive load cases (Coombs and Thornhill, 1967). Researchers of the Lovelace Foundation (1966) studied the influence of the impulse and the peak load on animal injuries. The closed-form formulas were brought up for rigid-plastic system (Abrahamson and Lindberg, 1976). P-I diagram method is also used for the assessment of injuries of animal and human subjected to a detonation (Smith and Hetherington, 1995). The least-square method was used to constitute universal formulas to fit the critical P-I diagram curves (Li and Meng, 2002). So P-I diagram is a powerful tool to evaluate the response of structural members under blast loads.

It has been widely admitted that the P-I diagram has three regions including an impulsive-controlled region, a peak pressure-controlled region, and a peak pressure and impulse combination-controlled region (Abrahamson and Lindberg, 1976; Smith and Hetherington, 1995; Li and Meng, 2002). The division of the three regions is shown in Table 2.1. Though there is small difference regarding the specific number of the dividing standard, they are similar because they are all based on the comparison with the natural period of a structure or structural members. The category of P-I diagram is illustrated as part □, □and □ in Fig. 2.6.

Table 2.1 Three regions of the P-I diagram

	Abrahamson 1971	Smith 1995
Impulse-controlled	$t_d \le 0.05T$	$0.4 > \omega t_d$
Peak pressure and impulse combination-controlled	$0.05T \le t_d \le 1.25T$	$0.4 \le \omega t_d \le 40$
Peak pressure controlled	$t_d \ge 1.25T$	$40 < \omega t_d$

Note: T is the natural period, ω is the natural vibration frequency, and t_d is the blast load duration.

There are three representative load types: (1) rectangular load with step rise, constant value, and step down, (2) triangular load with step rise and linear depreciation, (3) exponential load with step rise and exponential depreciation. For the same structural element the rectangular load gives the lower bound of the threshold curve, while the exponential load results in the upper bound. For the triangular load the corresponding curve is between the two boundary curves (Fig. 2.7). The maximum difference between the lower bound and the upper bound can be up to 40% (Abrahamson and Lindberg, 1976).

The advantage of the P-I diagram is the simplification of judgment to the safety of structural members or structures. Based on the P-I diagram, a certain load with the peak pressure and impulse above the critical curve will result in damage of the structures, vice versa, the structure is safe if the peak pressure and impulse combination locates below the curve.

Steel beams are indeed a kind of elasto-plastic structures. Since the elastic part of

material strength only absorbs very limited shock energy, the beam can be simplified as a rigid-plastic structure, which greatly simplify theoretical solution.

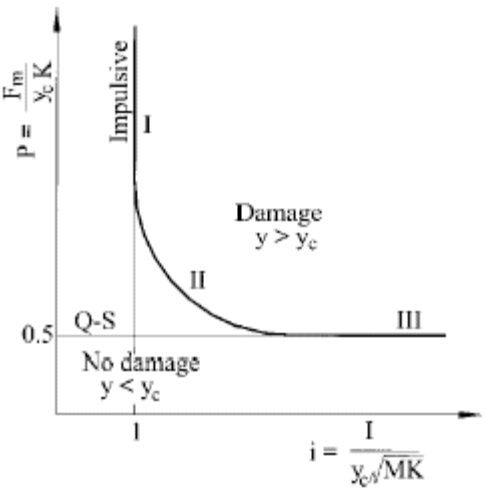

Fig. 2.6 Normalized P-I diagram.

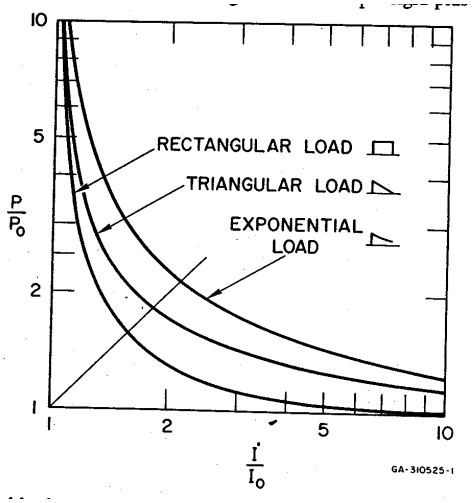

Fig. 2.7 Effect of impulse shape.

Some studies have conducted on theoretical modeling of rigid-plastic beams under blast loads, which can be roughly divided into two categories. The first category is based on single-degree-of-freedom (SDOF) model. The beam is simplified as a single mass and stiffness as a spring (Biggs, 1964; Smith and Hetherington, 1995). The maximum displacement is selected as a critical factor, which decides the safety of the beam. The equivalence of the mass, stiffness, and load has been discussed in details for structural members with different boundary conditions (Naval Facilities Engineering Command Design Manual 2.08, 1986). The SDOF model treats the beam as a whole and neglects the influence of shear force, which subsequently leads to the ignorance of shear failure. However, shear failure usually occurs when the ratio of span to height of the beams is very small or the detonation is very close to the structures.

The second category overcomes the deficiency by considering the impact of shear

force in the model. Based on experimental phenomena and mathematical derivation, five possible deformation profiles of beams under impact loads have been developed (Jones, 1989). The impact is simplified as an ideal impulse that is applied to the beam with no time duration. The model was further improved by considering the response of beam during impulse load duration and the standardized expression of critical deformation was put forward (Li and Jones, 1995). However, most results are expressed in an implicit form which caused inconvenience for the application in a specific computation. The difference between shear failure and bending failure is neglected as well.

2.6 Summary

In this chapter, the main theoretical background of nonlinear truss, cable and beam elements has been reviewed. With the application of Jaumann strains, these elements are proper for large deformation analysis. The inelasticity of material properties was introduced to improve the analysis accuracy. Two hardening models: isotropic hardening and dynamic hardening were reviewed and formulated. The change of stiffness during the nonlinear static analysis needs a special iterative algorithm for solution. Therefore, several algorithms including Newton Raphon's method, and Modified Riks method have been discussed. The corresponding solution methods for dynamic analysis are also explored using indirect method by modal analysis and the Newmark Beta method for direct numerical integration of nonlinear problems. The impulsive load is one of special dynamic loadings because of its high peak pressure and short duration. The pressure impulse method is introduced to provide a quick but efficient approach for individual member safety analysis.

Chapter 3 Geometrically Nonlinear Characteristics of Trusses, Cables and Beams

Truss, cable and beam elements are the basic components of guyed towers. They can be easily assembled in the field, which is an advantage in construction. Trusses can sustain large loads with relatively light weight. Cables are like one-directional trusses and they can only sustain tension. Beams can sustain bending moments and torsional loads in addition to shear and axial forces. They may have complicated static and dynamic behavior when fully geometric nonlinearity is involved.

This chapter will focus on the nonlinear behavior of truss, cable and beam elements of a full tower. Various scenarios, which are related to global analysis of a guyed tower, are considered to verify the capability of the developed finite element models. Linear analysis is employed for some parts to provide an alternative perspective.

3.1 Nonlinear static behaviors of trusses

Snap-through and snap-back are the common phenomena in highly flexible truss structures. Both of them usually result in very large deformation in the truss structures. To trace the deformation procedure, the modified Riks method is employed. Jaumann strains are used in the modeling because they are more accurate than Green- Lagrange strains for geometrically nonlinear problems (Pai, 2007).

An aluminum truss dome is used to demonstrate these phenomena. Young's modulus is 10.2×10^{6} psi. The geometry of the dome is shown in Figs. 3.1(a) and 3.1(b). The most outside ring is on a circle having a radius equal to 60m. The second ring's radius is 30m and the third one 15m. The cross section area is 0.3333 square

inch. The supports are on the ground and are fixed. The load is applied on the top center.

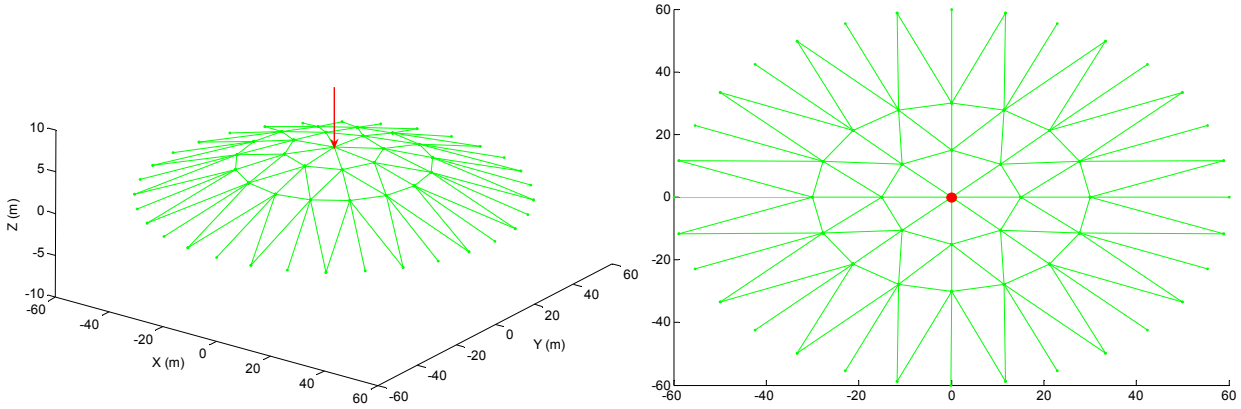

(a) (b)

Figure 3.1 (a) 3D view of the outlook of the dome, and (b) top view of the dome.

The load-deflection curve for the top node is shown in Fig. 3.2. It can be seen that when the tip load is below 2000 lb, as many as six types of deformation exist. When the tip deflection is between 1 m and 2 m, the tip resistance can be one of the three values. All the exact solutions are no longer uniquely decided by the external force or geometric shape. They also depend on the deformation and applied force history.

Different equilibrium states are shown in Fig. 3.3. It can be seen the deformation procedure is more complicated than normal star dome, which has only one snap-back (Geers, 1999). The buckling expanded gradually from the most inner ring to outer rings. The first snap-back happened when the smaller dome buckled. The continual sagging of the small ring caused the second ring to buckle. The most outside ring finally buckles when F= 6171.25 lb.

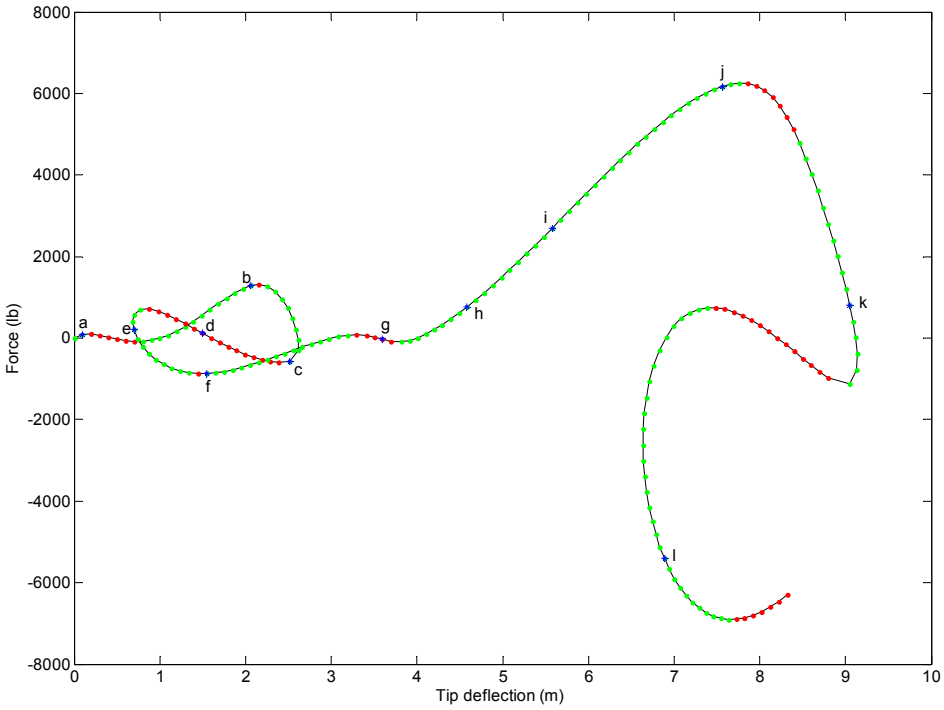

Figure 3.2 Load defection curve of the top node.

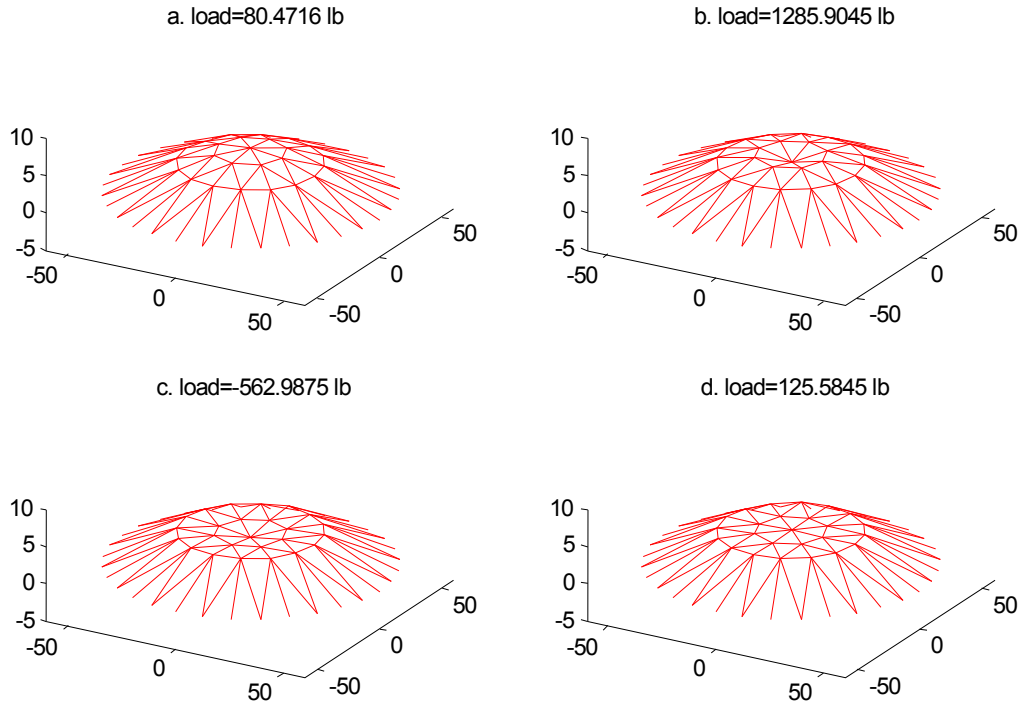

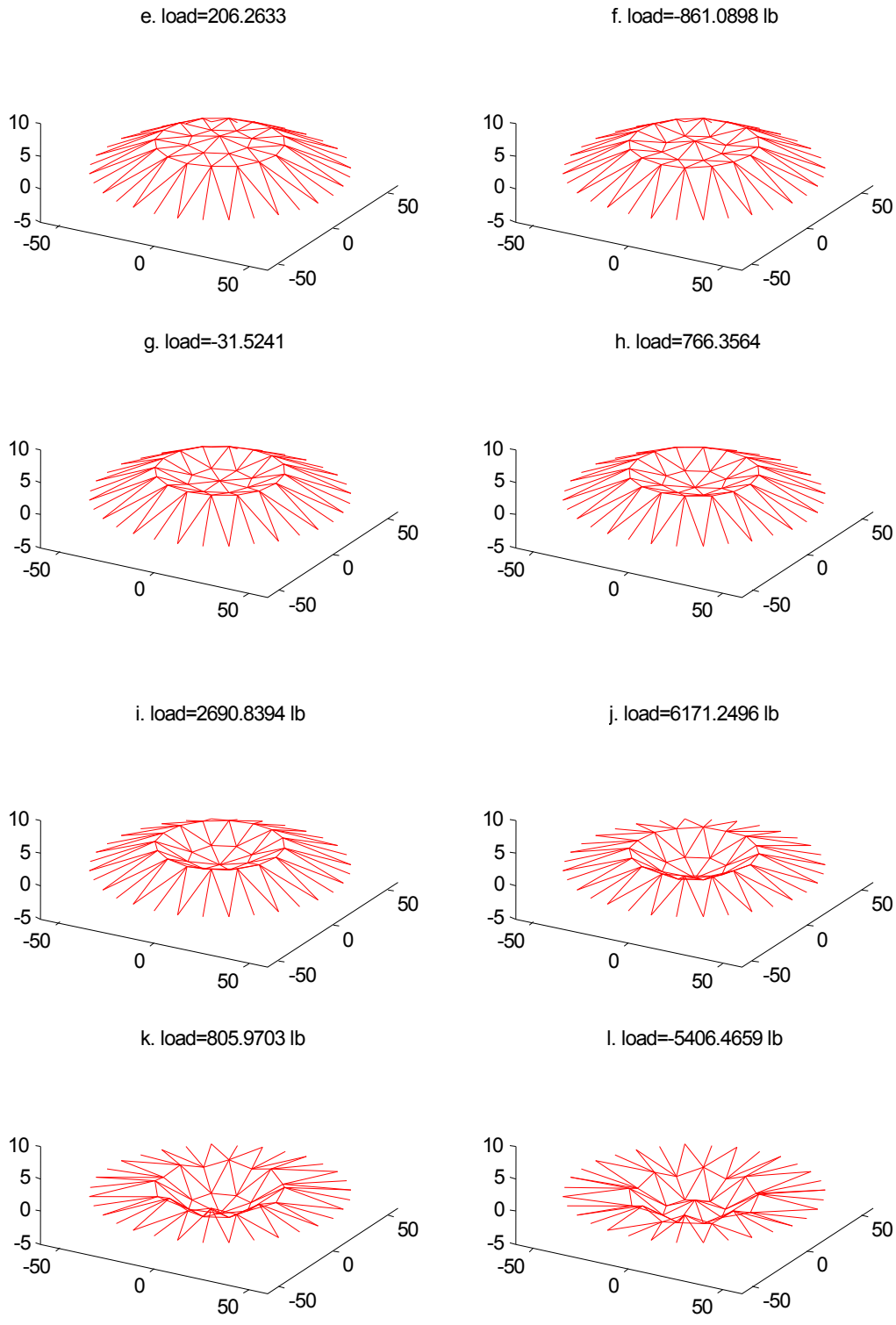

Figure 3.3 Deformation procedures with the adjusted load.

3.2 Nonlinear dynamic behaviors of trusses

Because geometric nonlinearities causes bifurcation and multiple solutions, dynamic deformation of a nonlinear structure is path dependent. Hence, step by step integration is necessary in order to obtain the time history of deformation of structures. To demonstrate the nonlinear effect, one self-standing tower (Fig. 3.4) is selected for the analysis. Both real time history analysis and modal analysis based on linear truss element are conducted.

3.2.1 Direct numerical integration analysis

The tower is composed of aluminum alloy pipes. The trusses at leg location have an outer radius of 0.03m and an inner radius of 0.028m. The braces have smaller cross sections with outer radius of 0.02m and inner radius of 0.01m. Young's modulus is $7\times10^{10}\,pa$ and mass density is $2800\,kg/m^3$. Poisson ratio is 0.29 and no prestress is applied. The tower has four floors and each floor's height is 8m. The base cross section is $2\times2\,m^2$. The four base points are fixed on the ground. The tower is assumed to sustain EI Centro earthquake in the X direction only.

Because the absolute displacement vector $\mathbf{U}$ consists of the relative deflection $\mathbf{u}$ and the rigid body motion $\mathbf{y}_s$, we have

$$\mathbf{U} = \mathbf{u} + \mathbf{y}_s \tag{3.1}$$

Because the tower is only subjected to a base excitation, the governing equation is given by

$$M\cdot\ddot{\mathbf{U}} + C\cdot\dot{\mathbf{U}} + K\cdot\mathbf{U} = 0 \tag{3.2}$$

However, because the rigid-body motion does not induce any elastic energy or

damping, we have

$$M \cdot \ddot{\mathbf{u}} + C \cdot \dot{\mathbf{u}} + K \cdot \mathbf{u} = -M \cdot \ddot{\mathbf{y}}_s \tag{3.3}$$

So the structure response is caused by the inertia force $-M \cdot \ddot{\mathbf{y}}_s$.

The deformations at different time instants are shown in Fig. 3.5. The dash lines represent the undeformed geometry of the tower. The solid lines represent the deformed geometry. The whole deflection history of a node at the tip of the tower is compared with the acceleration history of the ground motion in Fig. 3.6 (a). The increased intensity of acceleration does not induce large deformation immediately because of the time delay caused by wave propagation. It I s found that the maximum deflection of the tip is 0.1281m. Since the damping is neglected here, the oscillation does not die out with the elapse of time. Usually, the modal damping coefficient in civil structure would not excess 5 percent (Biggs, 1964). If the modal damping ratio is 0.03, the deflection would be significantly reduced as shown in Fig. 3.6(b). The maximum deflection becomes 0.0525m.

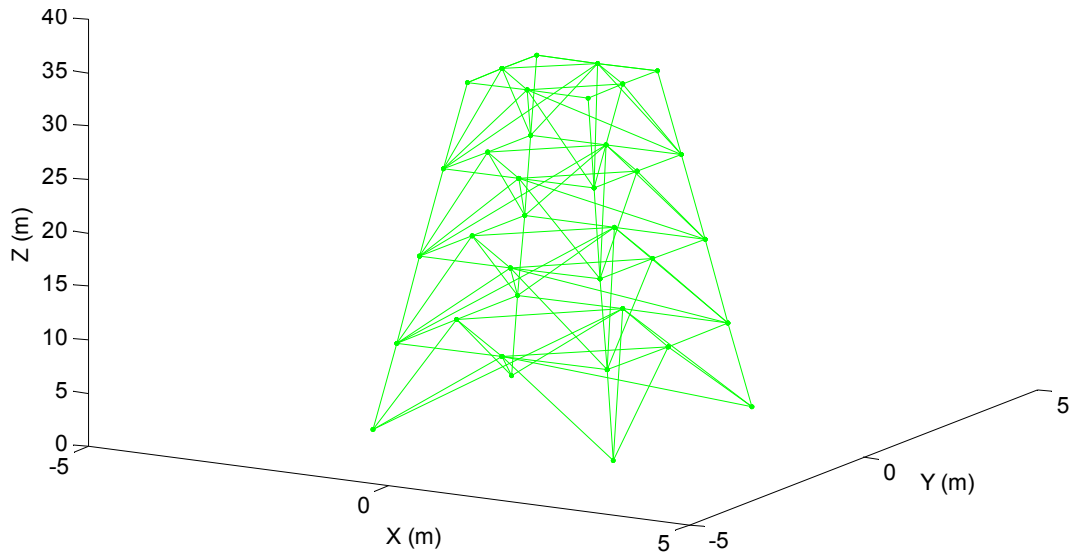

Figure 3.4 Undeformed geometry of the tower.

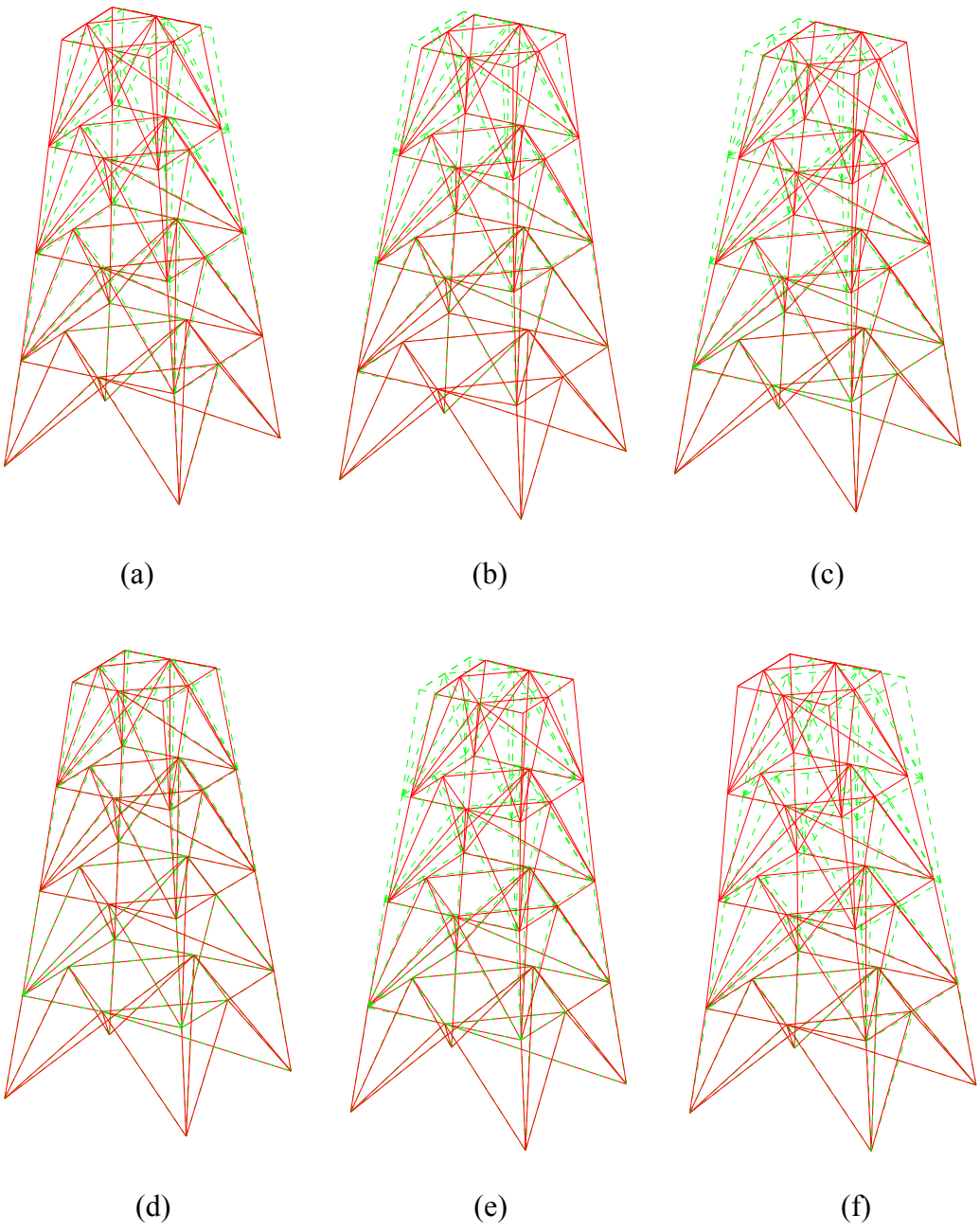

(a) (b) (c)

(d) (e) (f)

Figure 3.5 Tower deformation at different instants: (a) t = 2 sec, (b) t= 3 sec, (c) t = 5 sec, (d) t= 6 sec, (e) t = 8 sec, (f) t= 9 sec.

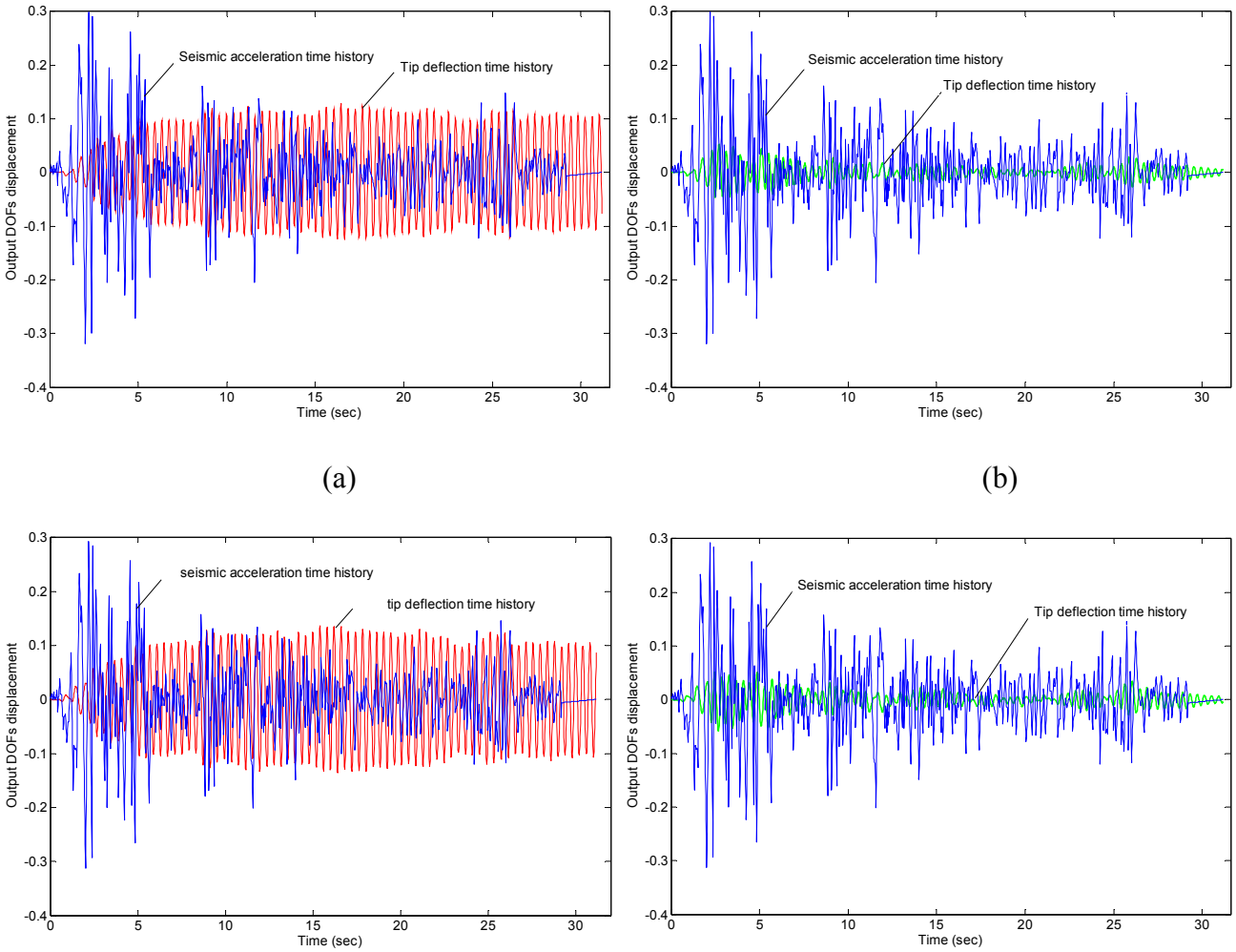

Figure 3.6 Time traces of deflection and ground seismic acceleration: (a) with no damping, (b) with 3% modal damping, (c) with no damping by large lumped stiffness method, and (d) with 3% modal damping by large lumped stiffness method.

An alternative approach to simulate the ground shaking is by adding large lumped stiffness to the base of the tower. Varying force will be applied to the lumped springs to simulate the ground motion. In this way, a displacement controlled problem can be translated to a force controlled problem, which is easier to be solved. The advantage of this approach is that it can simulate the process of wave propagation in the tower, especially very tall towers. Unlike the inertia force method, the seismic

load will be transferred to the top of the tower gradually instead of immediately. The maximum tip deflection for no damping case is 0.1371m, which is slightly higher than the previous result. The maximum tip deflection for 3% modal damping is 0.0591m. The difference is actually negligible for a 32m high tower.

3.2.2 Modal Analysis

For the purpose of comparison of the usual engineering approach, the tower's response is assumed to be linear and SRSS (Square Root of the Sum of the Squares) is employed for the estimation of the deformation of the tower. The response spectrum of a linear elastic SDOF system is obtained from the literature (Chopra, 2000). The first ten mode shapes are shown in Fig. 3.7. The third and sixth modes are torsion modes. The eighth and ninth modes have severe deformations on the top section of the tower. All the other modes are bending modes. In the first ten modes considered, the 2nd mode is along the y direction. Though it is included in the following calculation, it is found that it contributed very little and almost can be neglected because its modal participation factor is $4.6e10^{-3}$ of the 1st mode's. The modal participation factor (Biggs, 1964) can be calculated as

$$\Gamma_n = \frac{\sum_1^r M_r \cdot \phi_{rn}}{\sum_1^r M_r \cdot \phi_{rn}^{\,2}} \tag{3.4}$$

where M_r is the mass of the rth degree of freedom,

ϕ_{rn} is the modal shape component for the rth mass in the nth mode.

The product of the modal participation factor, the specific response from the response spectrum, and the characteristic shape coordinate gives the estimation of the maximum deflection. The maximum tip deflection is 0.0563m, which is almost half of

the result by real time analysis. Although the analysis is done quickly in this way, the accuracy is not good.

Table 3.1 Modal participation factors

Mode	Frequency (hz)	Participation factor
1	2.4916	-461.36
2	2.5562	-0.21237
3	6.5988	-11.35
4	9.0422	-1091.4
5	10.18	-0.45755
6	14.487	-33.617
7	17.216	1100
8	18.337	79.498
9	19.725	-16.732
10	19.777	9.658

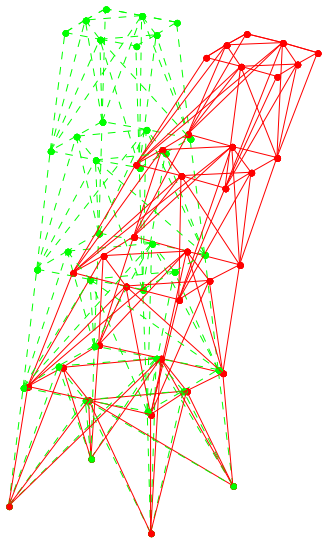

Mode 1

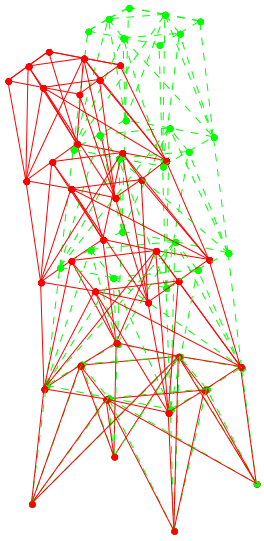

Mode 2

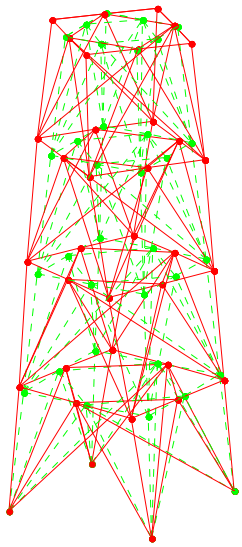

Mode 3

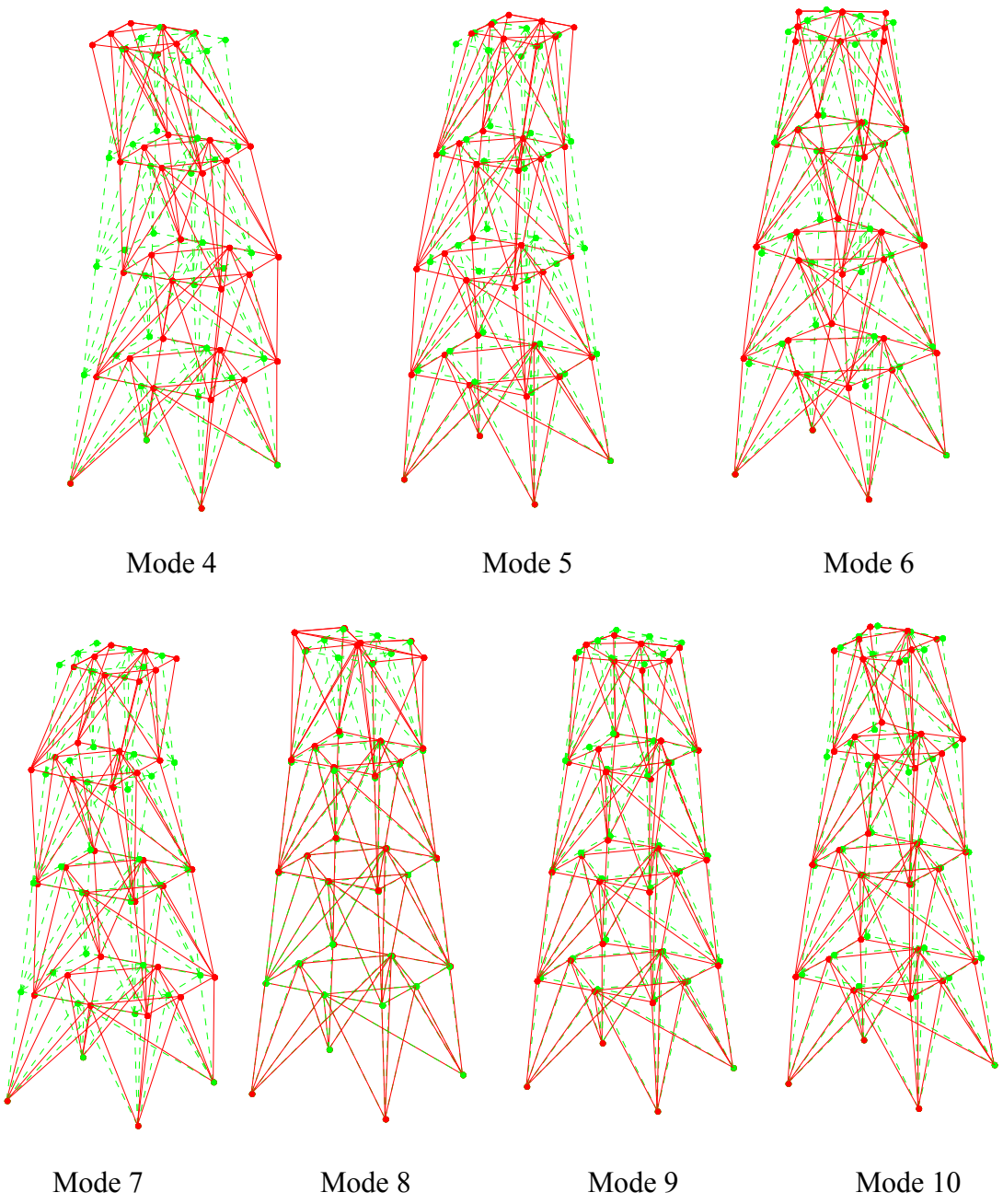

Figure 3.7 First ten mode shapes of the self standing tower.

3.3 Nonlinear static behaviors of cables

Cables are very flexible and behave nonlinearly under static loads. Irvine (1981) has developed analytical methods to analyze the response of cable. In this section, nonlinear FEM is applied to investigate the influence of geometric nonlinearities on

cables. A cable spacing from 600m high to the ground and 800m out under self weight, pretension and ice loading is modeled and the results are compared. The reason to consider ice loading is because it has a significant effect during an ice storm. The radial ice thickness has been reported as high as 8-9 in (Madugula, 2002). Modulus of elasticity for steel cables with a radius greater than $67\,mm$ is $159\,GPa$ (TIA/EIA-222-G.5).

Cables having the same geometric shape but different prestress levels can have very different sagging after installation. The discrepancy between linear and nonlinear model also varies with the prestress level (Fig. 3.8). The linear model can well predict the deformation of cable when the prestress level is higher than e0=0.1. But when the prestress level is as low as 0.001, the linear method can hardly work because the pretension in the cable is comparable to the self weight of the cable (Pai, 2007).

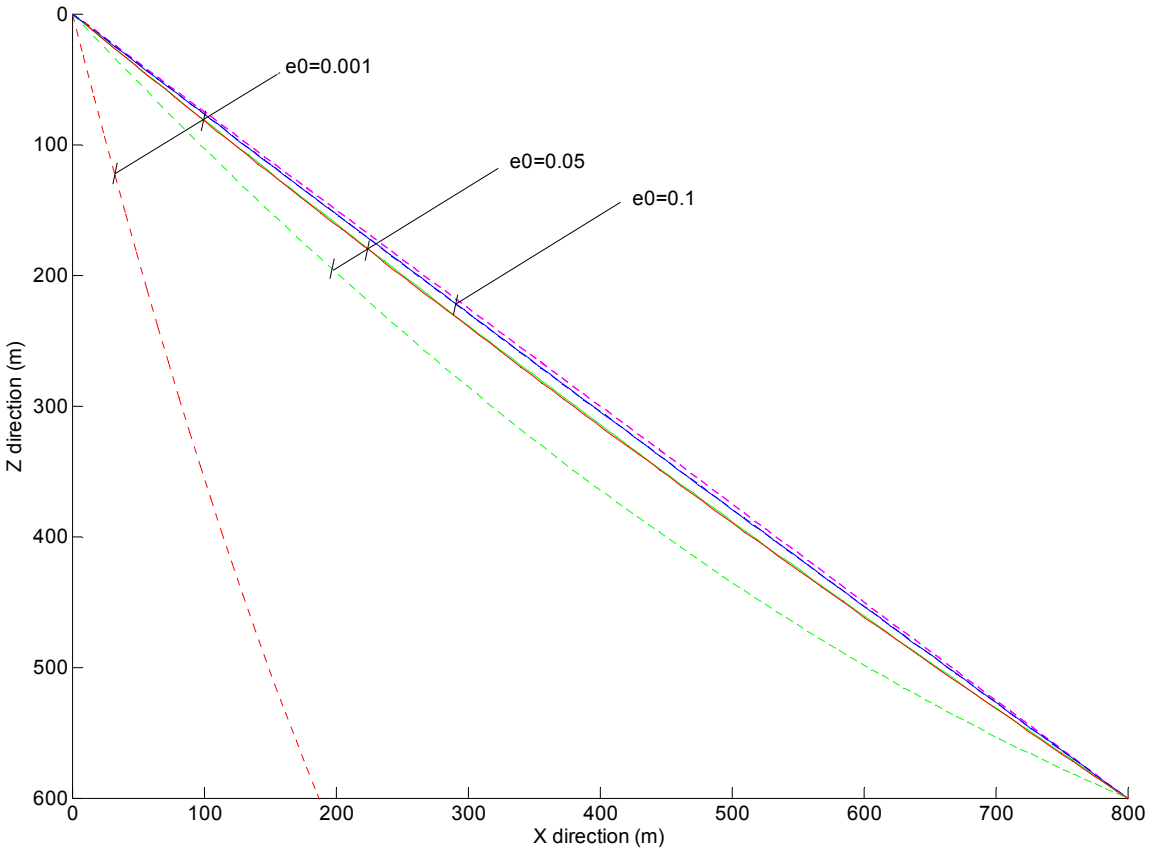

Figure 3.8 Comparison of linear and nonlinear static deformations under different

prestress levels.

Ice loading increases the mid sagging especially for long cables. The mid-point sag for the described cable under 0.001 prestress level is as large as 9.7602m and will be increased to 10.1261m under ice loading. The change of geometric shape under different static loads can be seen in Fig 3.9. With higher prestress level, the sag under self weight and ice loading decrease as shown in Fig. 3.9. When the prestress level is between 0.07 and 0.15 as specified in TIA/EIA-222-G.5 (2006), the maximum sag is less than 5.1054m under self weight and 5.5498m under the combination of self weight and ice loading. But no matter how high the prestress level is, the sag of long cables is inevitable.

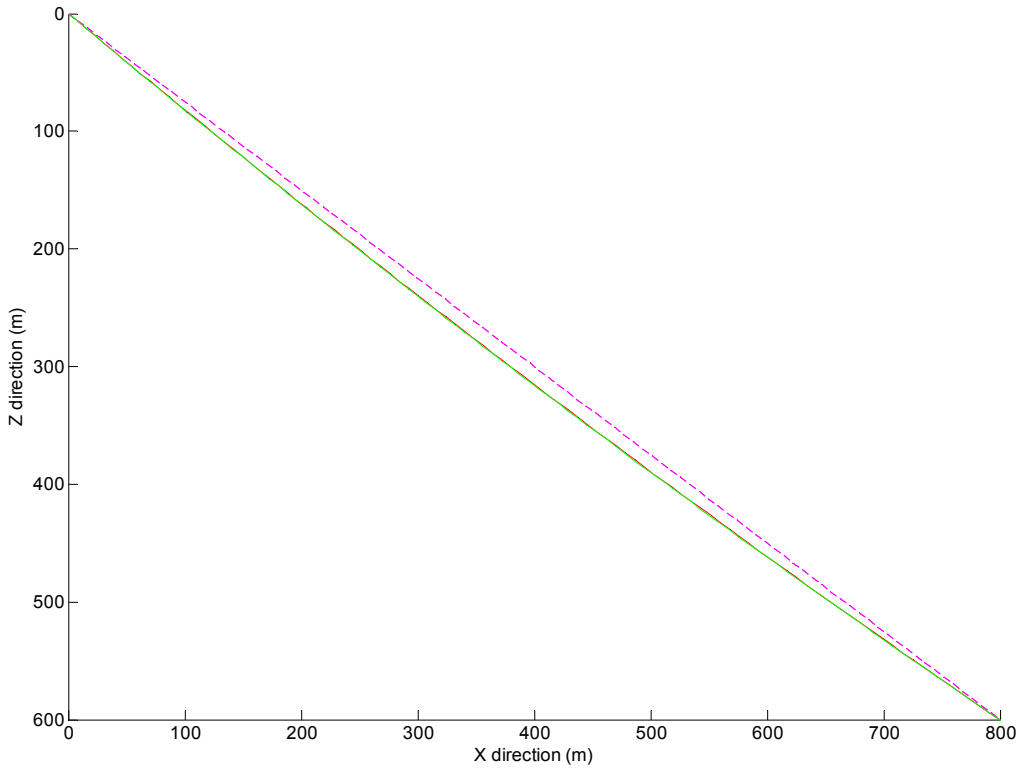

Figure 3.9 Deformation change w/o ice loading for e0=0.001.

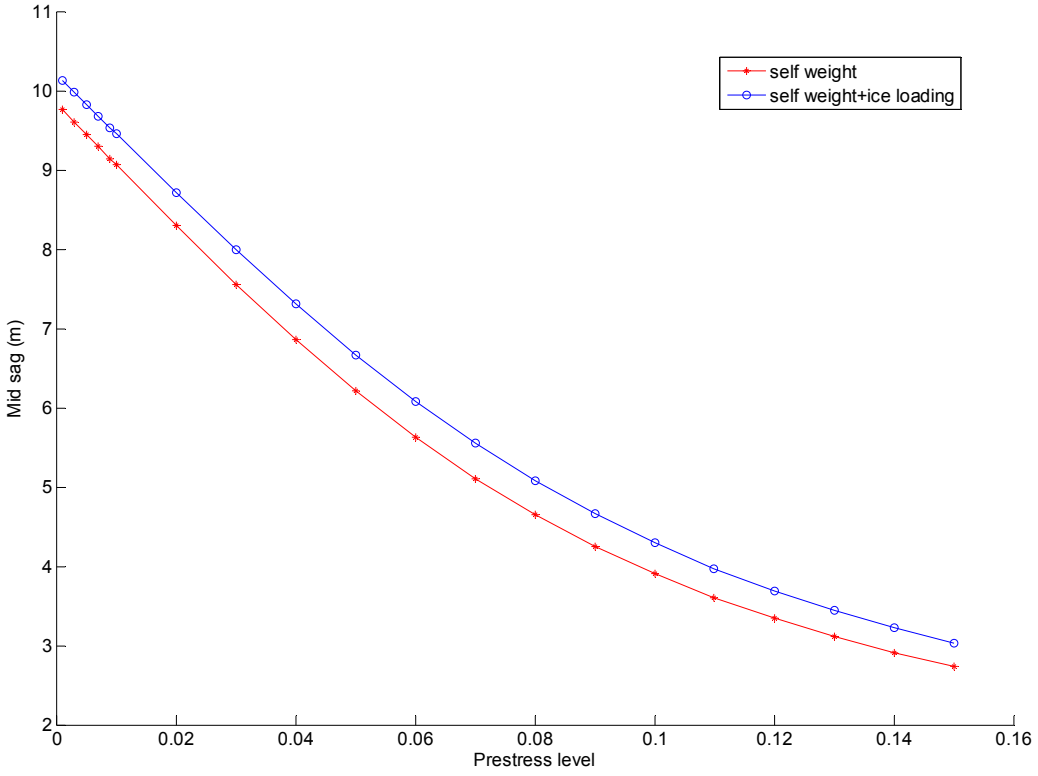

Figure 3.10 Mid sag under different prestress level.

The influence of ice loading varies with different prestress levels (Fig. 3.11). When prestress level increases from 0.001, the increase of mid sag due to ice loading increases as well. The maximum increase (0.4571m) appears at 0.05 prestress level, after which the sag increase will gradually diminish. The minimum sag increase is 0.2952m for 0.15 prestress level. Compared to the length of the cable, such sag increase is almost negligible.

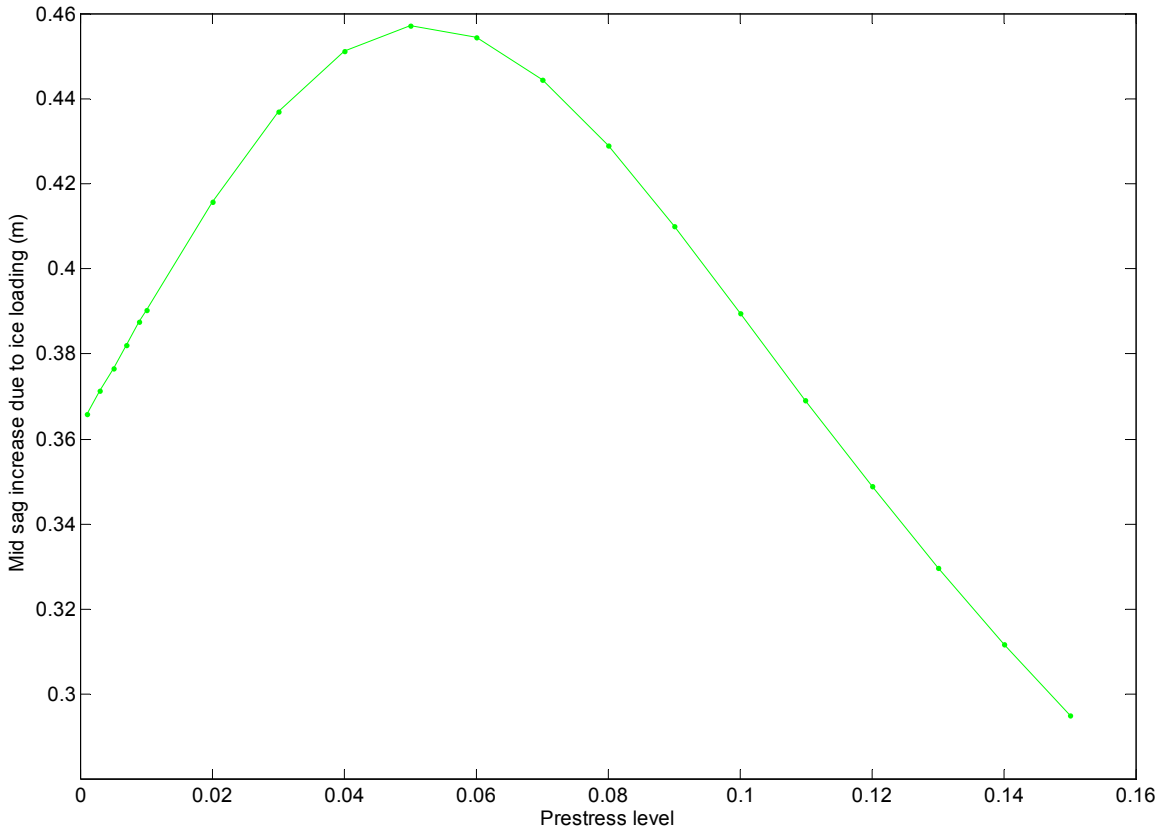

Figure 3.11 Mid sag increase at different prestress level.

3.4 Nonlinear dynamic behaviors of cables

Dynamic behaviors of cables are hard to predict with linear analysis. Since wind load is very common and sometimes critical to cables of guyed towers, a simplified model for a cable subject to varying wind loads is built and analyzed.

For wind loads on towers, there are several methods to evaluate them as introduced in the literature (Madugula, 2002). The second-order auto-regressive process is recommended for a time-varying structural analysis. However, the minimum time interval from this approach is 0.1s, which exceeds the accuracy limit of a nonlinear dynamic analysis. To simplify the analysis, the wind velocity is assumed to be the superimposition of constant velocity plus a sinusoidal velocity as proposed by Nabil (1993). By further referring to CSA (2001), the wind load hereby

applied is assumed as

$$W = W_c + W_r \cdot \sin \omega t \tag{3.5}$$

Where $W_c = P(C_d \cdot A_r)$

P = wind pressure, minimum is 300 Pa

$C_d = 1.2$ for guys

A_r = face area of guys

W_r = the magnitude of random wind load

ω = vibration frequency

Apparently, the vibration frequency has great impact on response of the cable. If it is close to the natural frequency of the cable, resonance can occur if there is no damping and the oscillation would be greatly amplified.

To explore the dynamic response of cables, one specific case is analyzed. The wind load is applied after the post- tension of the cable. So the wind load would be added to a sagged curve. The wind direction is assumed to be perpendicular to the plane of the cable. The wind pressure is assumed to be 300Pa. The diameter of the cable is 2 in. The prestress level is 0.01. The vibration frequency is taken to be the third modal frequency of the cable, which is 0.1435 Hz. The geometric prestressed shape under self weight is computed for the initial stiffness consideration. The first mode is shown as the red dotted line Fig 3.12. The 3D view of vibration shapes is shown in Fig 3.13. If viewed from the top, the vibration shapes clearly reveal the third mode.

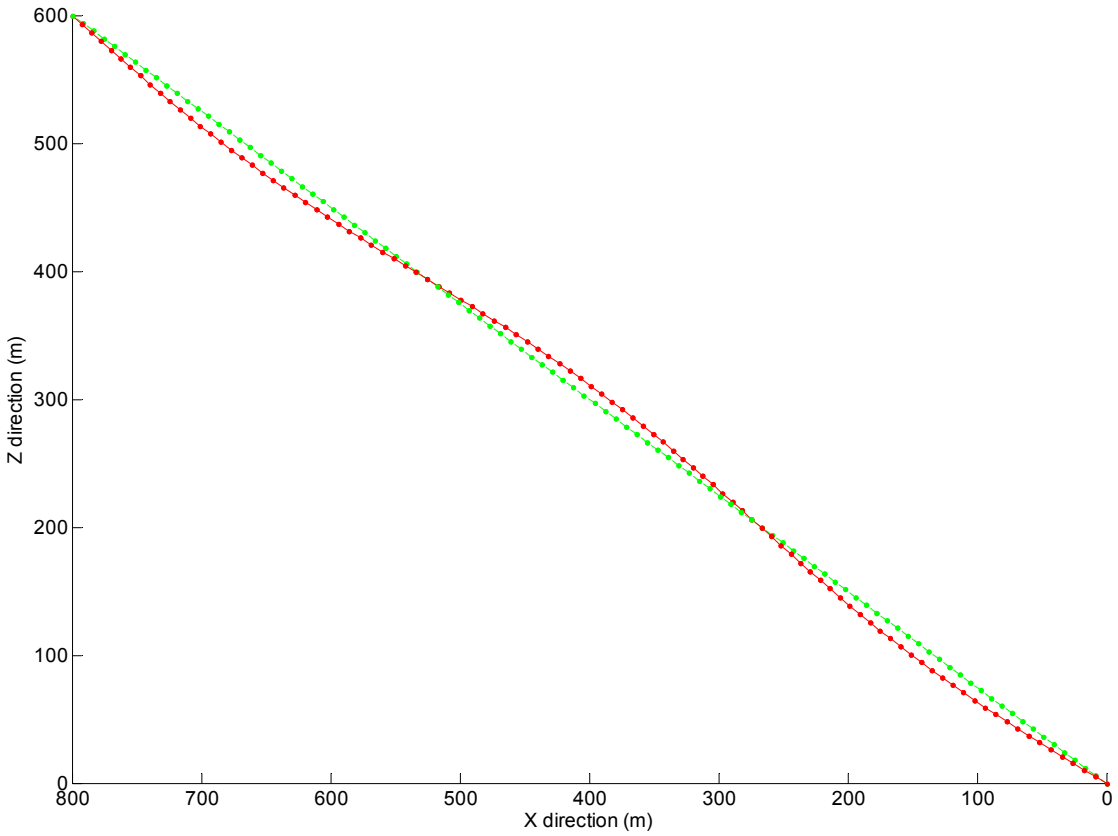

Figure 3.12 Third mode of 0.01 prestressed cable.

Figure 3.13 3D view of vibration shapes.

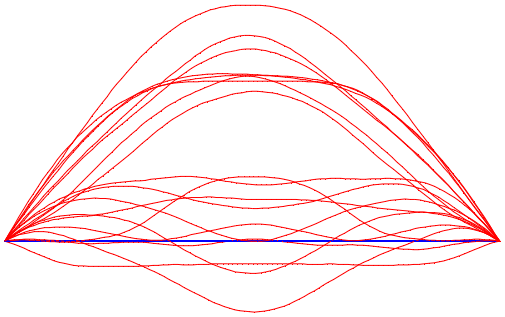

Figure 3.14 Top view of vibration shapes.

Fig. 3.15 reveals part of the vibration procedures. The time traces of the mid-points in Z and Y direction can be seen in Fig. 3.16 and Fig. 3.17. The vibration in the Y direction is more intensive than in the Z direction because the input wind load is in the Y direction.

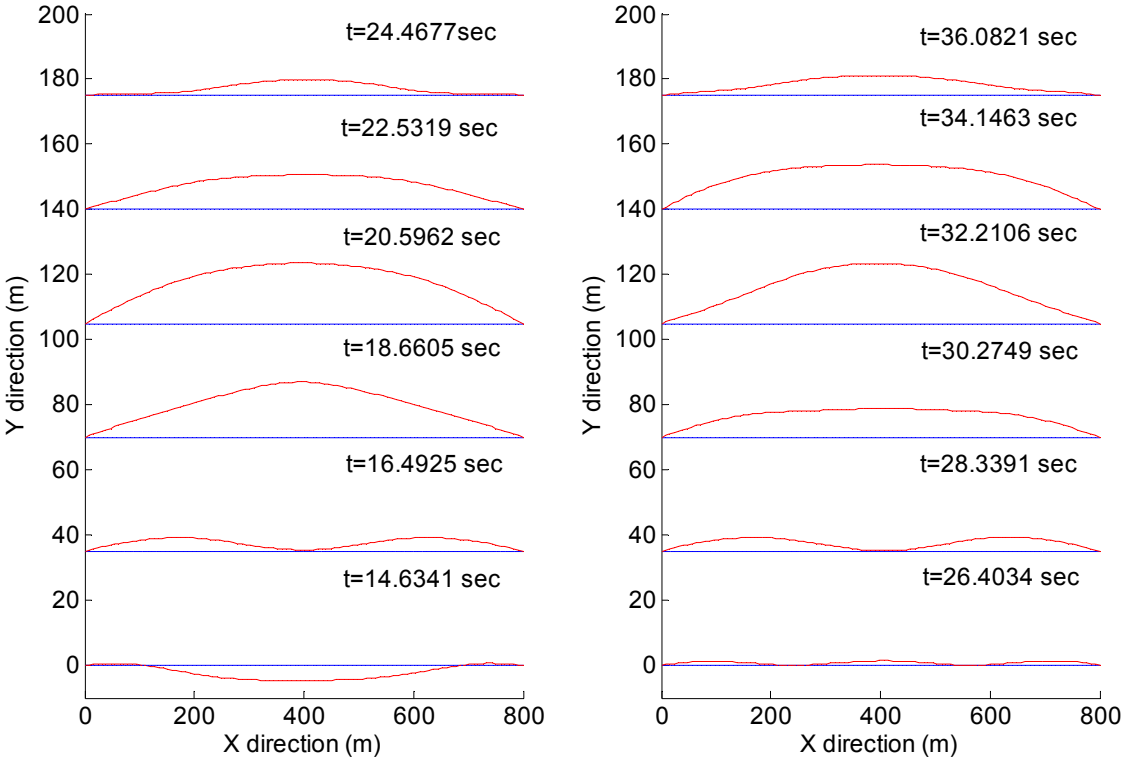

Figure 3.15 Top views of deflection shapes at different instants.

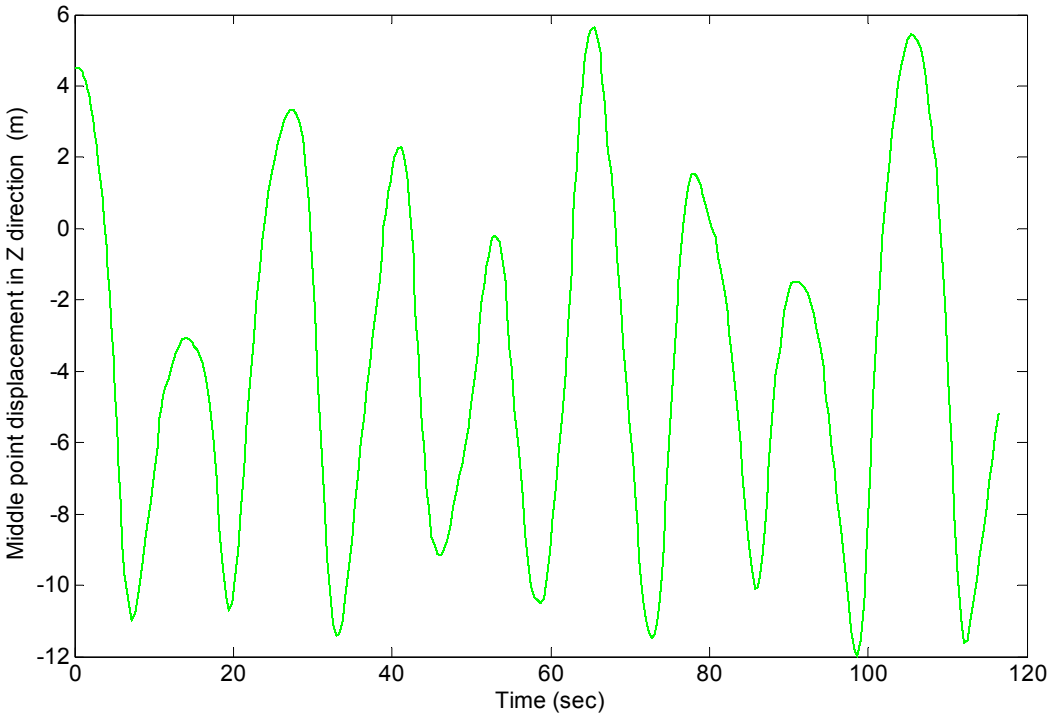

Figure 3.16 Time trace of defection of the middle point in the Z direction.

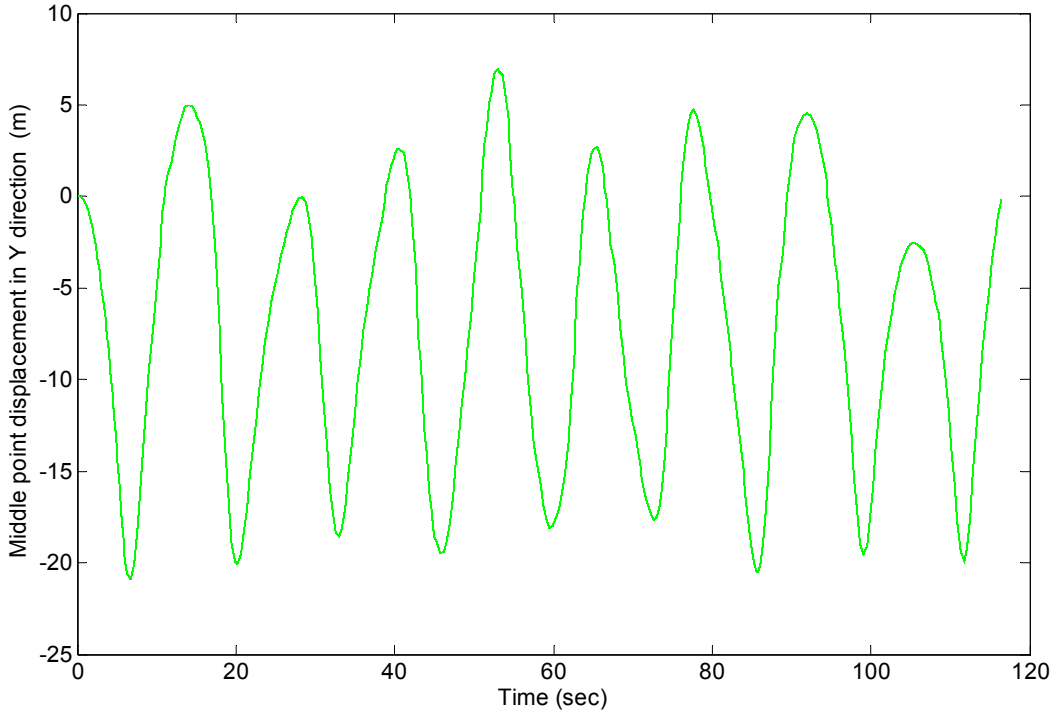

Figure 3.17 Time trace of defection of the middle point in the Y direction.

3.5 Nonlinear static behaviors of beams

To demonstrate the nonlinear behaviors of beam elements, a detailed example is examined. If an aluminum beam is clamped on the left end and imposed a constant end moment at the right side. The dimension of cross section (0.03m by 0.03m) is very small compared to the span (0.6m).

The linear solution for the deflection can be derived fromthe curvature and boundary conditions. From the linear beam theory,

$$y''(x) = \frac{M}{EI} \tag{3.6}$$

$y(0) = y'(0) = 0$ and M is constant. Hence

$$y(x) = \frac{M}{EI}\frac{x^2}{2} \tag{3.7}$$

The nonlinear solution can be obtained by the application of beam elements with

von karman nonlinearity. Suppose the end moment is $\frac{2\pi}{10}\frac{EI}{L}$, the deformed geometry of the beam is as shown in Fig 3.18. From the comparison, it can be seen that the linear beam theory neglects the influence of axial stretch, which make the beam stiffer. And the difference of the tip deflection of the beam is significant.

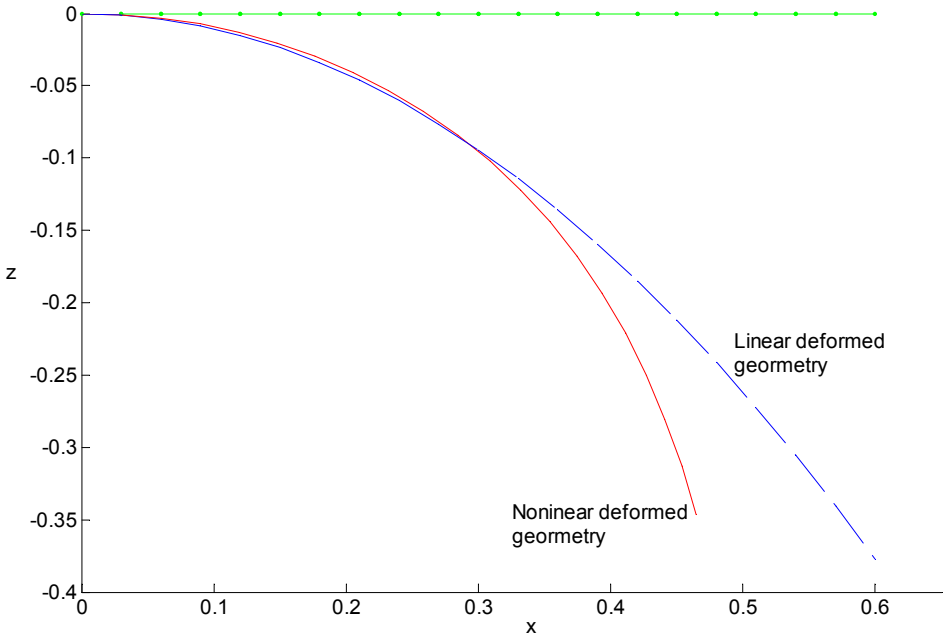

Figure 3.18 Comparison of deformed geometry of the beam.

Fig 3.19 further illustrates the influence of geometric nonlinearity. When the end moment is small, there is no difference between the linear case and the nonlinear one. With the increasing magnitude of external load, the nonlinear beam first becomes softer and then becomes stiffer when the load further increases. Thus geometric nonlinearity can not be neglected when the deflection is significant.

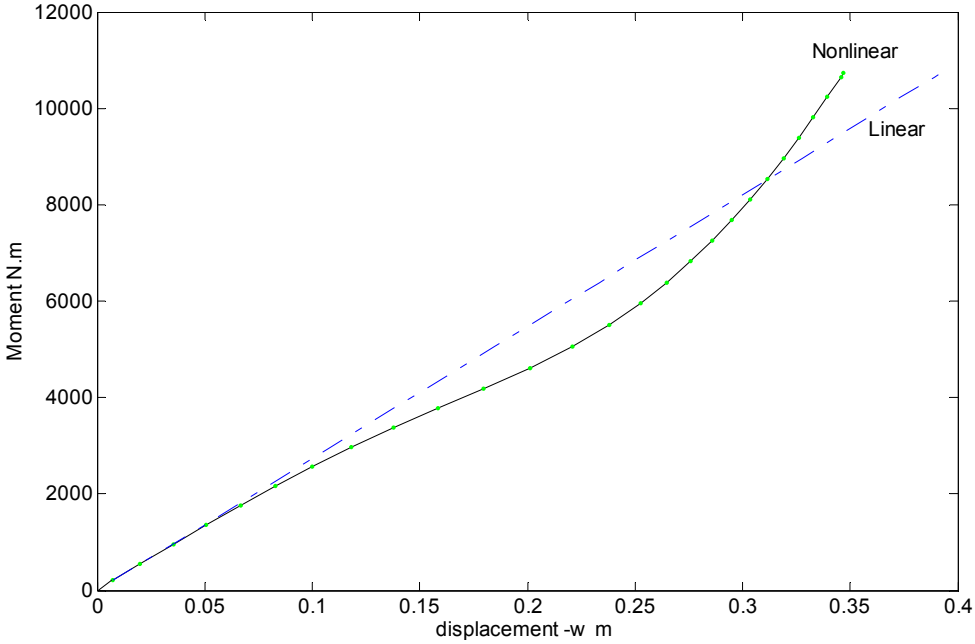

Figure 3.19 Comparison of load-deflection of the beam under increasing loads.

3.6 Nonlinear dynamic behaviors of beams

To capture the dynamic behavior of beams, two approaches are usually applied. The first one is the direct numerical integration and the second one is modal analysis. The following will conduct both analyses to gain a better understanding about the difference of these methodologies.

A meter long Aluminum (6061-T6) cantilevered beam is clamped at the left end and free on the right end. The depth of the beam is 2mm and the width is 3cm. The base is excited with a sinusoidal displacement with amplitude of 2mm and a frequency of 10.2753 Hz, which is exactly the second modal frequency. The base shaking velocity is 0.0206 m/s. The modal damping ratio is assumed to be 0.01. The dynamic response of the beam will be analyzed using the direct numerical integration and the modal analysis method.

3.6.1 Direct numerical integration analysis

The deflection shapes at different time instants are shown in Fig 3.20. It clearly reveals that the second mode dominates the response. The right tip deflection history is as shown in Fig 3.21.

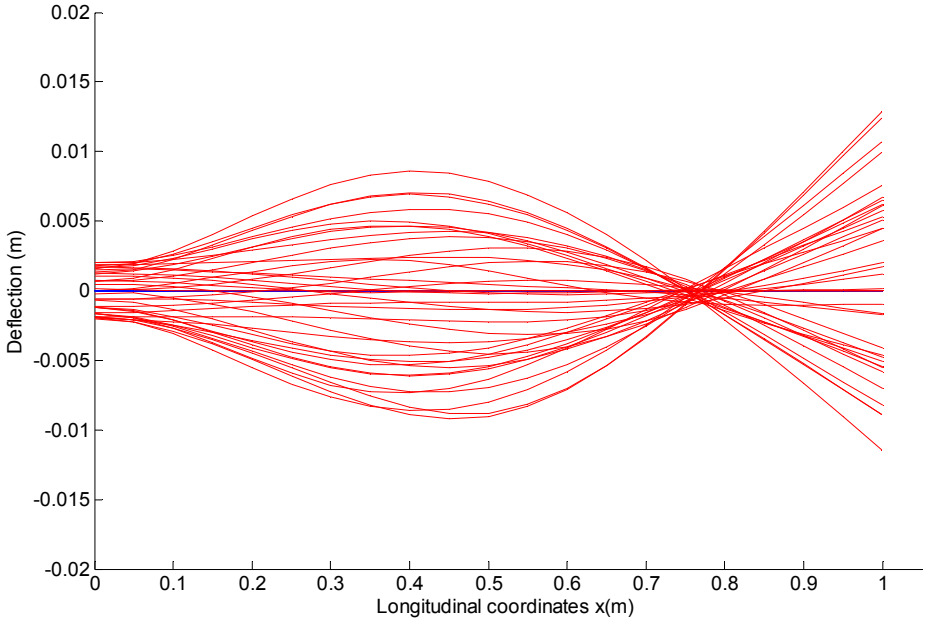

Figure 3.20 Deflection shapes at different time instants.

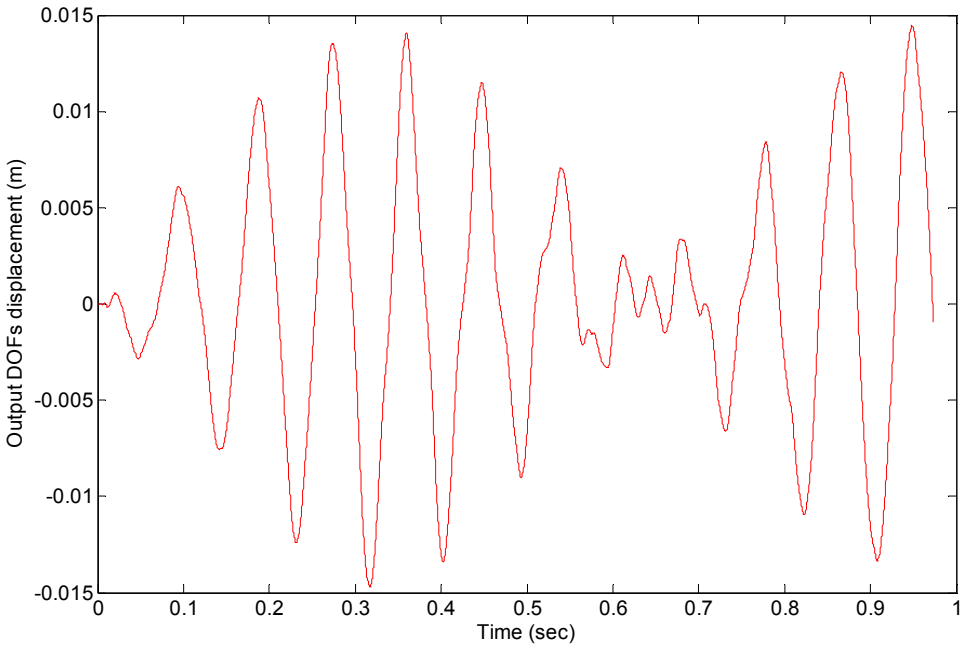

Figure 3.21 Time trace of the right tip.

It is also found that the velocity of base shaking greatly affect the response.

3.6.2 Modal analysis

The governing equation for the Euler-Bernouli beam (Pai, 2007) is

$$mw_{tt} + cw_t + EIw_{xxxx} = 0 \tag{3.8}$$

where m is the mass per unit length; w is the transverse displacement; c is the damping coefficient; E is Young's modulus; I is the moments of inertia; t is the time and x is the spatial coordinator along the beam. Because the highest order of special derivatives of w is four, four corresponding boundary conditions are needed, which are $w\big|_{x=0,t} = b\sin(\Omega t)$, $w_x\big|_{x=0,t} = 0$, $EIw_{xx}\big|_{x=L,t} = 0$, and $EIw_{xxx}\big|_{x=0,t} = 0$ for a clamped-free beam. Two initial conditions are set as $w\big|_{x,t=0} = 0$ and $w_t\big|_{x,t=0} = 0$.

Assume $w = W + b\sin(\Omega t)$, the boundary conditions are changed into $W\big|_{x=0,t} = 0$; $W_x\big|_{x=0,t} = 0$; $EIW_{xx}\big|_{x=L,t} = 0$ and $EIW_{xxx}\big|_{x=0,t} = 0$. And the initial conditions are changed to $W\big|_{x,t=0} = 0$ and $W_t\big|_{x,t=0} = -b\Omega$.

Assume the solution can be expressed as the product of a spatial function and a time function as $w(x,t) = X(x)\cdot T(t) + b\sin(\Omega t)$, the governing equation can be transformed into

$$mX(x)T_{tt}(t) + cX(x)T_t(t) + EIX_{xxxx}(x)T(t) = mb\Omega^2\sin(\Omega t) - cb\Omega\cos(\Omega t) \cong mb\Omega^2\sin(\Omega t) \tag{3.9}$$

To solve Eq. (3.9), first the homogeneous equation needs to be solved.

$$\frac{T_{tt}(t)}{T(t)} + \frac{c}{m}\frac{T_t(t)}{T(t)} + \frac{EI}{m}\frac{X_{xxxx}(x)}{X(x)} = 0 \tag{3.10}$$

This equation can be separated into two equations as

$$\therefore \frac{EI}{m}\frac{X_{xxxx}(x)}{X(x)} = \omega^2 \quad \text{and} \quad \frac{T_{tt}(t)}{T(t)} + \frac{c}{m}\frac{T_t(t)}{T(t)} = -\omega^2$$

The solution of the first one (Inman, 2001) is

$$X(x) = \frac{1}{\sqrt{mL}}\left[\cosh\beta_n x - \cos\beta_n x - \sigma_n\left(\sinh\beta_n x - \sin\beta_n x\right)\right] \tag{3.11}$$

where $\beta_n L =$ 1.87510407, 4.69409113, 7.85475744, 10.99554073, 14.13716839, for $n = 1\ldots5$, $\frac{2n-1}{2}\pi$ for $n > 5$, and $\sigma_n = \frac{\sinh\beta_n L - \sin\beta_n L}{\cosh\beta_n L + \cos\beta_n L}$.

Because of the orthogonality of the mode shapes, $\int_0^L \mathbf{X}(x)m\mathbf{X}(x)dx = [\mathbf{I}]$. Apply the integration at both sides of the governing equation to obtain

$$\int_0^L \mathbf{X}(x)\left(mX(x)T_{tt}(t) + cX(x)T_t(t) + EIX_{xxxx}(x)T(t)\right)dx = \int_0^L \mathbf{X}(x)\left(mb\Omega^2\sin(\Omega t)\right)dx$$

$$T_{tt}(t) + 2\zeta\omega T_t(t) + \omega^2 T(t) = \int_0^L \mathbf{X}(x)dx \cdot mb\Omega^2\sin(\Omega t) = F_0\sin(\Omega t)$$

The initial conditions are changed into $T(0) = 0$ and $T_t(0) = \int_0^L \mathbf{X}(x)dx \cdot (-bm\Omega)$

The solution is

$$T(t) = Ae^{-\zeta\omega t}\sin(\omega_d t + \phi) + A_0\sin(\Omega t - \phi_0) \tag{3.12}$$

where $A_0 = \frac{F_0}{\sqrt{\left(\omega^2 - \Omega^2\right)^2 + (2\zeta\omega\Omega)^2}}$, $\phi_0 = \tan^{-1}\frac{2\zeta\omega\Omega}{\omega^2 - \Omega^2}$,

$$A = \frac{\sqrt{\omega_d{}^2\left(T(0) + A_0\sin\phi_0\right)^2 + \left(T_t(0) + \zeta\omega\left(T(0) + A_0\sin\phi_0\right) - \Omega A_0\cos\phi_0\right)^2}}{\omega_d}$$

$$\phi = \tan^{-1}\frac{\omega_d\left(T(0) + A_0\sin\phi_0\right)}{T_t(0) + \zeta\omega\left(T(0) + A_0\sin\phi_0\right) - \Omega A_0\cos\phi_0}, \quad \omega_d = \omega\sqrt{1-\zeta^2}$$

The modal participation in the vibration can be seen in Fig 3.22. The second mode composes the major part and increases its weight with the time. The first mode also has a constant contribution in the response. All other modes actually have nearly

no contribution to the response. Time traces of specific points on the beam are plotted in Fig 3.23. Except at the constrained base, the amplitude of vibration amplifies gradually. The fully excited deflection is clearly revealed in Fig 3.24, which has the characteristic of the second mode shape. Compared with the nonlinear analysis, the linear analysis requires much less computational effort. But it can not discover the effect of base shaking velocity. For increased shaking amplitude, the linear analysis will simply amplify the response by the increased factor, which is actually not true.

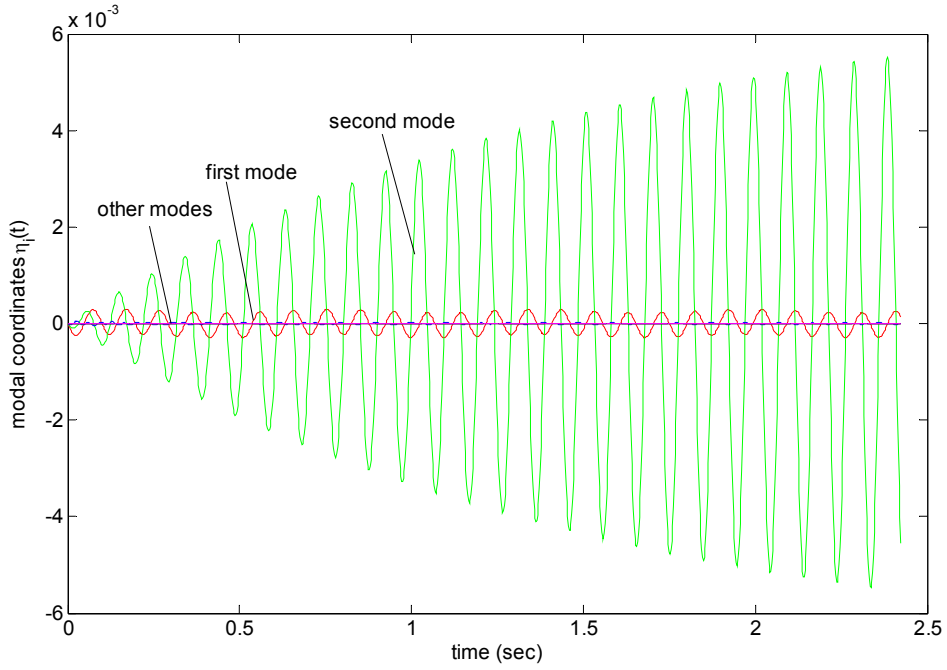

Figure 3.22 Modal coordinates for all the participated modes.

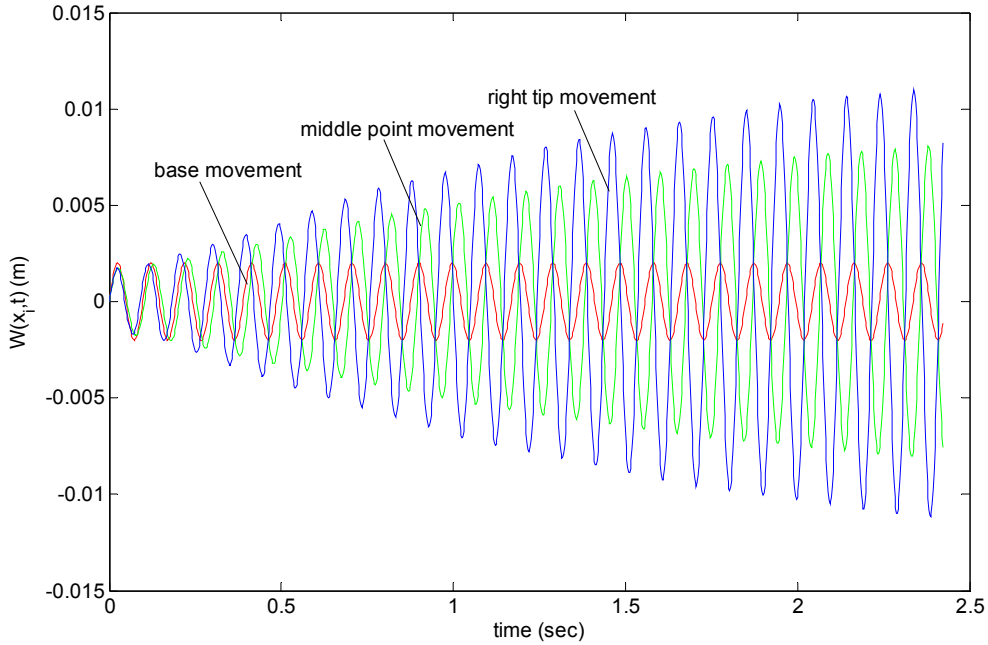

Figure 3.23 Time trace of deflection of base, middle point and tip.

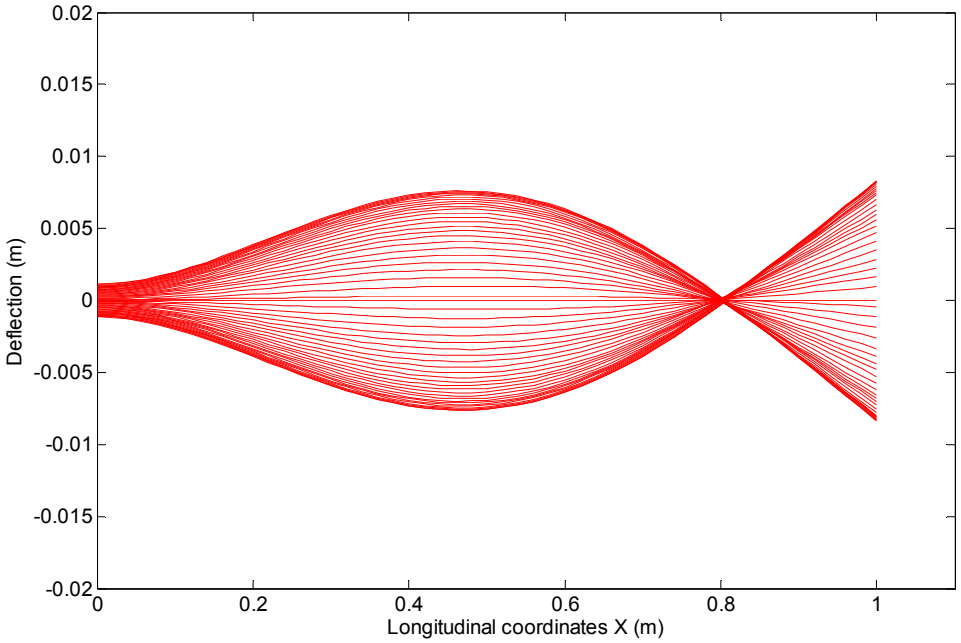

Figure 3.24 Deflection at different instants.

3.7 Summary

This chapter investigates the influences of geometrical nonlinearity on truss, cable and beam elements. Various examples were used to demonstrate the influence.

It can be seen that the nonlinear truss element can be used to track the post buckling response of truss domes. The comparison of linear modal analysis and direct numerical integration for truss towers subject to the EI Centro earthquake excitation showed that the results of direct numerical integration almost double the results from linear modal analysis. It is also found that two different dynamic simulation approaches (direct application of inertia force and large additional spring stiffness) actually produce similar results.

The static analysis of cables under self weight and ice loading with different prestress levels confirms that linear analysis can only predict the sag of heavily prestressed cables. The influence of ice loading on cables is almost negligible. Using the Newmark Beta iterative algorithm, the nonlinear response of cables in the wind can be well predicted. When the wind frequency matches with a modal frequency, the cable will vibrate with the specific mode shape.

For beam elements, nonlinear static analysis deviates from linear analysis when deflection is high. The modal analysis of beam vibration agrees with direct numerical integration to some extent. But in modal analysis the vibration amplitude keep increasing with time, which is inconsistent with the nonlinear analysis result.

Chapter 4 Material Nonlinearity Analysis

Material nonlinearity has significant effect on structural response. Without consideration of inelasticity, the material will stay infinitely elastic, which does not represent actual material behavior. Thus, in order to better simulate the real response, isotropic and dynamic hardening are implemented in the analysis. For cycling loads, dynamic hardening is more appropriate than isotropic hardening, because the latter will keep hardening until it eventually responds elastically. Based on the algorithm by other researchers (Bhatti, 2006; Reddy, 2004), the following procedure will be implemented to analyze the inelastic response.

4.1 Isotropic hardening in truss

First, the stress and strain of each step will be computed. If it is in the elastic range, the original procedure can be adopted without any modification. But once the material enters the inelastic range, the element tangent stiffness must be adjusted with the changed material modulus. If truss elements are under consideration, the governing equation is

$$[k]\{u\} = \sigma Al\{\phi\} \tag{4.1}$$

where σ is the stress in the element. The tangent stiffness matrix is modified in the same manner as

$$\begin{aligned}[\breve{k}] &= \frac{\partial([k]\{u\})}{\partial\{u\}} \\ &= \frac{\partial\sigma}{\partial\{u\}} EAl\{\phi\} + \sigma Al\frac{\partial\{\phi\}}{\partial\{u\}}\end{aligned} \tag{4.2}$$

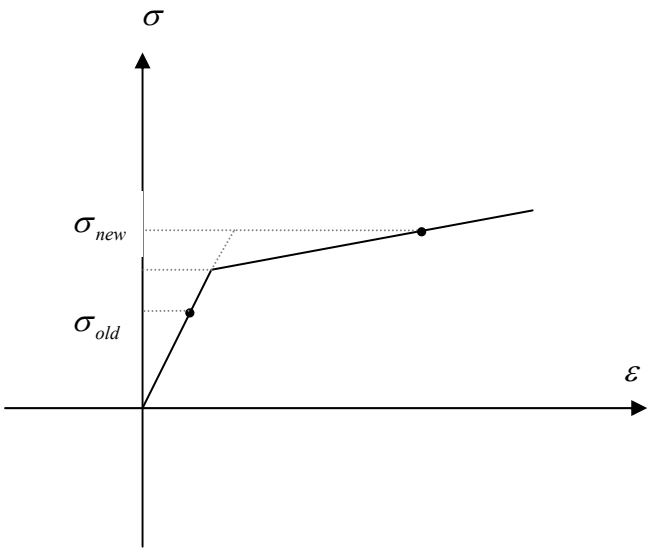

Figure 4.1 Elastic-to-plastic transition.

Because the stress is a function of strain, it can be expressed as

$$\sigma = \sigma_0 + ER\varepsilon + E_t(1-R)\varepsilon \tag{4.3}$$

where σ_0 is stress for previous step, E is Young's modulus, R is a factor that can be determined from Fig.4.1, ε is the current strain, and E_t is tangent modulus . It is found that R=1 for elastic state and R=0 for plastic state. Hence, we have

$$\begin{aligned}\frac{\partial\sigma}{\partial\{u\}} &= ER\frac{\partial\varepsilon}{\partial\{u\}} + E_t(1-R)\frac{\partial\varepsilon}{\partial\{u\}} \\ &= \left(ER + E_t(1-R)\right)\{\phi\}\end{aligned} \tag{4.4}$$

The status of each element (elastic or yielded) should be updated during iterations as well. The detailed procedure is given in Fig 4.2.

To illustrate the influence of inelasticity, a three-bar truss is analyzed. The material is Aluminum Alloy 6061 T6. Young's modulus is $E = 10.6\times10^6$ psi and the plastic modulus is assumed to be one tenth of the elastic modulus $E_t = 1.06\times10^6$ psi. The yield stress Y is 40×10^3 psi. The geometry is shown in Fig 4.3. For the detailed geometrically nonlinear analysis readers are referred to chapter 4 of Pai

(2007).

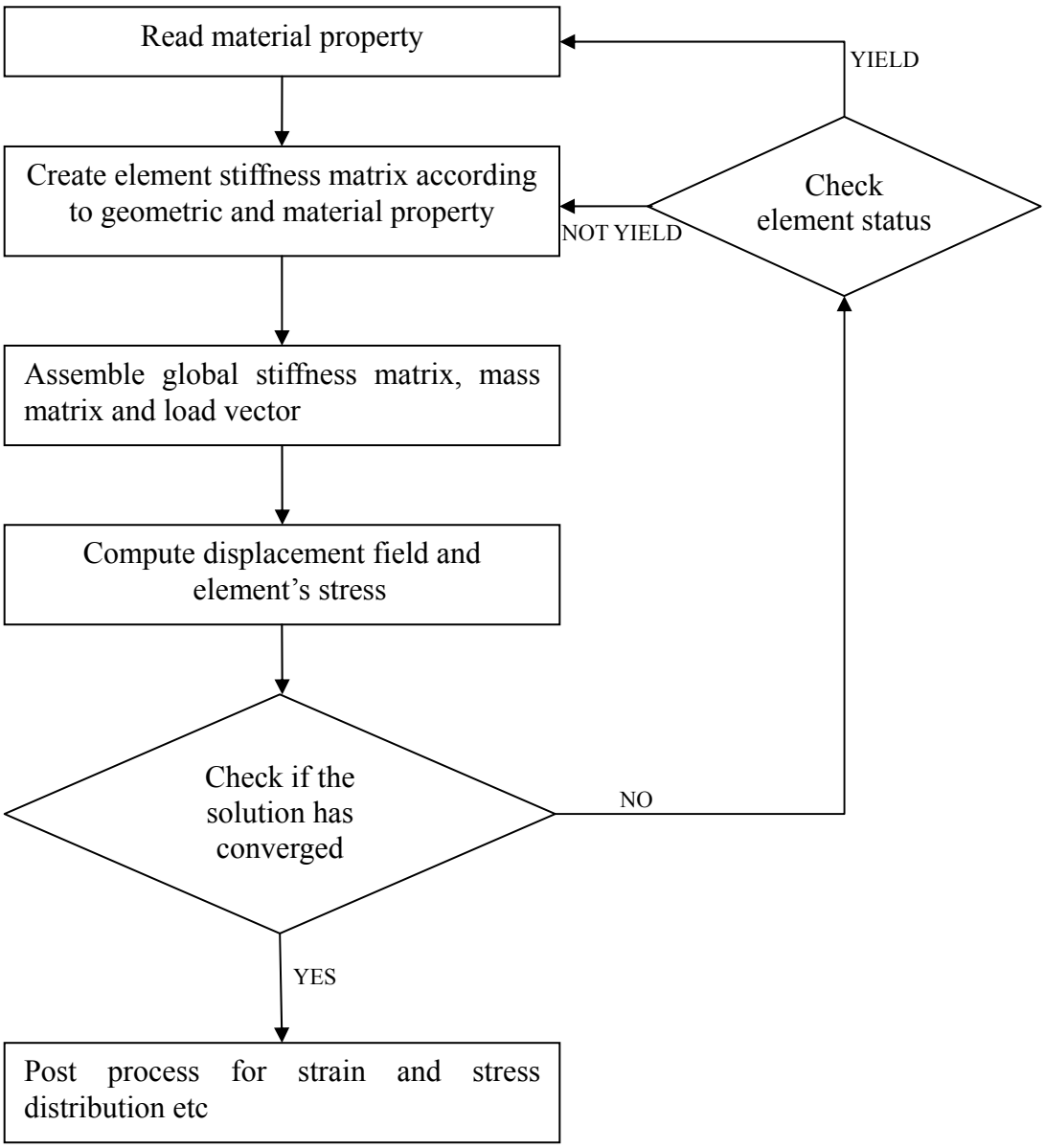

Figure 4.2 Flow chart for material nonlinearity iteration.

Once material nonlinearity is included in the analysis, it is found that resistance of the truss has significantly dropped. There are two turning points in the curve, each of them indicate the beginning of hardening. After the first turning point, the slope of the load deflection curve is greatly decreased. This is because the modulus of material has been dropped from elastic E to inelastic Et. The second turning point marks the beginning of isotropic hardening in tension. Without the set of ductility of the material,

the curve can go up forever. The snap-through phenomena still exists (Fig 4.4).

Theoretical solution for a inelastic load deflection curve is derived as follows. Assume the vertical deflection is x and the unreformed length of each truss member is L, the strain in each truss member can be obtained as

$$\varepsilon = \frac{\sqrt{(h-x)^2 + l^2}}{L}$$

When the strain is greater than $\frac{Y}{E}$, where Y is the initial yielding stress, it entered the inelastic hardening zone. The tangent stiffness has been changed to $Et = \frac{E \cdot H}{E + H}$, where H is the plastic modulus. If the strain stopped increasing, that means it began the unloading. The modulus is resumed to be E. After the opposite strain reaches the amplified yield strain, it will begin another round of hardening.

The stress strain curve is shown in Fig 4.5. The Geometric and Material Nonlinear Analysis (GMNA) result is exactly the same as the theoretical results. The loading zone can be categorized as elastic and plastic parts. But the unloading is always elastic. The load capacity comparison is shown in Fig 4.6.

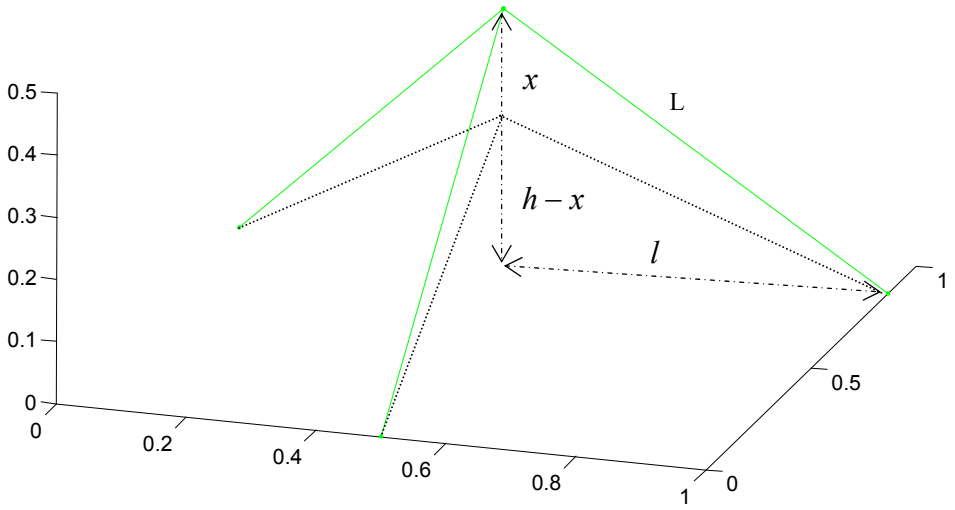

Figure 4.3 Geometry of the 3-bar truss.

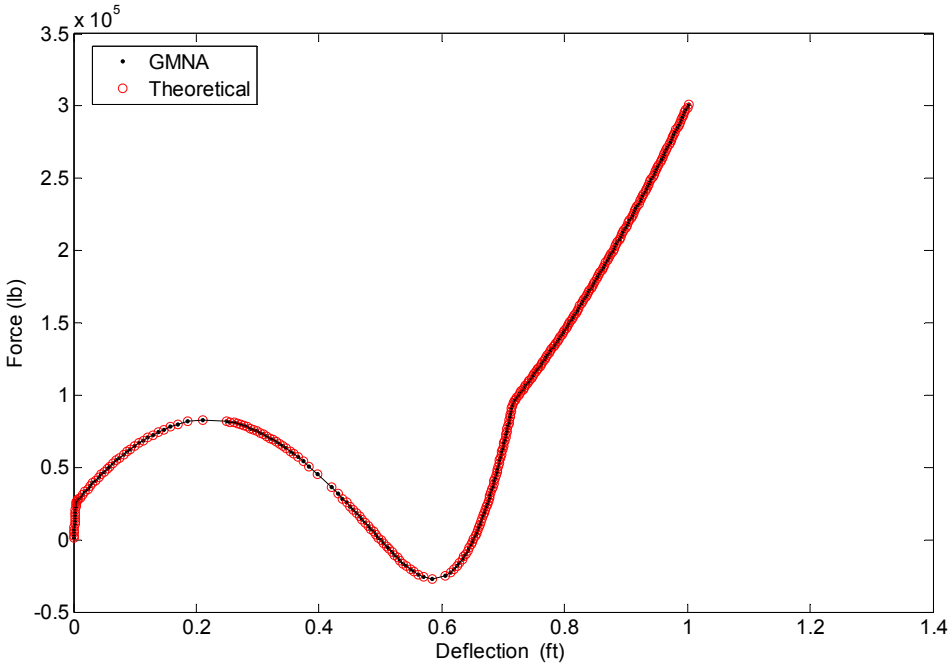

Figure 4.4 Inelastic snap-through of the 3-bar truss.

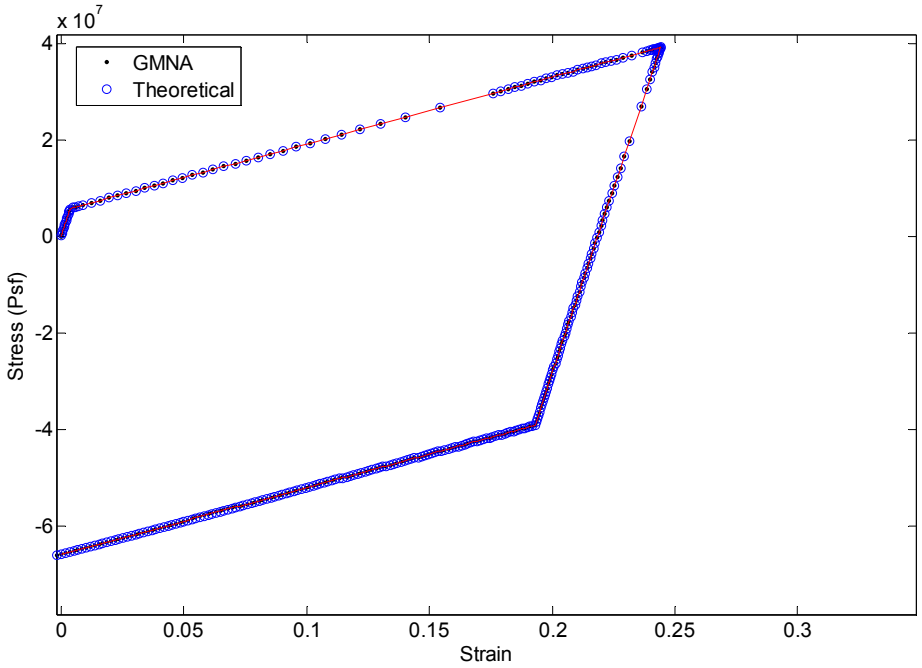

Figure 4.5 A stress- strain model for isotropic hardening.

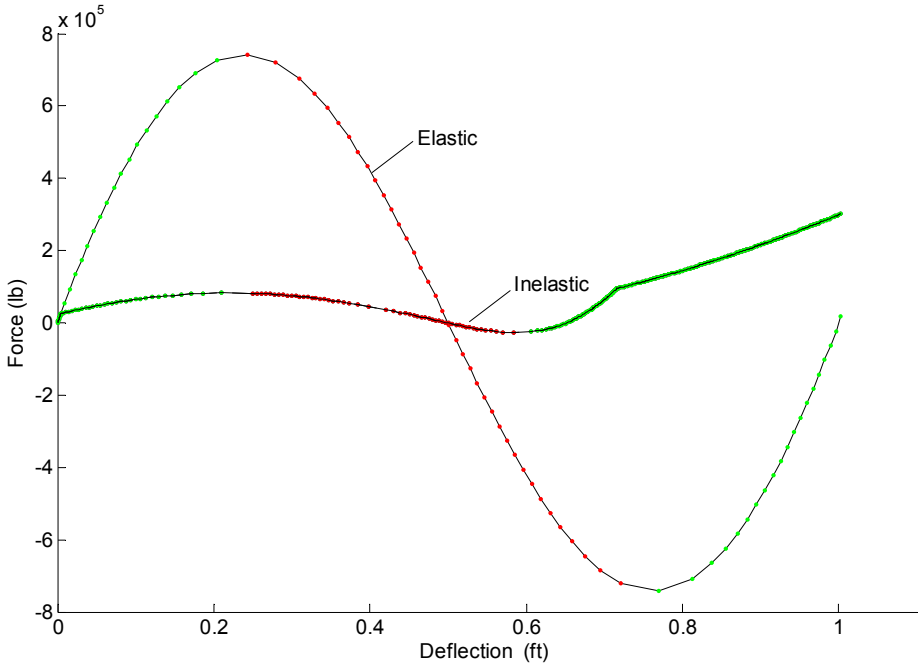

Figure 4.6 Comparison of load- deflection of elastic and inelastic 3-bar truss.

The interesting instants during the deformation process are captured in Fig 4.7. It can be seen that the 3-bar truss yielded in compression after very small deflection, which caused the first abrupt change of the slope of the load-deflection curve. Then the structure reaches its maximum resistance during continuous hardening. When the 3-bar turns to be horizontal, the resistance is decreased to zero. After that, the external force is changed from pression to tension in order to keep tracing the snap-through phenomena. After the tension reach the maximum, the external force is gradually changed from tension to pression and the resistance is again increased. Once the stress level in the 3-bar truss reaches the tension yield point, the load-deflection curve has its second turning points, where the slope is changed abruptly.

The influence of plastic modus in the resistance is discussed in Fig 4.8. With the increase of plastic modulus, the load capacity of the 3-bar truss is greater and greater. But as long as the isotropic hardening effect exists, the difference remains.

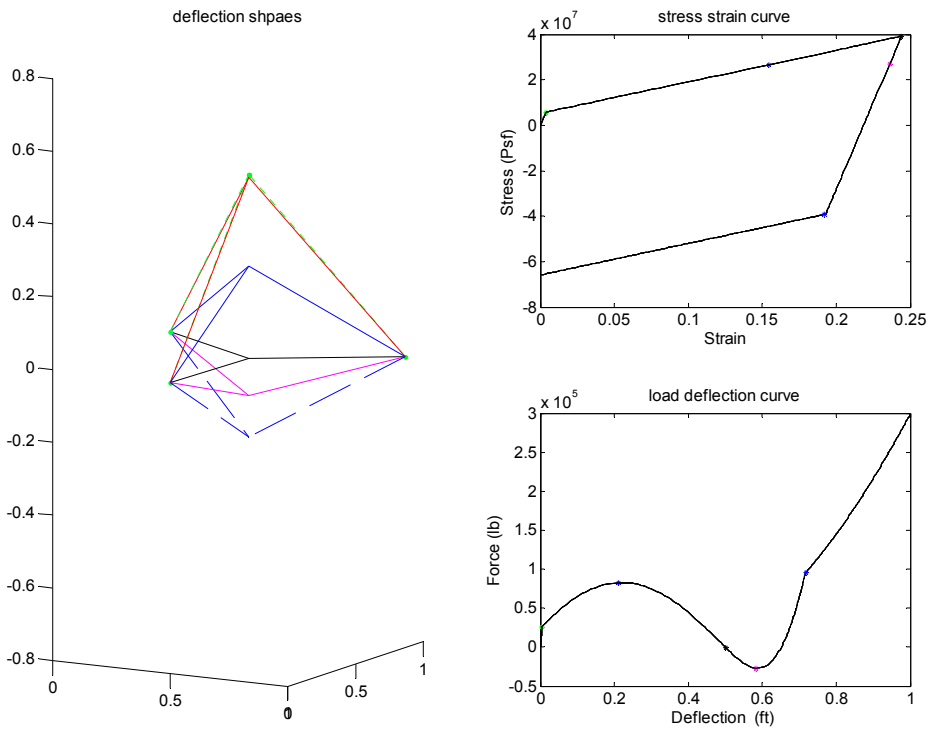

Figure 4.7 Interesting instants for the inelastic 3-bar truss.

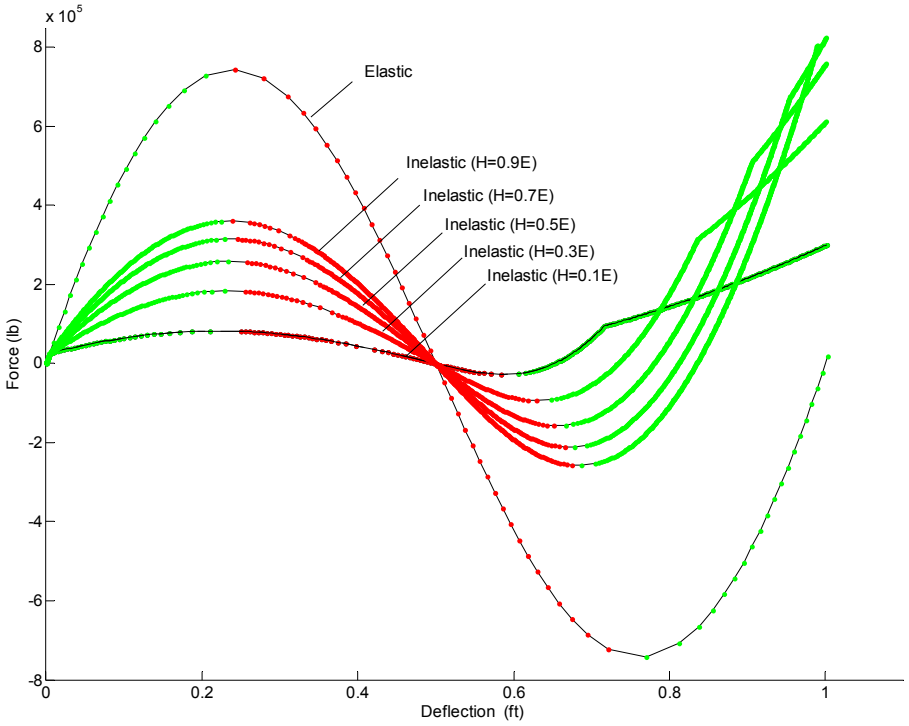

Figure 4.8 Comparison of load- deflection curves of elastic and inelastic 3-bar truss with different plastic modulus.

4.2 Dynamic hardening in truss

If the tower shown in Fig 3.4 is under 5 times EI Centro earthquake in the X direction and dynamic hardening is considered for the material, the response of the tower is found to be smaller than that of the totally elastic model (Fig 4.9). The reason is that under no modal damping circumstance, material yielding becomes the seismic energy dissipation mechanism.

The first four leg elements enter plastic zone before 4.5 seconds. After that, elements 13, 14, 17, 18, 21, 22, 23, 24 have plastic deformation one by one. Under the maximum deflection, 12 elements including elements 29, 30, 31, 32 are in the plastic zone at the same time as shown in Fig 4.10 and 4.11.

The corresponding stress strain history in elements 1, 13, 21, 30, 40 are shown in Figs. 4.12-4.16. It is found that the strain in the lateral members, such as element 13 and 21, has a larger range than the leg elements, such as elements 1 and 30. The stress in other elements always remains in elastic range.

The time history for the stress and strain in elements 1, 13, 21, 30, 40 as shown in Fig 4.17 and 4.18, again reveals that the lateral members maintain higher stress level than the leg parts. And all strains of these members drifts between the limits of ductility, which is 0.15 (Boresi and Schmidt, 2003). This indicates no fracture in the members.

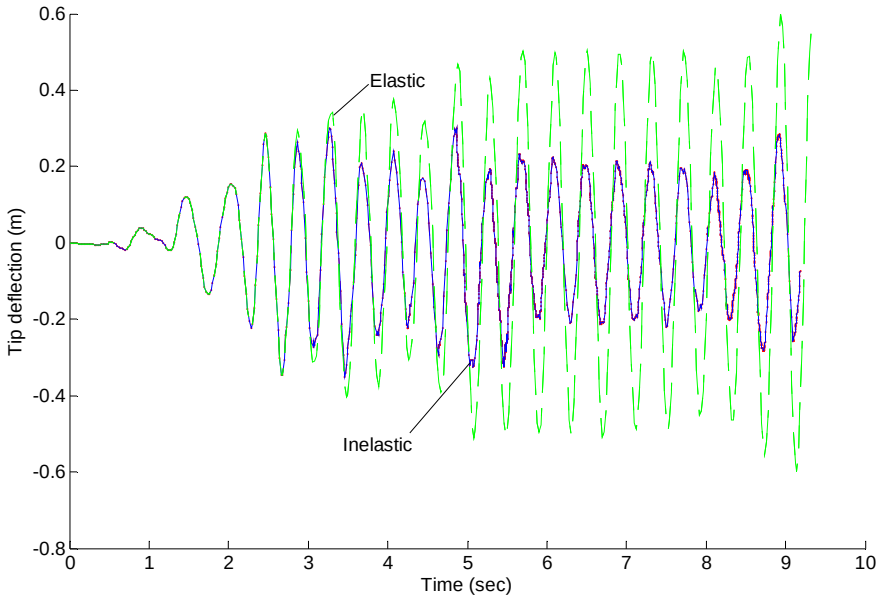

Figure 4.9 Comparison of tip deflection under strong earthquake.

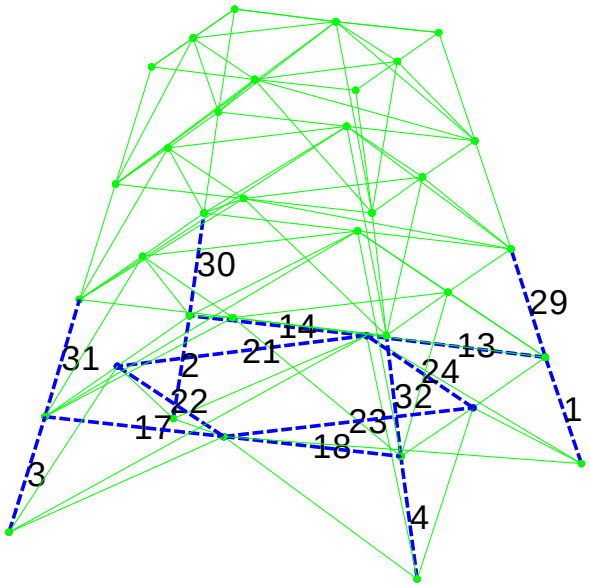

Figure 4.10 Yielded members in the tower.

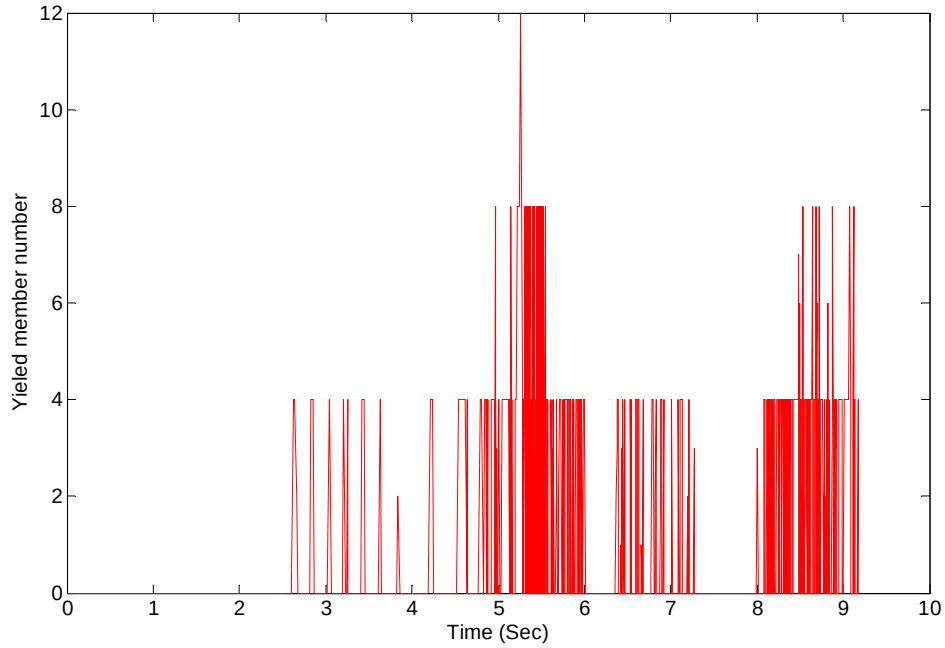

Figure 4.11 The number of yielded members versus time.

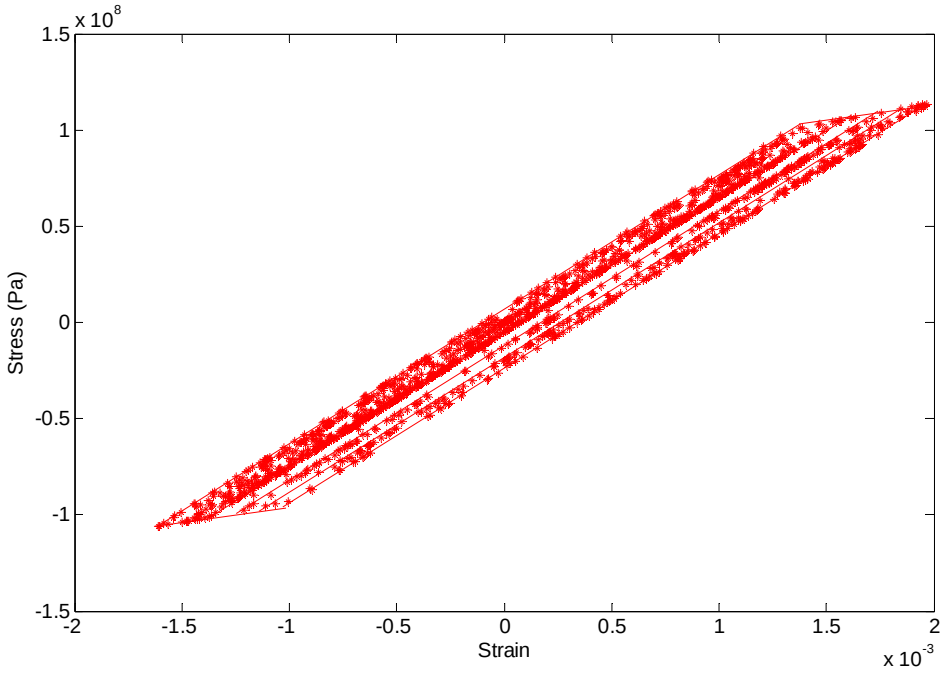

Figure 4.12 Stress strain history in the member #1.

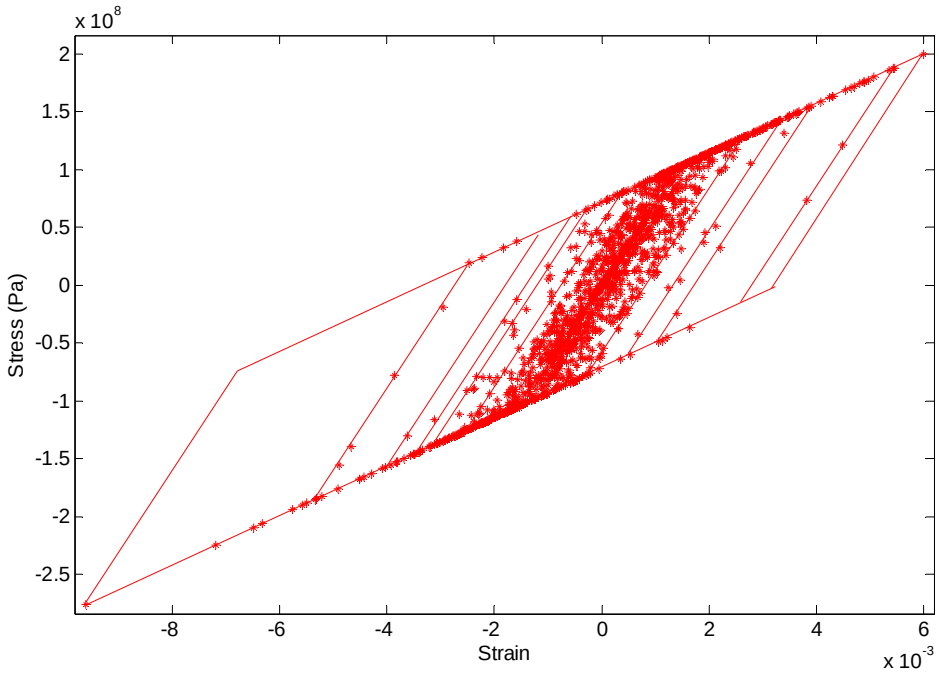

Figure 4.13 Stress strain history in member #13.

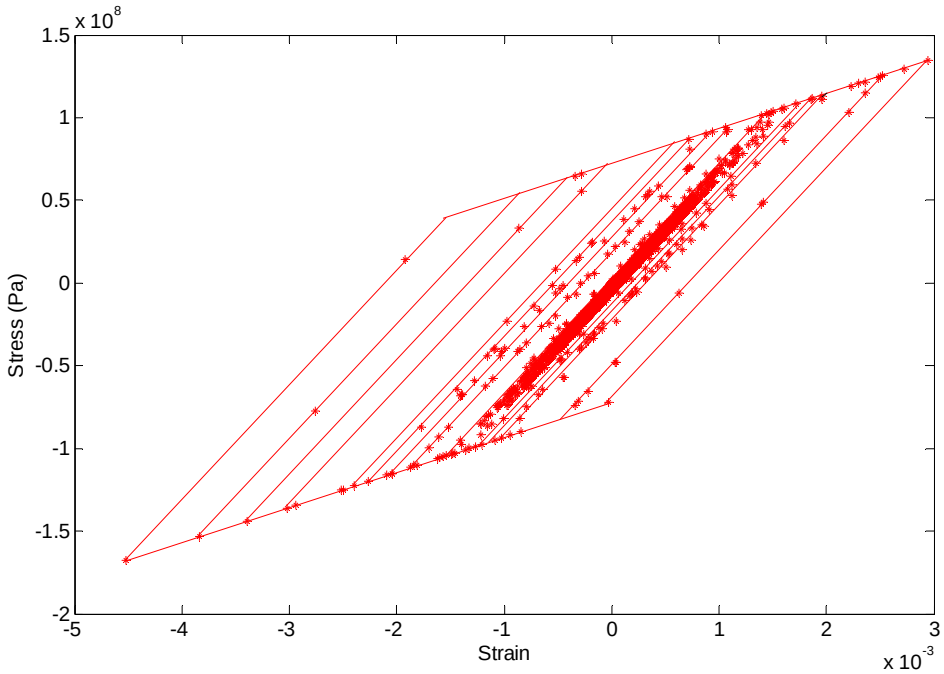

Figure 4.14 Stress strain history in member #21.

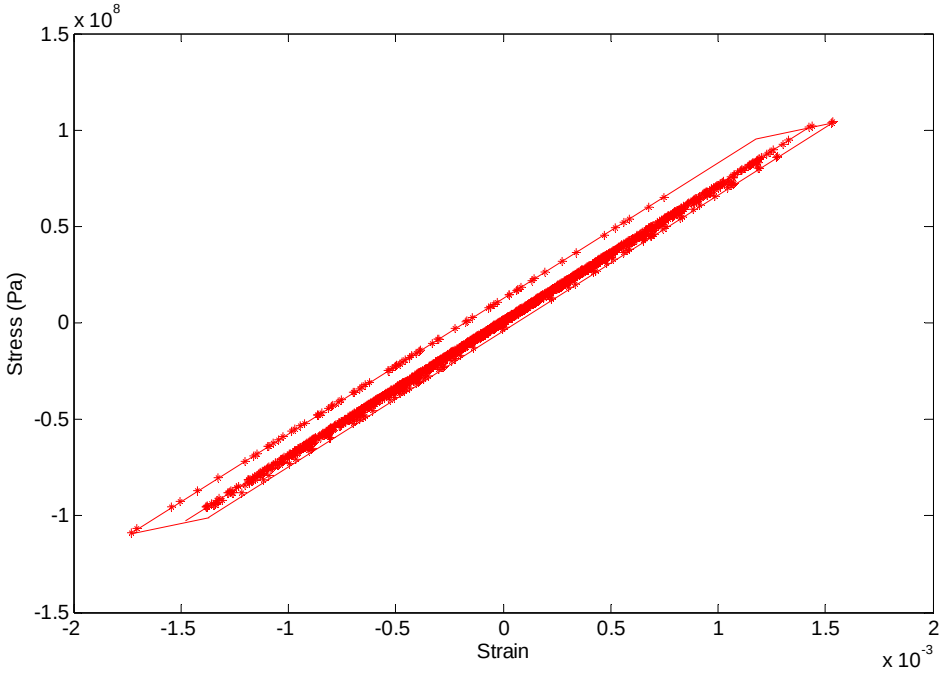

Figure 4.15 Stress strain history in member #30.

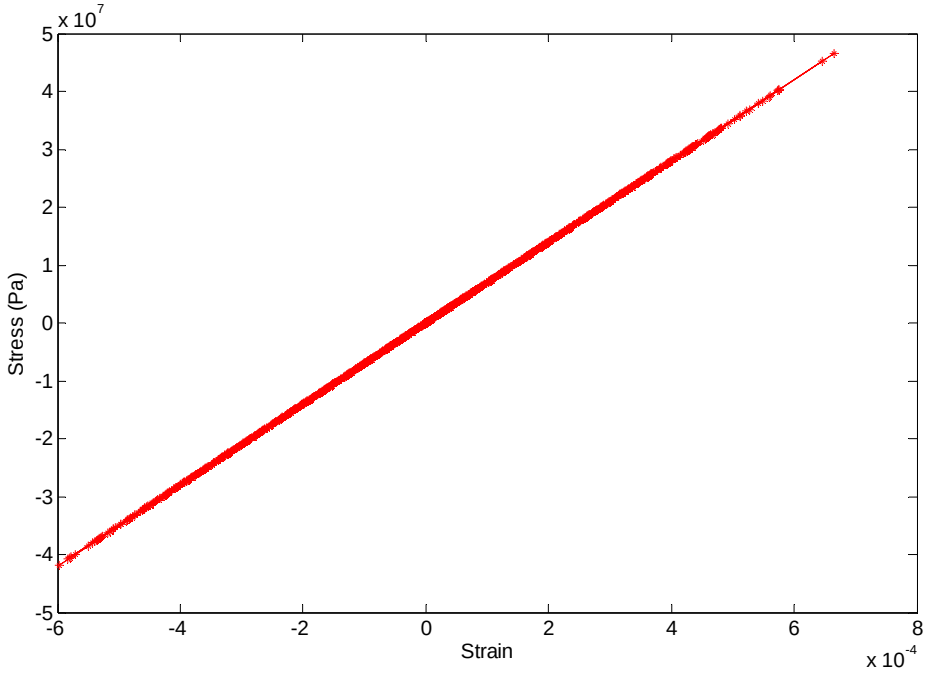

Figure 4.16 Stress strain history in member #40.

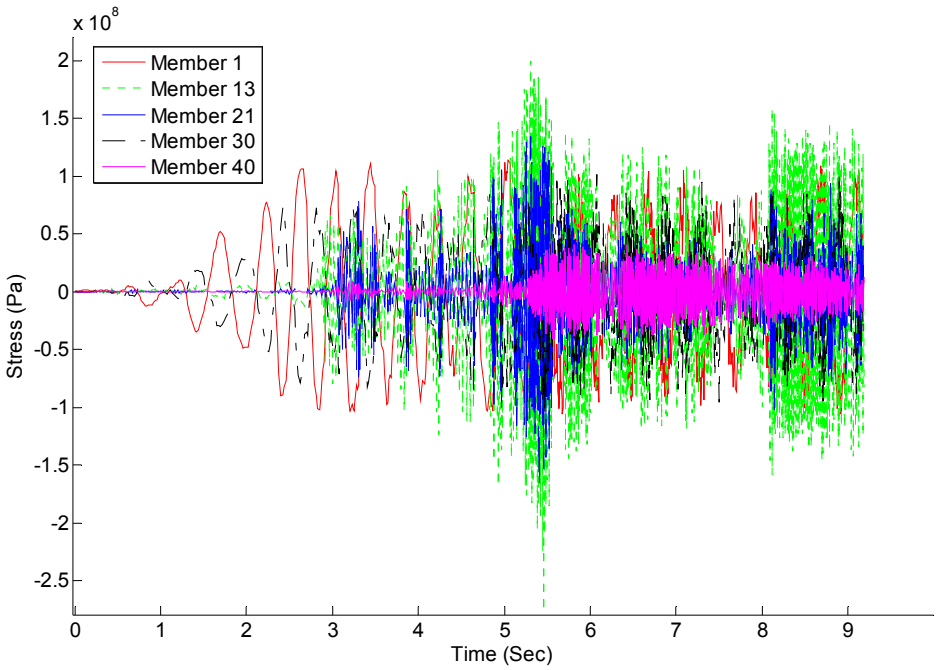

Figure 4.17 Stress histories for selected members.

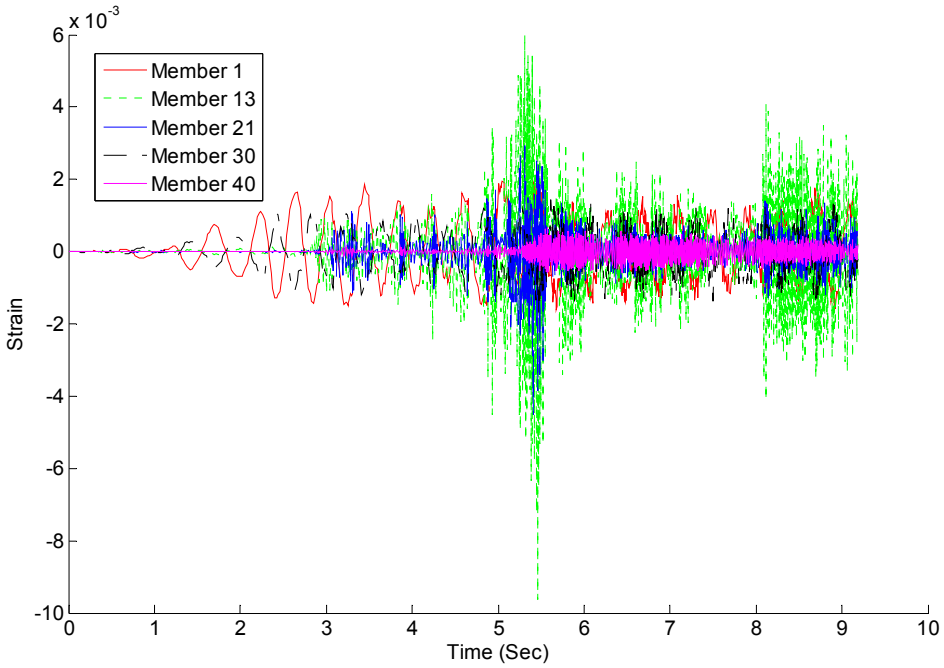

Figure 4.18 Strain histories for selected members.

4.3 Material nonlinearity in cables

Following the derivation in Section 4.1, the material nonlinearity in the cable can result in the following change in the formulation of the FEM cable element.

$$\begin{aligned}[k]\{u\} &= \int_l A_0[1-\upsilon e]^2\sigma[D]^T\{\phi\}ds \\ &= A_0[1-\upsilon e]^2\sigma[D]^T\{\phi\}l\end{aligned} \tag{4.5}$$

Referring to Eq. (4.3), it can be found that

$$\begin{aligned}\frac{\partial\sigma}{\partial\{u\}} &= ER\frac{\partial\varepsilon}{\partial\{u\}} + E_t(1-R)\frac{\partial\varepsilon}{\partial\{u\}} \\ &= (ER + E_t(1-R))\{\phi\}^T[D]\end{aligned} \tag{4.6}$$

Thus, the tangent stiffness can be modified as

$$\begin{aligned}[\tilde{k}] &= \frac{\partial([k]\{u\})}{\partial\{u\}} \\ &= \frac{\partial\sigma}{\partial\{u\}}A_0[1-\upsilon e]^2[D]^T\{\phi\}l + A_0(-2\upsilon+2\upsilon^2 e)\frac{\partial e}{\partial\{u\}}\sigma[D]^T\{\phi\}l \\ &\quad + A_0[1-\upsilon e]^2\sigma[D]^T\frac{\partial\{\phi\}}{\partial\{u\}}l \\ &= (ER+E_t(1-R))\{\phi\}^T[D]A_0[1-\upsilon e]^2[D]^T\{\phi\}l \\ &\quad + A_0(-2\upsilon+2\upsilon^2 e)\{\phi\}^T[D]\sigma[D]^T\{\phi\}l \\ &\quad + A_0[1-\upsilon e]^2\sigma[D]^T[\gamma][D]l \\ &= \left[(ER+E_t(1-R))A_0[1-\upsilon e]^2 + A_0(-2\upsilon+2\upsilon^2 e)\sigma\right][D]^T\{\phi\}\{\phi\}^T[D]l \\ &\quad + A_0[1-\upsilon e]^2\sigma[D]^T[\gamma][D]l\end{aligned}$$

The tensile strength for the cables is 1520 MPa and their Young's modulus is 159GPa (ASTM, 2007). The ductility limit is 4%. The prestrain level is set to be 0.005. When the uniform load is increased gradually, the deflection is increased as shown in Fig 4.22. The yielded members are labeled in Fig 4.19 from 1 to 13. The number sequence also indicates their yield consequence.

The stress strain curve in element 1 and 7 is shown in Fig 4.20 and 4.21. It is seen that element 1 is the first to yield and have the longest hardening history.

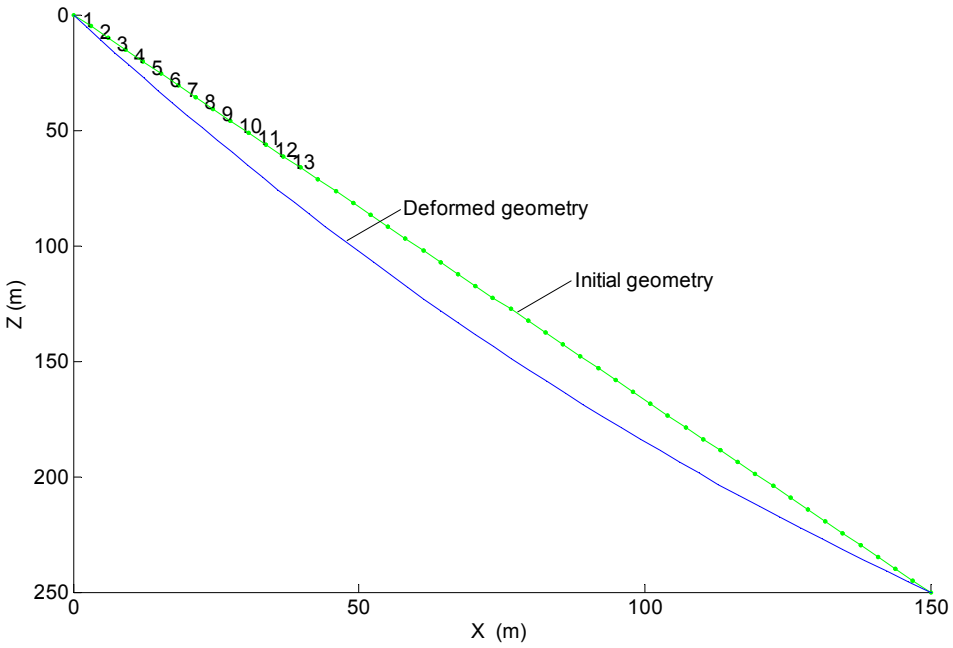

Figure 4.19 Deformation of a 0.5% prestrained lean cable under self weight and 800 N/m uniform vertical load.

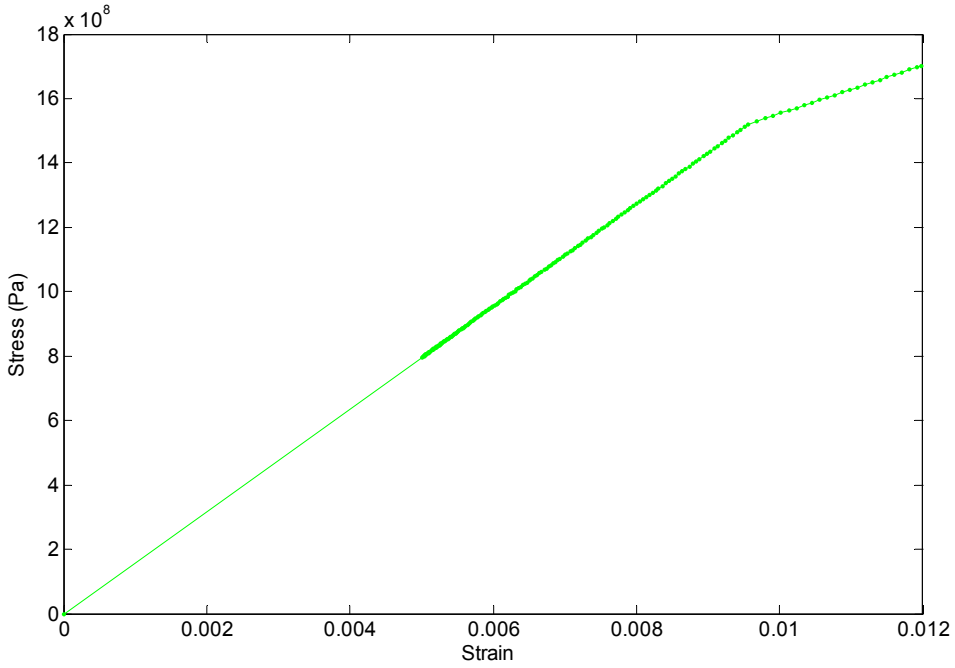

Figure 4.20 Stress-strain history in element #1.

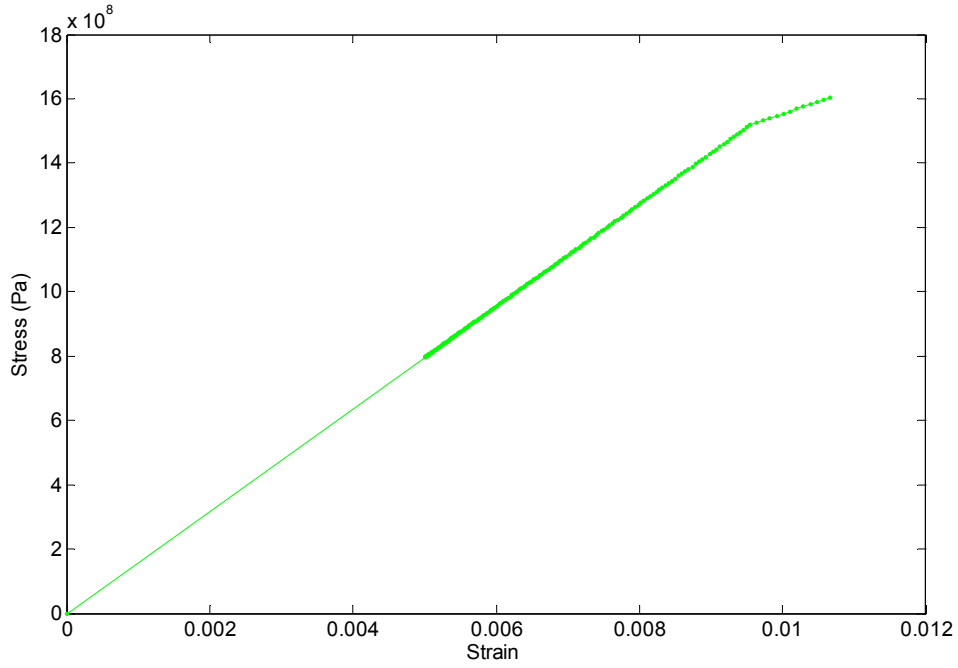

Figure 4.21 Stress-strain history in element #7.

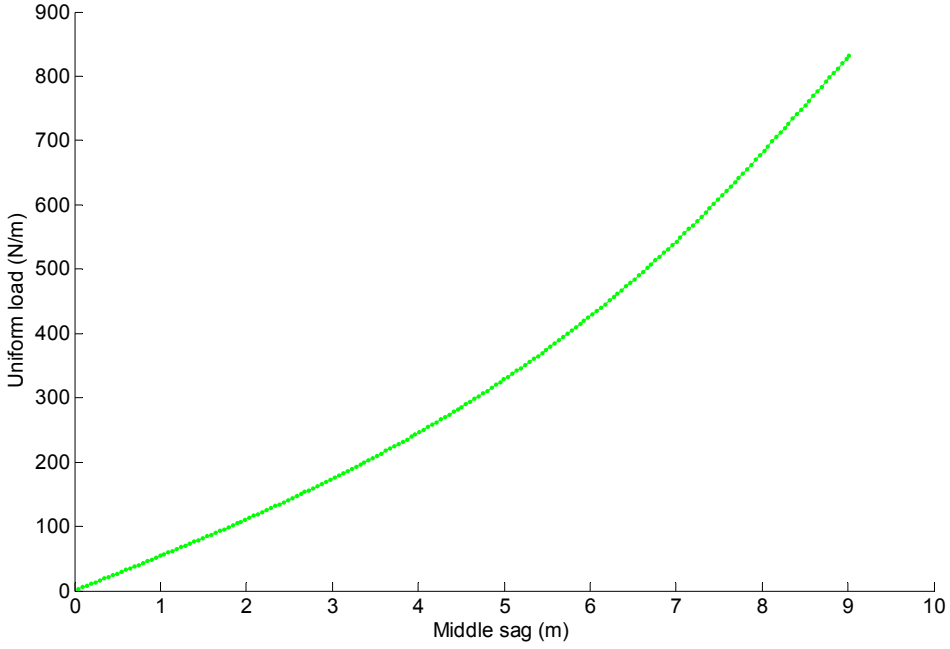

Figure 4.22 Uniform vertical load versus middle sag.

As for dynamic hardening model for cables, the methodology is the same as the one for truss elements. But the usual material like steel has very high modulus and

yield strength, which makes it physically almost impossible to yield and harden during dynamic response. Therefore, detailed discussion is neglected here.

4.4 Summary

Two inelastic models (isotropic hardening for static case and dynamic hardening for dynamic case) have been applied in the analysis along with geometric nonlinearity. It is found that inelasticity under static loading can greatly reduce the resistance capacity of truss structures. The transition from elastic state to plastic state will result in a turning point in the load deflection curve. The finite element analysis results agree well with theoretical results. In dynamic analysis, inelasticity helps dissipate the seismic energy transmitted into the truss tower. With the increased intensity, different members come into plasticity in turn. The tip deflection is thus suppressed in the inelastic model. For a cable under static loads, yielding will start from the top elements and expands towards the root.

Chapter 5 Nonlinear Analysis of Guyed Towers

When all the nonlinear elements are implemented with proper algorithms, the nonlinear response of guyed towers under large static loads and severe earthquakes can be predicted accurately. This chapter will focus on the applications of nonlinear finite element methods in the analysis of guyed towers. Two basic towers are chosen as representative of guyed towers. The first one is a tower with taut cables, which is appropriate for guyed towers with relatively low heights. The second one is for towers with sagged cables, which is usually the case for high towers. For each type of tower, both static and dynamic analyses are conducted through detailed examples. Simplified linear static analysis for towers with taut cables is also performed to compare with the nonlinear results. Material nonlinearity is further implemented in the analysis to improve accuracy of analysis.

5.1 Nonlinear static analysis of a 50 ft guyed tower

The mast arm is composed of steel pipes with Young's modulus 29×10^{6} psi. The outside rim diameter of the pipe is 1.25 inch and the inside diameter is 1.04 inch. The lateral and oblique struts between the poles are made of round steel bars with a radius of 7/16 inch. The steel cables have two layers, which are anchored separately. The radius of the lower-layer cables is 5/32 inch and the upper-layer cables is 3/16 inch. The initial prestress for the lower-layer cables is 900 lbs and the upper-layer cables is 100 lbs.

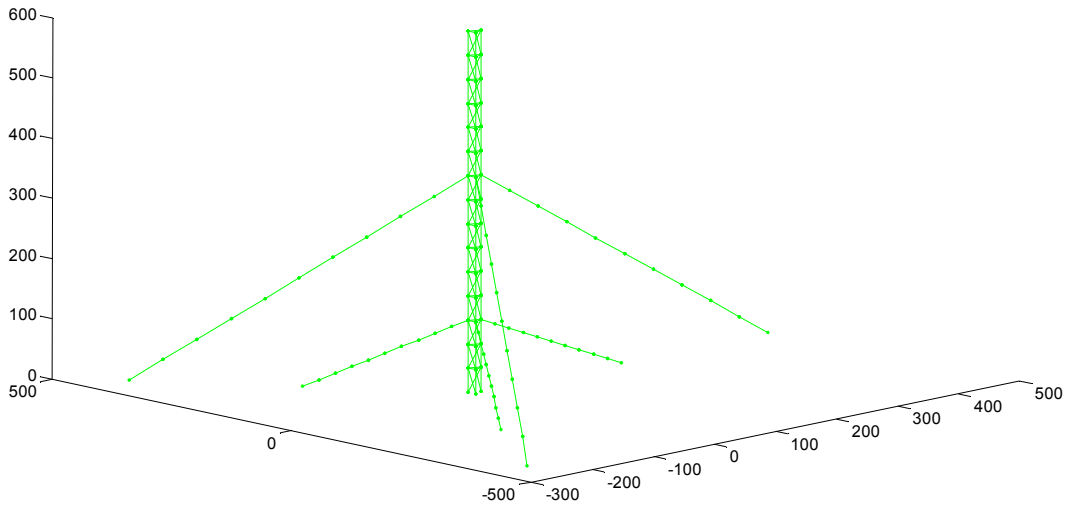

Figure 5.1 Geometry of the guyed tower.

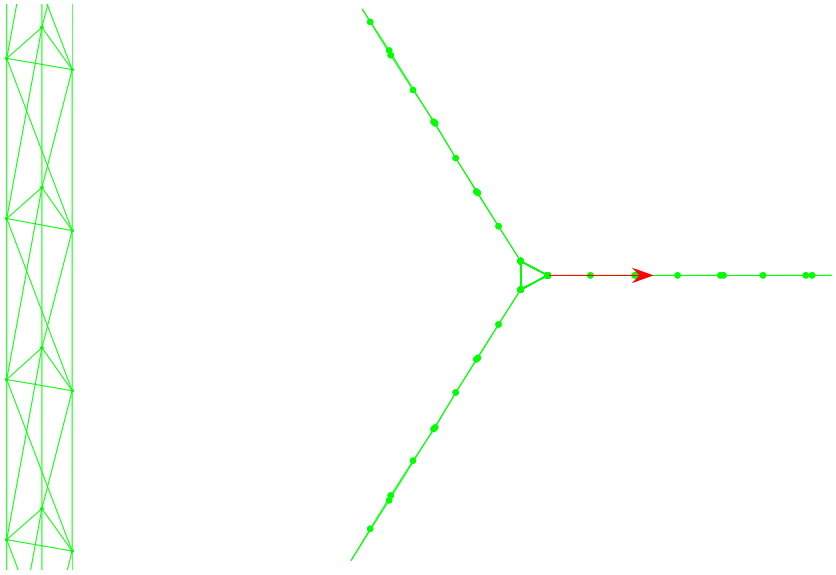

(a) (b)

Figure 5.2 (a) Cross section of the mast, and (b) top view of the applied force.

The concentrated load is applied on the tip of the mast. To trace the nonlinear response, the load is increased gradually at small increments. Once a converged solution for the current load step is achieved after iterations, the load level will be updated and

new solution loop will be started. The loop will continue until desired criteria such as maximum displacement on a specific part or the maximum load has been reached.

The final deformation shape is shown in Fig 5.3. The tip deflects as much as 83.75 inch under a concentrated load 6,584 lbs. But the lateral drift for the upper cable cluster connection point is much smaller than the tip deflection. There is almost no deflection for the lower cable cluster connection point. So the deformation mechanisms for the tip unrestrained mast is like a cantilever beam under tip point load. But the whole mast behaves more like a multiple supported beam under tip load.

The load-deflection curve in Fig 5.4 clearly shows that the tower is softened after the first 10 inch deflection. When the deflection reaches 45 inch, the structure turns to be stiffer with the increase of deflection. But the global stiffness is still less than the original elastic stiffness because the slope of load-deflection curve is smaller than the beginning slope of the curve.

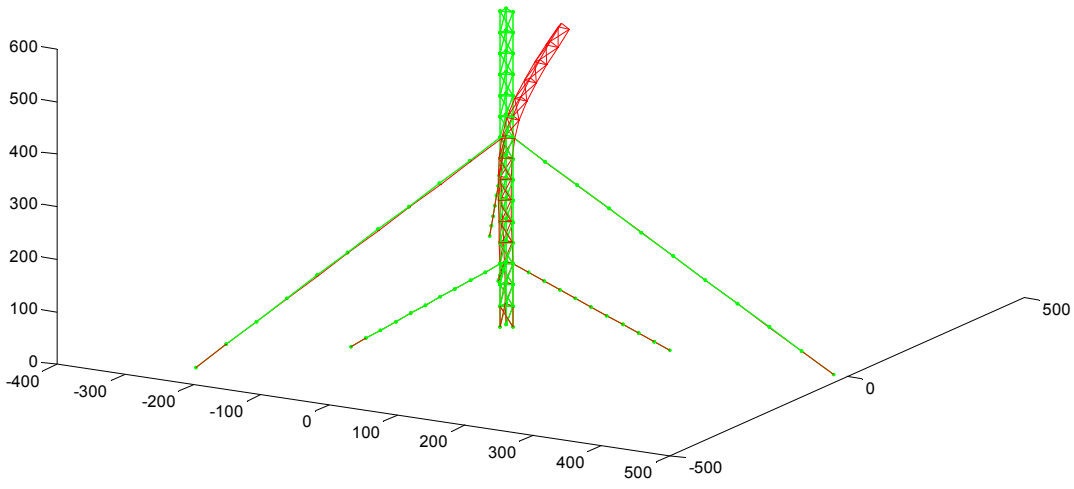

Figure 5.3 Deformation of the guyed tower under tip point load.

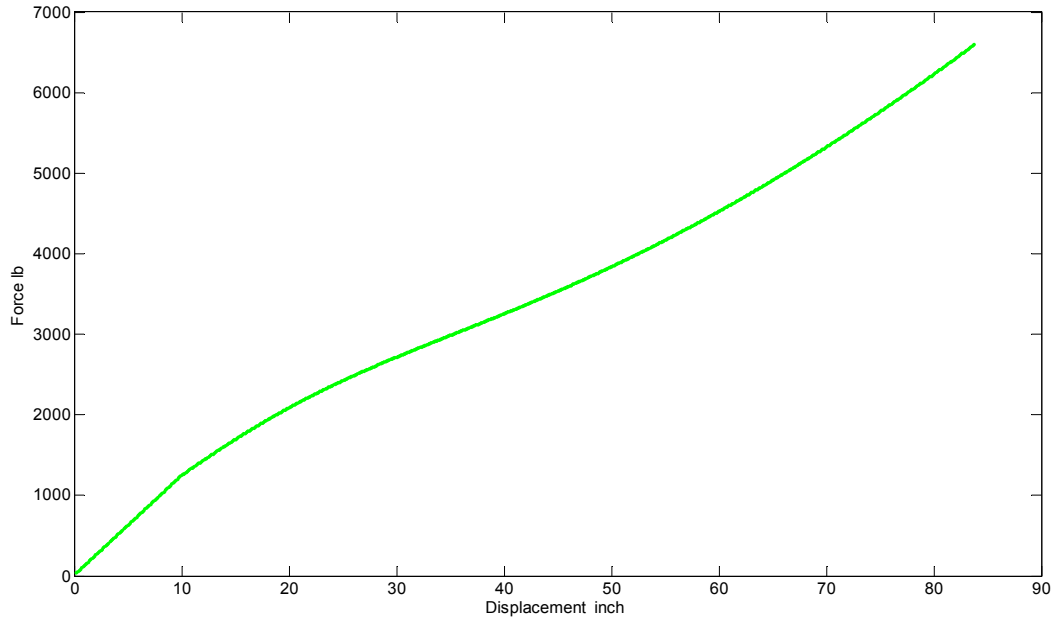

Figure 5.4 Load deflection curve.

The same model is also analyzed by ANSYS and SAP2000 for comparison. Link 8 is used for modeling of struts. Link 10 (tension-only) is applied for the modeling of cables. The pole is simulated by beam 4. The large static analysis option is turned on to capture the large deformation. The final deformed geometry is shown in Fig. 5.5, which is very similar to Fig. 5.4. Under 6000 lb external tip loads the maximum deflection is 97.362 inch. The load-deflection curve is compared in Fig. 5.7. Though the analysis is nonlinear, the results are still linear because the deflection is proportional to loads.

In the analysis of SAP2000, nonlinear and large deformation option in analysis is also chosen. The deflection shape under 6000lb external tip loads by SAP2000 is shown in Fig. 5.6. The deflection shape is more flexible than in Fig. 5.6, which indicates that the tower responds stiffer in SAP2000 than in ANSYS. This is verified in Fig. 5.7, because the slope of load-deflection curve by SAP2000 is greater than by ANSYS. The results by SAP2000 well match results by geometrical nonlinear analysis when deflection is small.

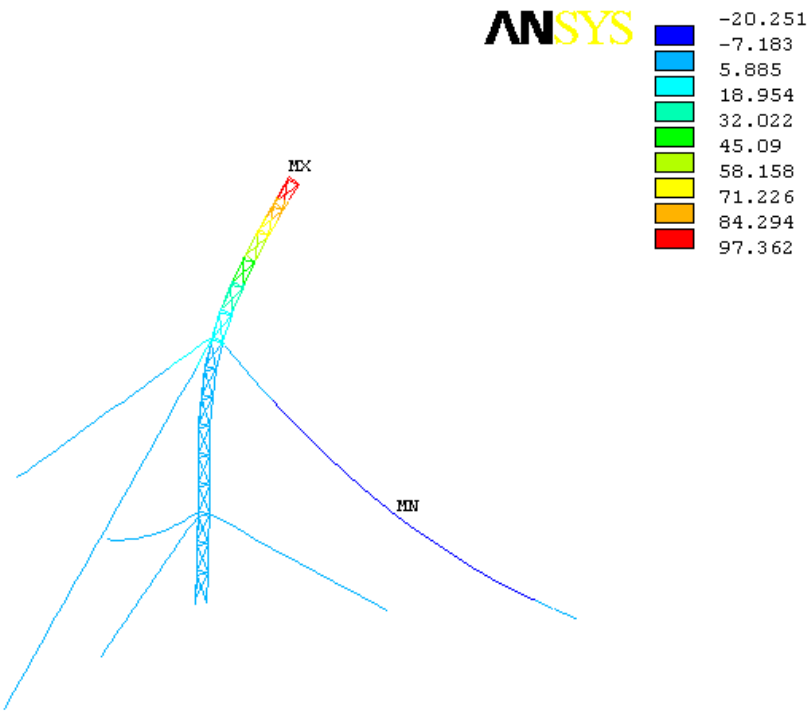

Figure 5.5 Deformed geometry by ANSYS.

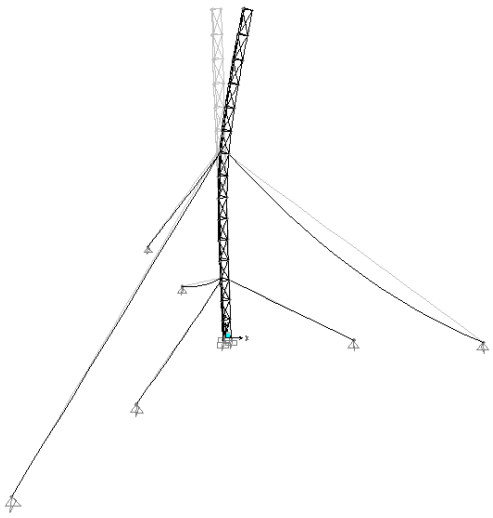

Figure 5.6 Deformed geometry by SAP2000.

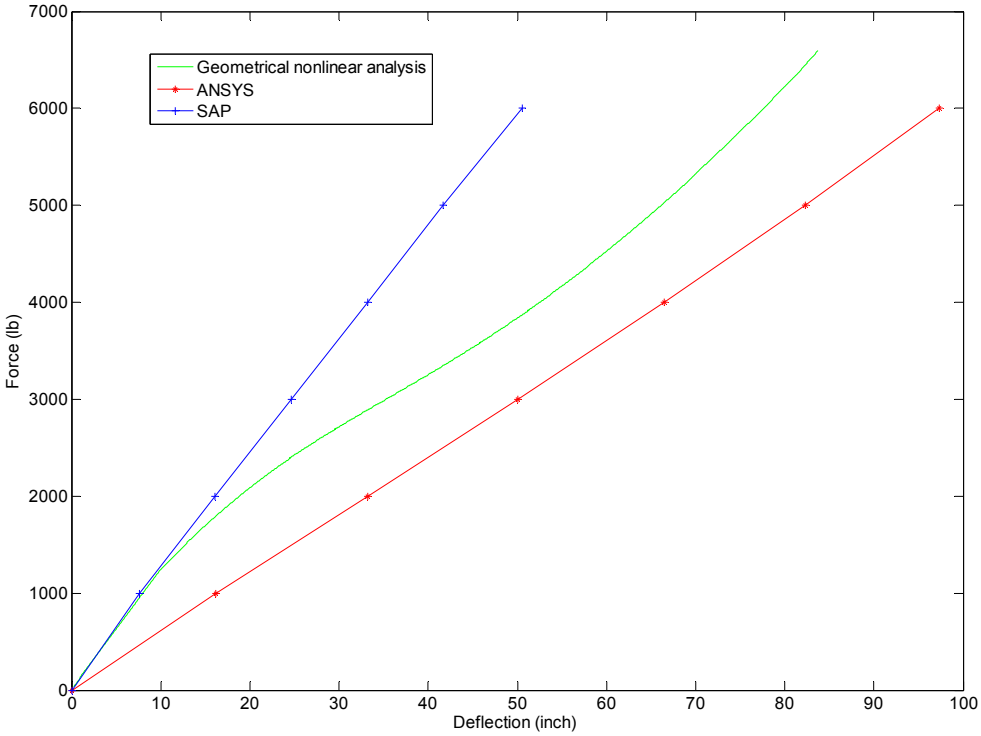

Figure 5.7 Comparison of load deflection curves.

From the comparison, it can be seen that large deflection analysis of guyed tower by different softwares usually gives different results. Though the analysis is based on nonlinear algorithm, the results are still linear. The nonlinear property can only be traced by proposed methodology.

5.2 Linear static analysis of the 50 ft guyed tower

The pole is treated as a beam with a constant cross-section as shown in Fig. 5.8. The equivalent bending stiffness is

$$I = \frac{\pi}{4}\left(0.625^4 - 0.5204^4\right)\times 3 + \pi\left(0.625^2 - 0.5204^2\right)\times\left(\frac{\sqrt{3}}{6}\times 16.75\right)^2 \times 2$$
$$+ \pi\left(0.625^2 - 0.5204^2\right)\times\left(\frac{\sqrt{3}}{3}\times 16.75\right)^2 + \pi\times 0.2188^2\times\left(\frac{\sqrt{3}}{6}\times 16.75\right)^2$$
$$+ \pi\times 0.2188^2\times\left(\left(0.5-\frac{\sqrt{3}}{6}\right)\times 16.75\right)^2 \times 2$$
$$= 60.2599\ in^4$$

Three different scenarios have been used to simplify the analysis. Because the height and span of the cables are not large, they are actually taut under 10% prestress. The lateral deflection is very small compared to the tip deflection. So the first simplification (Fig. 5.9) is only to simulate the top fraction of the tower as a clamped beam. The tip deflection is $\frac{FL_1^3}{3EI}$.

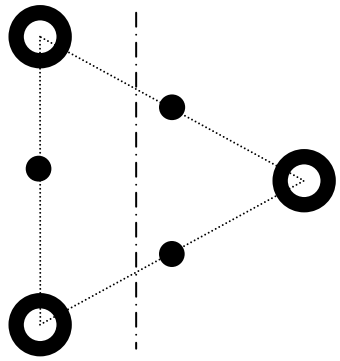

Figure 5.8 Equivalent cross section of the guyed tower.

Although the lateral deflection of the second cluster point is negligible, the rotation at this point greatly affects the tip deflection. Thus, the second simplification (Fig. 5.9) releases the restraint at the guy cluster points. Using the force method (Kassimali, 2005) to solve the indeterminate beams, two support reaction forces are assumed and the

deflections at these two supports must comply with the constraint conditions.

$$\Delta_1 = \frac{F_1 L_1^{\,2}}{6EI}(L_1 - 3L_1) - \frac{F_2 L_1^{\,2}}{6EI}(L_1 - 3L_2) + \frac{F L_1^{\,2}}{6EI}(L_1 - 3L) = 0$$

$$\Delta_2 = \frac{F_1 L_1^{\,2}}{6EI}(L_1 - 3L_2) - \frac{F_2 L_2^{\,2}}{6EI}(L_2 - 3L_2) + \frac{F L_2^{\,2}}{6EI}(L_2 - 3L) = 0$$

where L_1 is the distance from the tip to the upper cluster point; L_2 is the distance from the tip to the lower cluster point; and L is the height of the tower. The tip defection is

$$\Delta_{tip} = \frac{F_1 L_1^{\,2}}{6EI}(L_1 - 3L) - \frac{F_2 L_2^{\,2}}{6EI}(L_2 - 3L) + \frac{F L^2}{6EI}(L - 3L)$$

If the lateral stiffness of the guy cluster is considered, the equations become

$$\Delta_1 = \frac{F_1 L_1^{\,2}}{6EI}(L_1 - 3L_1) - \frac{F_2 L_1^{\,2}}{6EI}(L_1 - 3L_2) + \frac{F L_1^{\,2}}{6EI}(L_1 - 3L) = \frac{F_1}{K_1}$$

$$\Delta_2 = \frac{F_1 L_1^{\,2}}{6EI}(L_1 - 3L_2) - \frac{F_2 L_2^{\,2}}{6EI}(L_2 - 3L_2) + \frac{F L_2^{\,2}}{6EI}(L_2 - 3L) = \frac{F_2}{K_2}$$

where the equivalent lateral stiffness of the upper taut guy cluster (Madugula,2002) is

$$K_j = \sum \frac{EA_i}{l_i} \cdot \cos^2\theta_i \cdot \cos^2\beta_i$$

where l_i is the chord length of the cables;

A_i is the cross section of the cables;

θ_i is the vertical angle between the chord line and horizontal reference;

β_i is the horizontal angle between the cable and the direction of mast displacement.

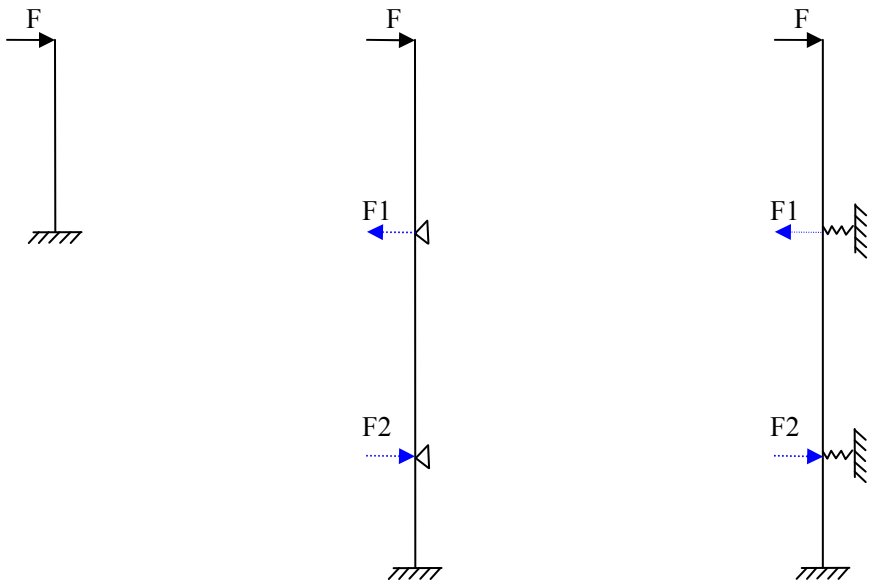

(a) (b) (c)

Figure 5.9 Simplification scenarios (a) clamped support at the upper cluster, (b) simply supported at clusters, and (c) spring supported at clusters.

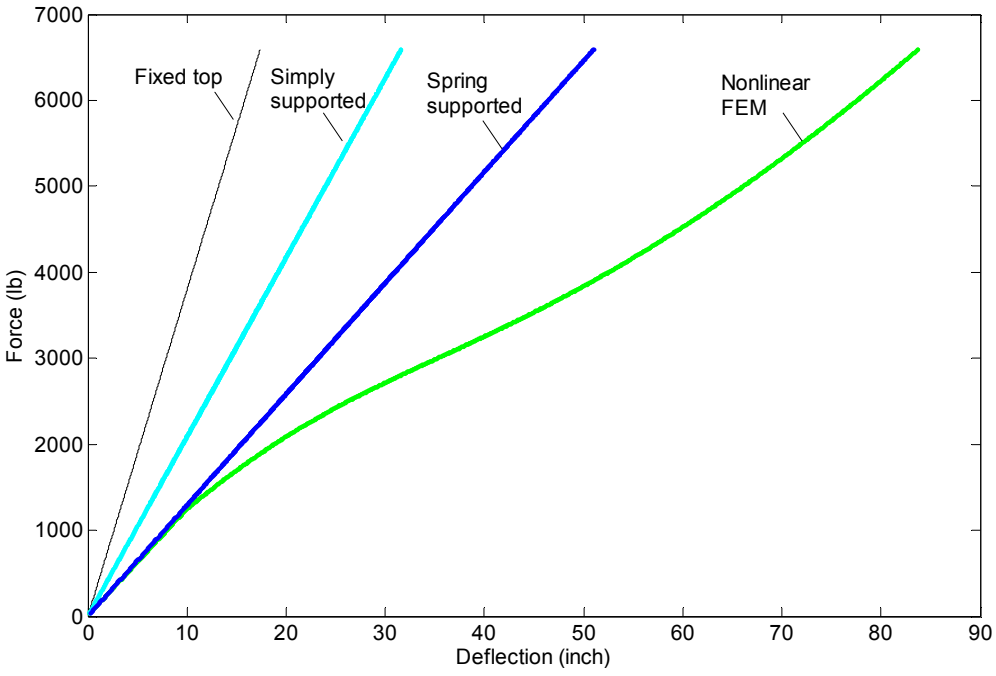

Figure 5.10 Comparison of simplified load-deflection curves.

The results from the three simplified methods are compared in Fig 5.10. It is clear that with the release of constrains, the equivalent beam becomes softer and more close to the real response. The spring supported beam matches with the response very well in the linear range. After that, none of the simplified methods can provide valuable estimation for the large deformation of the mast.

5.3 Nonlinear dynamic analysis of a 50 ft guyed tower

When the tower is subjected to the EI Centro earthquake in X-direction as shown in Fig 5.11 (a), the response is irregular. Figs. 5.12-5.17 represent the response of the guyed tower at different time steps. It is clear that when the ground shaking just begins, the structure almost has no deformation as shown in Fig 5.12. As the intensity of ground motion increases, the mast begins to defect and the cables start to swing.

The time history of the relative tip deflection (compared with the ground motion) is as shown in Fig 5.18. The maximum deflection is around 20 inches at 5 seconds, when the ground acceleration is not the most intensive. The absolute tip deflection history is shown in Fig 5.19, of which the maximum is close to 16 inches.

When the shaking direction is changed to Y-direction, the tower response at 3 second and 3.5 second is as shown in Figs 5.20 and 5.21. The relative and absolute tip deflection is plotted in Figs 5.22 and 5.23. From the comparison, it is seen that the response pattern under the different direction is very similar. The difference only lies in the specific value of tip deflection.

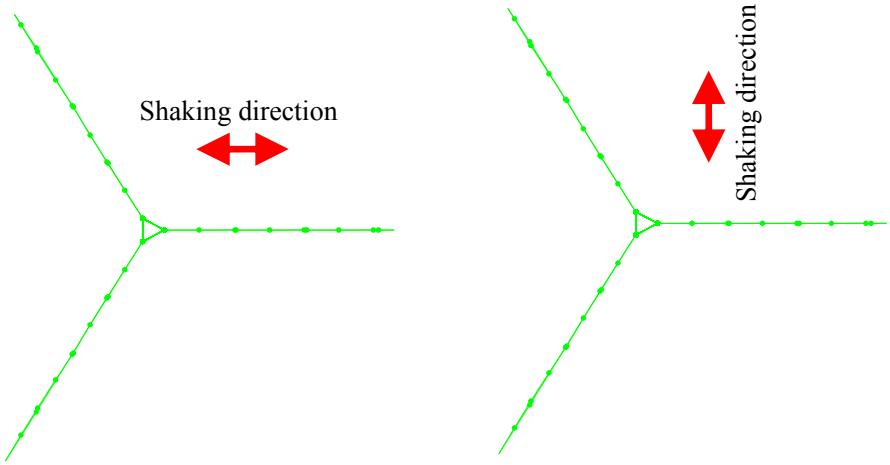

(a) (b)

Figure 5.11 (a) EI Centro earthquake input in the windward cable direction, (b) EI Centro earthquake input in the direction perpendicular to windward cable direction.

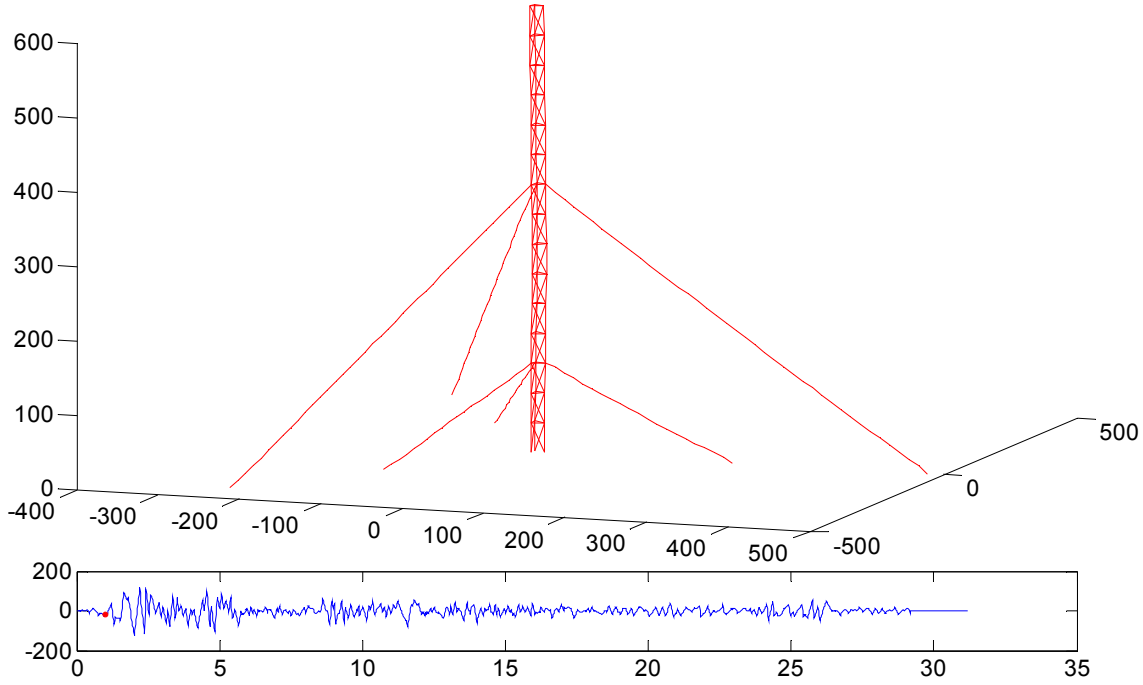

Figure 5.12 Tower deformation at t=1 second (in X-direction).

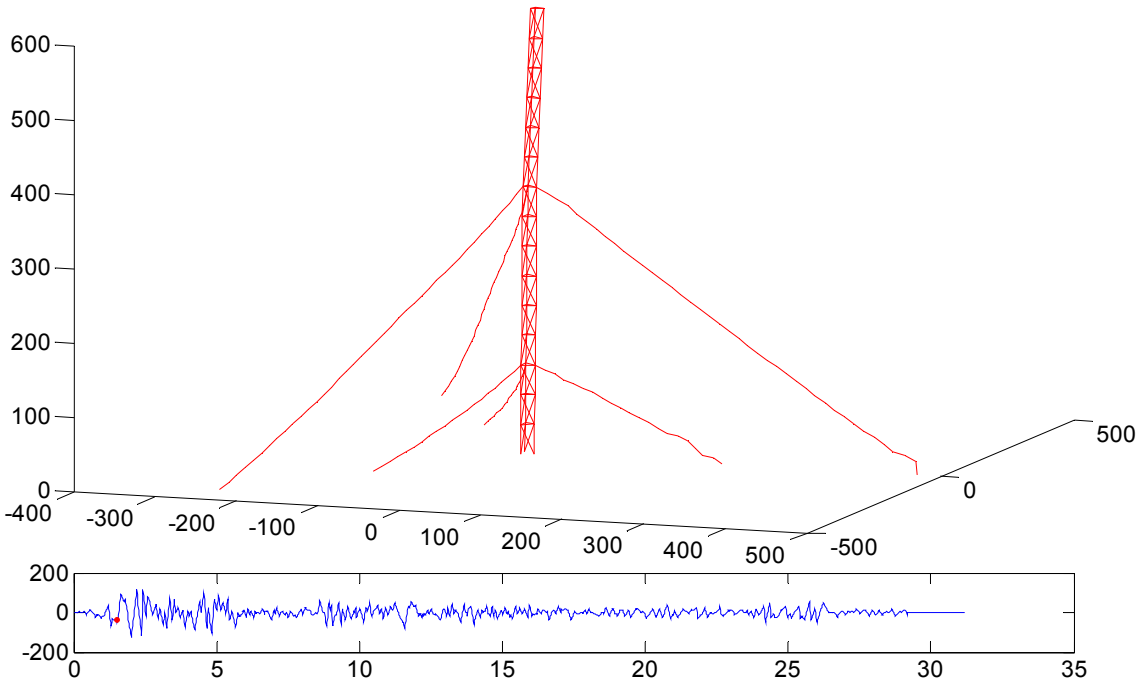

Figure 5.13 Tower deformation at t=1.5 second (in X-direction).

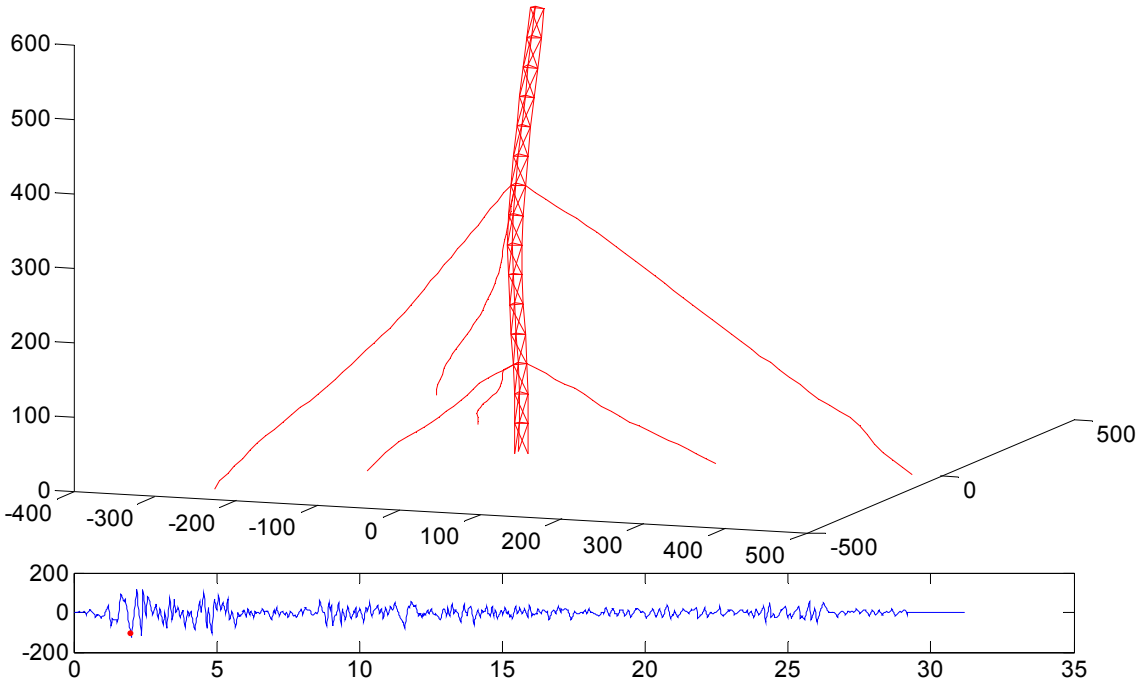

Figure 5.14 Tower deformation at t=2 second (in X-direction).

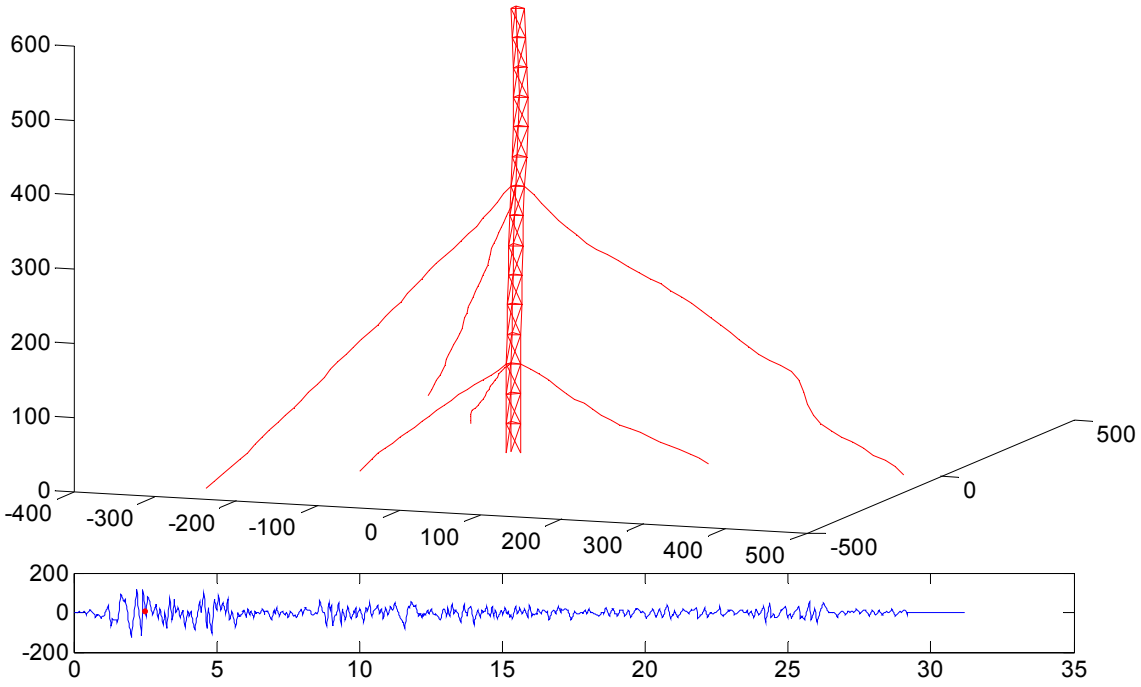

Figure 5.15 Tower deformation at t=2.5 second (in X-direction).

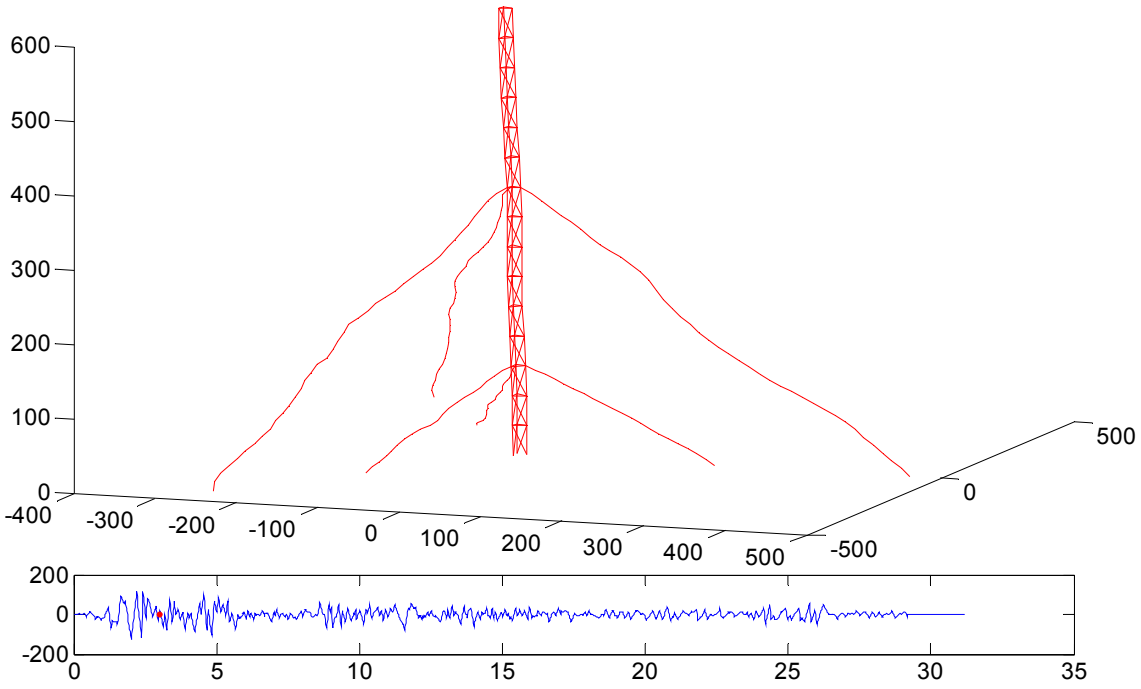

Figure 5.16 Tower deformation at t=3 second (in X-direction).

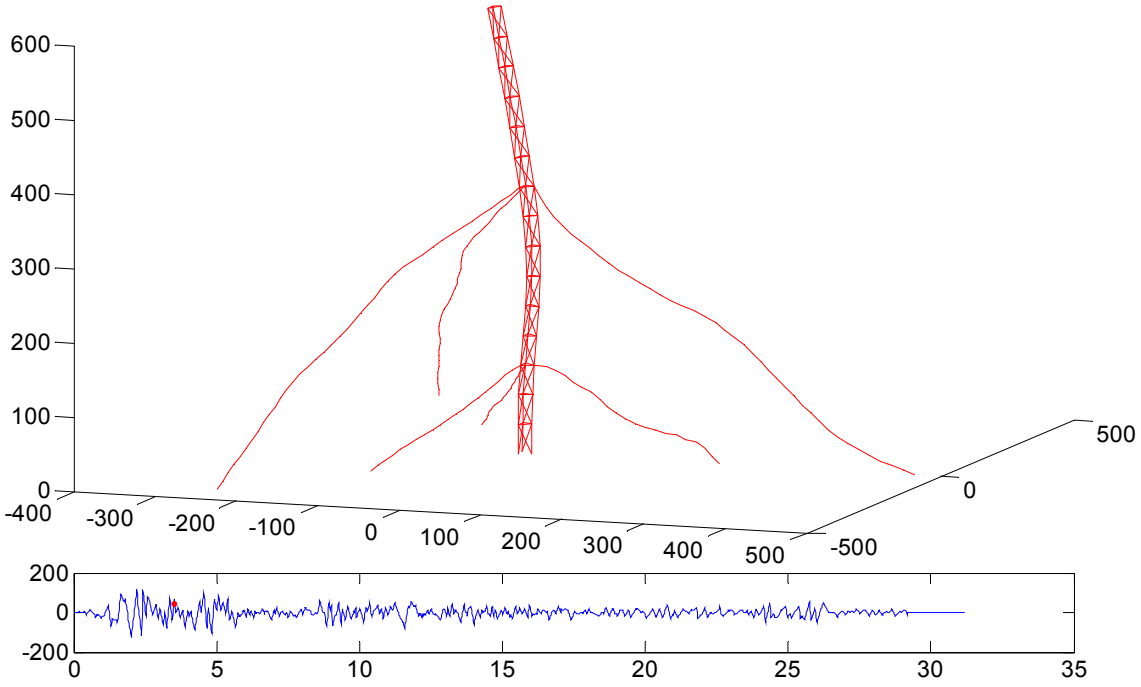

Figure 5.17 Tower deformation at t=3.5 second (in X-direction).

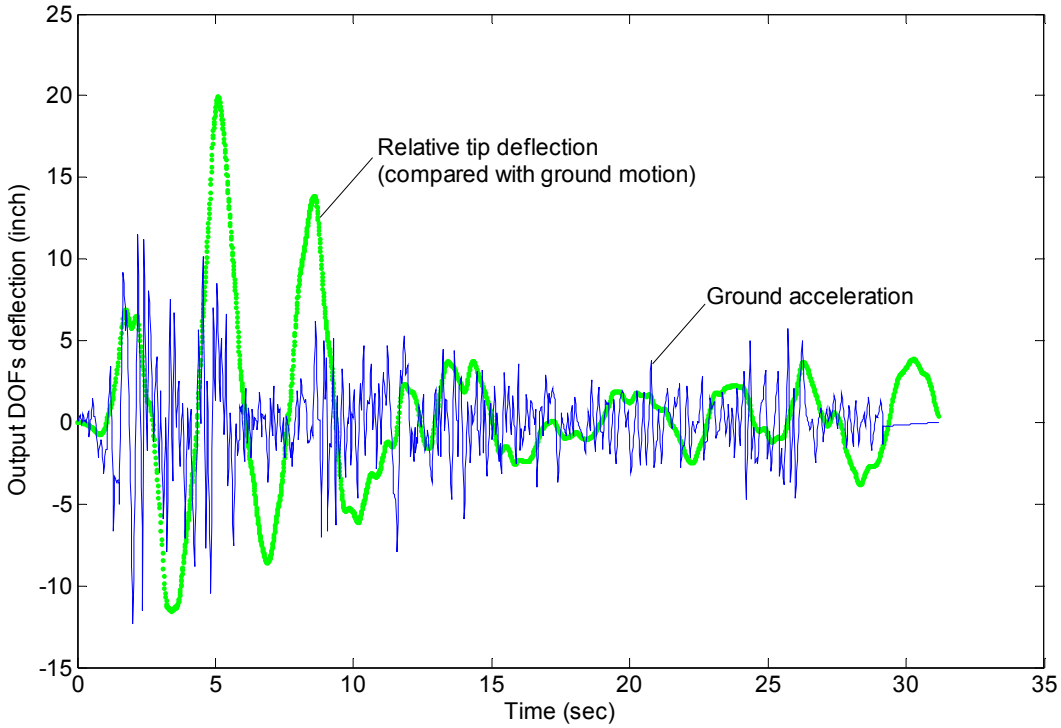

Figure 5.18 Time trace of relative tip deflection (in X-direction).

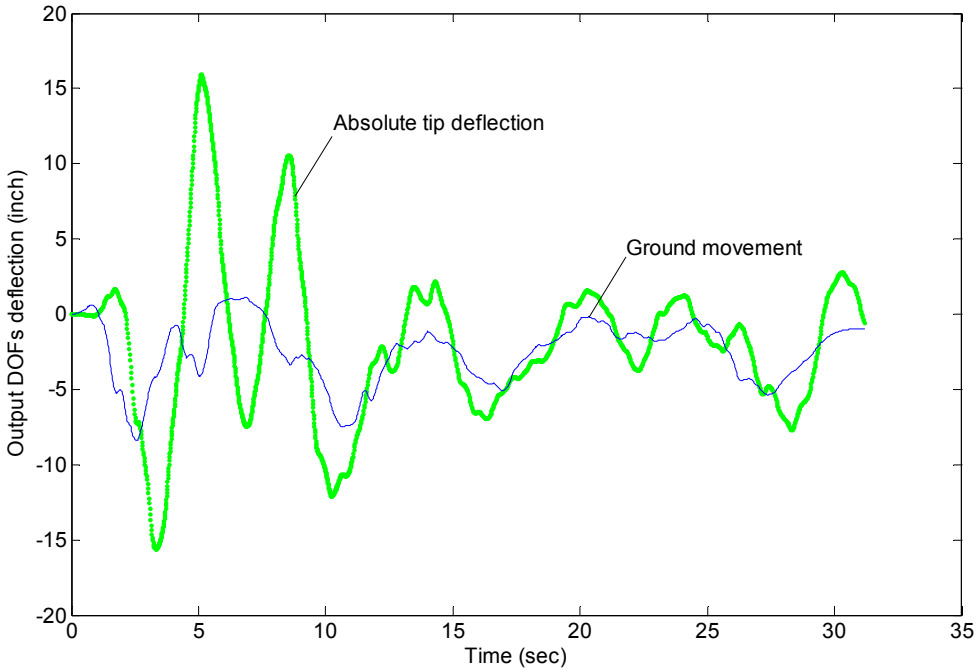

Figure 5.19 Time trace of absolute tip deflection (in X-direction).

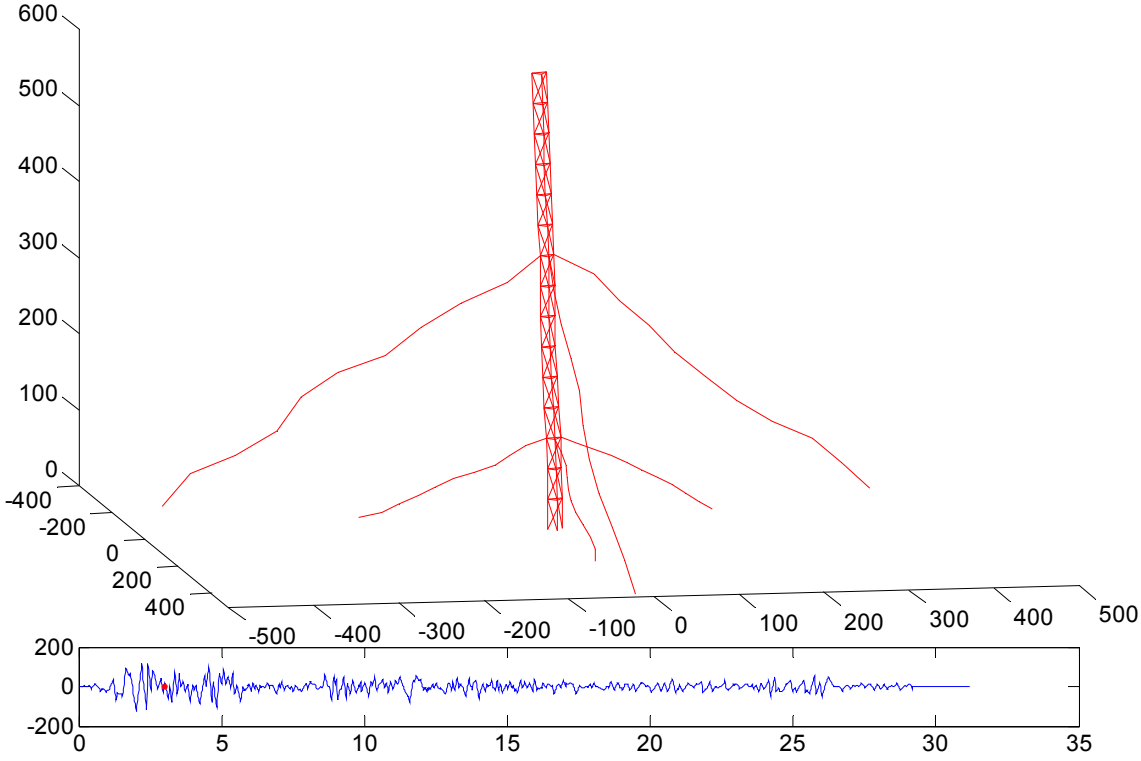

Figure 5.20 Tower deformation at t=3 second (in Y-direction).

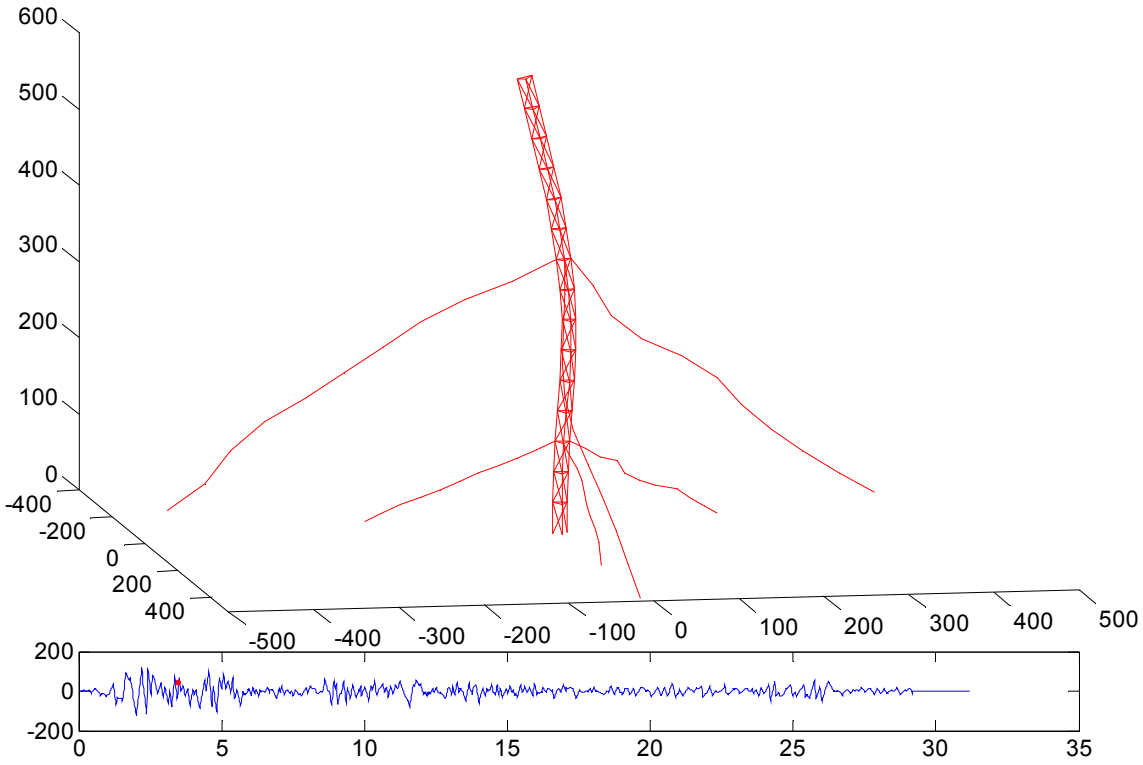

Figure 5.21 Tower deformation at t=3.5 second (in Y-direction).

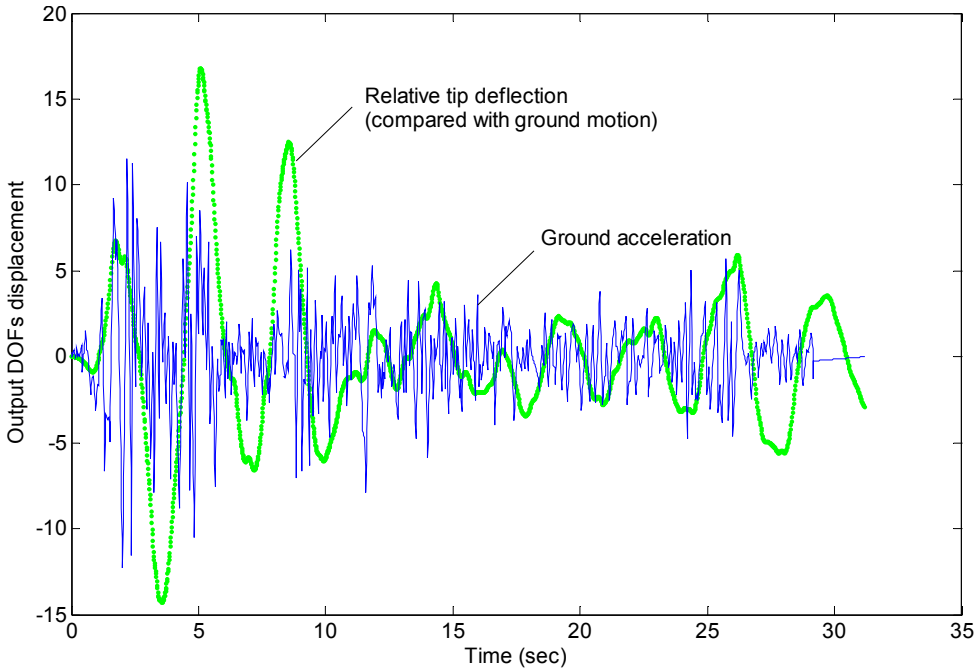

Figure 5.22 Time trace of relative tip deflection (in Y-direction).

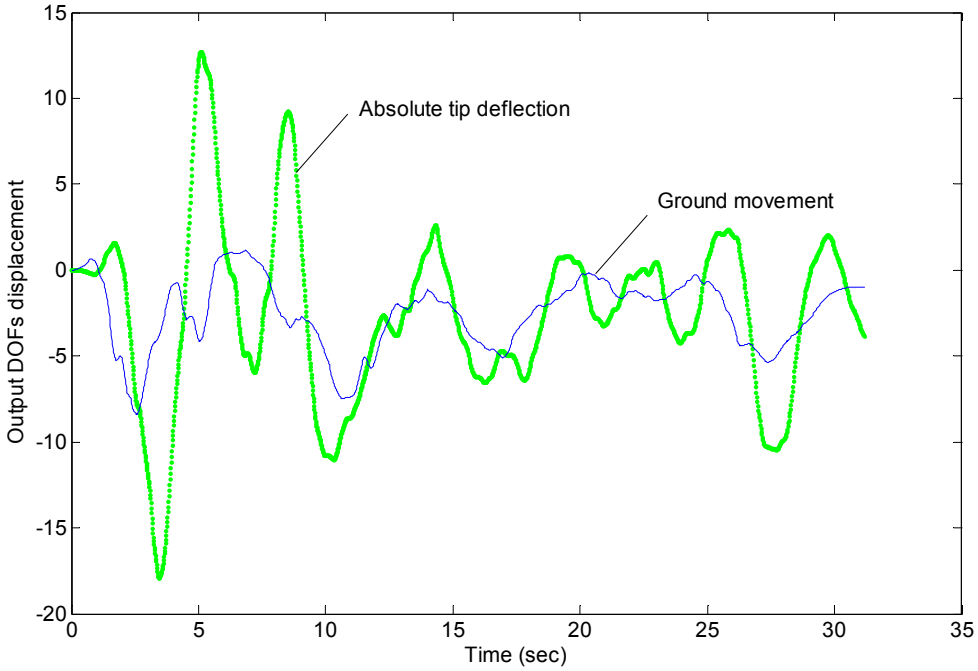

Figure 5.23 Time trace of absolute tip deflection (in Y-direction).

5.4 Nonlinear static analysis of a 100 m guyed tower

With the increase of height of the tower, the cables are inevitably sagged due to the self-weight. To explore the nonlinearity that was introduced by the sag of the cables, a 100 m high guyed tower is simulated. The poles and struts in the mast arm are composed of steel bars. Corresponding Young's modulus is 199×10^9 Pa. The steel pipes that constitute the poles have an outside rim diameter of 10cm and an inside rim diameter of 4cm. The plane section of the mast is an equilateral triangle similar to Fig 5.2(b). The side length of the triangle is 20cm. The prestress forces in all the three layers of cables are 100 N. All struts' and cables' diameters are assumed to be 4cm. The section detail can be seen in Fig 5.24.

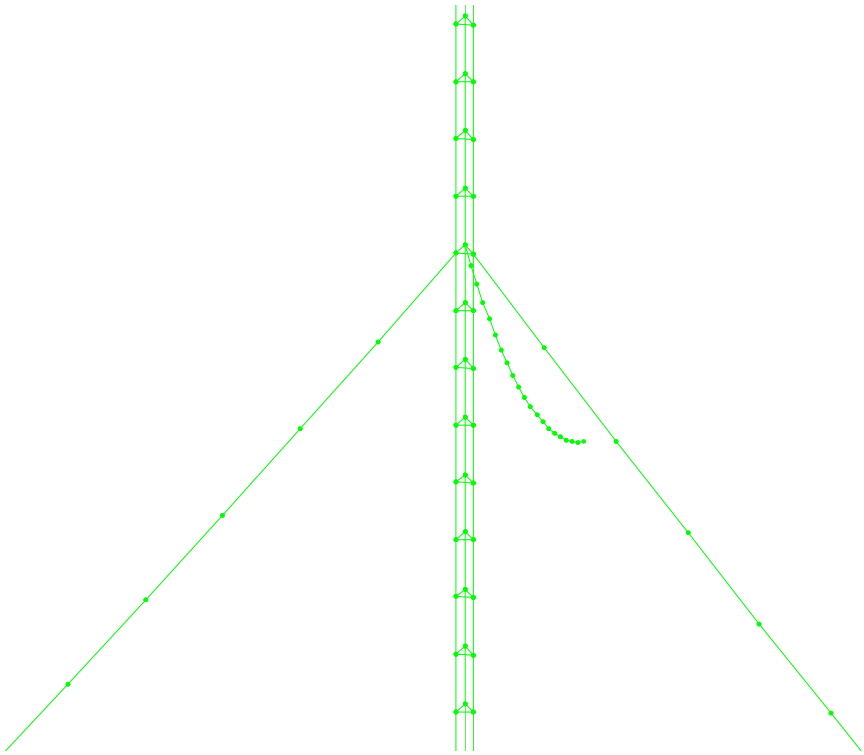

Figure 5.24 Detailed section of the guyed tower.

After the entire load steps, the deformed geometry of the tower is shown in Figs 5.25 and 5.26. The load deflection curve for the tip of pole is as shown in Fig 5.27. At the beginning, the lateral force just tightens up the slacken cables. After that, load deflection curve's slope climb sharply because of the lateral support from the stressed cables.

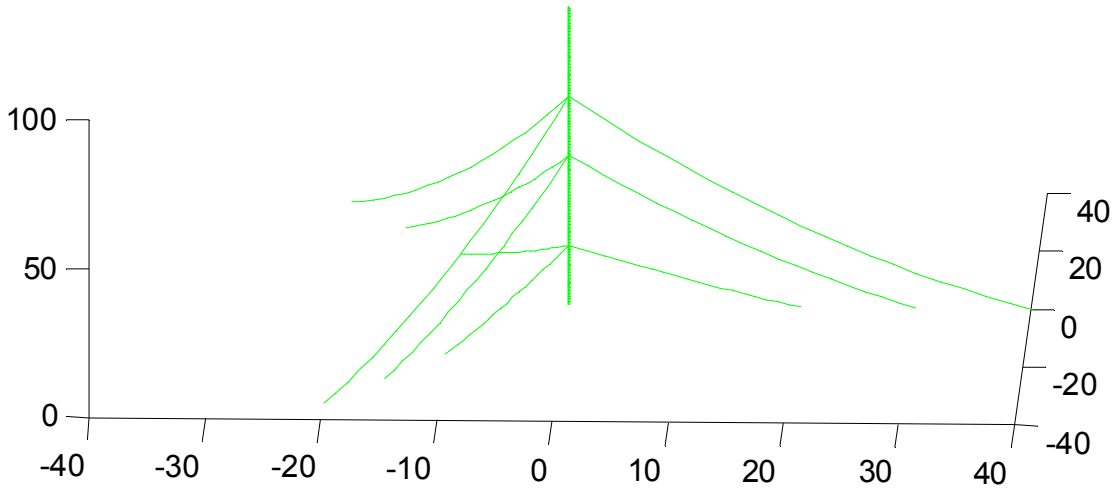

(a)

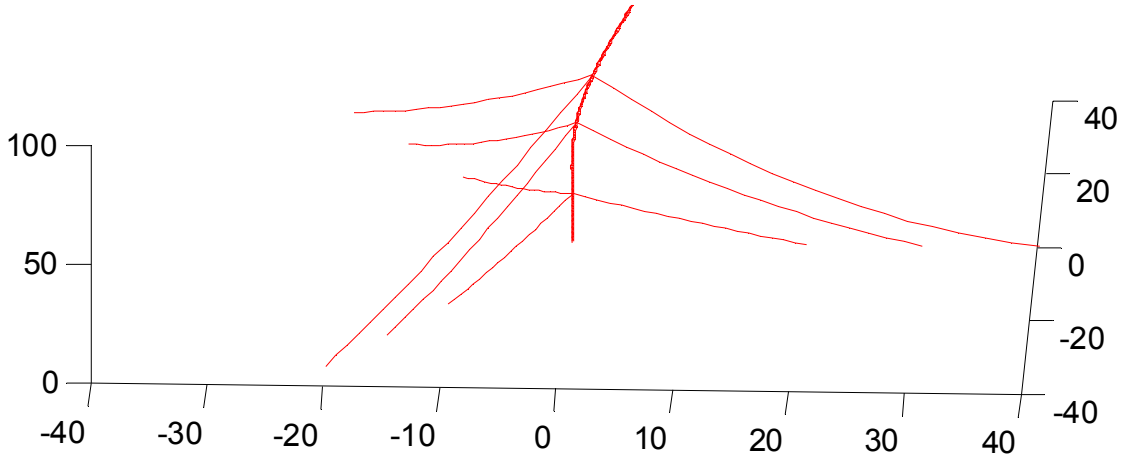

(b)

Figure 5.25 (a) The undeformed geometry, and (b) the deformed geometry of a 100 m guyed tower.

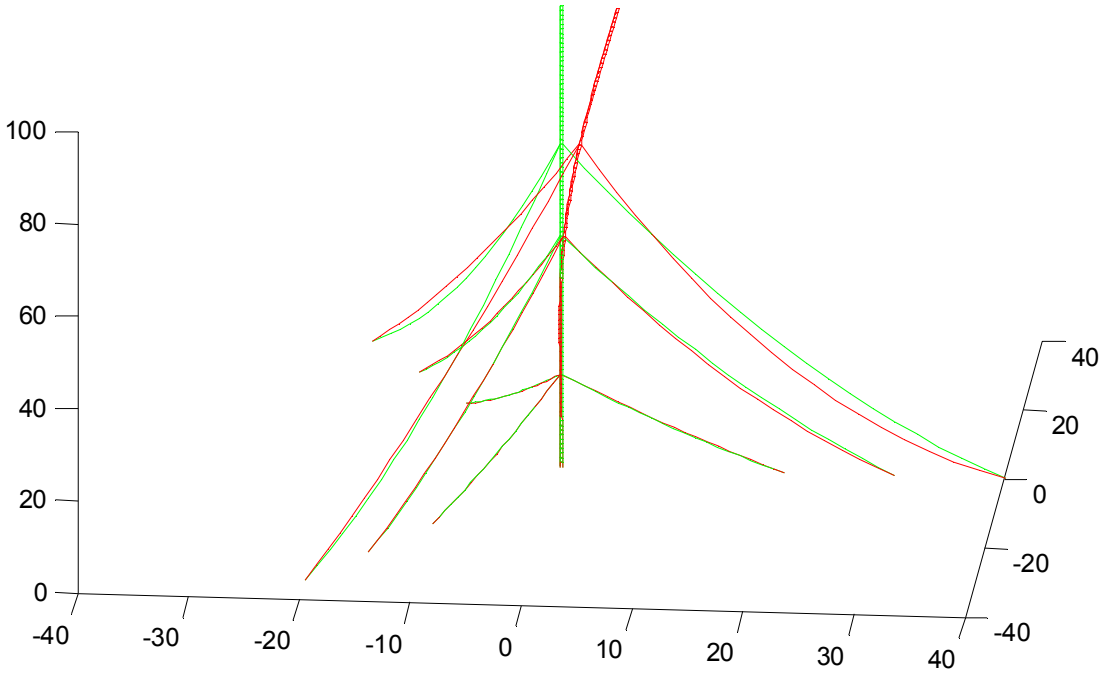

Figure 5.26 Deformed and undeformed geometres of a 100 m guyed tower.

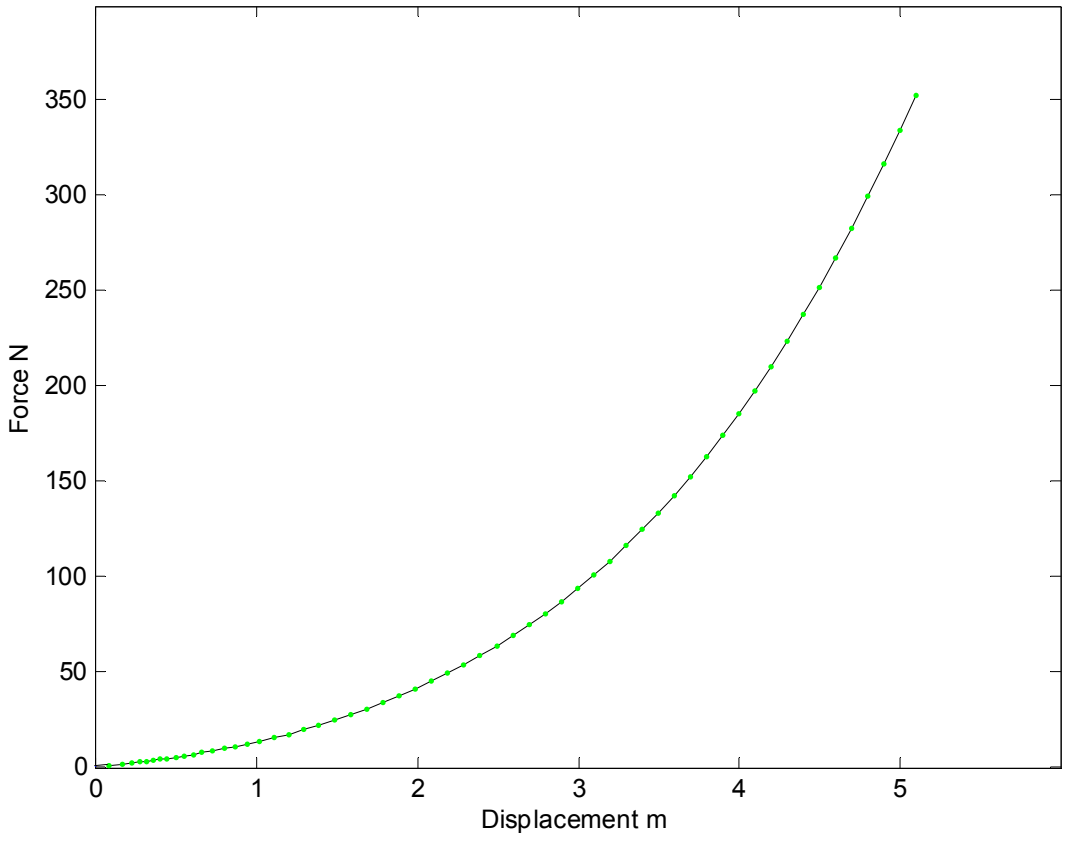

Figure 5.27 Load deflection curve of the tip.

5.5 Nonlinear dynamic analysis of a 100 m guyed tower

If the same tower is subjected to the EI Centro earthquake in X-direction, as shown in Fig 5.11(a), the responses at different instants are shown captured in Figs 5.28-5.42. With the passing of time, the tower is agitated by the ground motion gradually. In the first two seconds, there is little deformation (Figs 5.43 and 5.44). Significant deflection in the mast appears after 3 seconds. The entire computation is very intensive because all the elements used here are nonlinear. It took more than 24 hours for a single round computation. Due to this reason, the time trace for the tip deflection is terminated around 10 seconds, which already used 6,000 iterations.

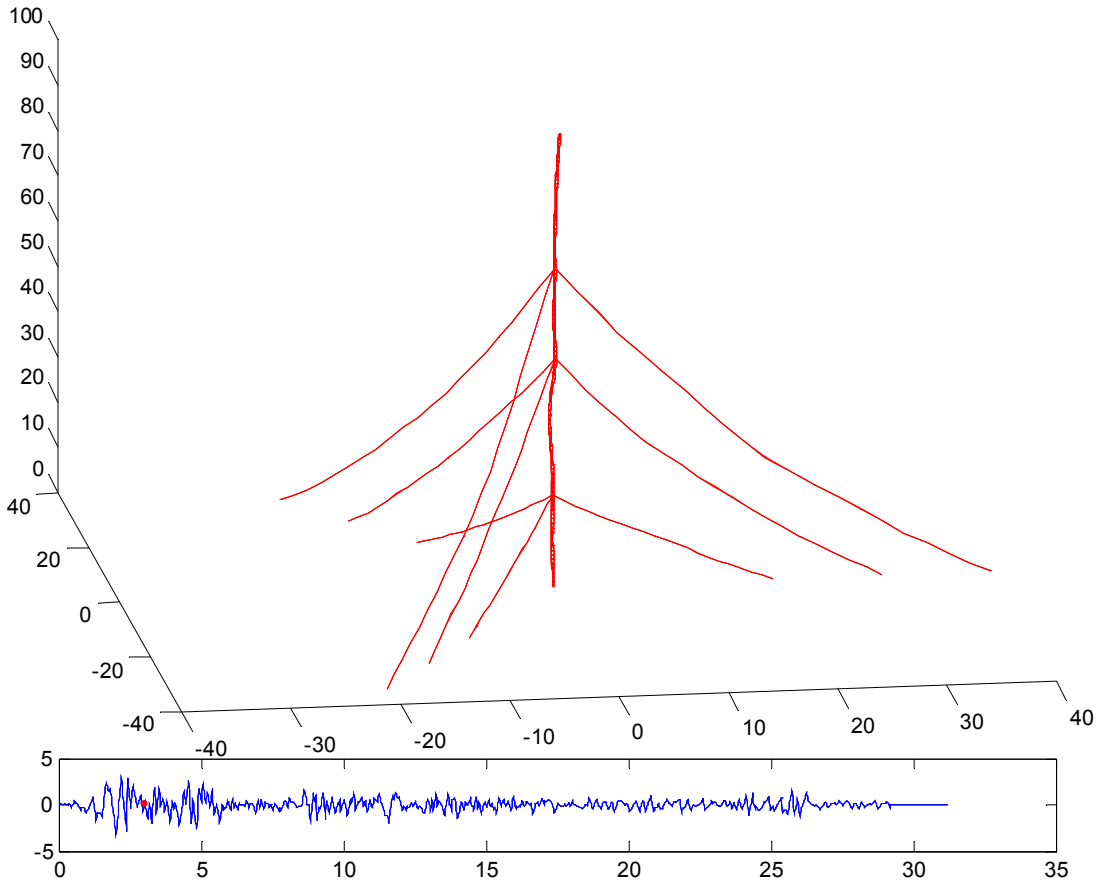

Figure 5.28 Response at t=3.0 second.

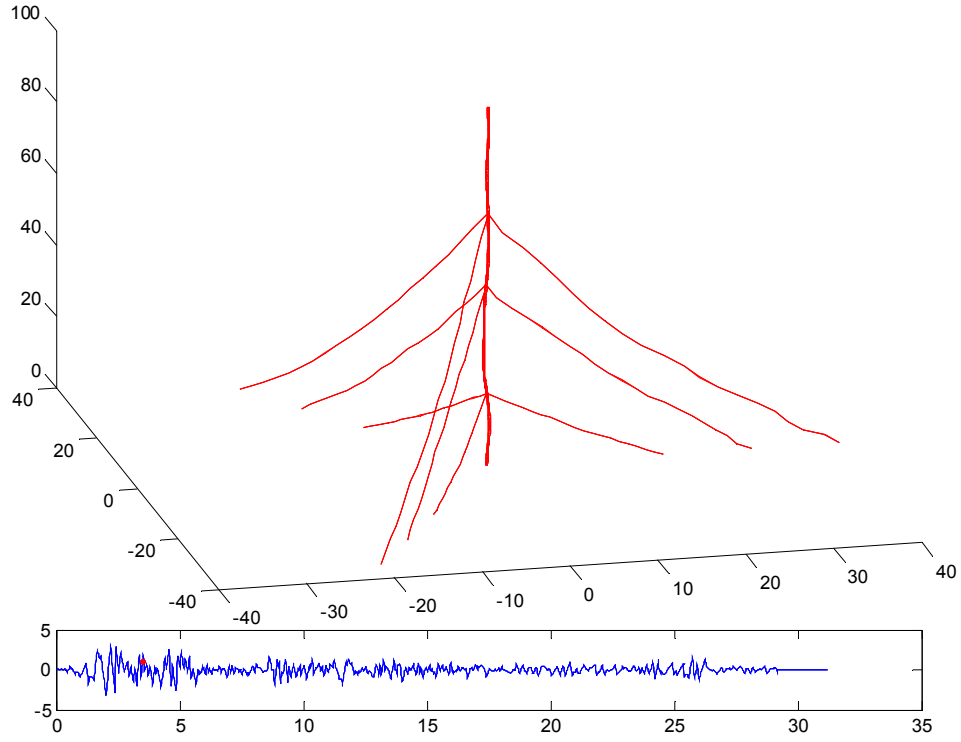

Figure 5.29 Response at t=3.5 second.

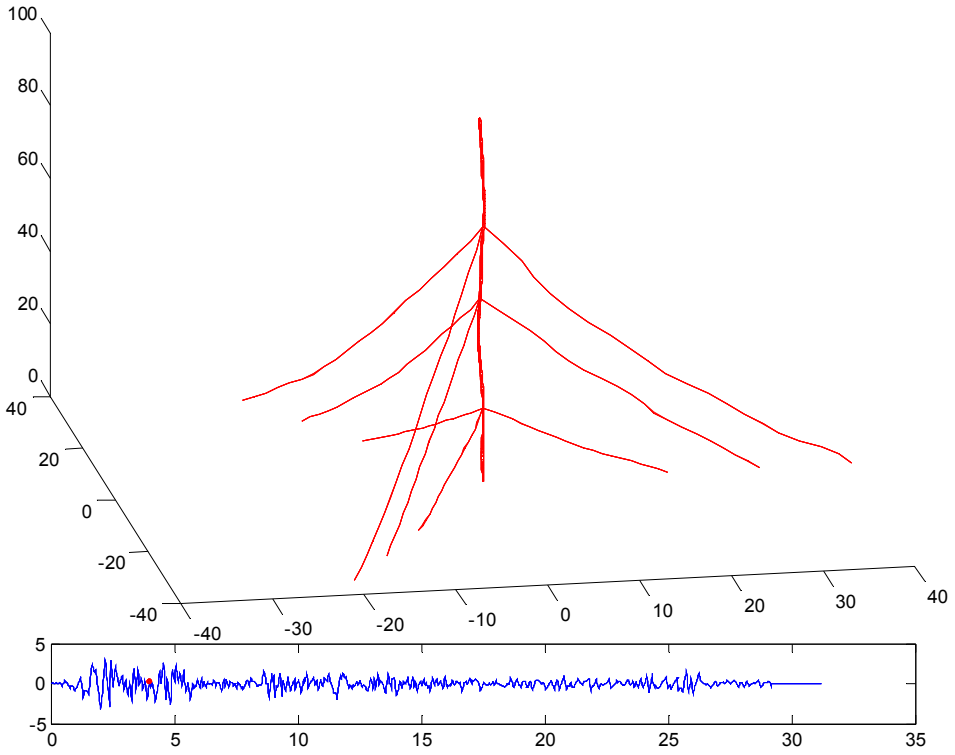

Figure 5.30 Response at t=4.0 second.

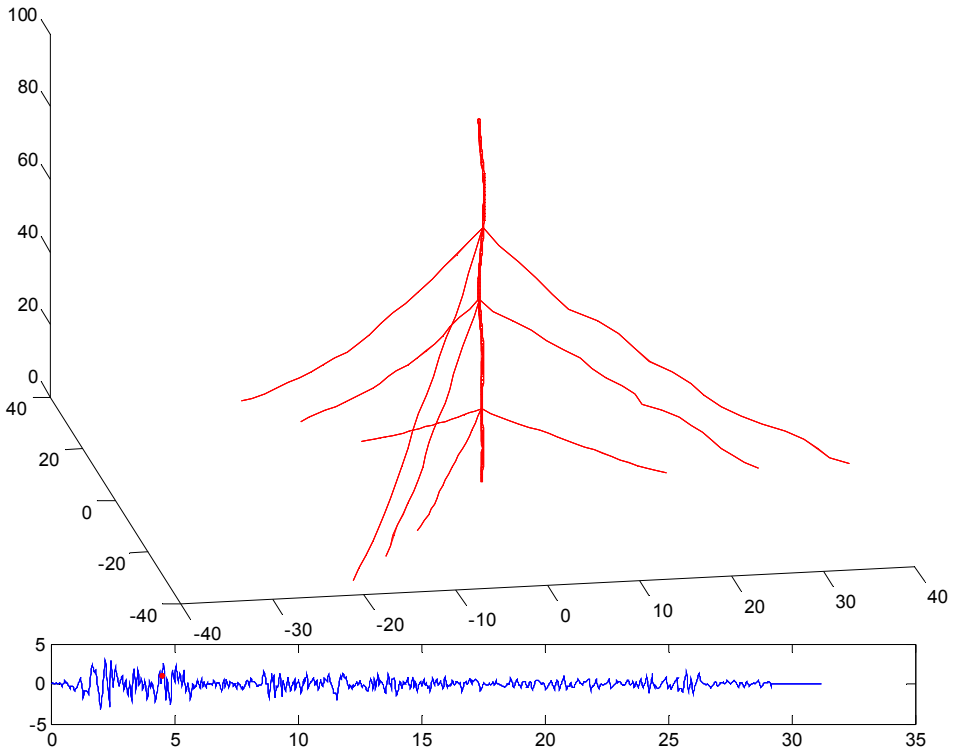

Figure 5.31 Response at t=4.5 second.

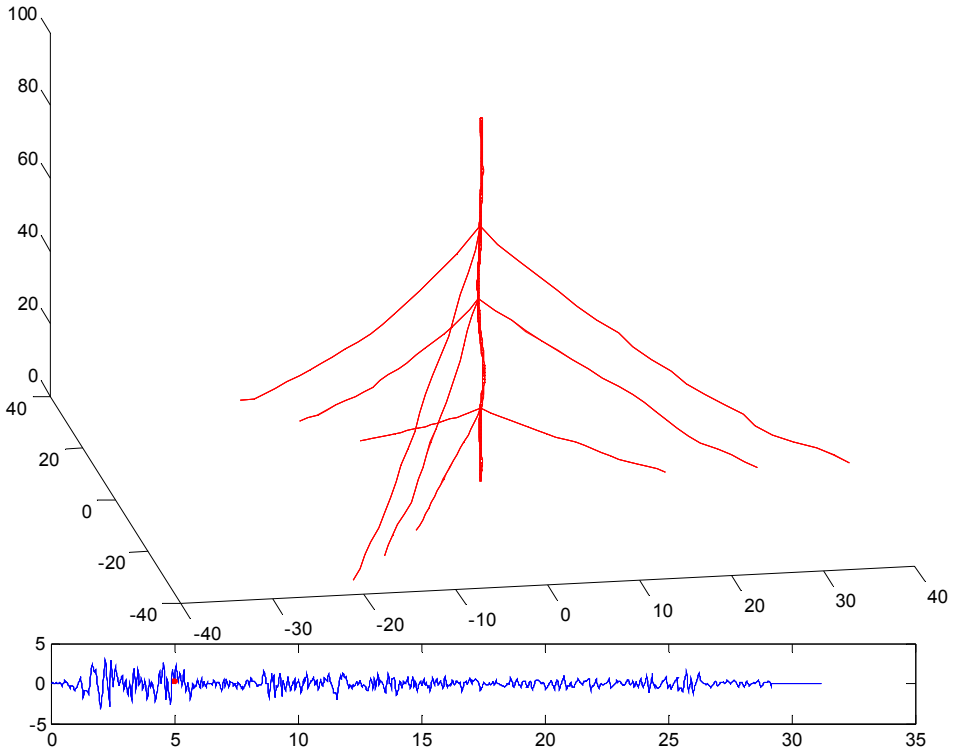

Figure 5.32 Response at t=5 second.

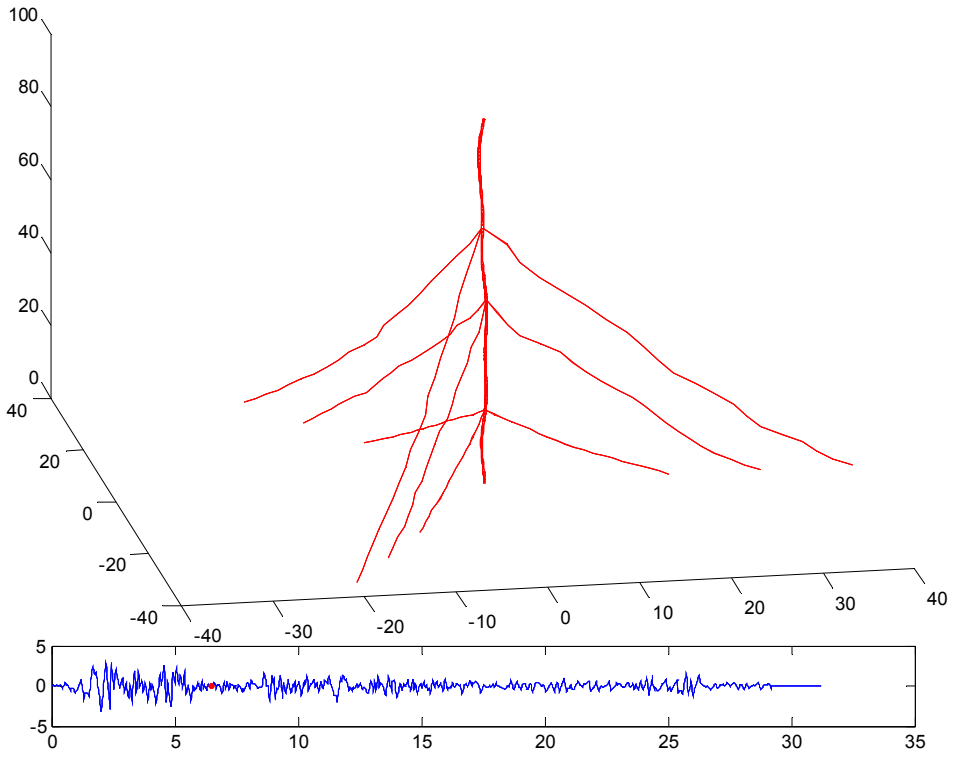

Figure 5.33 Response at t=5.5 second.

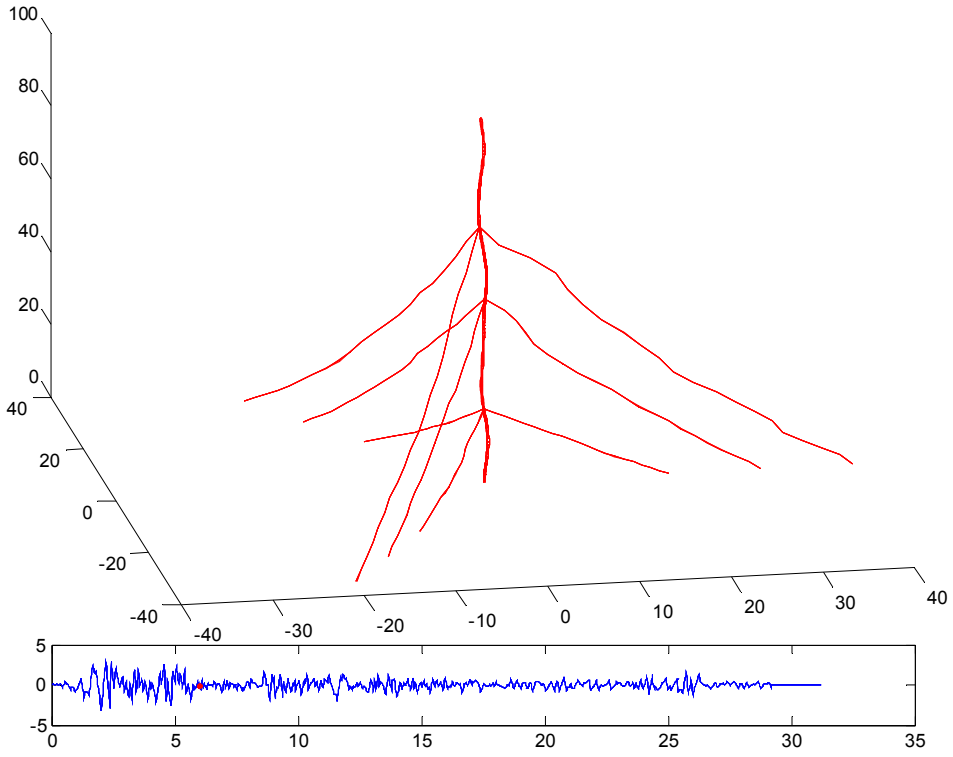

Figure 5.34 Response at t=6 second.

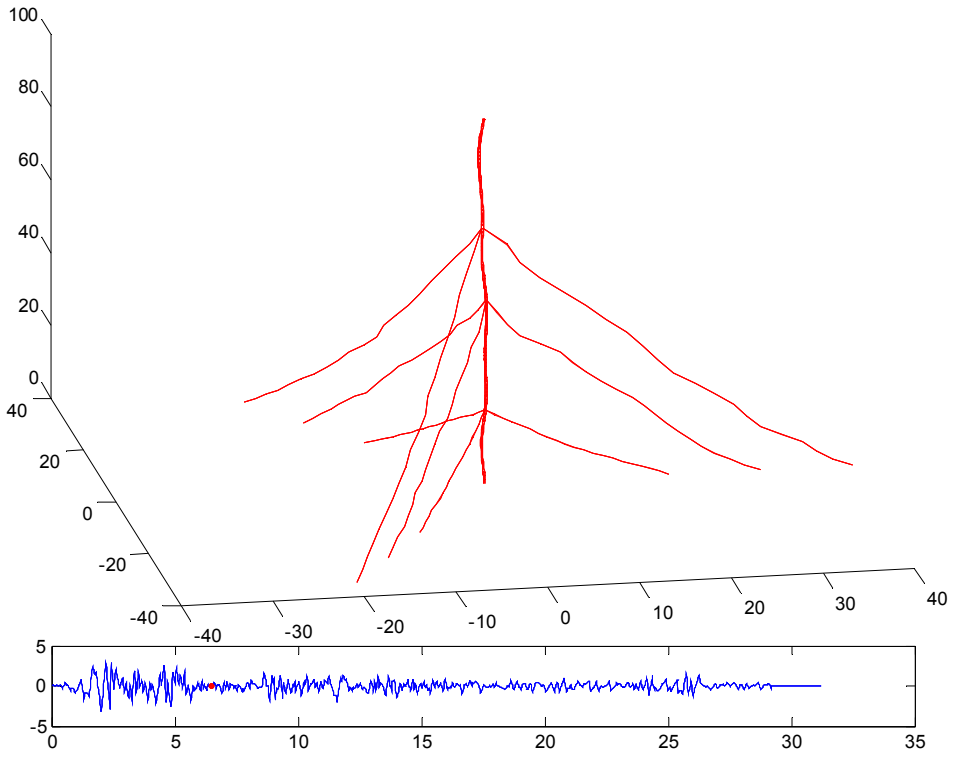

Figure 5.35 Response at t=6.5 second.

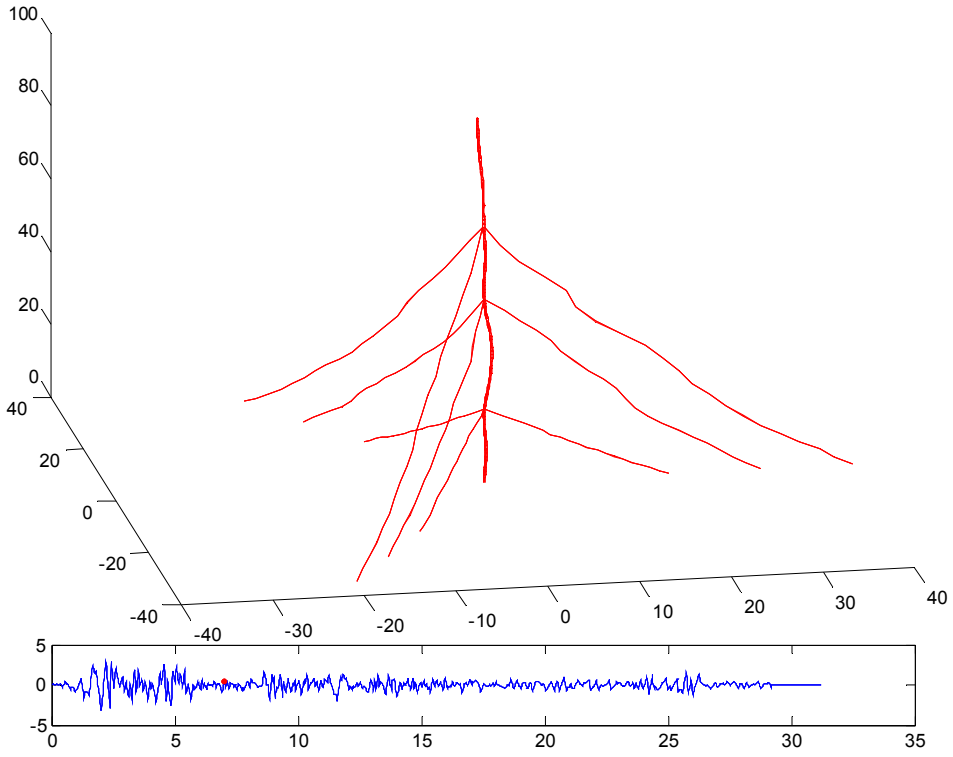

Figure 5.36 Response at t=7 second.

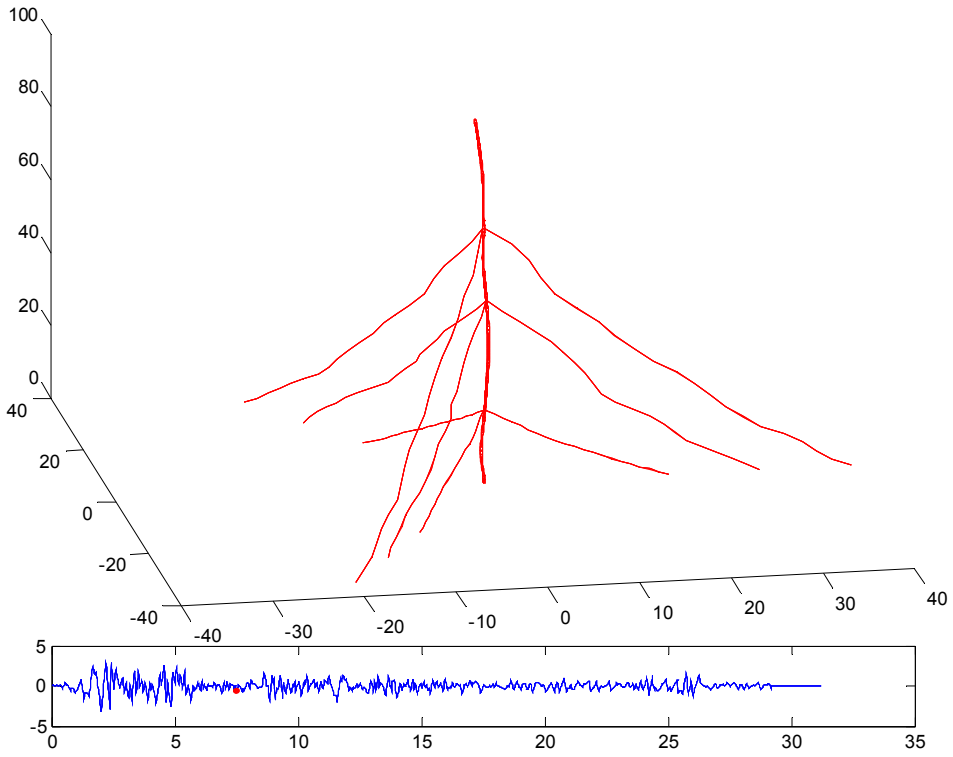

Figure 5.37 Response at t=7.5 second.

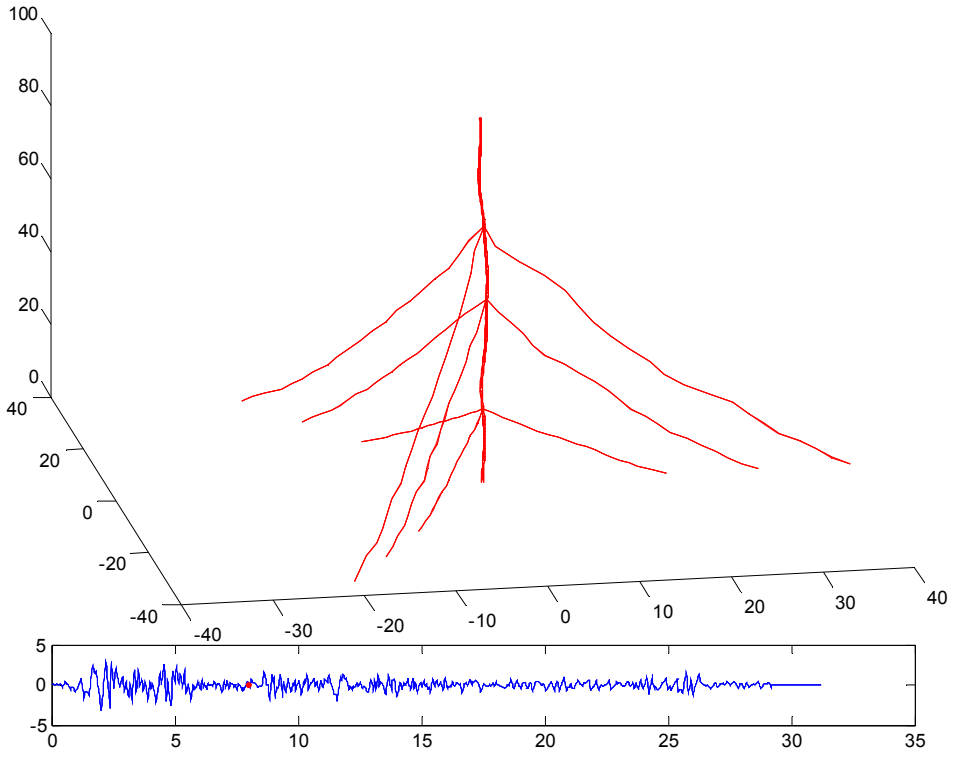

Figure 5.38 Response at t=8 second.

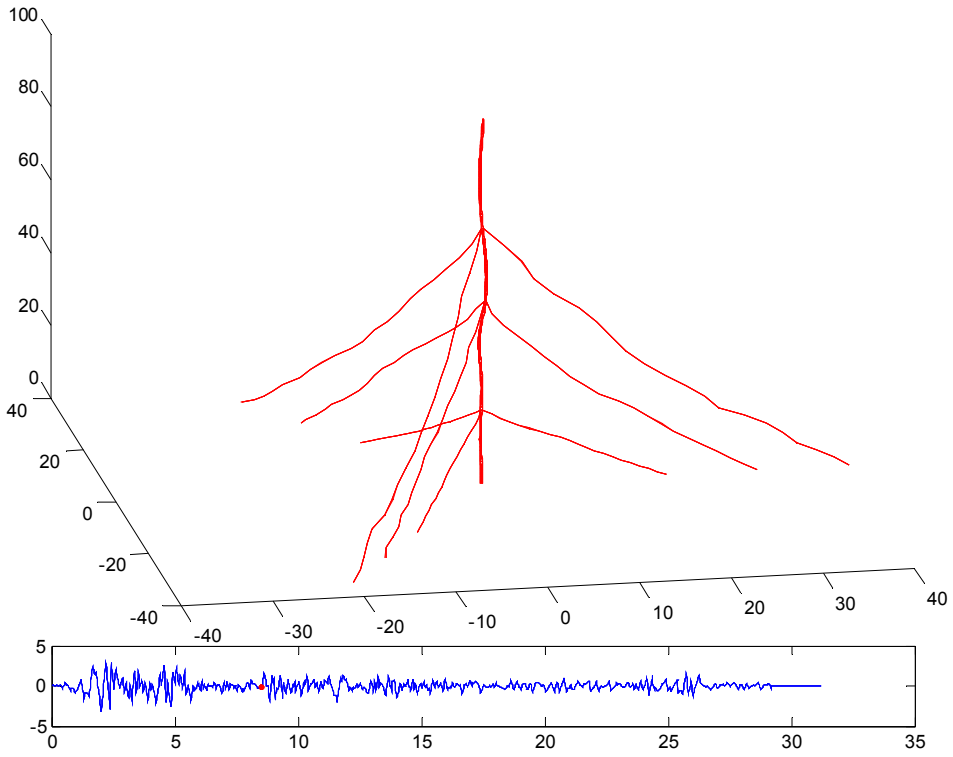

Figure 5.39 Response at t=8.5 second.

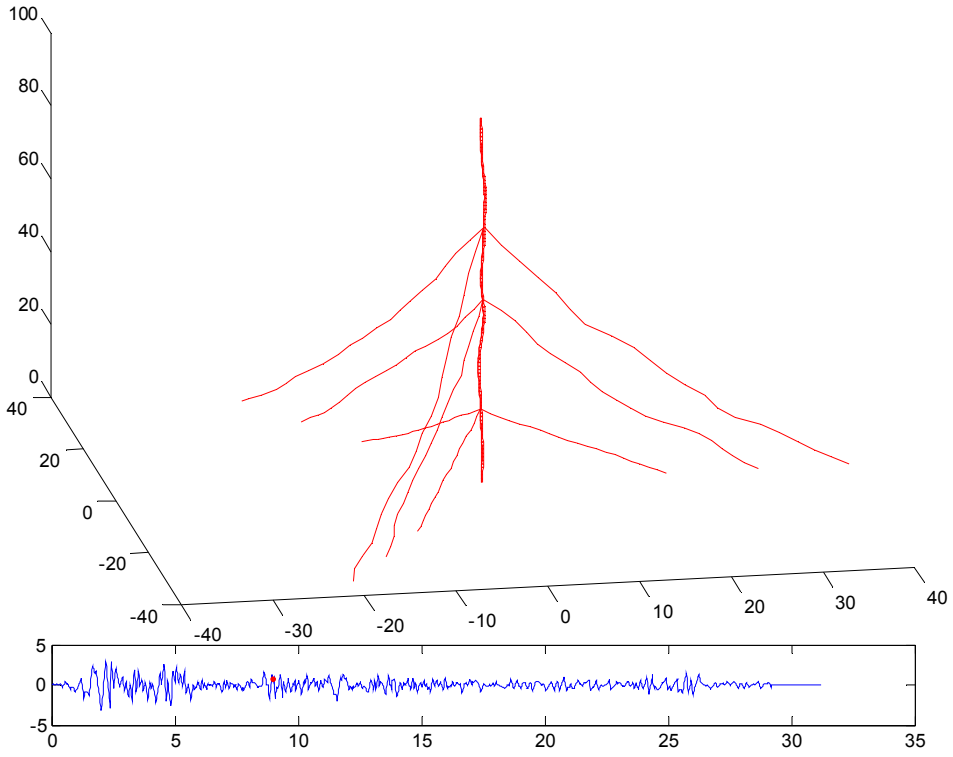

Figure 5.40 Response at t=9 second.

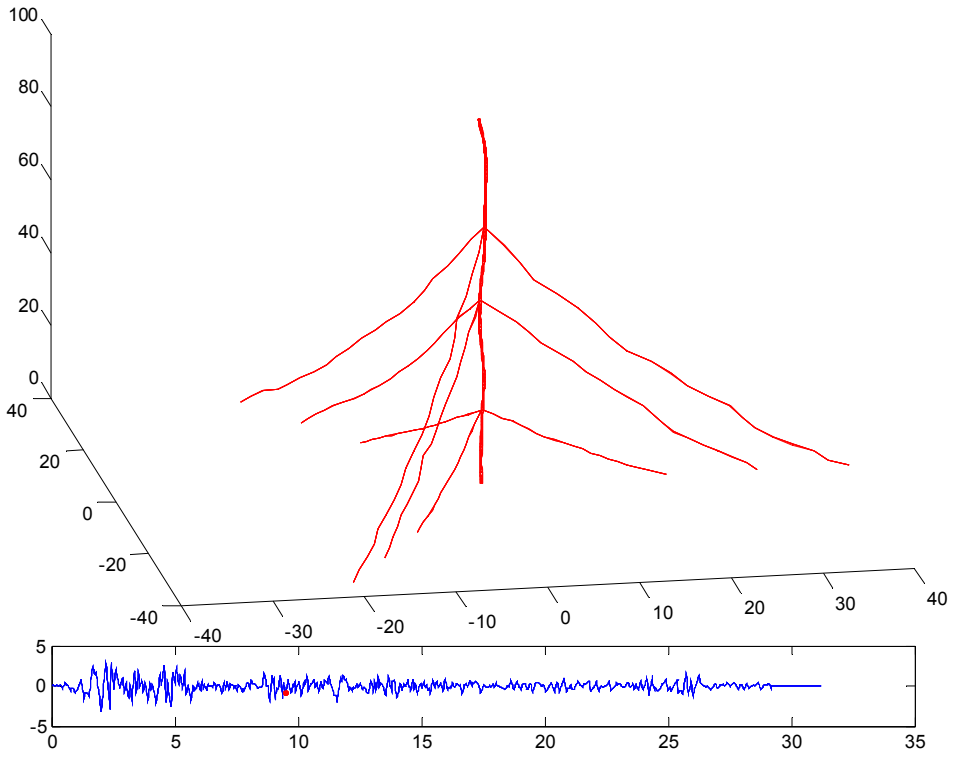

Figure 5.41 Response at t=9.5 second.

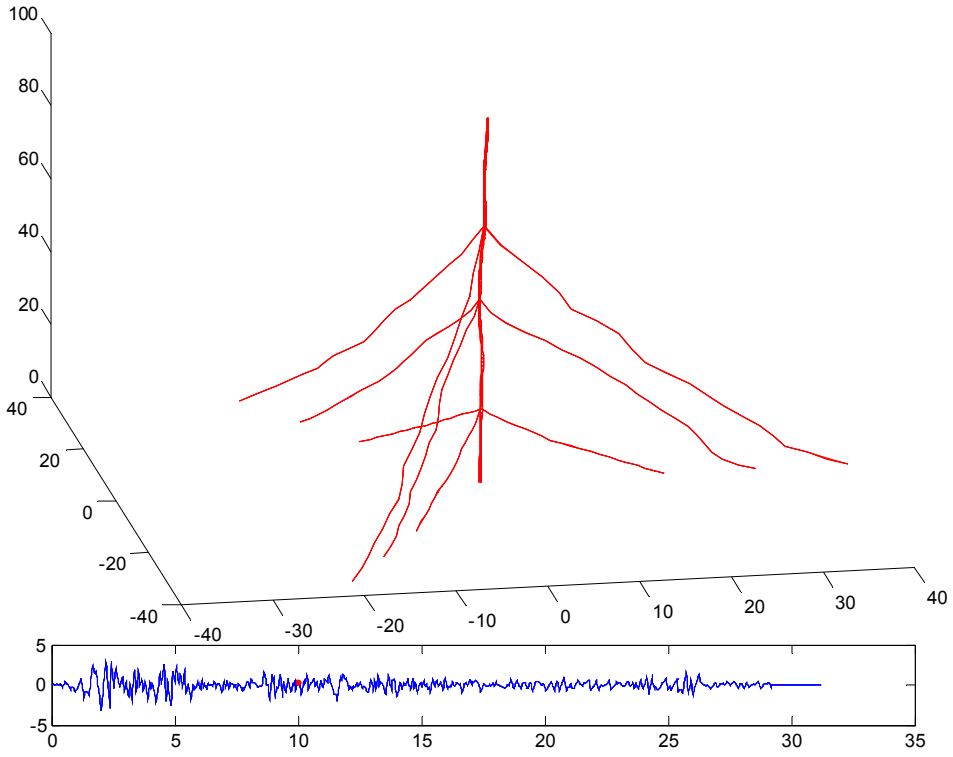

Figure 5.42 Response at t=10 second.

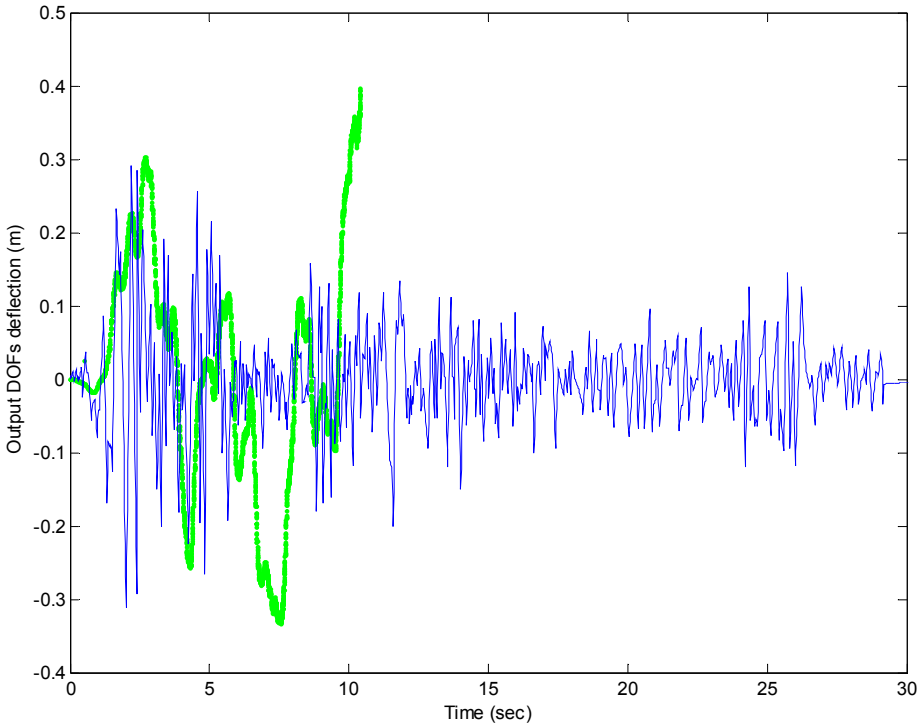

Figure 5.43 Time trace of the relative tip deflection.

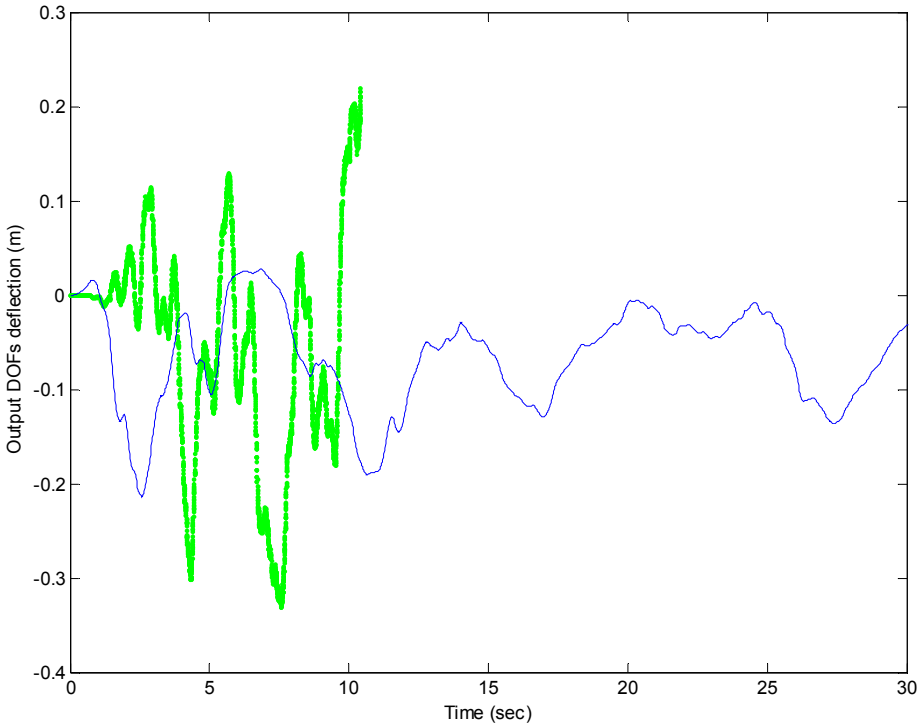

Figure 5.44 Time trace of the absolute tip deflection.

5.6 Geometric and Material Nonlinear static analysis of a 50 ft guyed tower

If the tower in Fig 5.1 is composed of truss and cable elements, the structure is stiffened as shown in Fig 5.45. When isotropic hardening effect is included in the simulation, the stiffness of the structure is decreased because some members yield with the increase of load. Truss member as element 7 is yielded with compression. The stress strain curve is shown in Fig 5.46. The stress-strain curves of truss elements 40 and 180 are shown in Figs 5.47 and 5.48. The upper two layers of cables are also yielded. The locations of yielded members are shown in Fig 5.49.

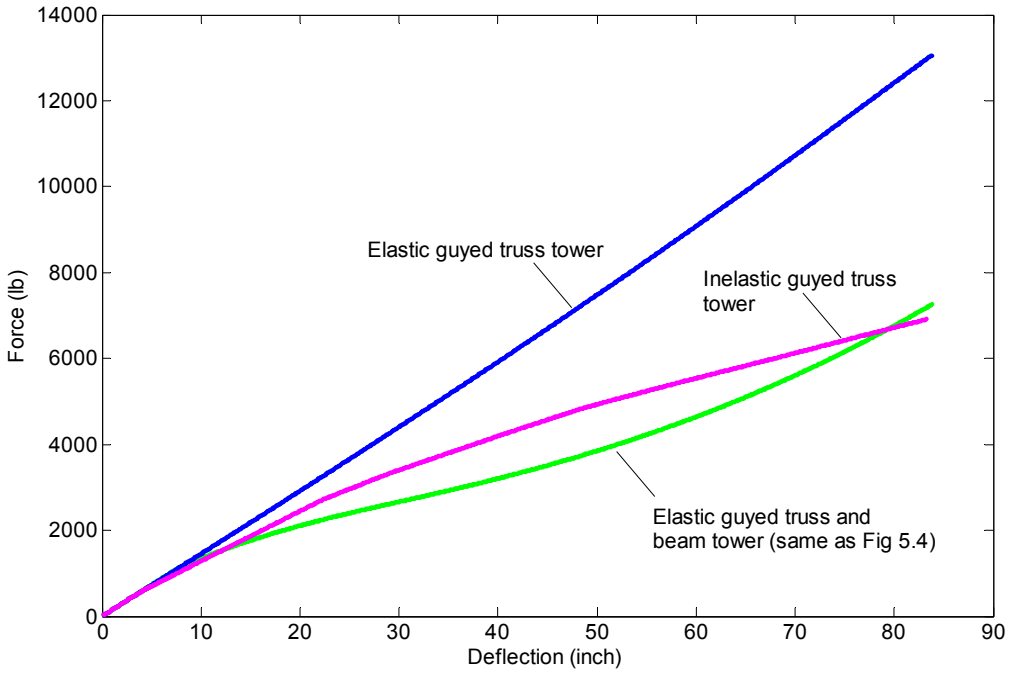

Figure 5.45 Comparison of load-deflection curves.

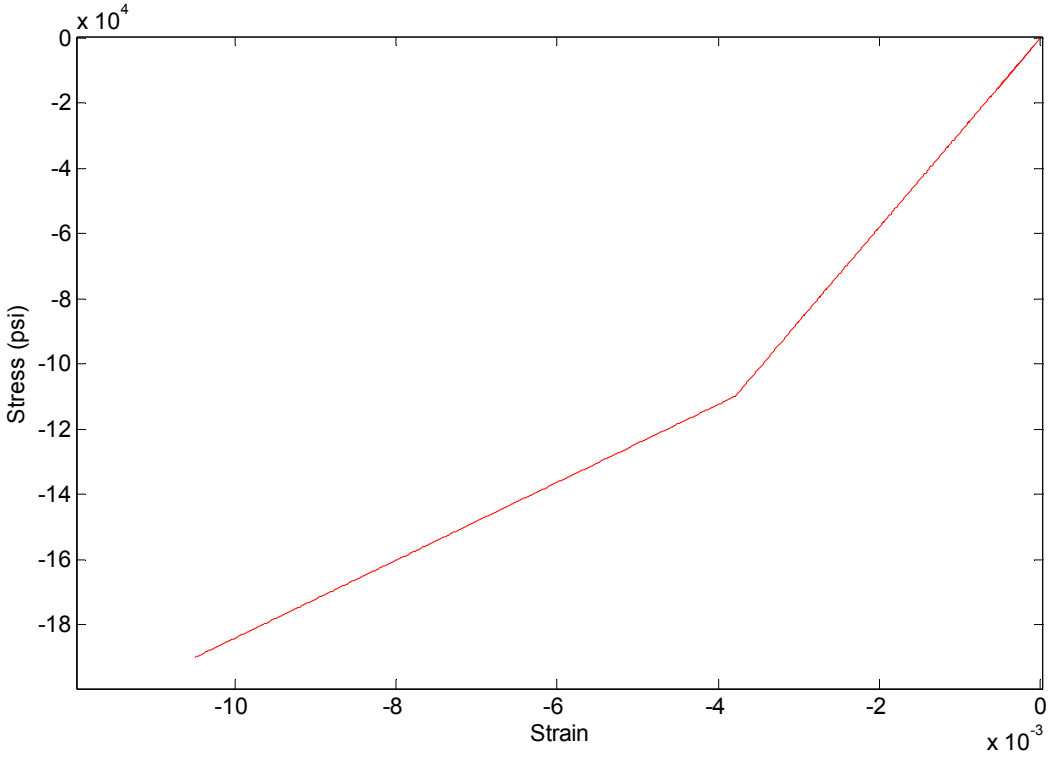

Figure 5.46 Stress strain curve of 7th element.

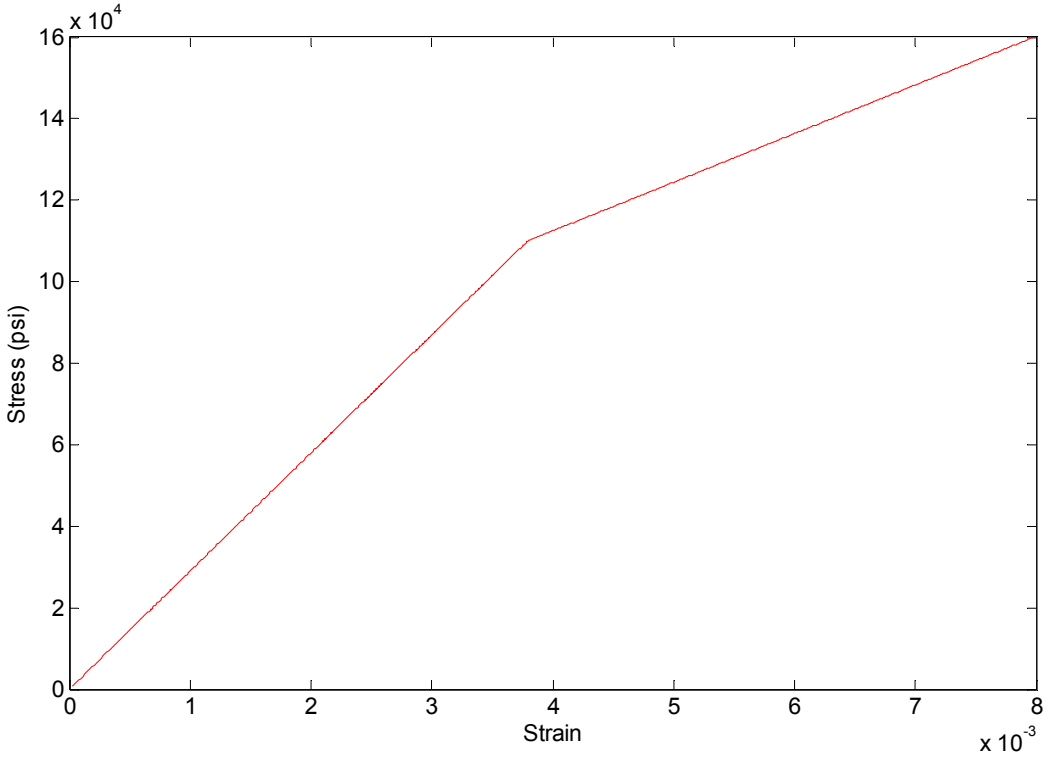

Figure 5.47 Stress strain curve of 40th element.

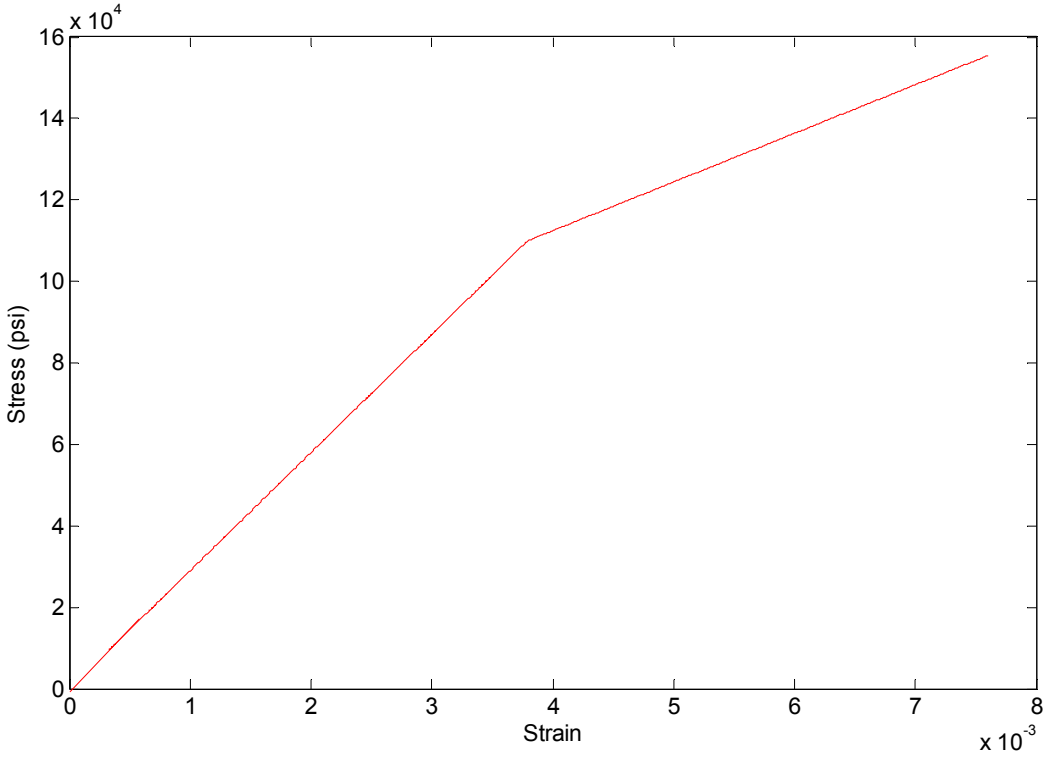

Figure 5.48 Stress-strain curve for 180th element.

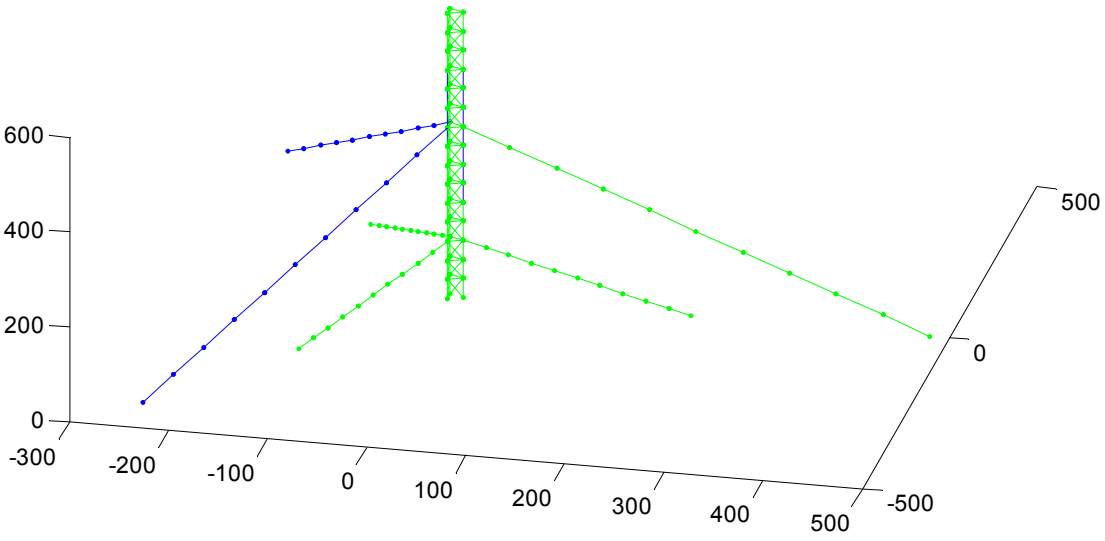

Figure 5.49 Yielded member locations in the tower.

5.7 Summary

With proper elements and algorithms, the nonlinear static and dynamic responses were accurately traced. Consideration of material nonlinearity along with geometric nonlinearity further closed the gap between analysis and reality.

The comparison of taut guyed towers under static loads shows that their results are similar when deflection is small. The release of constraints in rotation and deflection on the supports for the equivalent beam method can greatly improve the analysis accuracy. The different transited angle of seismic wave can result in different amplitudes of vibration. But the response pattern is similar.

For high guyed towers, computation becomes more intensive due to the size of stiffness matrix. It is found that at the beginning of deflection, the structure is relatively soft because the cables do not provide lateral support. With the increase of deflection, the cables are gradually tightened up and can restrain the mast by tension force, which make the whole structure stiffer. In the dynamic analysis, the wave propagation in the mast is clear.

Under small deflection, the elastic model and the inelastic model predict the same results. But under large deformation, in which some of components become yielded, the results are very different. The inelastic structures appear softer than the elastic ones.

Chapter 6 Response under Impulsive Load

Towers are open space structures that generally do not intercept shock front waves passing through them. So impulse load on any member of a tower is usually much lower than close space structures'. However, for large scale guyed towers, the leg member's size is much larger than normal guyed towers. If the impulsive load is intensive enough, certain damage can be caused. So there is a need for large towers to be evaluated for their possible damage or failure mechanism under impulsive load in order to prevent it.

This chapter will first discuss the proper evaluation methods for impulsive loads on individual members in the guyed towers. The P-I diagram method is then applied and developed for the further safety evaluation of members of towers. Global stability will be explored finally to accomplish the global safety evaluation.

6.1 Impulsive load estimation

There are three types of blast wave structure interaction (Smith and Hetherington, 1994). The first one is for a large structure and large scale blast wave, which is usually intrigued by nuclear weapons. The blast wave will reach and reflect on the front surface of the structure. At the same time, it will diffract around the sides and the rear face of a building. Finally, it will engulf and crush the structure. The duration can usually be counted by seconds. The major part of interaction is diffraction. The second type of interaction is for small size structure and large blast wave. The shock wave will squash and damage the structure as well. But the main impulsive effect is the drag effect. The third one is for a large structure under small size blast wave. The

size of the structure causes the delay of the applied impulsive load. So the actual loading is sequential.

When the tower is under consideration, the size of the tower can be large compared to the blast wave. But since the members are actual loading units, which are obviously small, the main impulsive effect on the tower members is drag effect.

Researchers (Brode, 1955; Henrych, 1979; TM5-1300, 1991; Bangash, 1999) have proposed various empirical estimations for impulsive loads. One of the evaluation methods (Bangash, 1999) is applied in this section. The overpressure P_{so} can be expressed as

$$P_{so} = 6784 \cdot \frac{W}{R^3} + 93\left(\frac{W}{R^3}\right)^{\frac{1}{2}} \tag{6.1}$$

where W = total charge weight in TNT (tonne)

R = stand-off distance to the detonation in meters

The reflected pressure is

$$P_R = 2P_{so} \cdot \left(\frac{7P_o + 4P_{so}}{7P_o + P_{so}}\right) \tag{6.2}$$

The ambient atmospheric pressure is $P_o \approx 1\,bar$. The reflected pulse time is

$$T_C = \frac{3S}{U} \tag{6.3}$$

where S = the smaller of half width and height of object

$U = \sqrt{\frac{6P_{so} + 7P_o}{7P_o}} \cdot a_o$, speed of shock front wave

$a_o \approx 340\ m/s$ speed of sound in air at ambient pressure

The shock pulse duration

$$T_B = \begin{cases} 9.04\left(\frac{W}{P_{so}}\right)^{\frac{1}{3}} & when\ P_{so} < 2\ bar \\ 14.35\frac{W^{\frac{1}{3}}}{P_{so}} & when\ P_{so} \geq 2\ bar \end{cases} \tag{6.4}$$

The drag coefficient for the rear face varies from -0.25 to -0.5. The drag coefficient for the front face varies from 0.8 to 1.6.

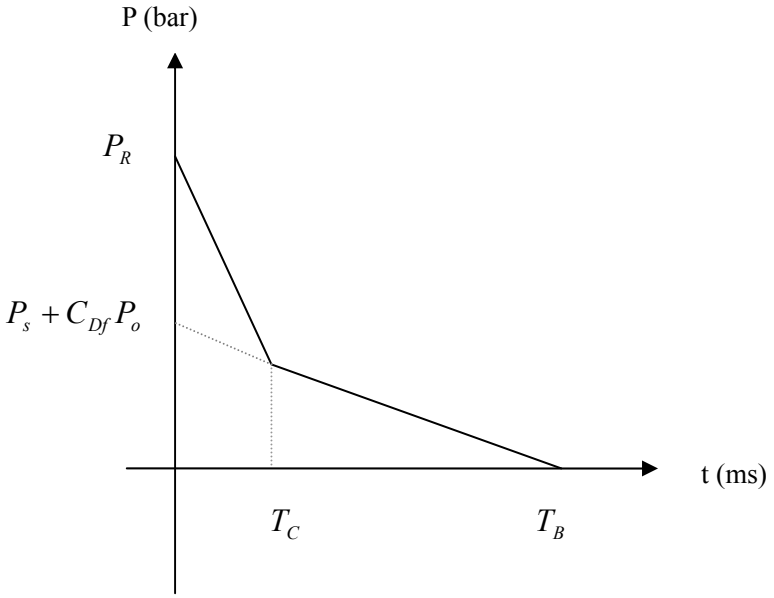

Figure 6.1 Pressure on the front surface.

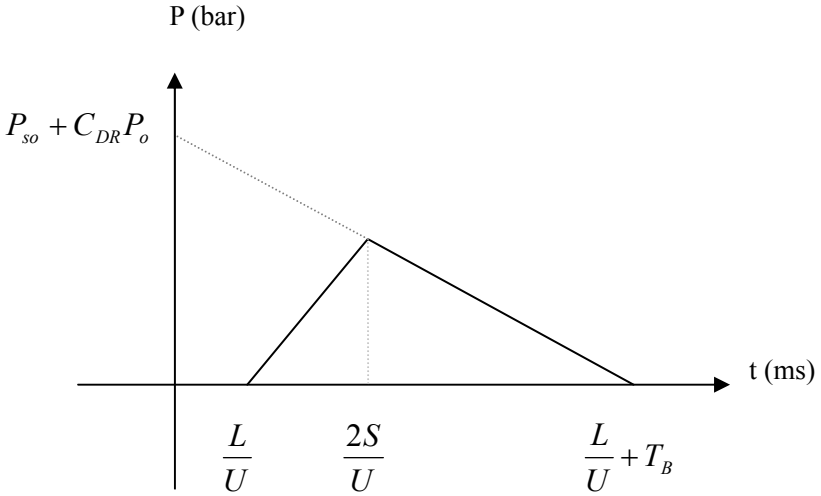

Figure 6.2 Pressure on the rear surface.

To illustrate the impulsive load on the members of tower, three loading cases (Figs. 6.3- 6.5) are considered. The member is assumed to be 0.1 m wide and 0.4 m high in the cross section. It can be seen with the increase of load intensity, the duration of drag phase is shortened. The reflected pressure is dropped while the instant pressure on the front face increased. The dramatic change happens on the rear surface. For lower but longer impulsive load, the drag effect by aerodynamics overcomes the instant pressure so that the net effect is to pull the member toward the blast wave direction. When the load gets increased, the net effect is close to zero because the magnitude of drag force is almost the same as instant pressure. With the further increased load, the instant pressure dominates and the pressure on the rear surface will push back the deflected member toward the source to the shock front wave.

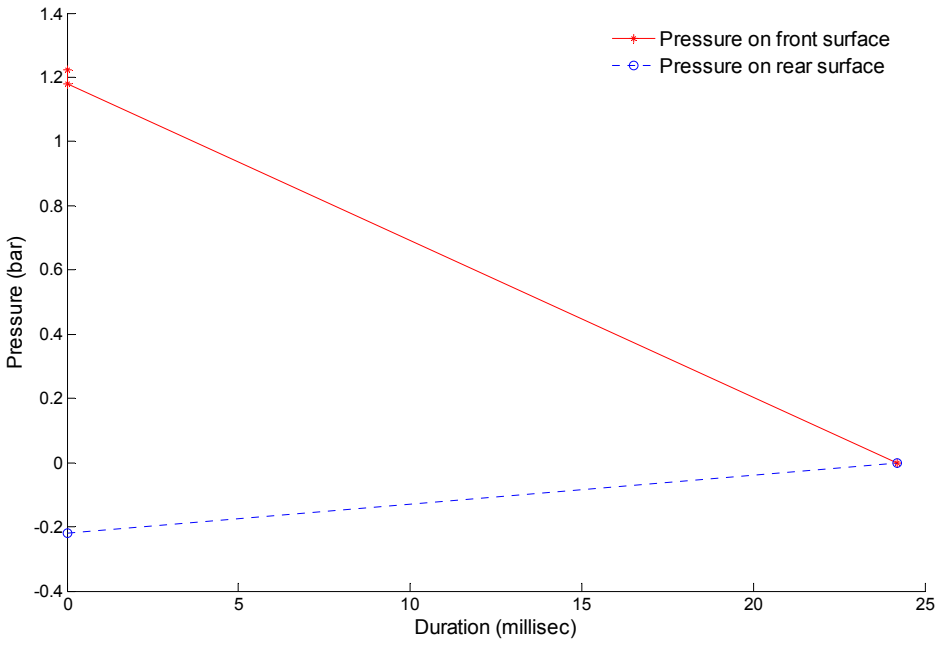

Figure 6.3 Pressure on the front and rear surface for 1 ton TNT at 70 m stand-off distance.

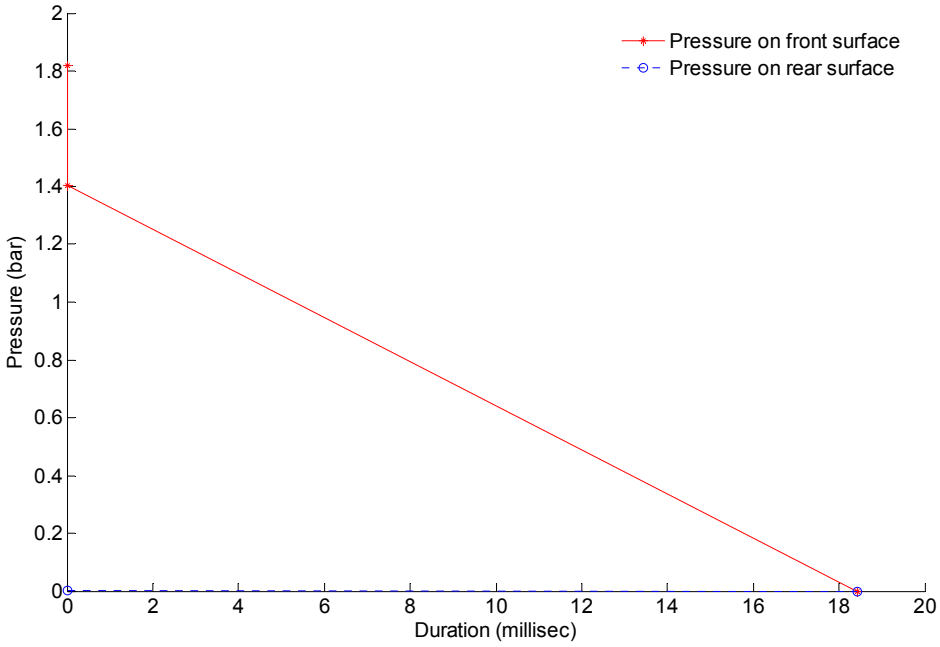

Figure 6.4 Pressure on the front and rear surface for 1.5 ton TNT at 50 m stand-off distance.

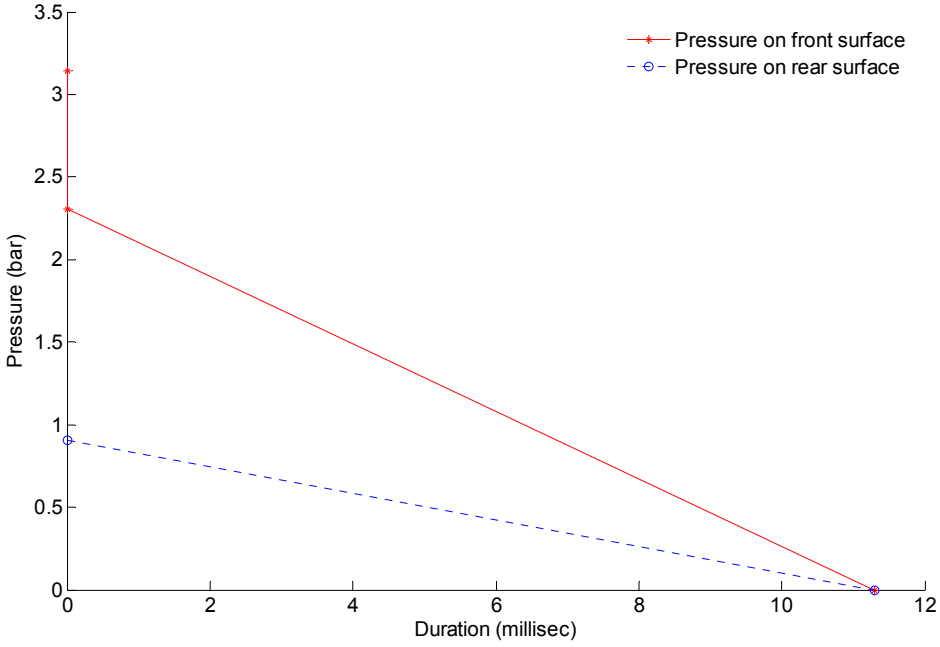

Figure 6.5 Pressure on the front and rear surface for 2 ton TNT at 30 m stand-off distance.

6.2 Impulsive response of members

In this section, the characteristic of bending failure and shear failure is discussed. With the adoption of damage criteria for shear failure and bending failure of beams (Krauthammer, 2004), the critical standard for the discrimination of both failure types are determined. A closed form of theoretical solutions for simply supported and fully clamped beams are then presented. P-I diagrams are subsequently used to assist the discrimination of failure. Comparisons of the threshold of shear failure and bending failure are conducted after the simplification of critical discriminants. The difference between the results of the two theoretical models is further discussed.

Under explosion loads most beams in the buildings fail due to insufficient bending capacity. The failure zone usually locates at the center of the beams due to excessive bending deformation (Fig 6.6 (a)). Such response is usually analyzed using a SDOF model. The beam will be simplified as a single mass vibrating under the stimulation of impulse loads (Biggs, 1964; Smith and Hetherington, 1995). The maximum displacement is selected as the fatal factor, which determines the safety of beams. The P-I diagram is applied to present critical status of beams in bending failure because of its straightforward expression form (Abrahamson and Lindberg, 1976; Smith and Hetherington, 1995; Li and Meng, 2002).

A SDOF model represents the beam as a whole and neglects the influence of shear force, which subsequently leads to the ignorance of shear failure. However, shear failure usually happens when the ratio of span to height of the beams is very small or when the detonation is very close to the structures. Compared with bending failure shear failure is sometimes brittle failure and may cause severe collapse of structures. The failure zone usually is at the sides of the beams because the maximum

shear force exists at both sides (Fig. 6.6 (b)).

Based on experimental observations and mathematical derivation, Jones (1989) developed five possible deformation profiles of beams under impact loads (Fig. 3.3). The impact is simplified as an ideal impulse that is applied to the beam with no time duration. Li and Jones (1995) improved the study by considering the response of beam during impulse load duration and put forward the standardized expression of critical deformation. Ma *et al* (2006) further studied the response and developed P-I diagram equations for rigid-plastic beams under rectangular blast loadings. However, most results are expressed in an implicit form and can't be used directly in a specific computation.

In this study, the shear force of beams is considered in another theoretical model (Fig. 6.7). The performance of beams under impulse loads and self weight is considered separately. Explicit criteria of failure are derived for each situation.

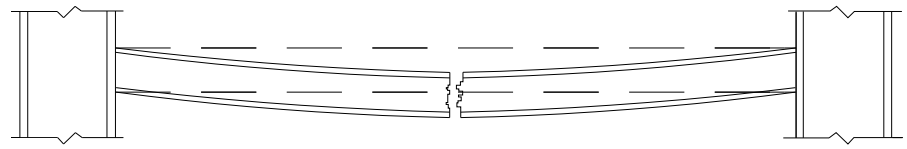

(a)

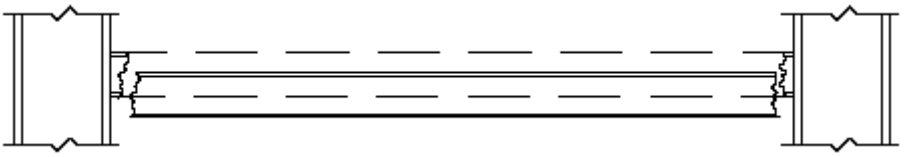

(b)

Figure 6.6 Failure mode profiles: (a) bending failure profile, and (b) shear failure profile.

6.3 Discrete rigid plastic beam model

In this model (Fig. 6.7) the beam was treated as many strongly linked differential elementsso that the shear effect between the small masses can be considered. The governing equation for the dominant shear effect is

$$\frac{\partial Q}{\partial x} = -p + m\ddot{y} \tag{6.5}$$

where Q is the shear force, x is the abscissa on the beam, p is the external uniform pressure, m is the mass per unit length, y is the transverse displacement of the beam, and $\ddot{y}$ is the acceleration of the unit mass.

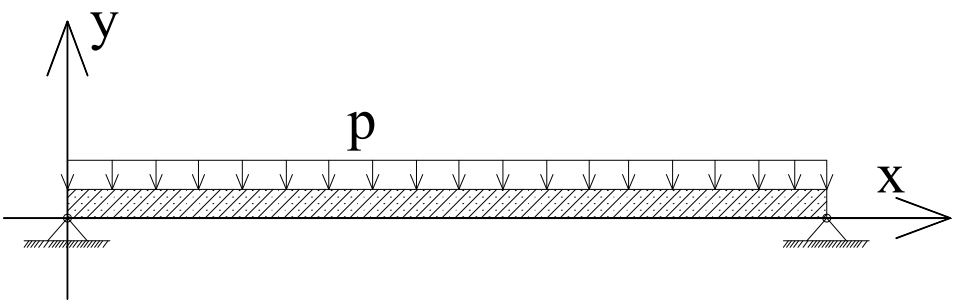

Figure 6.7 Discrete rigid-plastic beam model.

Integrate the acceleration with time and consider the initial displacement and velocity, then the final deformation of the beam can be derived. For this research, a rigid-plastic simply supported beam is selected as the object. According to Jones (1989), the transverse velocity profile of the beam change significantly with different values of the dimensionless shear-bending ratio

$$\upsilon = \frac{Q_0 L}{2M_0} \tag{6.6}$$

where Q_0 is the shearing resistance and M_0 is the bending resistance of the beams.

Fig. 6.8 shows the five possible transverse velocity profiles (Jones, 1989; Li and

Jones, 1995). $\dot{y}_m$ is the transverse velocity at the center, $\dot{y}_s$ is the transverse velocity at the support, L is a half of the beam length and ξ_0 is the length of dynamic bending zone. The deformation is induced by the impulse loads and is terminated when the beam's kinetic energy is totally consumed by the shear hinges or bending hinges. Fig. 6.8 (a) shows the response of a beam with strong bending moment capacity and relatively weak shearing strength. When it is loaded with a shock wave pressure, shear hinges emerge at both sides. The beam maintains the consistent deformation tendency until it reaches the ultimate shear deformation. Fig. 6.8 (b) describes the deformation of a beam with relative weak bending resistance. Before the shear sliding commences, there is already a plastic hinge in the center which keeps stationary throughout the whole procedure. Fig. 6.8 (c) depicts a beam whose bending and shearing resistance is between the ones in Fig. 6.8 (a) and Fig. 6.8 (b). Under impulse loads, such kind of beam not only has shear slides at the support but also has bending deformation at the central part. After the short duration of the load the shear slide will stop first and then bending will be terminated subsequently. A beam with weaker bending resistance is analyzed as shown in Fig. 6.8 (d). Bending hinges compose a small zone at the center of the beam. The two plastic hinge at the edge of the zone moves toward the center as the beam deforms. As the two hinges converge at the center the following deformation is similar to the deformation depicted in Fig. 6.8 (b). Fig. 6.8 (e) represents the most complicated case, which is a beam with moderate bending and shearing strength. It begins with both shearing hinges at both sides and a bending hinge zone in the center. The shear slide will terminate first and then the two bending hinges will converge together. Finally the beam will stop rotation around the stationary plastic hinge at the center and reach the

maximum displacement.

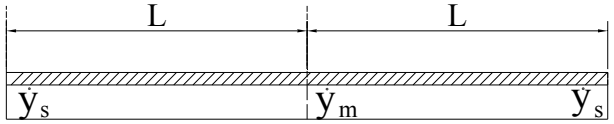

(a)

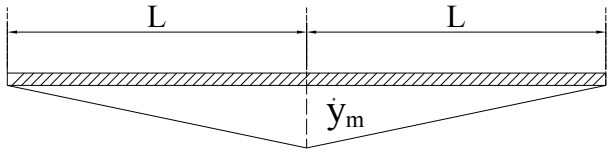

(b)

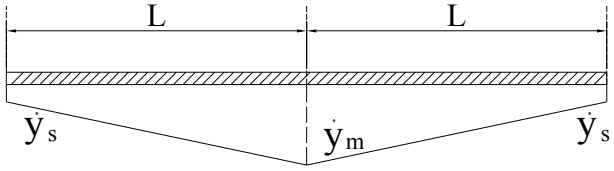

(c)

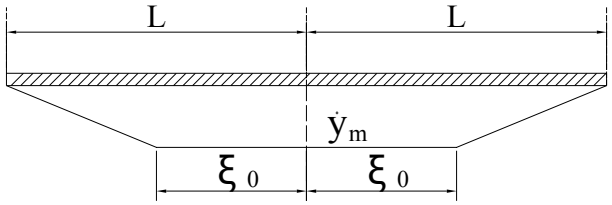

(d)

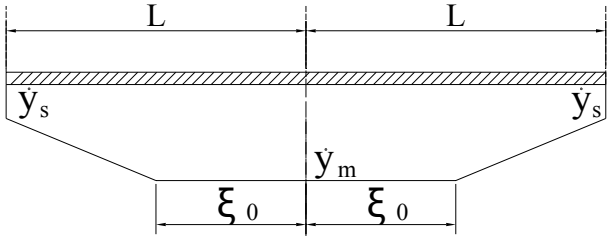

(e)

Figure 6.8 Transverse velocity profiles: (a) shear hinge at support, (b) stationary bending hinge in the center, (c) shear hinge at support and stationary bending hinge in

the center, (d) dynamic bending hinge zone in the center, and (e) shear hinge at support and dynamic bending hinge zone in the center.

6.4 Response under simplified blast load

There are three kinds of classic simplified loads: rectangular load, triangular load and exponential load. In this chapter, the performance of a beam under the former two kinds of loading will be discussed.

Rectangular load has a longer duration than the other load. It can represent the shock wave loads which usually endure a comparative long time. The peak pressure of triangular load drops quickly, which is the characteristic of conventional explosions. Compared with rectangular load, triangular load is more proper to simulate the real blast loads.

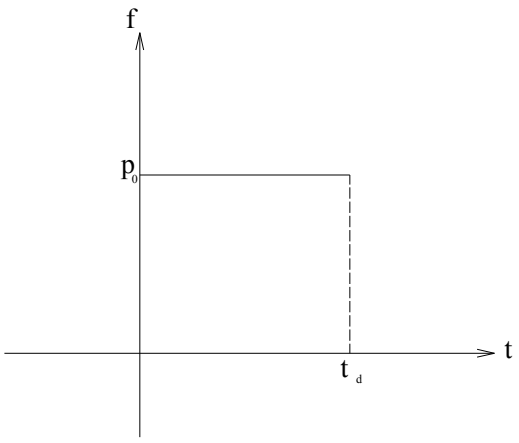

Figure 6.9 Rectangular loads.

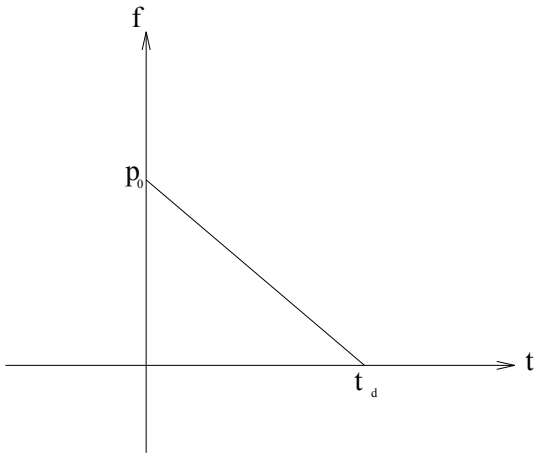

Figure 6.10 Triangular loads.

6.4.1 Response under rectangular loads

The pressure of the load is

$$f = \begin{cases} p_0 & t \le t_d \\ 0 & t > 0 \end{cases}$$

(6.7)

Li and Jones (1995) presented transverse velocity profiles for different pairs of pressure and υ. The maximum deformation and the duration of motion are derived in implicit form. However, the effect of impulse on the deformation hasn't been mentioned, which remains as a flaw. According to the velocity profiles proposed by Li and Jones (1995), corresponding derivation is conducted and the results are improved by including the influence of impulse in the critical equations. The final critical P-I equation is as shown in Fig. 6.11 and TableA.1 (Appendix A).

When $\upsilon \le 1$ and $p_0 \le \frac{2M_0}{L^2}\upsilon$ or $\upsilon \ge 1$ and $p_0 \le \frac{2M_0}{L^2}$, there will be no motion at all due to the rigid plasticity of the beam. It means that the pressure is too small to induce deformation.

Mode I. When $\upsilon \le 1$ and $p_0 \ge \frac{2M_0}{L^2}\upsilon$, shear failure

The beam deforms as shown in Fig. 6.8 (a). There are two phases throughout the deformation as shown in Mode I of Appendix A. At the end of first phase, which is the impulse load phase, the beam reaches maximum velocity. In the subsequent phase, the acceleration value becomes negative which means the velocity decreases untill the beam reach the maximum displacement.

When $t = \frac{p_0 L}{Q_0} t_d$, the beam's final transverse displacement is

$$y_f = \frac{L p_0^2 t_d^2}{2mQ_0} - \frac{p_0 t_d^2}{2m} \tag{6.8}$$

where L is half the length of the beam, and Q_0 is the shear strength of the beam. It

is interesting to notice that the time to reach the maximum deformation can also be derived by law of conservation of momentum because the kinetic energy is totally depleted by shear hinges.

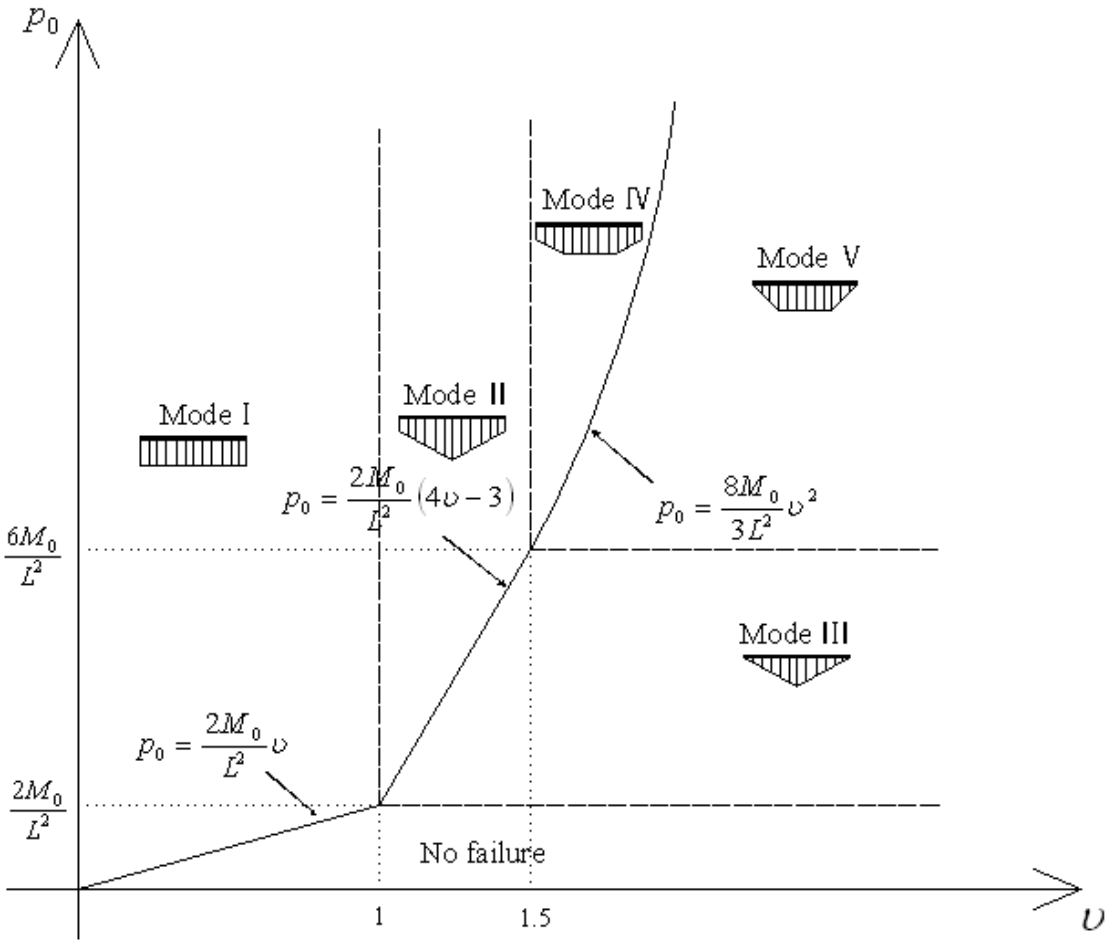

Figure 6.11 Failure profiles and criteria.

Krauthammer (2004) presented the damage criteria for shear failure induced by impact loads as shown in Table 6.1 (page 143). Moreover, Collins *et al*. (2003) derived the relationship between the average strain and the displacement along a given fracture zone as

$$d = Le \tag{6.9}$$

where d is the displacement, L is the fracture length and e is the average strain. According to the strain displacement equations (Boresi, 1985), the shear strain is

$$\gamma_v = \frac{\partial y_f}{\partial x} \tag{6.10}$$

where y_f is the vertical deformation and x is the abscissa on the beam (Fig. 6.7). If the size of shear hinge is assumed to be of similar size of the height of the cross section of the beam, integration of the average shear strain is equal to the displacement, i.e.

$$y_f = \int_0^h \gamma_v dx = h\gamma_v \tag{6.11}$$

Applying Eq. (6.11) as a shear damage criteria, critical pressure and impulse for a shear failure can be found.

$$\frac{2mh\gamma_v}{I^2} + \frac{1}{p_0} = \frac{L}{Q_0} \tag{6.12}$$

where h is the height of beam, γ_v is the average maximum shear strain.

Since the shear-bending ratio υ doesn't appear in Eq. (6.12), it can be concluded that when shearing strength is weak enough or bending moment capacity is strong enough the critical impulse and pressure is entirely determined by the shearing strength. The increase of bending reinforcement has no influence on the result.

Mode II. When $1 \le \upsilon \le 1.5$ and $p_0 > \frac{2M_0}{L^2}(4\upsilon - 3)$, shear and bending failure

The beam deforms as depicted in Fig. 6.8 (c) and goes through three phases (Mode II of Appendix A). The first one is the load phase, at the end of which both the shear slide motion and the bending motion reach the maximum velocity. The next phase is terminated when the shear slide stops at

$$t_s = \frac{p_0 \cdot t_d \cdot L^2}{2(4\upsilon - 3)M_0} \tag{6.13}$$

when the shear slide displacement is

$$y_s = \frac{p_0^2 t_d^2 L^2}{4M_0 m(4\upsilon - 3)} - \frac{p_0}{2m} t_d^2 \tag{6.14}$$

In the third phase, the excessive dynamic energy keeps the beam bending. However, the bending will finally stop at

$$t_f = \frac{p_0 \cdot t_d \cdot L^2}{2M_0} \tag{6.15}$$

The maximum deformation is located in the center.

$$y_f = \frac{(6\upsilon - 5) p_0^2 t_d^2 L^2}{4M_0 m(4\upsilon - 3)} - \frac{p_0}{2m} t_d^2 \tag{6.16}$$

The value of υ obviously affects the final deformation. Using the same method as in the derivation of Mode I, the critical equations for shear failure in terms of the peak pressure and the impulse can be obtained.

$$\frac{2mh\gamma_v}{I^2} + \frac{1}{p_0} = \frac{L\upsilon}{Q_0(4\upsilon - 3)} \tag{6.17a}$$

The critical equations for bending failure in terms of the peak pressure and the impulse can be obtained as well.

$$\frac{2mL\beta}{I^2} + \frac{1}{p_0} = \frac{L^2 \cdot (6\upsilon - 5)}{2M_0(4\upsilon - 3)} \tag{6.17b}$$

where β is the ratio of centerline deflection to span, which is prevalent criteria for bending failure.

Mode III. When $1 \le \upsilon \le 1.5$ and $\frac{2M_0}{L^2} \le p_0 \le \frac{2M_0}{L^2}(4\upsilon - 3)$

or $1.5 \le \upsilon$ and $\frac{2M_0}{L^2} \le p_0 \le \frac{6M_0}{L^2}$, bending failure

Before the shear hinges emerge, the rotation of stationary bending hinge in the center absorbs all the impact energy as shown in Fig. 6.8 (b). Two phases exist during

the whole deformation process (Mode III of Appendix B). The first phase is the impulse load phase and the second phase is the free load phase.

In the second phase, the rotation will stop at

$$t_f = \frac{p_0 \cdot t_d \cdot L^2}{2M_0} \tag{6.18}$$

The final deformation is

$$y_f = \frac{3p_0^2 t_d^2 L^2}{8M_0 m} - \frac{3p_0}{4m} t_d^2 \tag{6.19}$$

The critical equation for bending failure in terms of the peak pressure and the impulse is

$$\frac{4mL\beta}{3I^2} + \frac{1}{p_0} = \frac{L^2}{2M_0} \tag{6.20}$$

According to the energy conservation principle the final cease time also can be calculated because only the bending plastic hinge can dissipate the impact energy.

Mode IV. When $1.5 \le \upsilon$ and $p_0 > \frac{8M_0}{3L^2}\upsilon^2$, shear and bending failure

There are four phases before the deformation finally ceases (Mode IV of Appendix A). The shear hinges and bending hinges both appear at the very beginning as illustrated in Fig. 6.8 (e). In the first phase both the shear slide and bending deformation reach the maximum velocity. In the second phase, the shear slide ceases at

$$t_s = \frac{3L^2 p_0 \cdot t_d}{8M_0 \upsilon^2} \tag{6.21}$$

when the maximum shear slide distance is

$$y_s = -\frac{p_0 t_d^2}{2m} + \frac{3p_0^2 L^2 t_d^2}{16M_0 m\upsilon^2} \tag{6.22}$$

The bending hinge zone keeps invariable when the shear hinges slide. The length of the hinge zone is

$$\xi_0 = \frac{2\upsilon - 3}{2\upsilon} L \tag{6.23}$$

The hinge zone will reduce to a point when $\upsilon = 1.5$, which corresponds to Mode II. After the shear slide ceases, the third phase commence and the bending hinges begin to move toward the center with velocity

$$\dot{\xi} = \frac{-3M_0}{p_0 t_d (L - \xi)} \tag{6.24}$$

The shift of bending hinges is terminated at

$$t_1 = \frac{p_0 t_d L^2}{6M_0} \tag{6.25}$$

At the end of the third phase, the transverse velocity profile changes into Fig. 6.8 (b).In the fourth phase, the beam rotates around the plastic bending hinge and reaches the maximum displacement when

$$t_f = \frac{p_0 t_d L^2}{2M_0} \tag{6.26}$$

The maximum displacement is

$$y_f = \frac{p_0^2 L^2 t_d^2}{3M_0 m} - \frac{p_0}{2m} t_d^2 \tag{6.27}$$

The following equation for shear failure can be derived from Eqs. (6.22) in terms of the peak pressure and impulse as

$$\frac{2mh\gamma_v}{I^2} + \frac{1}{p_0} = \frac{3L}{4Q_0\upsilon} \tag{6.28a}$$

For bending failure, the critical equation derived from Eq. (6.27) is

$$\frac{2mL\beta}{I^2}+\frac{1}{p_0}=\frac{2L^2}{3M_0} \tag{6.28b}$$

Mode V. When $1.5 \le \upsilon$ and $\frac{6M_0}{L^2} \le p_0 \le \frac{8M_0}{3L^2}\upsilon^2$, bending failure

No shear slide appears and there is a bending zone in the center of the beam (Fig. 6.8 (d)). There exist three phases including the impulse loads phase, the shift of bending hinges phase and the motion-cease phase (Mode V of Appendix A). The length of the hinge zone in the first phase can be calculated by

$$\xi_0 = L-\sqrt{\frac{6M_0}{p_0}} \tag{6.29}$$

In the second phase, the zone decreases to a hinge point with the velocity

$$\dot{\xi}=\frac{-3M_0}{p_0 t_d (L-\xi)} \tag{6.30}$$

The hinges points coalesce in the center at

$$t_1=\frac{p_0 t_d L^2}{6M_0} \tag{6.31}$$

In the third phase, the beam deforms as depicted in Fig. 6.8 (b). When

$$t_f=\frac{p_0 t_d L^2}{2M_0} \tag{6.32}$$

the displacement is

$$y_f=\frac{p_0^2 L^2 t_d^2}{3M_0 m}-\frac{p_0}{2m}t_d^2 \tag{6.33}$$

The following equation for bending failure can be derived from Eq. (6.32) in terms of the peak pressure and the impulse

$$\frac{2mh\gamma_v}{I^2}+\frac{1}{p_0}=\frac{2L^2}{3M_0} \tag{6.34}$$

The results are summarized in Fig. 6.11 and Table A.1 (Appendix A). The number in Fig 6.11 represents the discrimination equations in TableA.1 (Appendix A). The failure mode varies from shear failure to bending failure as the two parameters υ and p_0 change. When $\upsilon \le 1$, shear failure is the predominant failure mode. But when $1.5 \le \upsilon$ and $p_0 \le \frac{8M_0}{3L^2}\upsilon^2$, bending failure is the only failure mode. Other failure modes need discrimination separately because both shear and bending failure are possible. Generally speaking, the beam is more vulnerable to bending failure as the value of υ is higher. When υ is fixed, high peak pressure leads to the occurrence of shear failure. For shear failure, the decrease of υ results in the lower critical values of pressure and impulse, which indicates the beam becomes more vulnerable (Fig. 6.12). However, for bending failure, the decrease of υ leads to the decrease of the critical value of pressure and impulse (Fig. 6.13).

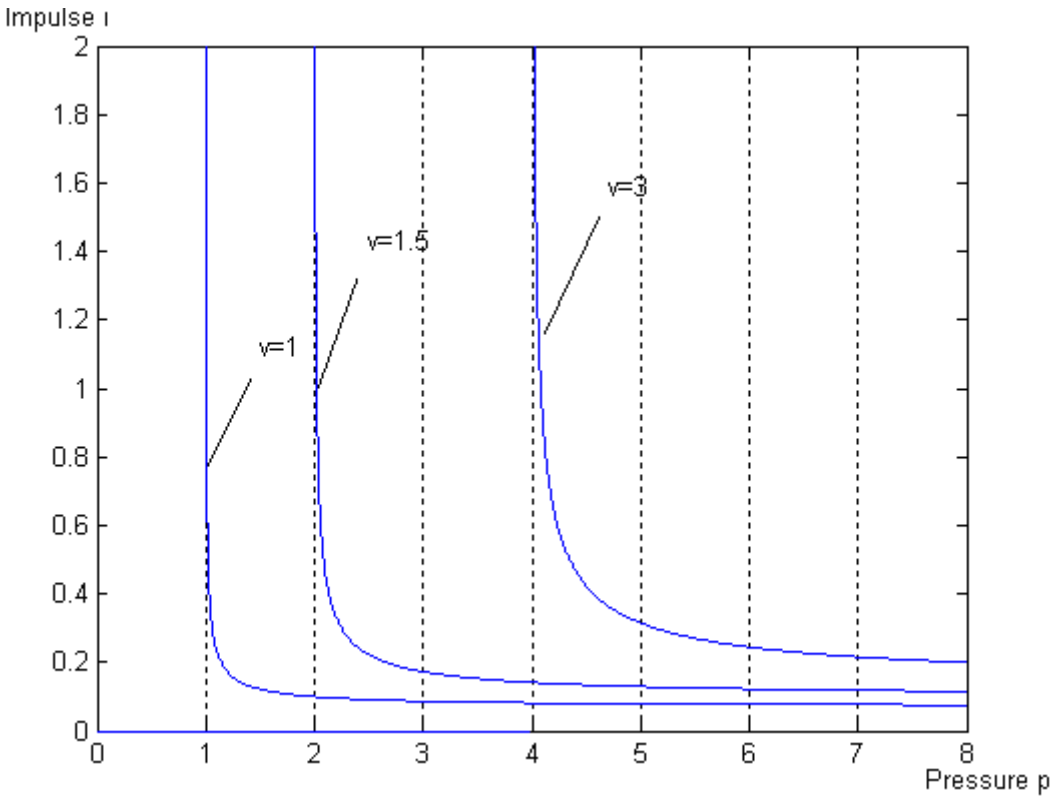

Figure 6.12 P-I diagram for shear failure.

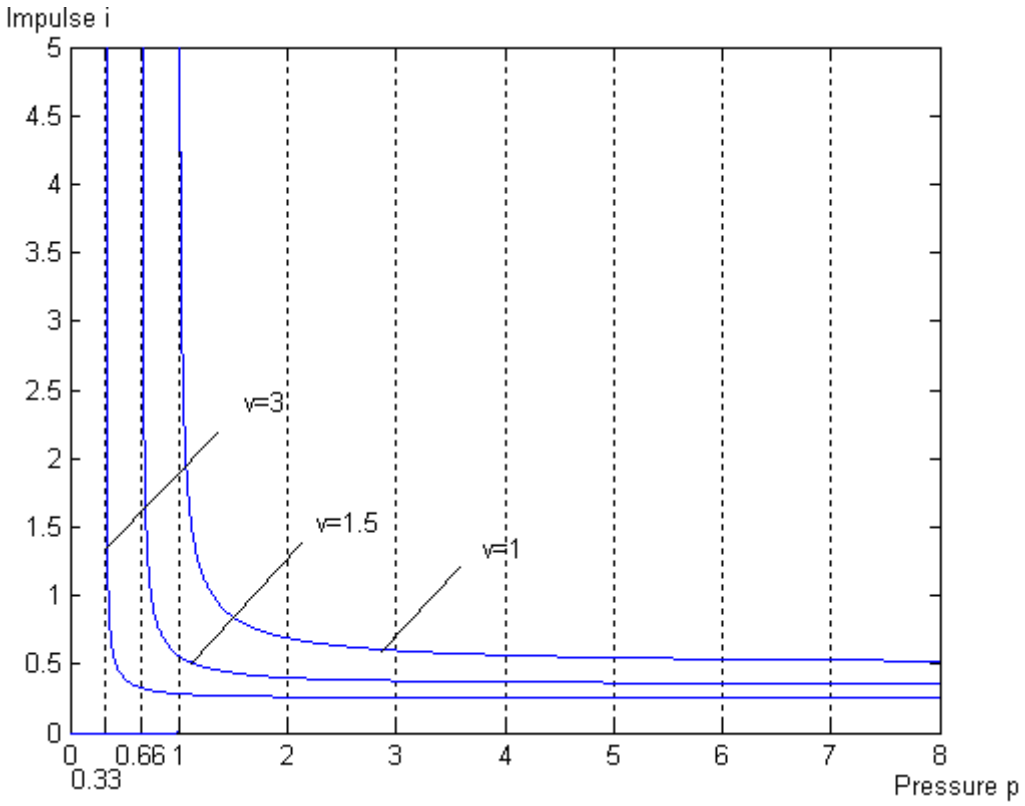

Figure 6.13 P-I diagram for bending failure.

6.4.2 Response under triangular loads

The pressure of the load is defined by

$$f = \begin{cases} P_0 \cdot \left(1 - \dfrac{t}{t_d}\right) & t \le t_d \\ 0 & t > 0 \end{cases} \tag{6.35}$$

Li and Jones (1995) have developed implicit results for simply supported beams under triangular loads. However, when the discrimination is conducted with critical pressure and impulse, it is found that more partition needs to be made to discriminate the failure. Through derivation the final critical P-I equation is as shown in Table B.1 (Appendix B). The performance of the beam is similar to those under rectangular load, though there are more categories. For details of each mode please refer to the corresponding part in Appendix B.

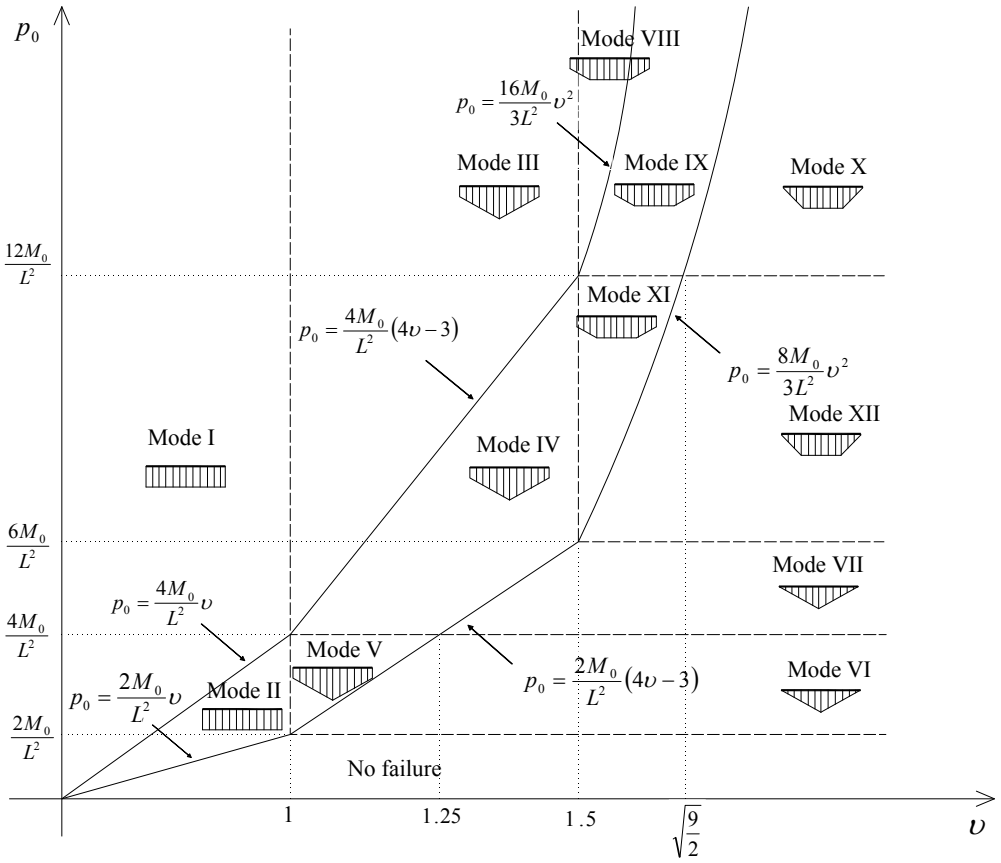

Figure 6.14 Failure modes for triangular pulse load.

Mode I. When $\upsilon \le 1$ and $\frac{4M_0\upsilon}{L^2} \le p_0$, shear failure

Shear slide occurs at both supports (Fig. 6.8 (a)). There are two phases including the loading phase and the post-loading phase. The beam reaches its maximum transverse velocity at the end of the loading phase and decelerates in the subsequent post-loading phase. In the post-loading phase, the deformation will cease at

$$t_f = \frac{p_0 L}{2Q_0} t_d \tag{6.36}$$

when the transverse displacement of the beam becomes

$$y_f = \frac{p_0(3p_0 L - 4Q_0)}{24mQ_0} t_d^2 \tag{6.37}$$

The following equation for shear failure can be derived from Eq. (6.35) in terms

of the peak pressure and the impulse

$$\frac{1.6mh\gamma_v}{I^2}+\frac{4}{3p_0}=\frac{L}{Q_0} \tag{6.38}$$

where h is the height of beam, γ_v is the average maximum shear strain, I is the impulse which equals $\frac{1}{2}p_0t_d$ for triangular load.

Mode II. When $\upsilon \le 1$ and $\frac{2M_0\upsilon}{L^2} \le p_0 \le \frac{4M_0}{L^2}\upsilon$, shear failure

The transverse velocity profile is the same as that for Mode I. But there is only one phase of the motion. The shear slide will cease in the loading phase because the blast pressure is relatively weak compared to the shear strength of the beam.

$$t_f = (1-\frac{Q_0}{p_0L})2t_d \tag{6.39}$$

The final shear sliding displacement is

$$y_f = \frac{2p_0t_d^2}{3m}\left(1-\frac{Q_0}{p_0L}\right)^3 \tag{6.40}$$

The following equation for shear failure can be derived from Eq. (6.40) in terms of the peak pressure and the impulse

$$\left(\frac{0.3mp_0h\gamma_v}{I^2}\right)^{\frac{1}{3}}+\frac{Q_0}{p_0L}=1 \tag{6.41}$$

Mode III. When $1 \le \upsilon \le 1.5$ and $\frac{4M_0}{L^2}(4\upsilon-3) < p_0$, shear and bending failure

There are shear slide and bending deformation simultaneously as shown in Fig. 6.8 (c). Three phases exist before the beam deformation ceases. In the first phase (loading phase) both shear slide and bending deformation reach the maximum velocity.

In the second phase (post-loading phase), the shear slide stops at

$$t_s = \frac{p_0 \cdot t_d \cdot L^2}{4(4\upsilon - 3)M_0} \tag{6.42}$$

and the shear sliding displacement is

$$y_s = \frac{p_0^2 t_d^2 L^2}{16 M_0 m(4\upsilon - 3)^2} - \frac{p_0}{6m} t_d^2 \tag{6.43}$$

In the third phase (post-loading phase), the beam continue bending till the central part reaches the maximum displacement at

$$t_f = \frac{p_0 \cdot t_d \cdot L^2}{4M_0} \tag{6.45}$$

when the bending displacement is

$$y_f = \frac{(6\upsilon - 5)p_0^2 t_d^2 L^2}{16 M_0 m(4\upsilon - 3)} - \frac{p_0}{6m} t_d^2 \tag{6.46}$$

The following equation for shear failure can be derived from Eq. (6.43) in terms of the peak pressure and the impulse

$$\frac{0.8mh\gamma_v}{I^2} + \frac{2}{3p_0} = \frac{L\upsilon}{2Q_0(4\upsilon - 3)} \tag{6.47a}$$

The equation for bending failure can be derived from Eq. (6.46) in terms of the peak pressure and the impulse

$$\frac{mL\beta}{I^2} + \frac{2}{3p_0} = \frac{(6\upsilon - 5)L^2}{4M_0(4\upsilon - 3)} \tag{6.47b}$$

Mode IV. When $1 \le \upsilon \le 1.25$ and $\frac{4M_0}{L^2} < p_0 < \frac{2M_0}{L^2}(4\upsilon - 3)$,

or $1.25 \le \upsilon \le 1.5$ and $\frac{2M_0}{L^2}(4\upsilon - 3) < p_0 < \frac{4M_0}{L^2}(4\upsilon - 3)$, shear and bending failure

The performance of the beam is similar to that of Mode III and the motion has

three phases. But the shear slide will cease during the loading phases because of the decrease of intensity of blast pressure. In the first phase (loading phase), the shear slide will cease at

$$t_s = 2t_d - \frac{4(4\upsilon - 3)M_0 t_d}{p_0 L^2} \tag{6.48}$$

and the shear slide is

$$y_s = \frac{2\left[(6 - 8\upsilon)M_0 + L^2 p_0\right]^3 \cdot t_d^2}{3L^6 m p_0^2} \tag{6.49}$$

In the subsequent phase (loading phase), the beam is still under the pulse load and keeps accelerating until the commencement of the third phase. The third phase ends at

$$t_f = \frac{p_0 \cdot t_d \cdot L^2}{4M_0} \tag{6.50}$$

while the final central displacement as

$$y_f = \frac{t_d^2}{96L^6 M_0 m p_0^2}[256(4\upsilon - 3)^3 M_0^4 - 384(4\upsilon - 3)^2 M_0^3 p_0 L^2 + 192(4\upsilon - 3)M_0^2 p_0^2 L^4 - 56M_0 p_0^3 L^6 + 9L^8 p_0^4] \tag{6.51}$$

The following equation for shear failure can be derived from Eq. (6.49) in terms of the peak pressure and the impulse

$$\left(\frac{0.3mp_0 h\gamma_v}{I^2}\right)^{\frac{1}{3}} + \frac{(4\upsilon - 3)Q_0}{p_0 L\upsilon} = 1 \tag{6.52 a}$$

For bending failure, the critical equation is

$$\frac{12mL\beta}{I^2} + \frac{28}{p_0} = \frac{9L^2}{2M_0} + \frac{96(4\upsilon - 3)M_0}{p_0^2 L^2} - \frac{192(4\upsilon - 3)^2 M_0^2}{p_0^3 L^4} + \frac{128(4\upsilon - 3)^3 M_0^3}{p_0^4 L^6} \tag{6.52 b}$$

Mode V. When $1 \le \upsilon \le 1.25$ and $\frac{2M_0}{L^2}(4\upsilon - 3) < p_0 < \frac{4M_0}{L^2}$, shear and bending failure

There are only two phases during the motion process, both of which are in the loading phase (Fig. 6.8 (c)). Because the pressure is relatively small, the shear slide will cease in the first phase. The first phase ends when the shear slide cease at

$$t_s = 2t_d - \frac{4(4\upsilon - 3)M_0 t_d}{p_0 L^2} \tag{6.53}$$

and the shear slide is

$$y_s = \frac{2\left[(6 - 8\upsilon)M_0 + L^2 p_0\right]^3 \cdot t_d^2}{3L^6 m p_0^2} \tag{6.54}$$

The second phase stops at

$$t_f = \left(1 - \frac{2M_0}{p_0 L^2}\right) \cdot 2t_d \tag{6.55}$$

when the final central displacement is

$$\begin{aligned} y_f = \frac{2t_d^2}{3L^6 m p_0^2}[&8\left(-15 + 54\upsilon - 72\upsilon^2 + 32\upsilon^3\right)M_0^3 - 12\left(3 - 12\upsilon + 8\upsilon^2\right)M_0^2 p_0 L^2 \\ &+ 6(2\upsilon - 3)M_0 p_0^2 L^4 + L^6 p_0^3] \end{aligned} \tag{6.56}$$

The following equation for shear failure can be derived from Eq. (6.54) in terms of the peak pressure and the impulse

$$\left(\frac{0.3 m p_0 h \gamma_v}{I^2}\right)^{\frac{1}{3}} + \frac{(4\upsilon - 3)Q_0}{p_0 L \upsilon} = 1 \tag{6.57a}$$

For bending failure, the critical equation is

$$\frac{3mL\beta}{8I^2} - \frac{1}{p_0} = \frac{6(2\upsilon - 3)M_0}{p_0^2 L^2} - \frac{12\left(8\upsilon^2 - 12\upsilon + 3\right)M_0^2}{p_0^3 L^4} + \frac{8\left(32\upsilon^3 - 72\upsilon^2 + 54\upsilon - 15\right)M_0^3}{p_0^4 L^6}$$

[B]

(6.57b)

Mode VI. When $1 \le \upsilon \le 1.25$ and $\frac{2M_0}{L^2} < p_0 < \frac{2M_0}{L^2}(4\upsilon - 3)$

or $1.25 \le \upsilon \le 1.5$ and $\frac{2M_0}{L^2} < p_0 < \frac{4M_0}{L^2}$, bending failure

Only one phase exists during the whole motion process. The bending motion ceases during the loading phase (Fig. 6.8 (c)) at

$$t_f = \left(1 - \frac{2M_0}{p_0 L^2}\right) \cdot 2t_d \tag{6.58}$$

The final maximum displacement exists at the mid-span of the beam

$$y_f = \frac{\left(p_0 - \frac{Q_0}{L\upsilon}\right)^3}{mp_0^2} \cdot t_d^2 \tag{6.59}$$

The following equation for bending failure can be derived from Eq. (6.59) in terms of the peak pressure and the impulse

$$\left(\frac{mp_0 L\beta}{4I^2}\right)^{\frac{1}{3}} + \frac{2M_0}{p_0 L^2} = 1 \tag{6.60}$$

Mode VII. When $1.25 \le \upsilon \le 1.5$ and $\frac{4M_0}{L^2} < p_0 < \frac{2M_0}{L^2}(4\upsilon - 3)$

or $1.5 \le \upsilon$ and $\frac{4M_0}{L^2} < p_0 < \frac{6M_0}{L^2}$, bending failure

Two phases exists in this mode while there is only bending deformation motion of the beam (Fig. 6.8 (c)). The first phase is the loading phase which terminates at t_d. The second phase (post-loading phase) stops at

$$t_f = \frac{p_0 \cdot t_d \cdot L^2}{4M_0} \tag{6.61}$$

and the final maximum displacement exists in the central portion of the beam

$$y_f = \frac{3p_0^2 t_d^2 L^2}{32 M_0 m} - \frac{p_0}{4m} t_d^2 \tag{6.62}$$

The following equation for bending failure can be derived from Eq. (6.62) in terms of the peak pressure and the impulse

$$\frac{mL\beta}{I^2} + \frac{1}{p_0} = \frac{3L^2}{8M_0} \tag{6.63}$$

Mode VIII. When $1.5 \le \upsilon$ and $p_0 > \frac{16M_0}{3L^2}\upsilon^2$, shear and bending failure

There is not only shear slide at the support but also bending hinge zone at the mid-span of the beam (Fig. 6.8 (d)). The motion can be divided into four phases. The first phase is the loading phase. The length of the bending hinge zone is

$$\xi_0 = \frac{2\upsilon - 3}{2\upsilon} L \tag{6.64}$$

The shear slide motion will cease in the second phase (post-loading phase) at

$$t_s = \frac{3L^2 p_0 \cdot t_d}{16 M_0 \upsilon^2} \tag{6.65}$$

and the shear slide displacement is

$$y_s = -\frac{p_0 t_d^2}{6m} + \frac{3p_0^2 L^2 t_d^2}{64 M_0 m \upsilon^2} \tag{6.66}$$

In the third phase (post-loading phase), the positions of bending hinges begin to travels from $x = \xi_0$ to the mid-span after the shear slide ceases. The traveling velocity is

$$\dot{\xi} = \frac{-6M_0}{p_0 t_d (L - \xi)} \tag{6.67}$$

In the fourth phase (post-loading phase), the bending hinges coalesce at the mid-span

at

$$t_1 = \frac{p_0 t_d L^2}{12 M_0} \tag{6.68}$$

Then, the beam continues bending motion till

$$t_f = \frac{p_0 t_d L^2}{4 M_0} \tag{6.69}$$

while the final central displacement is

$$y_f = \frac{p_0^2 L^2 t_d^2}{12 M_0 m} - \frac{p_0}{6m} t_d^2 \tag{6.70}$$

The following equation for shear failure can be derived from Eq. (6.66) in terms of the peak pressure and the impulse

$$\frac{0.8 m h \gamma_v}{I^2} + \frac{2}{3 p_0} = \frac{3L}{8 Q_0 \upsilon} \tag{6.71 a}$$

For bending failure, the critical equation is

$$\frac{3 m L \beta}{2 I^2} + \frac{1}{p_0} = \frac{L^2}{2 M_0} \tag{6.71 b}$$

Mode IX. When $1.5 \le \upsilon \le \sqrt{\frac{9}{2}}$ and $\frac{8M_0}{3L^2}\upsilon^2 \le p_0 \le \frac{12M_0}{L^2}$, shear and bending failure

The deformation process is similar to Mode VIII and can be divided into four phases. The difference exists in the time for the process of shear slides and bending hinges' traveling. In the first phase (loading phase), the shear slide motion will cease at

$$t_s = 2 t_d \cdot \left(1 - \frac{8 M_0 \upsilon^2}{3 p_0 L^2} \right) \tag{6.72}$$

and the shear slide displacement is

$$y_s = \frac{2t_d^2\left(3p_0L^2 - 8M_0\upsilon^2\right)^3}{81mL^6p_0^2} \tag{6.73}$$

The bending hinges begin to coalesce to the center of the beam in the second phase (loading phase) until the end of the pulse load. In the third phase (post-loading phase), the coalescence is continued until the hinge zone merges into a point.

$$t_1 = \frac{p_0L^2t_d}{12M_0} \tag{6.74}$$

and the corresponding displacement is

$$y_m = \frac{p_0}{2m}t_d^2\left(\frac{p_0L^2}{12M_0} - \frac{1}{3}\right) \tag{6.75}$$

In the last phase (post-loading phase), the bending motion stops at

$$t_f = \frac{p_0 \cdot t_d \cdot L^2}{4M_0} \tag{6.76}$$

The final displacement is

$$y_f = \frac{\left(-2M_0 + p_0L^2\right)}{12M_0m} \cdot p_0t_d^2 \tag{6.77}$$

The following equation for shear failure can be derived from Eq. (6.73) in terms of the peak pressure and the impulse

$$\left(\frac{8.1mp_0h\gamma_v}{I^2}\right)^{\frac{1}{3}} + \frac{4Q_0\upsilon}{p_0L} = 3 \tag{6.78a}$$

For bending failure, the critical equation is

$$\frac{mL\beta}{I^2} + \frac{2}{3p_0} = \frac{L^2}{3M_0} \tag{6.78b}$$

Mode X. When $1.5 \le \upsilon$ and $\frac{12M_0}{L^2} \le p_0 \le \frac{8M_0}{3L^2}\upsilon^2$, bending failure

The transverse velocity profile is shown as Fig. 6.8(e). There is three phase in the

deformation process. No shear slide happens and the length of bending hinge zone is

$$\xi_0 = L - \sqrt{\frac{6M_0}{p_0}} \tag{6.79}$$

The bending hinge zone decreases to the central point at

$$t_1 = \frac{p_0 t_d L^2}{12M_0} \tag{6.80}$$

The final displacement is

$$y_f = \frac{p_0^2 L^2 t_d^2}{12M_0 m} - \frac{p_0}{6m} t_d^2 \tag{6.81}$$

The corresponding equations for bending failure in terms of the peak pressure and the impulse is

$$\frac{mL\beta}{I^2} + \frac{2}{3p_0} = \frac{L^2}{3M_0} \tag{6.82}$$

Mode XI. When $1.5 \le \upsilon \le \sqrt{\frac{9}{2}}$ and $\frac{8M_0}{3L^2}\upsilon^2 \le p_0 \le \frac{12M_0}{L^2}$, shear and bending failure

The deformation process is similar to Mode IX regarding to the timing of stopping shear deformation. The second phase (loading phase) begins with the coalescing of bending hinges and end with the loading phase.

$$t_1 = 2t_d \cdot \left(1 - \frac{6M_0}{p_0 L^2}\right) \tag{6.83}$$

and the corresponding displacement of the middle point is

$$y_m = \frac{2t_d^2 \left(p_0 L^2 - 6M_0\right)^2 \left(12M_0 + p_0 L^2\right)}{3mL^6 p_0^2} \tag{6.84}$$

The third phase (loading phase) terminates at the end of pulse loads. In the last phase (post-loading phase), the bending motion stops at

$$t_f = \frac{p_0 \cdot t_d \cdot L^2}{4M_0} \tag{6.85}$$

The final displacement is

$$y_f = \frac{\left(6912M_0^4 - 3456M_0^3 p_0 L^2 + 576M_0^2 p_0^2 L^4 - 56M_0 p_0^3 L^6 + 9p_0^4 L^8\right)}{96L^6 M_0 m p_0^2} \cdot t_d^2 \tag{6.86}$$

The following equation for shear failure can be derived from Eq. (6.73) in terms of the peak pressure and the impulse

$$\left(\frac{8.1mp_0 h\gamma_v}{I^2}\right)^{\frac{1}{3}} + \frac{4Q_0\upsilon}{p_0 L} = 3 \tag{6.87a}$$

For bending failure, the critical equation derived from Eq. (6.86) is

$$\frac{mL\beta}{I^2} - \frac{288M_0^3}{p_0^4 L^6} + \frac{144M_0^2}{p_0^3 L^4} - \frac{24M_0}{p_0^2 L^2} + \frac{7}{3p_0} = \frac{3L^2}{8M_0} \tag{6.87b}$$

Mode XII. When $1.5 \le \upsilon \le \sqrt{\frac{9}{2}}$ and $\frac{6M_0}{L^2} \le p_0 \le \frac{8M_0}{3L^2}\upsilon^2$

Or $\sqrt{\frac{9}{2}} \le \upsilon$ and $\frac{6M_0}{L^2} \le p_0 \le \frac{12M_0}{L^2}$, shear and bending failure

There are three phase for the whole deformation procedure. During the first loading phase, the bending deformation initiates together with the traveling of bending hinges. The traveling hinges coalesce at the center of the beam at

$$t_1 = 2t_d \cdot \left(1 - \frac{6M_0}{p_0 L^2}\right) \tag{6.88}$$

In the second loading phase, the beam continues bending till the end of impulse load. The bending deformation ends in the third phase (post-loading phase) at

$$t_f = \frac{p_0 \cdot t_d \cdot L^2}{4M_0} \tag{6.89}$$

The final deformation at mid-span is

$$y_f = \frac{\left(6912M_0^4 - 3456M_0^3 p_0 L^2 + 576M_0^2 p_0^2 L^4 - 56M_0 p_0^3 L^6 + 9p_0^4 L^8\right)}{96L^6 M_0 m p_0^2} \cdot t_d^2 \quad (6.90)$$

The corresponding critical P-I diagram equation for bending failure is

$$\frac{mL\beta}{I^2} - \frac{18M_0^3}{p_0^4 L^6} + \frac{9M_0^2}{p_0^3 L^4} - \frac{3M_0}{2p_0^2 L^2} + \frac{7}{48p_0} = \frac{3L^2}{128M_0} \quad (6.91)$$

6.5 Discrimination of failure mode

It can be seen that during impulsive loading both shear failure and bending failure are likely to happen. To take pertinent measures to protect buildings it is vital to discriminate the failure modes, which is presented next.

6.5.1 Discrimination criteria

Krauthammer (2004) concluded the discrimination standard as shown in Table 6.1. It applies the ratio of centerline deflection to span as the criteria for bending failure, and average shear strain as the criteria for shear failure.

Table 6.1 Discrimination criteria

TYPE OF FAILURE	CRITERIA	LIGHT DAMAGE	MODERATE DAMAGE	SEVERE DAMAGE
Global Bending/ Membrane Response	Ratios of Centerline Deflection to Span, D/L	4%	8%	15%
Shear	Average Shear Strain across Section, γ_v	1%	2%	3%

6.5.2 Normalization of the discrimination equation

If simplification is introduced as

$$i = \frac{I}{\sqrt{\frac{2mQ_0}{L}}} = \frac{I}{\sqrt{\frac{4mM_0\upsilon}{L^2}}} \tag{6.92}$$

$$p_0 = \frac{P_0}{\left(\frac{Q_0}{L}\right)} = \frac{P_0}{\left(\frac{2M_0\upsilon}{L^2}\right)} \tag{6.93}$$

Then for rectangular load the discrimination equations transform into simple form.

Table 6.2 Critical P-I equation for rectangular impulsive load

Mode	Shear failure	Bending failure
I	$\frac{2mh\gamma_v}{I^2} + \frac{1}{p_0} = \frac{L}{Q_0}$	N/A
II	$\frac{2mh\gamma_v}{I^2} + \frac{1}{p_0} = \frac{L\upsilon}{2Q_0(2\upsilon-3)}$	$\frac{2mL\beta}{I^2} + \frac{1}{p_0} = \frac{L^2\cdot(3\upsilon-5)}{4M_0(2\upsilon-3)}$
III	N/A	$\frac{4mL\beta}{3I^2} + \frac{1}{p_0} = \frac{L^2}{4M_0}$
IV	$\frac{2mh\gamma_v}{I^2} + \frac{1}{p_0} = \frac{3L}{2Q_0\nu}$	$\frac{2mL\beta}{I^2} + \frac{1}{p_0} = \frac{L^2}{3M_0}$
V	N/A	$\frac{2mL\beta}{I^2} + \frac{1}{p_0} = \frac{L^2}{3M_0}$

Table 6.3 Critical P-I equation for triangular impulsive load

Mode	Shear failure	Bending failure
I	$\frac{1.6mh\gamma_v}{I^2}+\frac{4}{3p_0}=\frac{L}{Q_0}$	N/A
II	$\left(\frac{0.3mp_0h\gamma_v}{I^2}\right)^{\frac{1}{3}}+\frac{Q_0}{p_0L}=1$	N/A
III	$\frac{0.8mh\gamma_v}{I^2}+\frac{2}{3p_0}=\frac{L\upsilon}{2Q_0(4\upsilon-3)}$	$\frac{mL\beta}{I^2}+\frac{2}{3p_0}=\frac{(6\upsilon-5)L^2}{4M_0(4\upsilon-3)}$
IV	$\left(\frac{0.3mp_0h\gamma_v}{I^2}\right)^{\frac{1}{3}}+\frac{(4\upsilon-3)Q_0}{p_0L\upsilon}=1$	$\frac{12mL\beta}{I^2}+\frac{28}{p_0}=\frac{9L^2}{2M_0}+\frac{96(4\upsilon-3)M_0}{p_0^2L^2}-\frac{192(4\upsilon-3)^2M_0^2}{p_0^3L^4}+\frac{128(4\upsilon-3)^3M_0^3}{p_0^4L^6}$
V	$\left(\frac{0.3mp_0h\gamma_v}{I^2}\right)^{\frac{1}{3}}+\frac{(4\upsilon-3)Q_0}{p_0L\upsilon}=1$	$\frac{3mL\beta}{8I^2}-\frac{1}{p_0}=\frac{6(2\upsilon-3)M_0}{p_0^2L^2}-\frac{12(8\upsilon^2-12\upsilon+3)M_0^2}{p_0^3L^4}+\frac{8(32\upsilon^3-72\upsilon^2+54\upsilon-15)M_0^3}{p_0^4L^6}$
VI	N/A	$\left(\frac{mp_0L\beta}{4I^2}\right)^{\frac{1}{3}}+\frac{2M_0}{p_0L^2}=1$
VII	N/A	$\frac{mL\beta}{I^2}+\frac{1}{p_0}=\frac{3L^2}{8M_0}$
VIII	$\frac{0.8mh\gamma_v}{I^2}+\frac{2}{3p_0}=\frac{3L}{8Q_0\upsilon}$	$\frac{3mL\beta}{2I^2}+\frac{1}{p_0}=\frac{L^2}{2M_0}$
IX	$\left(\frac{8.1mp_0h\gamma_v}{I^2}\right)^{\frac{1}{3}}+\frac{4Q_0\upsilon}{p_0L}=3$	$\frac{mL\beta}{I^2}+\frac{2}{3p_0}=\frac{L^2}{3M_0}$
X	N/A	$\frac{mL\beta}{I^2}+\frac{2}{3p_0}=\frac{L^2}{3M_0}$

XI	$\left(\frac{8.1mp_0h\gamma_v}{I^2}\right)^{\frac{1}{3}}+\frac{4Q_0\upsilon}{p_0L}=3$	$\frac{mL\beta}{I^2}-\frac{288M_0^3}{p_0^4L^6}+\frac{144M_0^2}{p_0^3L^4}-\frac{24M_0}{p_0^2L^2}+\frac{7}{3p_0}=\frac{3L^2}{8M_0}$
XII	N/A	$\frac{mL\beta}{I^2}-\frac{18M_0^3}{p_0^4L^6}+\frac{9M_0^2}{p_0^3L^4}-\frac{3M_0}{2p_0^2L^2}+\frac{7}{48p_0}=\frac{3L^2}{128M_0}$

6.5.3 Discrimination diagram

The P-I diagram method has the advantage to evaluate conveniently the structural safety against impact load (Ma, Shi and Shu, 2006). To demonstrate the usage of P-I diagram, a beam with length of $4\,m$ and height of $0.4\,m$ is calculated. Normalized P-I diagrams are plotted in Figs. 6.15-6.17.

A. Rectangular impulsive load

The failure mode varies from shear failure to bending failure as the two parameters υ and p_0 change. For simply supported beams, when $\upsilon \le 1$, shear failure is the predominant failure mode. But when $1.5 \le \upsilon$ and $p_0 \le \frac{8M_0}{3L^2}\upsilon^2$, bending failure is the only failure mode. Other failure modes need discrimination separately because both shear and bending failure are possible. Generally speaking, the beam is more vulnerable to bending failure as the value of υ is higher. When υ is fixed, high peak pressure leads to the occurrence of shear failure. For shear failure, the decrease of υ results in the lower critical values of pressure and impulse, which indicates the beam becomes more vulnerable. However, for bending failure, the decrease of υ leads to the decrease of the critical value of pressure and impulse. For fully clamped

beams similar rules exist in the change tendency of critical P-I diagram with the change of υ. When $\upsilon \le 2$, there is only shear failure. when $3 \le \upsilon$ and $p_0 \le \frac{4M_0}{3L^2}\upsilon^2$, bending failure is the only failure mode.

When $\upsilon \le 1$, both simply supported beam and fully clamped beam has the same critical discriminant for shear failure because when shear hinge emerge at both sides the difference between boundary condition disappears. When $\upsilon \ge 1$, a fully clamped beam has a stricter requirement for the prevention of shear failure compared with simply supported beams. When $\upsilon \ge 2$, beams with both boundary conditions can fail due to extreme bending effect. Simply supported beams can bear less impact loads than fully clamped beams.

B. Triangular impulsive load

It is found when $\upsilon \le 1$ ($\upsilon \le 2$ for fully clamped beams) shear failure is the only failure type (Fig. 6.15). Both shear failure and bending failure become possible when $1 \le \upsilon \le 4.4$ ($2 \le \upsilon \le 8.8$ for fully clamped beams). Four different failure combinations are denoted as A, B, C, and D in Fig. 6.16. In region A, both failures may occur. In region B, no shear failure may happen and no bending failure in region C. The beam keeps safe in region D. When $\upsilon \ge 4.4$ ($\upsilon \ge 8.8$ for fully clamped beams), the failure combination changes into three regions A, B, C. In region C, there is no failure. In region B, only bending failure exist. In region A, shear failure accompanies the bending failure.

As υ increases, shear failure tendency descends. However, bending failure becomes more possible due to the downward drift of the threshold (Fig. 6.18). When $\upsilon \le 1$, shear failure is the dominant failure type. But when $4.4 \le \upsilon$ and

$p_0 \le \frac{8M_0}{3L^2}\upsilon^2$, the bending failure precedes the shear failure.

For beams with the same parameter υ, the boundary condition influences the failure type as well (Fig. 6.19). Fully clamped beams are more vulnerable to shear failure compared with simply supported beams. However their bending resistances are more likely to sustain the bending than simply supported ones, which is consistent to previous research (Ma, Shi and Shu, 2006).

It can be easily seen from Fig 6.20 that a P-I diagram for triangular loading merges with the ones for rectangular loading at impulse-controlled part and peak-pressure controlled part. This demonstrates that when an ideal impulse is imposed to the beam, the response will be decided by the impulse and will no longer be affected by loading shape. The same phenomena happen at the quasi-static part when the loading duration is much longer than the natural vibration period of the beam. But at Peak pressure and impulse combination-controlled area, the difference is significant and can not be neglected.

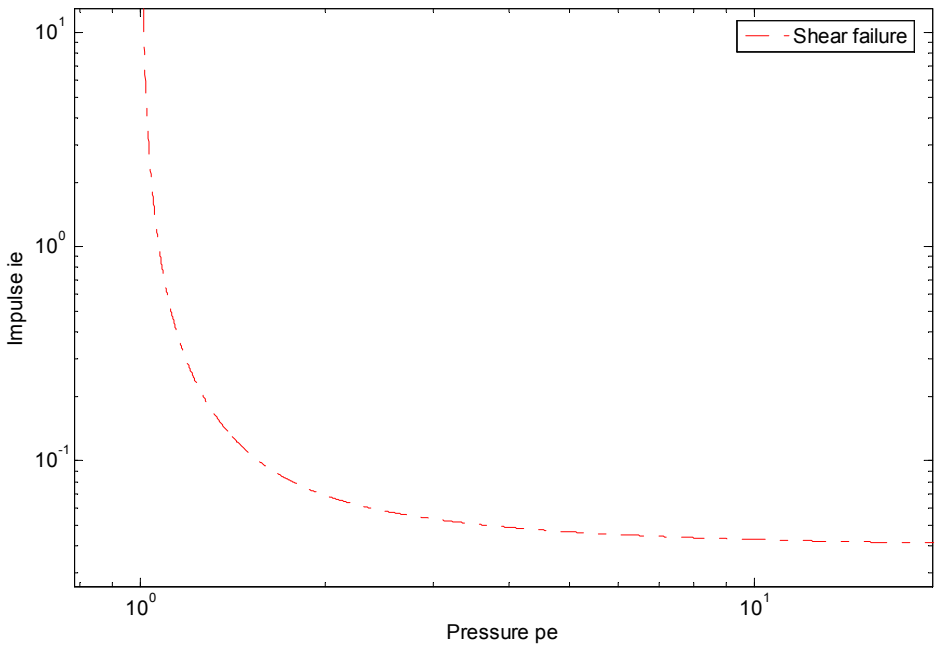

Figure 6.15 Comparison of failure modes with $\upsilon \le 1$.

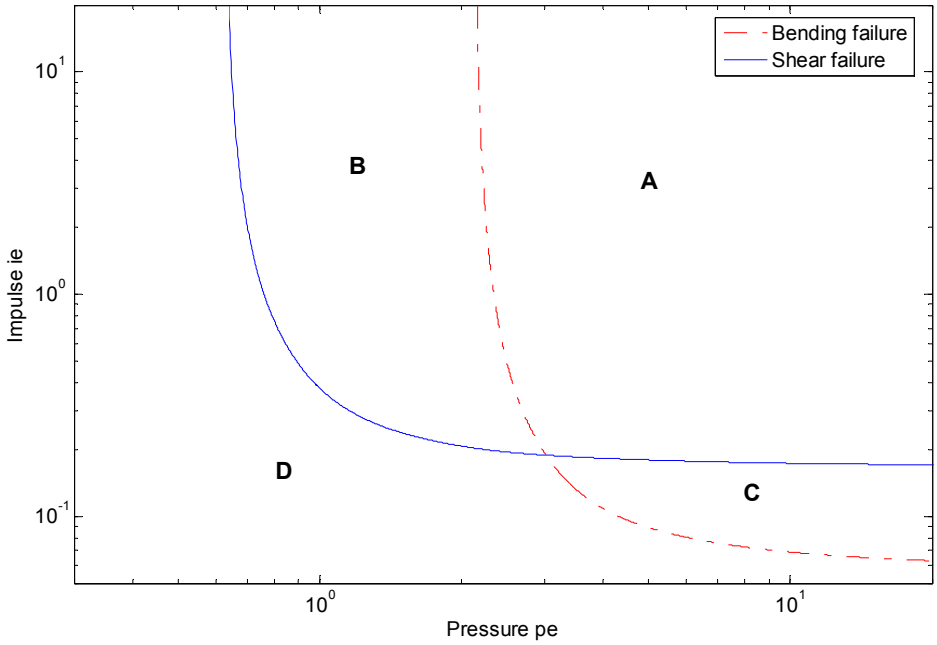

Figure 6.16 Comparison of failure modes with $1 \le \upsilon \le 4.4$.

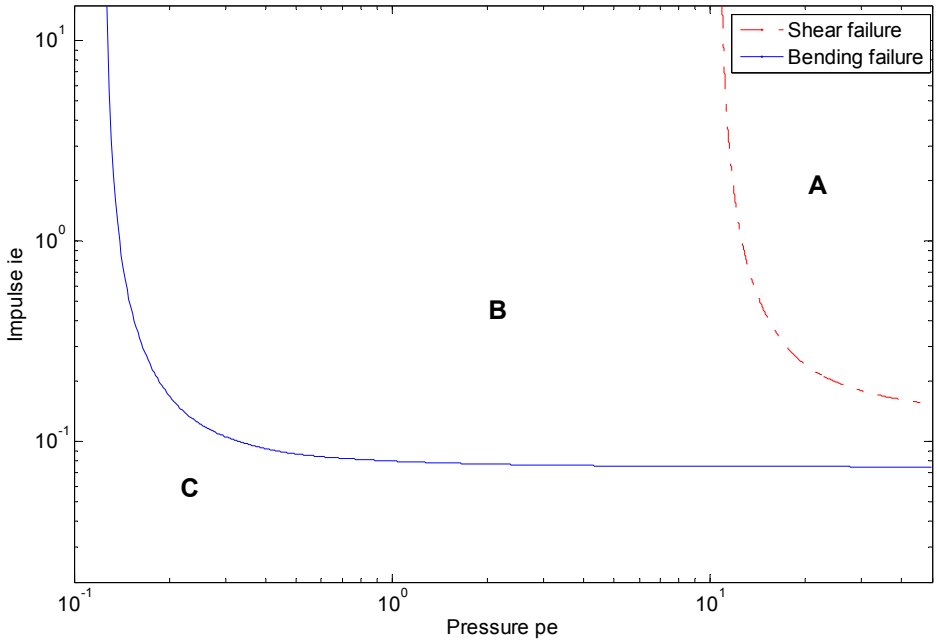

Figure 6.17 Comparison of failure modes with $4.4 \le \upsilon$.

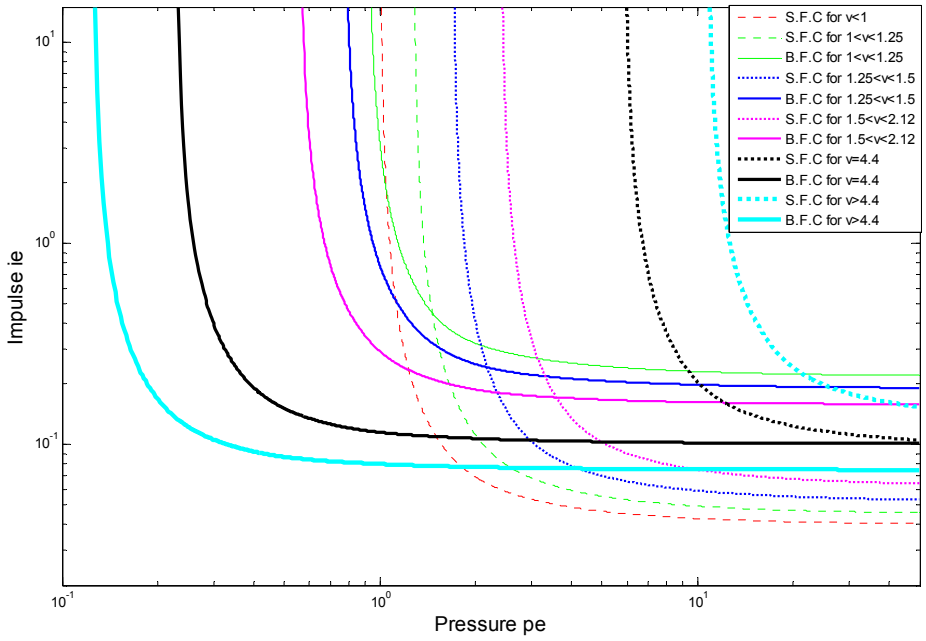

Figure 6.18 Failure modes for triangular pulse load.

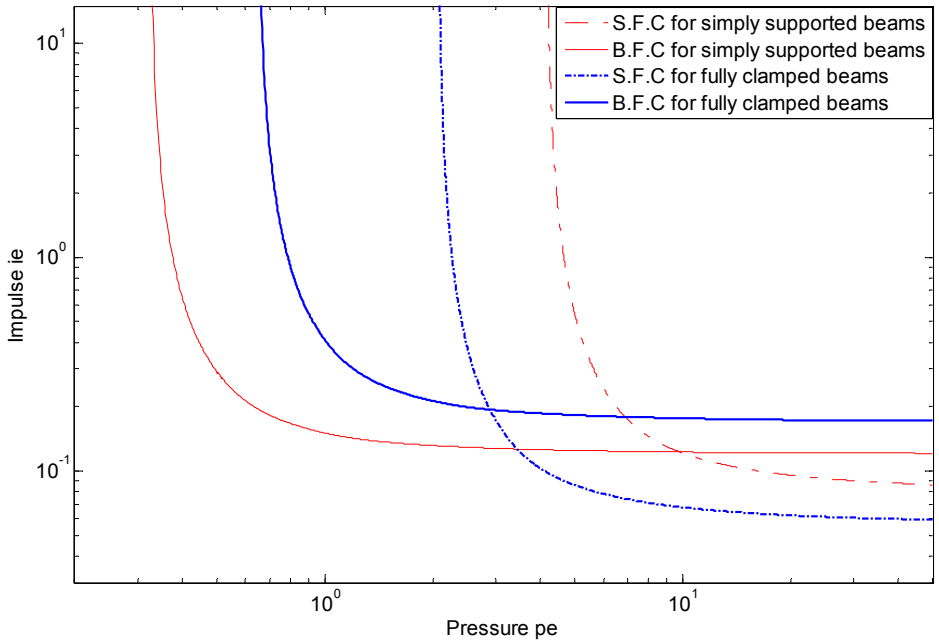

Figure 6.19 Critical P-I curves for different boundary conditions with same υ.

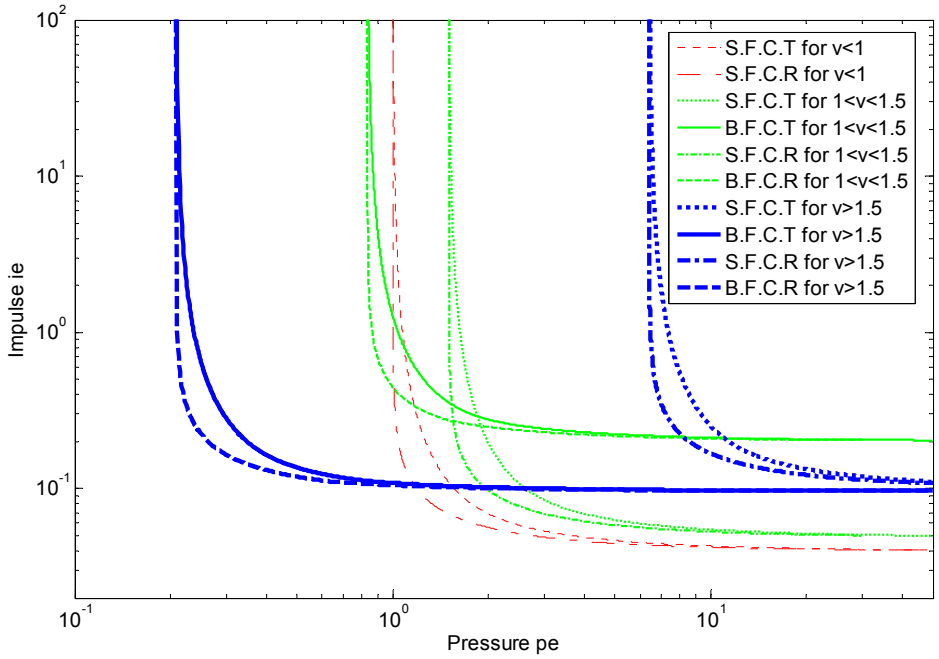

Figure 6.20 Critical P-I curves for different pulse shape.

Note: S.F.C.T means Shear Failure critical Curve under Triangular loading,

S.F.C.R means Shear Failure critical Curve under Rectangular loading,

B.F.C.T means Bending Failure critical Curve under Triangular loading,

B.F.C.R means Bending Failure critical Curve under Rectangular loading.

6.6 Global estimation of guyed tower under impulsive load

The proposed methodology is to use the derived P-I diagram to evaluate the performance of individual members. If one member fails, the corresponding stiffness contribution will be eliminated. The global stiffness matrix will then be reevaluated by the eigenvalues of the structure. If it is negative, the structure becomes unstable. The procedure is shown in the flow chart of Fig. 6.21.

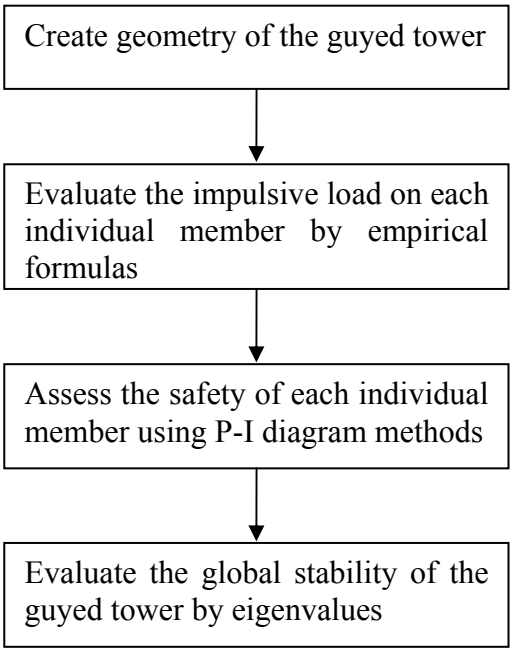

Figure 6.21 Flow chart for global stability assessment.

In a rigid plastic rectangular beams, the shear stress is

$$\tau = \frac{Q\frac{1}{2}bh\frac{1}{4}h}{\frac{1}{12}bh^3 b} = \frac{3Q}{2bh} \tag{6.94}$$

If Tresca yield criterion is admitted, the maximum shear stress is

$$\tau = \frac{1}{2}\sigma_0 \tag{6.95}$$

Thus,

$$Q_0 = \frac{\sigma_0}{3}bh \tag{6.96}$$

$$M_0 = \frac{\sigma_0}{4}bh^2 \tag{6.97}$$

So $\upsilon = \frac{Q_0 L}{2M_0} = \frac{2L}{3h}$, which means the index υ in some extent reflects the factored ratio of beam's length to depth.

To determine the stability of a structure, the eigenvalues check is used as described by Pai (2007). Because

$$[K]\{\Delta D\} = \{\Delta F\} \tag{6.98}$$

Where $[K]$ is the global stiffness matrix; $\{\Delta D\}$ is the displacement vector; $\{\Delta F\}$ is the force vector. If $\{\Delta F\} = \lambda\{\Delta D\}$,

$$([K] - \lambda[I])\{\Delta D\} = \{0\} \tag{6.99}$$

Where λ is eigenvector; $[I]$ is an unit vector. If $\lambda_i < 0$, the variation of energy is

$$\Delta W = \frac{1}{2}\{\Delta F\}\{\Delta D\} = \frac{1}{2}\lambda_i \{\Delta D\}^T \{\Delta D\} < 0$$

That means the structure will release energy during deformation, which actually is impossible. So if any eigenvalue becomes less than zero, the structure becomes unstable.

To demonstrate the application, one specific example is provided in this section. The height of the mast is 150m and has four layers of cables that are connected at 30, 60, 100, 140 meters (Fig 6.22). The mast of the tower is an equilateral triangle of 1m length. The cross section of the pole is assumed to 0.05×0.05m and the strut is 0.02×0.05m (Fig 6.27 (a)). The radius of the cables is 3.16cm. The material is AISI-3140 steel with a yield stress of 620 MPa. The charge is 1 tonne TNT with standoff of 100m.

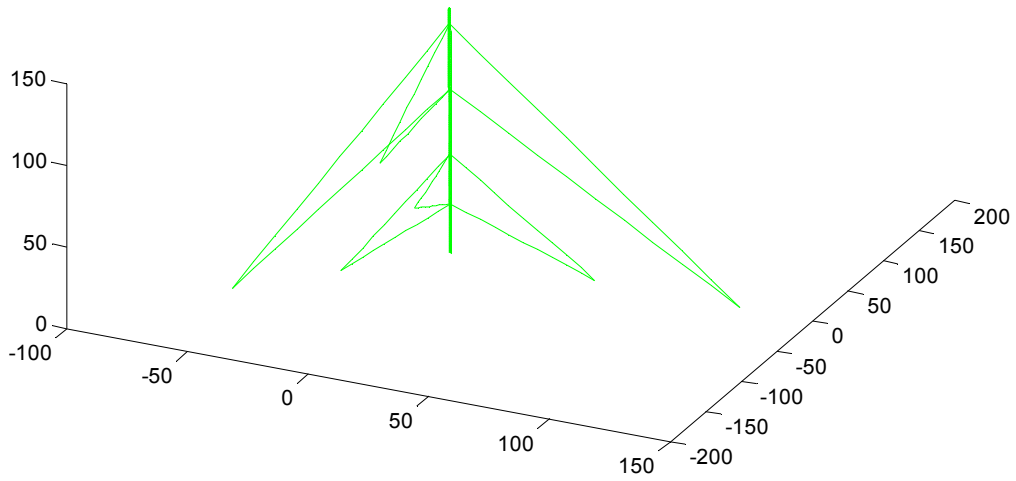

Figure 6.22 Geometry of guyed tower.

Because the members in the tower are slim, the failure associated is bending failure. Shear failure is another possible failure mode, which requires much higher peak pressure. The critical P-I diagrams for each type of components are as shown in Figs 6.23-6.26. For pole elements and lateral struts, the external impulsive loads are less than the critical loads. This indicates they are safe for such loads. But for diagonal struts, their loads exceed the strength. All of the loads are in the zone of failure mode 7.

The impulsive load blows off all diagonal slim struts in the mast as shown in Fig6.27 (b). But all lateral strut and pole elements have survived, which maintains the guyed tower's integrity and stability. By using eigenvector analysis, it is found that the minimum eigenvalue of the tower is greater than zero, which indicates that the structure is still stable and won't collapse under specified impulsive loading.

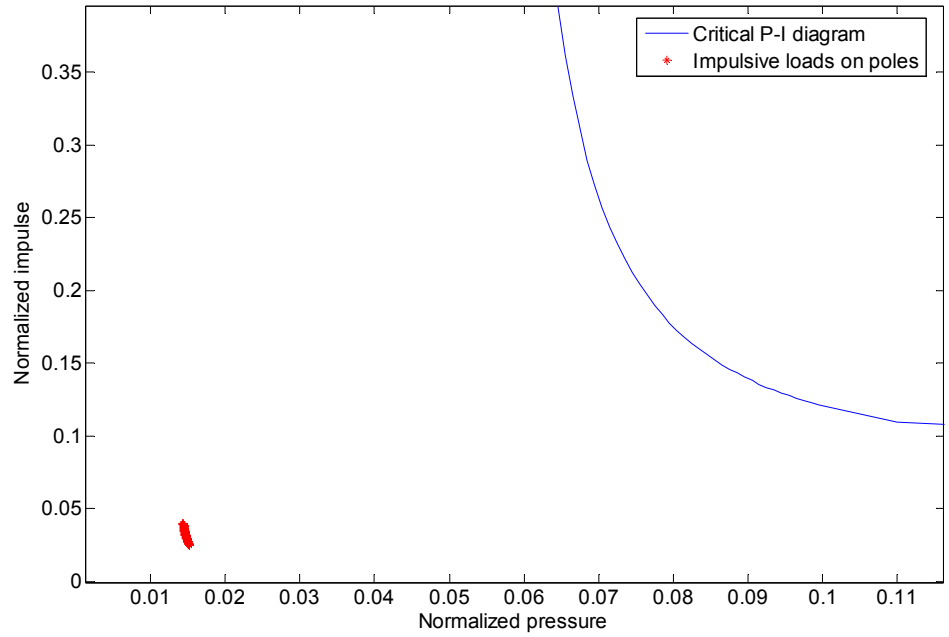

Figure 6.23 P-I diagram and impulsive loads for poles.

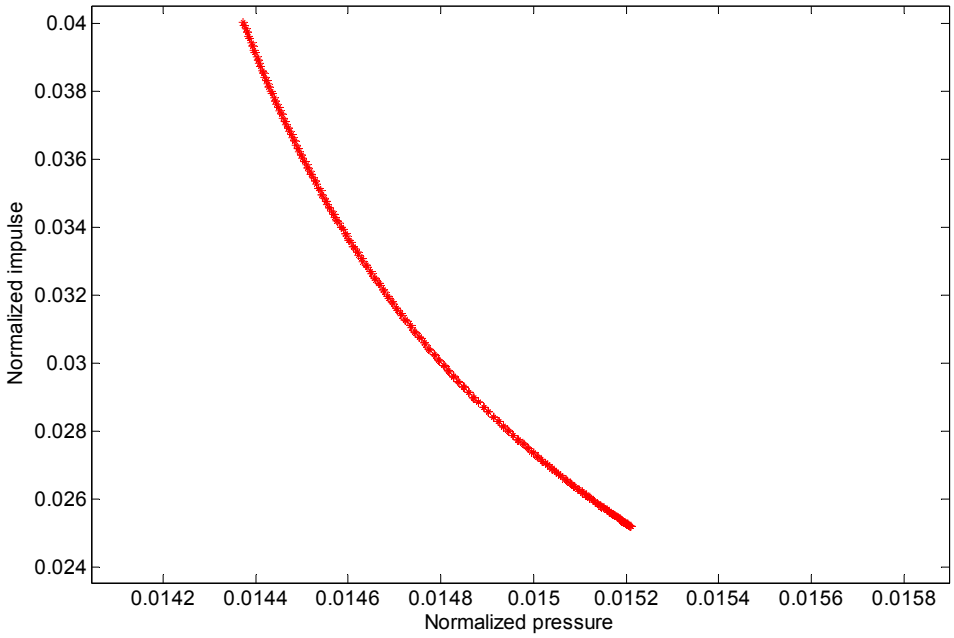

Figure 6.24 Impulsive loads for poles.

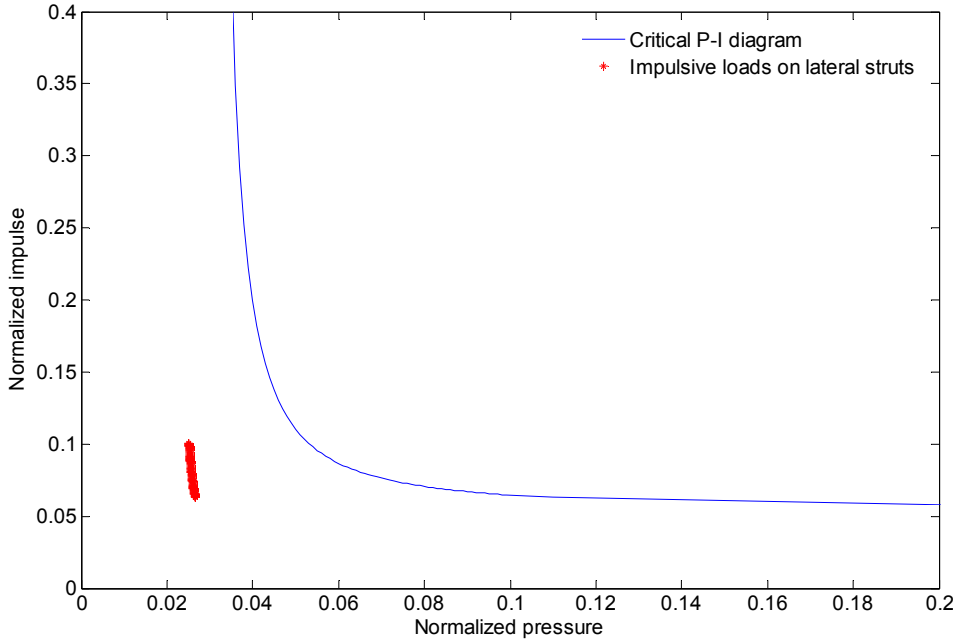

Figure 6.25 P-I diagram and impulsive loads for lateral struts.

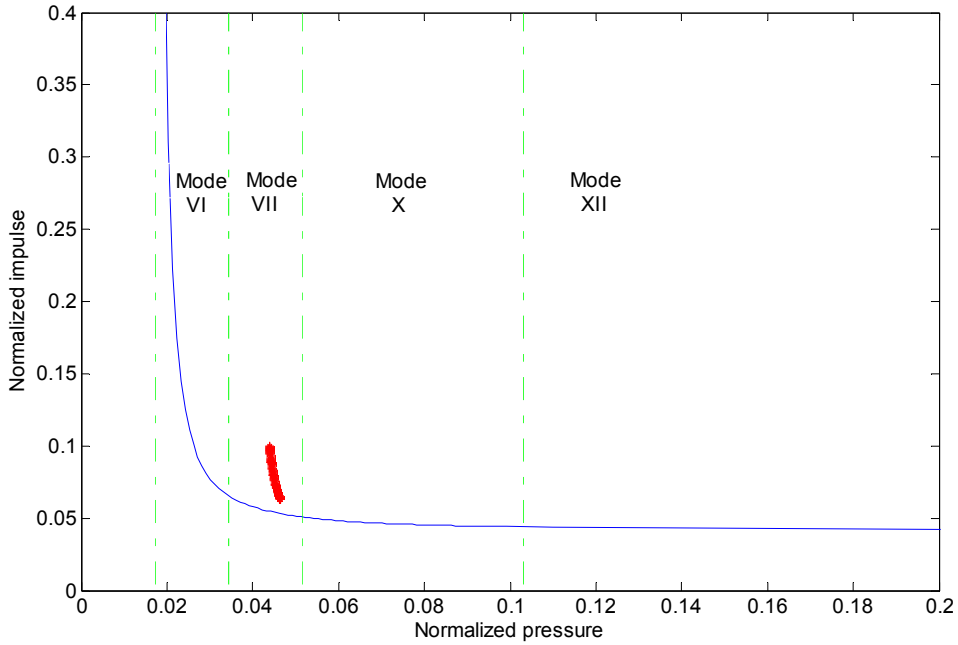

Figure 6.26 P-I diagram and impulsive loads for diagonal struts.

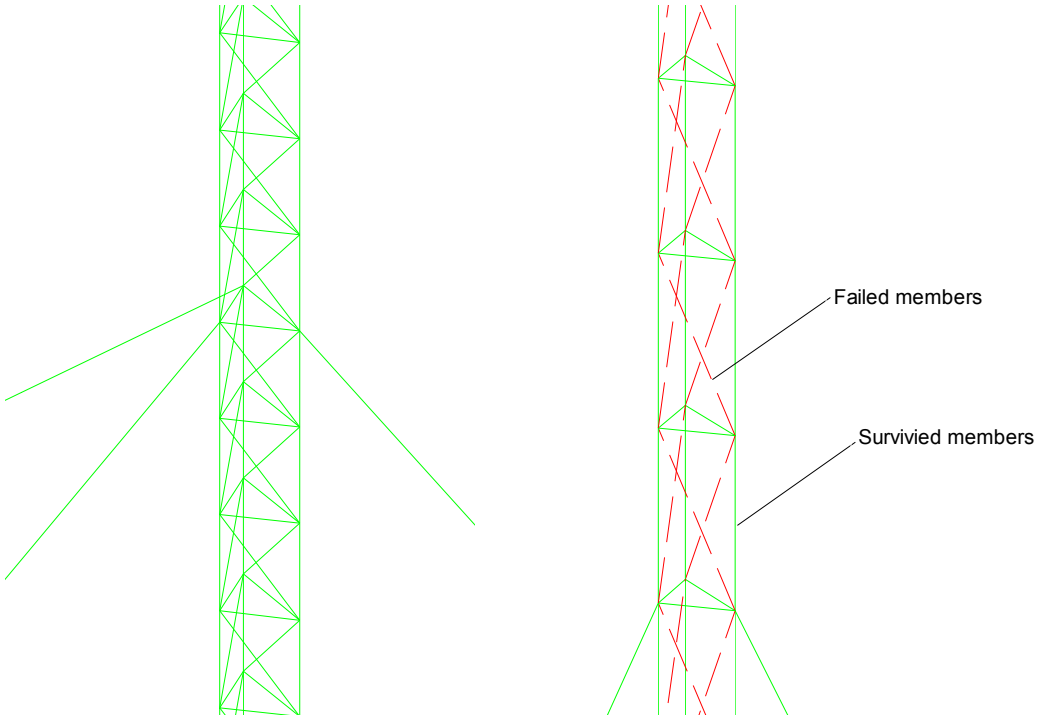

(a) (b)

Figure 6.27 Mast components (a) before the impulsive loading, and (b) after the impulsive loading.

6.7 Summary

The proposed methodology is effective in the individual load assessment, safety evaluation and global safety evaluation. Certain empirical formula can easily predict the intensity of impulsive load on big guyed towers. The developed P-I formulas can efficiently facilitate engineers in the assessment of survivability of truss and beam members under impulsive load. Different boundary conditions (simply supported or clamped) and impulsive load type (rectangular or triangular) will lead to different P-I thresholds. Critical curves for rectangular and triangular loads merge together in impulse-controlled and peak pressure-controlled regions. The global stability of a guyed tower can be determined by the eigenvalues of the structure. Due to the

inherent redundancy in guyed towers, they are expected to survive most types of light or medium impulsive loads.

Chapter 7 Conclusion and Future Work

7.1 Summary

In this dissertation we have extensively explored the nonlinear responses of guyed towers under large static loads and seismic loads. Two types of nonlinearities are included in the modeling: geometrical nonlinearity and material nonlinearity. Nonlinear characteristics of trusses, cables and beams are studied using various demonstrating examples. Material nonlinearity is added into the formulation of truss and cable elements to enable simulating of cases that not only have large deformation but also have large strain. Two types of guyed towers (short guyed tower with taut cables and high guyed tower with sagged cables) are analyzed with the implementation of truss, cable and beam elements. Both static and dynamic simulations are conducted. Material nonlinearity is finally included in the large static deformation.

The response and global stability of guyed towers under impulsive loads was evaluated in chapter 6. The impulsive load on specific members is assessed by empirical formulas. Two failure types, shear failure and bending failure, are realized next. With five possible transverse velocity profiles, response of rigid plastic beam is formulated for rectangular and triangular impulsive loads. The influence of boundary conditions was discussed as well. Five failure modes for rectangular loads and twelve modes for triangular loads were differentiated. A specific example of a guyed tower under impulsive load was conducted to demonstrate the comprehensive application of the P-I diagram method with nonlinear finite element analysis.

7.2 Conclusion

The application of nonlinear finite element and algorithms can successively trace static and dynamic response of guyed towers. Consideration of geometric nonlinearity is sufficient for large deformation with small strain. The dynamic analysis for a high guyed tower can be time consuming because of the large size of degrees of freedom.

Linear analysis may be proper and efficient for guyed towers that have small static deformation. Beyond some critical points, linear analysis is no longer accurate and nonlinear analysis is needed. For truss towers under seismic loads, linear modal analysis usually underestimates the corresponding vibration intensity, but it requires much less computation effort.

Consideration of material nonlinearity is very necessary for large deformation with large strain. An isotropic hardening model is proper for static cases and dynamic hardening can represent material constitution under dynamic loads. It is seen that inelasticity make structures behave softer than elastic ones. The inelasticity also helps in the dissipation of seismic response of truss towers, which is beneficial to structural safety as long as the strain remains below ductility limits.

The proposed methodology for global safety assessment for a guyed tower is effective. The developed P-I formulas are convenient to check the safety of individual member. It is also found that shear failure is a relatively rare phenomenon for mast members because they are usually slim. But some struts can have bending failure and form a potential failure mechanism.

7.3 Future work

Following tasks should be accomplished in the future to improve analysis.

1. Implementation of material nonlinearity in beam elements. Because the strain in beam element includes axial strain and bending strain, the combination of these results should be considered.
2. Parameter study of various indices for guyed towers, such as height, cable number and prestress level. Further study can include optimization to assist structural design.
3. If the impulsive loads are evaluated by FEM software like LS-DYNA, the impulsive loads on each member would be more accurate and the global safety evaluation would be more close to reality.

References

Abrahamson, G.R., and Lindberg, H.E. (1976). "Peak load-impulse characterization of critical pulse loads in structural dynamics." *Nuclear Engineering and Design*, 37, 35-36.

Amiri,G. G. (1997). *Seismic Sensitivity of Tall Guyed Telecommunication Towers*, Ph.D. Thesis, Department of Civil Engineering and Applied Mechanics, McGill University, Montreal, Canada.

ASTM A586-04a. (2007). *Standard Specification for Zinc-Coated Parallel and Helical Steel Wire Structural Strand*. American Society for Testing and Materials.

Bangash, M.Y. H. (1999). *Prototype Building Structures: Analysis and Design*, Thomas Telford, London.

Bangash, M.Y. H. and Bangash, T. (2006). *Explosion-Resistant Buildings analysis and design*, Springer, Germany.

Bathe, K.J. and Wilson, E.L. (1976). *Numerical Methods in Finite Element Analysis,* Prentice-Hall, Englewood Cliffs, N.J.

Bhatti, M.A. (2005). *Fundamental Finite Element Analysis and Applications : with Mathematica and MATLAB Computations*, John Willey & Sons, New Jersy.

Bhatti, M.A. (2006). *Advanced Topics in Finite Element Analysis of Structures*, John Willey & Sons, New Jersy.

Biggs, J.M. (1964). *Introduction to Structural Dynamics*, McGraw-Hill Book Company, New York.

Boresi, A.P. and Schmidt, R.J. (2003). *Advanced Mechanics of Materials*, John Willey

& Sons.

BSI. (1994). *British Standard: Lattice Towers and Masts: Part 4, Code of Practice for Lattice Masts.* BS 8100 Part 4, British Standards Institution, London, UK.

Brode, H.L. (1955). "*Numerical solution of spherical blast waves*", Journal of Applied Physics, 26, 766-775.

CEN. (1997). *European Pre-Standard ENV 1993-3-1:1997: Eurocode 3: Design of Steel Structures-Part 3-1: Towers, Masts and Chimneys – Towers and Masts*, Comité Européan de Normalisation, Brussels.

Chopra, A. K. (2000), *Dynamics of Structures Theory and Application to Earthquake Engineering*, Prentice Hall

Collins, G.S., Melosh, H.J., and Ivanov, B.A. (2003). "Modeling damage and deformation in impact simulations", *Meteoritics and Planetary Science*, 39(2), 217-231

Coombs, A., and Thornhill, C.K. (1967). "An Underwater explosive shock gun", *Journal of Fluid Mechanics*, 29, 373-383.

CSA. (1994). *Antennas, Towers, and Antenna-Supporting Structures*. CSA S37-94, Canadian Standards Association, Etobicoke, Ontario, Canada.

CSA. (2001), *Antennas, Towers, and Antenna-Supporting Structures*. Canadian Standards Association, Toronto, Ontario, Canada.

Davis, H. T. and Thomson. K. T. (2000). *Linear algebra and linear operators in engineering : with applications in Mathematica*, Academic Press, San Diego.

Galvez, C. (1995). *Static Method for Aseismic Design of Self –supporting Towers*. M. Eng. Project Report G95-08, Department of Civil Engineering and Applied Mechanics,

McGill University , Montreal, Quebec, Canada.

Geers, M.G.D. (1999). Enhanced solution control for physically and geometrically non-linear problems. Part II- comparative performance analysis, *Int.J. Numer. Meth. Engng.*, 46 , 205-230

Henrych. J. (1979). *The Dynamics of Explosion and Its Use*, Elsevier Science Publisher.

Hussam, M.M. (2005), Dynamic analysis of guyed towers for seismic loads, PhD dissertation, University of Windsor, Ontario, Canada.

Inman, D.J. (2001). *Engineering Vibration,* 2nd version, Prentice-Hall.

Irvine, H. M. (1981), *Cable Structures*, The MIT Press.

Jones, N. (1989). *Structural Impact*, Cambridge University Press.

Kassimali, A. (2005). Structural Analysis, Thomson Canada.

Kornhauser, M. (1954). "Prediction and evaluation of sensitivity to transient accelerations." *Journal of Applied Mechanics*, 21, 371-380.

Krauthammer, T. (1998). "Blast mitigation technologies: developments and numerical considerations for behavior assessment and design." *Proceedings of International Conference on Structures under Shock and Impact*, SUSI, Thessaloniki, Greece, 1-10.

Li, Q.M., and Jones, N. (1995). "Blast loading of fully clamped beams with transverse shear effects", *Mechanics of Structural and Machines*, 23(1), 59-86.

Li, Q.M., and Meng, H. (2002). "Pressure-impulse diagram for blast loads based on dimensional analysis and single-degree-of-freedom model." *Journal of Engineering Mechanics*, 128, 87-92.

Ma,G.W., Shi, H.J. and Shu, D.W. (2007). “P-I diagram method for combined failuremodes of rigid-plastic beams.” *International Journal of Impact Engineering,* 34, 1081-1094.

Madenci, E. and Guven, I. (2006). *The Finite Element Method and Applications in Engineering Using ANSYS,* Springer Science, New York.

Madugula, M.K.S. (2002), Dynamic response of lattice towers and guyed masts, American Society of Civil Engineers.

Mortion, H.S. (1954). *Scaling the effects of air blast on typical targets*, The John Hopkins Univ., Applied Physics Laboratory, Contract Now 62-0604-c, Technical Memorandum TG-733.

Nabil, B.K. (1993), Static and Dynamic Analysis of Guyed Towers, PhD dissertation, University of Wisconsin-Madison., Wisconsin, US.

Nayfeh, A.H. and Pai, P.F. (2004). *Linear and Nonlinear Structural Mechanics*, John Wiley, New Jersy.

Naval Facilities Engineering Command Design Manual 2.08. (1986). *Blast Resistant Structures*, SN 0525-CP-300-2092, US Army Engineer Research & Development Center.

Pai, P.F. (2007). *Highly Flexible Structures: Modeling, Computation, and Experimentation*, American Institute of Aeronautics and Astronautics (AIAA), Reston, Virginia.

Reddy, J.N. (2004). *An Introduction to Nonlinear Finite Element Analysis*, Oxford University Press, New York.

Sackmann, V. (1996). *Prediction of natural frequencies and mode shapes of self supporting lattice telecommunication towers*. Project Report- Diplomarbeit-Nr.76,

Department of Civil Engineering, McGill University, Montreal, Quebec, Canada.

Smith, P.D., and Hetherington, J.G. (1994). *Blast and Ballistic Loading of Structures*, Butterworth Heinemann.

TIA/EIA-222-G.5 (2006), *Structural Standard for Antenna Supporting Structures and Antennas*, Telecommunications Industry Association, Arlington, Virginia.

TM 5-1300 (1991), *Structures to Resist the Accidental Explosion*. US Department of the Army.

Wahba, Y.M.F. (1999), Static and dynamic analysis of guyed antenna towers, PhD dissertation, University of Windsor, Ontario, Canada.

Zienkiewicz, O.C., Taylor, R.L. and Zhu, J.Z. (2005). *The Finite Element Method : Its Basis and Fundamentals*, Elsevier Butterworth-Heinemann, Boston.

Appendix A

Derivation of P-I Diagrams for Combined Failure Mode of Simply Supported Beams subject to Rectangular Loads

Mode I. **When** $\upsilon \le 1$ **and** $p_0 > \frac{2M_0}{L^2}\upsilon$

(1) $t \le t_d$

The governing equation for the dominant shear effect is

$$\frac{\partial Q}{\partial x} = -p_0 + m\ddot{y} \tag{A.1}$$

Integrate with respect to x and consider the initial condition $Q = -Q_0$ when $x = L$,

$$-Q_0 = -p_0 \cdot L + m\ddot{y}L$$

Thus,

$$\ddot{y} = \frac{-Q_0}{mL} + \frac{p_0}{m} \tag{A.2}$$

Integrate Eq. (A.2) with respect to x and consider the initial condition $\dot{y} = 0$ when $t = 0$,

$$\dot{y} = \frac{-Q_0}{mL}t + \frac{p_0}{m}t \tag{A.3}$$

To initiate the motion $\dot{\omega} > 0$, so

$$p_0 L > Q_0, \text{ i.e., } p_0 > \frac{2M_0}{L^2}\upsilon$$

Integrate Eq. (A.3) with respect to x and consider the initial condition $y = 0$ when $t = 0$,

$$y = \frac{-Q_0}{mL}\frac{t^2}{2} + \frac{p_0}{m}\frac{t^2}{2} \tag{A.4}$$

At the end of loading, the velocity and displacement of the beam is

$$\dot{y} = \frac{-Q_0}{mL}t_d + \frac{p_0}{m}t_d \tag{A.5}$$

$$y = \frac{-Q_0}{mL}\frac{t_d^2}{2} + \frac{p_0}{m}\frac{t_d^2}{2} \tag{A.6}$$

(2) $t_d \le t \le t_f$

After t_d the load is removed, Eq. (A.1) turns into

$$\frac{\partial Q}{\partial x} = m\ddot{y} \tag{A.7}$$

Integrate Eq. (A.7) with respect to x

$$-Q_0 = m\ddot{y}L$$

$$\ddot{y} = \frac{-Q_0}{mL}$$

Due to continuity condition, i.e., Eq. (A.5) and Eq. (A.6),

$$\dot{y} = \frac{-Q_0}{mL}(t - t_d) + \left(\frac{-Q_0}{mL}t_d + \frac{p_0}{m}t_d\right) = \frac{-Q_0}{mL}t + \frac{p_0}{m}t_d$$

$$y = \frac{-Q_0}{mL}\frac{(t-t_d)^2}{2} + \left(\frac{-Q_0}{mL}t_d + \frac{p_0}{m}t_d\right)(t-t_d) + \frac{(p_0L - Q_0)}{2mL}t_d^2$$
$$= \frac{-Q_0}{2mL}t^2 - \frac{p_0}{2m}t_d^2 + \frac{p_0}{m}t_d \cdot t$$

The deformation will cease at

$$t_f = \frac{p_0 L}{Q_0}t_d \tag{A.8}$$

The final maximum deformation of the beam is

$$y_f = \frac{p_0\left(p_0 L - Q_0\right)}{2mQ_0} t_d^2 = \frac{Lp_0^2 t_d^2}{2mQ_0} - \frac{p_0 t_d^2}{2m} \tag{A.9}$$

If the average shear strain damage criteria is applied, then

$$h\gamma_v = \frac{p_0\left(p_0 L - Q_0\right)}{2mQ_0} t_d^2 \tag{A.10}$$

Set the impulse quantity $I = p_0 \cdot t_d$, the critical P-I diagram equation for shear failure is derived as

$$\frac{2mh\gamma_v}{I^2} + \frac{1}{p_0} = \frac{L}{Q_0} \tag{A.11}$$

Mode II. **When** $1 \le \upsilon \le 1.5$ **and** $p_0 > \frac{2M_0}{L^2}\left(4\upsilon - 3\right)$

From the transverse velocity profiles, it can

$$\dot{y} = \dot{y}_s + \left(\dot{y}_m - \dot{y}_s\right)\left(1 - \frac{x}{L}\right) \quad 0 \le x \le L \tag{A.12}$$

(1) $t \le t_d$

$$\frac{\partial Q}{\partial x} = -p_0 + m\ddot{y}_s + m\left(\ddot{y}_m - \ddot{y}_s\right)\left(1 - \frac{x}{L}\right) \tag{A.13}$$

Integrate with respect to x and consider the initial condition

$$Q = -Q_0 \text{ at } x = L$$

$$Q = 0 \text{ at } x = 0 \tag{A.14}$$

Eq. (A.13) can be turned into

$$Q = -p_0 x + m\ddot{y}_s x + m(\ddot{y}_m - \ddot{y}_s)\left(x - \frac{x^2}{2L}\right) \tag{A.15}$$

since $\frac{\partial M}{\partial x} = Q$, $M = M_0$ at $x = 0$ and $M = 0$ at $x = L$

Integration of Eq. (A.15) gives

$$M = -p_0 \frac{x^2}{2} + m\ddot{y}_s \frac{x^2}{2} + m(\ddot{y}_m - \ddot{y}_s)\left(\frac{x^2}{2} - \frac{x^3}{6L}\right) + M_0 \tag{A.16}$$

$$\begin{cases} -Q_0 = -p_0 L + m\ddot{y}_s L + m(\ddot{y}_m - \ddot{y}_s)\dfrac{L}{2} \\ 0 = -p_0 \dfrac{L^2}{2} + m\ddot{y}_s \dfrac{L^2}{2} + m(\ddot{y}_m - \ddot{y}_s)\dfrac{L^2}{3} + M_0 \end{cases} \tag{A.17}$$

Solve the above Eq. (A.16) and Eq. (A.17)

$$\ddot{y}_m = \frac{p_0}{m} - \frac{6M_0}{mL^2} + \frac{2Q_0}{mL} \tag{A.18}$$

$$\ddot{y}_s = \frac{p_0}{m} + \frac{6M_0}{mL^2} - \frac{4Q_0}{mL} \tag{A.19}$$

Integrate Eq. (A.18) and Eq. (A.19) with respect to time and consider the initial condition as

$\dot{y}_m = \dot{y}_s = 0$ and $y_m = y_s = 0$ at $t = 0$

$$\dot{y}_m = \frac{p_0}{m} t - \frac{6M_0}{mL^2} t + \frac{2Q_0}{mL} t = \left[\frac{p_0}{m} + \frac{2M_0}{mL^2}(2\upsilon - 3)\right] t \tag{A.20}$$

$$\dot{y}_s = \frac{p_0}{m} t + \frac{6M_0}{mL^2} t - \frac{4Q_0}{mL} t = \left[\frac{p_0}{m} + \frac{2M_0}{mL^2}(3 - 4\upsilon)\right] t \tag{A.21}$$

To initiate the shear slide motion it requires $p_0 > \frac{2M_0}{L^2}(4\upsilon - 3)$, otherwise it will keep still. Integrate Eq. (A.20) and Eq. (A.21) with respect to t

$$y_m = \frac{p_0}{m}\frac{t^2}{2} - \frac{6M_0}{mL^2}\frac{t^2}{2} + \frac{2Q_0}{mL}\frac{t^2}{2} \tag{A.22}$$

$$y_s = \frac{p_0}{m}\frac{t^2}{2} + \frac{6M_0}{mL^2}\frac{t^2}{2} - \frac{4Q_0}{mL}\frac{t^2}{2} \tag{A.23}$$

Substitute Eq. (A.22) and Eq. (A.23) into Eq. (A.12)

$$\therefore\ \dot{y} = \frac{p_0}{m}t + \frac{6M_0}{mL^2}t - \frac{4Q_0}{mL}t + \left(\frac{6Q_0}{mL}t - \frac{12M_0}{mL^2}t\right)\left(1 - \frac{x}{L}\right) \tag{A.24}$$

Integrate Eq. (A.24) with respect to time t

$$y = \frac{p_0}{m}\frac{t^2}{2} + \frac{6M_0}{mL^2}\frac{t^2}{2} - \frac{4Q_0}{mL}\frac{t^2}{2} + \left(\frac{6Q_0}{mL}\frac{t^2}{2} - \frac{12M_0}{mL^2}\frac{t^2}{2}\right)\left(1 - \frac{x}{L}\right) \tag{A.25}$$

(2) $t_d \le t \le t_s$

Eq. (A.1) turns into

$$\frac{\partial Q}{\partial x} = m\ddot{y}_s + m\left(\ddot{y}_m - \ddot{y}_s\right)\left(1 - \frac{x}{L}\right) \tag{A.26}$$

Integrate with respect to x and consider the initial condition $Q = 0$ at $x = 0$ and

$M = M_0$ at $x = 0$

$$Q = m\ddot{y}_s x + m\left(\ddot{y}_m - \ddot{y}_s\right)\left(x - \frac{x^2}{2L}\right)$$

$$M = m\ddot{y}_s \frac{x^2}{2} + m\left(\ddot{y}_m - \ddot{y}_s\right)\left(\frac{x^2}{2} - \frac{x^3}{6L}\right) + M_0$$

since $Q = -Q_0$ at $x = L$ and $M = 0$ at $x = L$

$$\begin{cases} -Q_0 = m\ddot{y}_s L + m\left(\ddot{y}_m - \ddot{y}_s\right)\dfrac{L}{2} \\ 0 = m\ddot{y}_s \dfrac{L^2}{2} + m\left(\ddot{y}_m - \ddot{y}_s\right)\dfrac{L^2}{3} + M_0 \end{cases} \tag{A.27}$$

Solve the Eq. (A.27)

$$\ddot{y}_m = -\frac{6M_0}{mL^2} + \frac{2Q_0}{mL} \tag{A.28}$$

$$\ddot{y}_s = \frac{6M_0}{mL^2} - \frac{4Q_0}{mL} \tag{A.29}$$

Integrate Eq. (A.28) and Eq. (A.29) with respect to time t and consider the initial condition as at $t = t_d$

$$\dot{y}_m = \frac{p_0}{m} t_d - \frac{6M_0}{mL^2} t_d + \frac{2Q_0}{mL} t_d$$

$$\dot{y}_s = \frac{p_0}{m} t_d + \frac{6M_0}{mL^2} t_d - \frac{4Q_0}{mL} t_d$$

$$y_m = \frac{p_0}{m} \frac{t_d^2}{2} - \frac{6M_0}{mL^2} \frac{t_d^2}{2} + \frac{2Q_0}{mL} \frac{t_d^2}{2}$$

$$y_s = \frac{p_0}{m} \frac{t_d^2}{2} + \frac{6M_0}{mL^2} \frac{t_d^2}{2} - \frac{4Q_0}{mL} \frac{t_d^2}{2}$$

The final solution is

$$\dot{y}_m = \frac{2}{mL}\left(-\frac{3M_0}{L} + Q_0\right)t + \frac{p_0}{m} t_d$$

$$\dot{y}_s = \frac{2}{mL}\left(\frac{3M_0}{L} - 2Q_0\right)t + \frac{p_0}{m} t_d$$

$$y_m = \frac{1}{mL}\left(-\frac{3M_0}{L} + Q_0\right)t^2 + \frac{p_0}{m} t \cdot t_d - \frac{p_0}{2m} t_d^2$$

$$y_s = \frac{1}{mL}\left(\frac{3M_0}{L} - 2Q_0\right)t^2 + \frac{p_0}{m} t \cdot t_d - \frac{p_0}{2m} t_d^2$$

It is evident that the transverse shear slide ceases at the supports when $\dot{\omega}_s = 0$

$$t_s = \frac{p_0 \cdot t_d \cdot L^2}{2(4\upsilon - 3)M_0} \tag{A.30}$$

when

$$\dot{y}_m = \frac{6 p_0 t_d}{m} \cdot \frac{\upsilon - 1}{4\upsilon - 3}$$

Since $\upsilon > 1$, $\dot{y}_m > 0$. Thus the beam has kinetic energy which should be dissipated in the next phase of motion.

So at the end

$$y_m = \frac{(10\upsilon - 9)p_0^2 t_d^2 L^2}{4M_0 m(4\upsilon - 3)^2} - \frac{p_0}{2m} t_d^2 \tag{A.31}$$

$$y_s = \frac{p_0^2 t_d^2 L^2}{4M_0 m(4\upsilon - 3)} - \frac{p_0}{2m} t_d^2 \tag{A.32}$$

(3) $t_s \le t \le t_f$

$$\frac{\partial Q}{\partial x} = m\ddot{y}_m \left(1 - \frac{x}{L}\right) \tag{A.33}$$

$\because Q = 0$ at $x = 0$

$$Q = m\ddot{y}_m \left(x - \frac{x^2}{2L}\right) \tag{A.34}$$

$\because \frac{\partial M}{\partial x} = Q$ and $M = M_0$ at $x = 0$

$$M = m\ddot{y}_m \left(\frac{x^2}{2} - \frac{x^3}{6L}\right) + M_0 \tag{A.35}$$

$\because M = 0$ at $x = L$

$$\ddot{y}_m = -\frac{3M_0}{mL^2} \tag{A.36}$$

When ensuring the continuity condition at $t = t_s$

$$\dot{y}_m = -\frac{3M_0}{mL^2}t + \frac{3p_0}{2m}t_d \tag{A.37}$$

$$y_m = -\frac{3M_0}{2mL^2}t^2 + \frac{3p_0}{2m}t_d \cdot t - \frac{p_0}{2m}t_d^2 + \frac{p_0^2 t_d^2 L^2}{8M_0 m(3-4\upsilon)} \tag{A.38}$$

So the motion finally ceased at

$$t_f = \frac{p_0 \cdot t_d \cdot L^2}{2M_0} \tag{A.39}$$

The final transverse displacement is

$$y_f = \frac{(6\upsilon-5)p_0^2 t_d^2 L^2}{4M_0 m(4\upsilon-3)} - \frac{p_0}{2m}t_d^2 \tag{A.40}$$

Apply the failure criteria, the critical P-I diagram equation for shear failure is

$$\frac{2mh\gamma_v}{I^2} + \frac{1}{p_0} = \frac{L\upsilon}{Q_0(4\upsilon-3)} \tag{A.41}$$

The critical P-I diagram equation for bending failure is

$$\frac{2mL\beta}{I^2} + \frac{1}{p_0} = \frac{L^2 \cdot (6\upsilon-5)}{2M_0(4\upsilon-3)} \tag{A.42}$$

Mode III. **When** $1 \le \upsilon \le 1.5$ **and** $\frac{2M_0}{L^2} \le p_0 \le \frac{2M_0}{L^2}(4\upsilon-3)$

or $1.5 \le \upsilon$ **and** $\frac{2M_0}{L^2} \le p_0 \le \frac{6M_0}{L^2}$

There will be no transverse shear slide at the support.

$$\dot{y} = \dot{y}_m\left(1-\frac{x}{L}\right) \quad 0 \le x \le L \tag{A.43}$$

(1) $t \le t_d$

$$\frac{\partial Q}{\partial x} = -p_0 + m\ddot{y}_m\left(1-\frac{x}{L}\right) \tag{A.44}$$

Integrate with respect to x and consider the initial condition $Q = 0$ at $x = 0$

$$Q = -p_0 x + m\ddot{y}_m\left(x-\frac{x^2}{2L}\right) \tag{A.45}$$

since $\frac{\partial M}{\partial x} = Q$, $M = M_0$ at $x = 0$ and $M = 0$ at $x = L$.

$$M = -p_0\frac{x^2}{2} + m\ddot{y}_m\left(\frac{x^2}{2}-\frac{x^3}{6L}\right) + M_0 \tag{A.46}$$

Solve Eq. (A.45)

$$\ddot{y}_m = \frac{3p_0}{2m} - \frac{3M_0}{mL^2} \tag{A.47}$$

Integrate Eq. (A.46) with time t

$$\dot{y}_m = \left[\frac{3p_0}{2m} - \frac{3M_0}{mL^2}\right]t \tag{A.48}$$

Integrate Eq. (A.47) with time t

$$y_m = \left[\frac{3p_0}{2m} - \frac{3M_0}{mL^2}\right]\cdot\frac{t^2}{2} \tag{A.49}$$

(2) $t_d \le t \le t_f$

$$\frac{\partial Q}{\partial x} = m\ddot{y}_m\left(1-\frac{x}{L}\right) \tag{A.50}$$

Integrate with respect to x and consider the initial condition $Q = 0$ at $x = 0$ and $M = M_0$ at $x = 0$

$$Q = m\ddot{y}_m\left(x - \frac{x^2}{2L}\right) \tag{A.51}$$

$$M = m\ddot{y}_m\left(\frac{x^2}{2} - \frac{x^3}{6L}\right) + M_0 \tag{A.52}$$

since $M = 0$ at $x = L$

$$0 = m\ddot{y}_m \frac{L^2}{3} + M_0$$

Solve the above equations

$$\ddot{y}_m = -\frac{3M_0}{mL^2} \tag{A.53}$$

Integrate with respect to time and consider the initial condition as at $t = t_d$

$$\dot{y}_m = -\frac{3M_0}{mL^2}t + \frac{3p_0}{2m}t_d \tag{A.54}$$

$$y_m = -\frac{3M_0}{2mL^2}t^2 + \frac{3p_0}{2m}t \cdot t_d - \frac{3p_0}{4m}t_d^2 \tag{A.55}$$

It is evident that the bending ceases at the supports when $\dot{y}_m = 0$ $t_f = \frac{p_0 \cdot t_d \cdot L^2}{2M_0}$

$$y_f = \frac{3p_0^2 t_d^2 L^2}{8M_0 m} - \frac{3p_0}{4m}t_d^2 \tag{A.56}$$

The critical P-I diagram equation for bending failure is

$$\frac{4mL\beta}{3I^2} + \frac{1}{p_0} = \frac{L^2}{2M_0} \tag{A.57}$$

Mode IV. **When** $1.5 \le \upsilon$ **and** $p_0 > \dfrac{8M_0}{3L^2}\upsilon^2$

There is shear slide at the support.

(1) $t \le t_d$

The transverse velocity field is like

$$\dot{y} = \begin{cases} \dot{y}_m & 0 \le x \le \xi_0 \\ \dot{y}_s + (\dot{y}_m - \dot{y}_s)\dfrac{L-x}{L-\xi_0} & \xi_0 \le x \le L \end{cases} \tag{A.58}$$

When $0 \le x \le \xi_0$, $Q = 0$ and $M = M_0$

$$\because \frac{\partial Q}{\partial x} = -p_0 + m\ddot{y}_m = 0$$

$$\therefore \ddot{y}_m = \frac{p_0}{m}$$

When $\xi_0 \le x \le L$

$$\frac{\partial Q}{\partial x} = -p_0 + m\ddot{y}_s + m(\ddot{y}_m - \ddot{y}_s)\cdot\frac{L-x}{L-\xi_0} \tag{A.59}$$

$$Q = -p_0(x-\xi_0) - \frac{m(x-\xi_0)((-2L+x+\xi_0)\ddot{y}_m + (-x+\xi_0)\ddot{y}_s)}{2(L-\xi_0)} \tag{A.60}$$

since $Q = 0$ at $x = \xi_0$.

$$\begin{aligned} M = \frac{L-x}{6(L-\xi_0)}[&3p_0(L+x-2\xi_0)(L-\xi_0) - m\ddot{y}_m(2L^2+2Lx-x^2-6L\xi_0+3\xi_0^2) \\ &- m\ddot{y}_s(L^2+Lx+x^2-3L\xi_0-3x\xi_0+3\xi_0^2)] \end{aligned} \tag{A.61}$$

since $M = 0$ at $x = L$.

Since $Q = -Q_0$ at $x = L$ and $M = M_0$ at $x = \xi_0$, solve the equations,

$$\ddot{y}_m = \frac{p_0}{m} - \frac{6M_0}{m(L-\xi_0)^2} + \frac{2Q_0}{m(L-\xi_0)} \tag{A.62}$$

$$\ddot{y}_s = \frac{p_0}{m} + \frac{6M_0}{m(L-\xi_0)^2} - \frac{4Q_0}{m(L-\xi_0)} \tag{A.63}$$

$$\because \ \ddot{y}_m = \frac{p_0}{m}$$

$$\therefore \ \xi_0 = \frac{2\upsilon - 3}{2\upsilon} L$$

$$\ddot{y}_s = \frac{p_0}{m} - \frac{4Q_0\upsilon}{3mL} = \frac{p_0}{m} - \frac{8M_0\upsilon^2}{3mL^2} \tag{A.64}$$

$$Q = -\frac{(3L - 2L\upsilon + 2x\upsilon)^2}{9L^2} Q_0 \tag{A.65}$$

$$M = \frac{2\upsilon(L-x)\left[2Lx\upsilon(9-4\upsilon) + 4x^2\upsilon^2 + L^2(27 - 18\upsilon + 4\upsilon^2)\right]}{27L^3} M_0 \tag{A.66}$$

To initiate the shear slide motion it requires $p_0 > \frac{8M_0}{3L^2}\upsilon^2$, otherwise it will keep still.

$$\dot{y}_m = \frac{p_0}{m} t \tag{A.67}$$

$$y_m = \frac{p_0}{2m} t^2 \tag{A.68}$$

$$\dot{y}_s = \left(\frac{p_0}{m} - \frac{8M_0\upsilon^2}{3mL^2} \right) t \tag{A.69}$$

$$y_s = \left(\frac{p_0}{m} - \frac{8M_0\upsilon^2}{3mL^2} \right) \frac{t^2}{2} \tag{A.70}$$

at the end of this phase

$$\dot{y}_m = \frac{p_0}{m} t_d \tag{A.71}$$

$$y_m = \frac{p_0}{2m} t_d^2 \tag{A.72}$$

$$\dot{y}_s = \left(\frac{p_0}{m} - \frac{8M_0 \upsilon^2}{3mL^2} \right) t_d \tag{A.73}$$

$$y_s = \left(\frac{p_0}{m} - \frac{8M_0 \upsilon^2}{3mL^2} \right) \frac{t_d^2}{2} \tag{A.74}$$

(2) $t_d \le t \le t_s$

When $0 \le x \le \xi_0$

$$\because Q = 0 \text{ and } M = M_0$$

$$\therefore \frac{\partial Q}{\partial x} = m\ddot{y}_m = 0 \;\Rightarrow\; \ddot{y}_m = 0$$

When $\xi_0 \le x \le L$

$$\frac{\partial Q}{\partial x} = m\ddot{y}_s - m\ddot{y}_s \cdot \frac{L-x}{L-\xi_0} \quad = m\ddot{y}_s \cdot \frac{x-\xi_0}{L-\xi_0}$$

since $Q = 0$ at $x = \xi_0$

$$Q = m\ddot{y}_s \cdot \frac{(x-\xi_0)^2}{2(L-\xi_0)} \tag{A.75}$$

since $Q = -Q_0$ at $x = L$

$$\ddot{y}_s = \frac{-2Q_0}{m(L-\xi_0)} \tag{A.76}$$

since $M = 0$ at $x = L$

$$M = -m\ddot{y}_s (L-x) \frac{x^2 + Lx + L^2 - 3L\xi_0 - 3x\xi_0 + 3\xi_0^2}{6(L-\xi_0)} \tag{A.77}$$

since $M = M_0$ at $x = \xi_0$

$\xi_0 = \frac{2\upsilon - 3}{2\upsilon} L$,which means that the plastic hinges region hasn't changed.

Thus,

$$\ddot{y}_s = \frac{-8\upsilon^2 M_0}{3mL^2} \tag{A.78}$$

$$\dot{y}_m = \frac{p_0}{m} t_d \tag{A.79}$$

$$y_m = \frac{p_0}{m} t_d t - \frac{p_0}{2m} t_d^2 \tag{A.80}$$

$$\dot{y}_s = \frac{p_0 \cdot t_d}{m} - \frac{8M_0\upsilon^2}{3mL^2} \cdot t \tag{A.81}$$

$$y_s = -\frac{4M_0\upsilon^2 t^2}{3mL^2} + \frac{p_0 t_d t}{m} - \frac{p_0 t_d^2}{2m} \tag{A.82}$$

So the motion will cease at $t_s = \frac{3L^2 p_0 \cdot t_d}{8M_0\upsilon^2}$ when

$$\dot{y}_m = \frac{p_0}{m} t_d \tag{A.83}$$

$$y_m = -\frac{\left(8M_0\upsilon^2 - 3L^2 p_0\right) \cdot p_0 t_d^2}{8M_0 m\upsilon^2} \tag{A.84}$$

$$\dot{y}_s = 0$$

$$y_s = -\frac{p_0 t_d^2}{2m} + \frac{3p_0^2 L^2 t_d^2}{16M_0 m\upsilon^2} \tag{A.85}$$

(3) $t_s \le t \le t_1$

At the end of last phase $\dot{y}_m \neq 0$ the beam has a kinetic energy that must be dissipated as plastic work. In this phase the position of bending hinges begin to travels from $x = \xi_0$ to the mid span till t_1.

When $0 \le x \le \xi$

$$\dot{y}_m = \frac{p_0}{m} t_d \tag{A.86}$$

$$y_m = \frac{p_0}{m} t_d t - \frac{p_0}{2m} t_d^2 \tag{A.87}$$

When $\xi \le x \le L$

$$\dot{y} = \dot{y}_m \cdot \frac{L-x}{L-\xi} = \frac{p_0}{m} t_d \cdot \frac{L-x}{L-\xi} \tag{A.88}$$

$$\because \ \ddot{y} = \frac{p_0}{m} t_d \cdot \frac{L-x}{(L-\xi)^2} \cdot \dot{\xi}$$

$$Q = p_0 t_d \cdot \frac{\dot{\xi}}{(L-\xi)^2} \cdot (x-\xi) \cdot \left[L - \frac{x+\xi}{2} \right] \tag{A.89}$$

$$M = M_0 + \frac{p_0 t_d \dot{\xi} (x-\xi)^2 \left(\frac{L}{2} - \frac{x}{6} - \frac{\xi}{3} \right)}{(L-\xi)^2} \tag{A.90}$$

Since $M = 0$ at $x = L$

$$\dot{\xi} = \frac{-3M_0}{p_0 t_d (L-\xi)} \tag{A.91}$$

Solve the above differential equation with the initial condition $t_s = \frac{3L^2 p_0 \cdot t_d}{8M_0 \upsilon^2}$

$$\xi = \xi_0 = \frac{2\upsilon - 3}{2\upsilon} L \tag{A.92}$$

$$\xi = L - \frac{\sqrt{6tM_0 p_0 t_d}}{p_0 t_d} \tag{A.93}$$

So $\xi = 0$, $t_1 = \dfrac{p_0 t_d L^2}{6M_0}$ when

$$y_m = \frac{p_0^2 t_d^2 L^2}{6M_0 m} - \frac{p_0}{2m} t_d^2 = \frac{p_0}{2m} t_d^2 \left(\frac{p_0 L^2}{3M_0} - 1 \right) \tag{A.94}$$

(4) $t_1 \le t \le t_f$

The transverse velocity field is

$$\dot{y} = \dot{y}_m \cdot \left(1 - \frac{x}{L} \right) \qquad 0 \le x \le L \tag{A.95}$$

$$\therefore Q = m\ddot{y}_m \left(x - \frac{x^2}{2L} \right) \tag{A.96}$$

$$M = M_0 + m\ddot{y}_m \left(\frac{x^2}{2} - \frac{x^3}{6L} \right) \tag{A.97}$$

since $M = 0$ at $x = L$

$$\ddot{y}_m = \frac{-3M_0}{mL^2} \tag{A.98}$$

$$\dot{y}_m = \frac{-3M_0}{mL^2}(t - t_1) + \frac{p_0 t_d}{m} \tag{A.99}$$

$$y_m = \frac{-3M_0}{mL^2} \frac{(t - t_1)^2}{2} + \frac{p_0 t_d}{m}(t - t_1) + \frac{p_0}{2m} t_d^2 \left(\frac{p_0 L^2}{3M_0} - 1 \right) \tag{A.100}$$

solve $\dot{y}_m = 0$

$$t_f = \frac{p_0 t_d L^2}{2M_0} \tag{A.101}$$

which predicts the mid-span displacement

$$y_f = \frac{p_0^2 L^2 t_d^2}{3M_0 m} - \frac{p_0}{2m} t_d^2 \tag{A.102}$$

Apply the failure criteria, the critical P-I diagram equation for shear failure is

$$\frac{2mh\gamma_v}{I^2} + \frac{1}{p_0} = \frac{3L}{4Q_0 \upsilon} \tag{A.103}$$

The critical P-I diagram equation for bending failure is

$$\frac{2mL\beta}{I^2} + \frac{1}{p_0} = \frac{2L^2}{3M_0} \tag{A.104}$$

Mode V. **When** $1.5 \le \upsilon$ **and** $\frac{6M_0}{L^2} \le p_0 \le \frac{8M_0}{3L^2}\upsilon^2$

There will be no transverse shear slide at the support.

(1) $t \le t_d$

The transverse velocity field is like

$$\dot{y} = \begin{cases} \dot{y}_m & 0 \le x \le \xi_0 \\ \dot{y}_m \dfrac{L-x}{L-\xi_0} & \xi_0 \le x \le L \end{cases} \tag{A.105}$$

So when $0 \le x \le \xi_0$, $Q = 0$ and $M = M_0$.

$$\because \frac{\partial Q}{\partial x} = -p_0 + m\ddot{y}_m = 0$$

$$\therefore \ddot{y}_m = \frac{p_0}{m}$$

When $\xi_0 \le x \le L$

$$\frac{\partial Q}{\partial x} = -p_0 + p_0 \cdot \frac{L-x}{L-\xi_0} \tag{A.106}$$

$$Q = -p_0(x-\xi_0) - \frac{p_0(x-\xi_0)(-2L+x+\xi_0)}{2(L-\xi_0)}$$
$$= -\frac{p_0(x-\xi_0)^2}{2(L-\xi_0)}$$

since $Q = 0$ at $x = \xi_0$.

$$M = \frac{L-x}{6(L-\xi_0)}\left[3p_0(L+x-2\xi_0)(L-\xi_0) - p_0(2L^2+2Lx-x^2-6L\xi_0+3\xi_0^2)\right]$$
$$= \frac{(L-x)p_0}{6(L-\xi_0)}\left[L^2+Lx+x^2-3(L+x)\xi_0+3\xi_0^2\right]$$

since $M = 0$ at $x = L$.

Since $M = M_0$ at $x = \xi_0$, solve the equations

$$\therefore \xi_0 = L - \sqrt{\frac{6M_0}{p_0}} \tag{A.107}$$

Thus if $\frac{6M_0}{L^2} \le p_0$, the bending part is a district. Otherwise it will be confined to only one bending hinge.

$$Q = -\frac{\sqrt{6p_0M_0}}{2} + (L-x)p_0 - \frac{\sqrt{6}}{12}(L-x)^2 p_0\sqrt{\frac{p_0}{M_0}} \tag{A.108}$$

$$M = \frac{\sqrt{6p_0M_0}}{2}(L-x) - \frac{(L-x)^2 p_0}{2} + \frac{\sqrt{6}}{36}(L-x)^3 p_0\sqrt{\frac{p_0}{M_0}} \tag{A.109}$$

at the end of this phase

$$\dot{y}_m = \frac{p_0}{m}t_d \tag{A.110}$$

$$y_m = \frac{p_0}{2m}t_d^2 \tag{A.111}$$

(2) $t_d \le t \le t_1$

In this phase the position of bending hinges begin to travels from $x = \xi_0$ to the mid span till t_1.

When $0 \le x \le \xi$

$$\dot{y}_m = \frac{p_0}{m} t_d \tag{A.112}$$

$$y_m = \frac{p_0}{m} t_d t - \frac{p_0}{2m} t_d^2 \tag{A.113}$$

When $\xi \le x \le L$

$$\dot{y} = \dot{y}_m \cdot \frac{L-x}{L-\xi} = \frac{p_0}{m} t_d \cdot \frac{L-x}{L-\xi} \tag{A.114}$$

$$\because \ \ddot{y} = \frac{p_0}{m} t_d \cdot \frac{L-x}{(L-\xi)^2} \cdot \dot{\xi}$$

$$Q = p_0 t_d \cdot \frac{\dot{\xi}}{(L-\xi)^2} \cdot (x-\xi) \cdot \left[L - \frac{x+\xi}{2} \right] \tag{A.115}$$

$$M = M_0 + \frac{p_0 t_d \dot{\xi} (x-\xi)^2 \left(\frac{L}{2} - \frac{x}{6} - \frac{\xi}{3} \right)}{(L-\xi)^2} \tag{A.116}$$

Since $M = 0$ at $x = L$

$$\dot{\xi} = \frac{-3M_0}{p_0 t_d (L-\xi)} \tag{A.117}$$

Solve the above differential equation with the initial condition $t = t_d$,

$$\xi = \xi_0 = L - \sqrt{\frac{6M_0}{p_0}} \tag{A.118}$$

$$\xi = L - \frac{\sqrt{6tM_0 p_0 t_d}}{p_0 t_d} \tag{A.119}$$

So $\xi = 0$, $t_1 = \dfrac{p_0 t_d L^2}{6M_0}$ when

$$\dot{y}_m = \frac{p_0}{m} t_d$$

$$y_m = \frac{p_0^2 t_d^2 L^2}{6M_0 m} - \frac{p_0}{2m} t_d^2 = \frac{p_0}{2m} t_d^2 \left(\frac{p_0 L^2}{3M_0} - 1 \right) \tag{A.120}$$

(3) $t_1 \le t \le t_f$

The transverse velocity field is

$$\dot{y} = \dot{y}_m \cdot \left(1 - \frac{x}{L} \right) \qquad 0 \le x \le L$$

$$\therefore Q = m\ddot{y}_m \left(x - \frac{x^2}{2L} \right) \tag{A.121}$$

$$M = M_0 + m\ddot{y}_m \left(\frac{x^2}{2} - \frac{x^3}{6L} \right) \tag{A.122}$$

since $M = 0$ at $x = L$

$$\ddot{y}_m = \frac{-3M_0}{mL^2} \tag{A.123}$$

$$\dot{y}_m = \frac{-3M_0}{mL^2} (t - t_1) + \frac{p_0 t_d}{m} \tag{A.124}$$

$$y_m = \frac{-3M_0}{mL^2} \frac{(t - t_1)^2}{2} + \frac{p_0 t_d}{m} (t - t_1) + \frac{p_0}{2m} t_d^2 \left(\frac{p_0 L^2}{3M_0} - 1 \right) \tag{A.125}$$

solve $\dot{y}_m = 0$

$$t_f = \frac{p_0 t_d L^2}{2M_0} \tag{A.126}$$

which predicts the mid-span displacement

$$y_f = \frac{p_0^2 L^2 t_d^2}{3M_0 m} - \frac{p_0}{2m} t_d^2 \tag{A.127}$$

Apply the failure criteria, the critical P-I diagram equation for bending failure is

$$\frac{2mL\beta}{I^2} + \frac{1}{p_0} = \frac{2L^2}{3M_0} \quad \text{[B]} \tag{A.128}$$

The results can be summarized in Table A.1 using the normalization criteria (Eqs. (6.92) and (6.93)).

Table A.1 Normalized P-I equations for rectangular impulsive loads

Failure Type	**Mode**	**Shear failure**	**Bending failure**
Simply Supported Beams	I	$\frac{h\gamma_v}{i^2} + \frac{1}{p_0} = 1$	N/A
	II	$\frac{h\gamma_v}{i^2} + \frac{1}{p_0} = \frac{\upsilon}{4\upsilon - 3}$	$\frac{L\beta}{i^2} + \frac{1}{p_0} = \frac{\upsilon(6\nu - 5)}{4\upsilon - 3}$
	III	N/A	$\frac{2}{3} \cdot \frac{L\beta}{i^2} + \frac{1}{p_0} = \upsilon$
	IV	$\frac{h\gamma_v}{i^2} + \frac{1}{p_0} = \frac{3}{4\upsilon}$	$\frac{L\beta}{i^2} + \frac{1}{p_0} = \frac{4\upsilon}{3}$
	V	N/A	$\frac{L\beta}{i^2} + \frac{1}{p_0} = \frac{4\upsilon}{3}$
Fully Clamped Beams	I	$\frac{h\gamma_v}{i^2} + \frac{1}{p_0} = 1$	N/A
	II	$\frac{h\gamma_v}{i^2} + \frac{1}{p_0} = \frac{\upsilon}{2(2\upsilon - 3)}$	$\frac{L\beta}{i^2} + \frac{1}{p_0} = \frac{\upsilon(3\nu - 5)}{2(2\upsilon - 3)}$
	III	N/A	$\frac{2}{3} \cdot \frac{L\beta}{i^2} + \frac{1}{p_0} = \frac{\upsilon}{2}$
	IV	$\frac{h\gamma_v}{i^2} + \frac{1}{p_0} = \frac{3}{2\upsilon}$	$\frac{L\beta}{i^2} + \frac{1}{p_0} = \frac{2\upsilon}{3}$
	V	N/A	$\frac{L\beta}{i^2} + \frac{1}{p_0} = \frac{2\upsilon}{3}$

Appendix B

Derivation of P-I Diagram for Combined Failure Mode of Simply Supported Beams subject to Triangular Loads

Mode I. When $\upsilon \le 1$ **and** $\frac{4M_0\upsilon}{L^2} \le p_0$

(1) $t \le t_d$

$$\frac{\partial Q}{\partial x} = -p_0\left(1-\frac{t}{t_d}\right) + m\ddot{y} \tag{B.1}$$

Solve Eq. (B.1),

$$\ddot{y} = \frac{-Q_0}{mL} + \frac{p_0}{m}\left(1-\frac{t}{t_d}\right) \tag{B.2}$$

Integrate Eq. (B.2) with respect to time t,

$$\dot{y} = \frac{-Q_0}{mL}t + \frac{p_0}{m}\left(t-\frac{t^2}{2t_d}\right) \tag{B.3}$$

If $p_0 L \le Q_0$, then the motion will not even begin. Integrate Eq. (B.3) with respect to time t,

$$y = \frac{-Q_0}{mL}\frac{t^2}{2} + \frac{p_0}{m}\left(\frac{t^2}{2}-\frac{t^3}{6t_d}\right) \tag{B.4}$$

At the end of loading, the velocity and displacement of the beam is

$$\dot{y} = \frac{-Q_0}{mL}t_d + \frac{p_0}{2m}t_d \tag{B.5}$$

$$y = \frac{-Q_0}{mL}\frac{t_d^2}{2} + \frac{p_0}{m}\frac{t_d^2}{3} \tag{B.6}$$

(2) $t_d \le t \le t_f$

$$\dot{y} = \frac{-Q_0}{mL}(t - t_d) + \left(\frac{-Q_0}{mL}t_d + \frac{p_0}{2m}t_d\right) = \frac{-Q_0}{mL}t + \frac{p_0}{2m}t_d \tag{B.7}$$

$$y = \frac{-Q_0}{mL}\frac{(t - t_d)^2}{2} + \left(\frac{-Q_0}{mL}t_d + \frac{p_0}{2m}t_d\right)(t - t_d) + \frac{(2p_0L - 3Q_0)}{6mL}t_d^2 \tag{B.8}$$

If $p_0 L \ge 2Q_0$, the deformation will cease at

$$t_f = \frac{p_0 L}{2Q_0}t_d \tag{B.9}$$

The final maximum deformation of the beam is

$$y_f = \frac{p_0(3p_0L - 4Q_0)}{24mQ_0}t_d^2 \tag{B.10}$$

Setting the impulse quantity $I = \frac{1}{2}p_0 \cdot t_d$ the critical P-I diagram equation for shear failure is derived as

$$\frac{2mQ_0h\gamma_v}{I^2} + \frac{4Q_0}{3p_0} = L \tag{B.11a}$$

which is equivalent to

$$\frac{2mh\gamma_v}{I^2} + \frac{4}{3p_0} = \frac{L}{Q_0} \tag{B.11b}$$

Mode II. When $\upsilon \le 1$ and $\frac{2M_0\upsilon}{L^2} \le p_0 \le \frac{4M_0}{L^2}\upsilon$

(1) $t \le t_d$

$$\frac{\partial Q}{\partial x} = -p_0\left(1-\frac{t}{t_d}\right)+m\ddot{y} \tag{B.12}$$

Solve Eq. (B.12),

$$\ddot{y} = \frac{-Q_0}{mL}+\frac{p_0}{m}\left(1-\frac{t}{t_d}\right) \tag{B.13}$$

Integrate Eq. (B.13) with respect to time t,

$$\dot{y} = \frac{-Q_0}{mL}t+\frac{p_0}{m}\left(t-\frac{t^2}{2t_d}\right) \tag{B.14}$$

If $p_0 L \le Q_0$, then the motion will not even begin.

$$y = \frac{-Q_0}{mL}\frac{t^2}{2}+\frac{p_0}{m}\left(\frac{t^2}{2}-\frac{t^3}{6t_d}\right) \tag{B.15}$$

At the end of loading, the velocity and displacement of the beam is

$$\dot{y} = \frac{-Q_0}{mL}t_d+\frac{p_0}{2m}t_d \tag{B.16}$$

$$y = \frac{-Q_0}{mL}\frac{t_d^2}{2}+\frac{p_0}{m}\frac{t_d^2}{3} \tag{B.17}$$

If $Q_0 \le p_0 L \le 2Q_0$, i.e., $\frac{2M_0\upsilon}{L^2} \le p_0 \le \frac{4M_0}{L^2}\upsilon$, then the motion will stop in this phase,

$$t_f = (1-\frac{Q_0}{p_0 L})\cdot 2t_d \tag{B.18}$$

then the maximum displacement is

$$y_f = \frac{2p_0 t_d^2}{3m}\left(1-\frac{Q_0}{p_0 L}\right)^3 \tag{B.19}$$

Setting the impulse quantity $I = \frac{1}{2} p_0 \cdot t_d$, the critical P-I diagram equation for shear failure is derived as

$$\left(\frac{3mp_0 h\gamma_v}{8I^2} \right)^{\frac{1}{3}} + \frac{Q_0}{p_0 L} = 1 \tag{B.20}$$

Mode III. When $1 \le \upsilon \le 1.5$ **and** $\frac{4M_0}{L^2}(4\upsilon - 3) < p_0$

There is shear slide at the support.

$$\dot{y} = \dot{y}_s + (\dot{y}_m - \dot{y}_s)\left(1 - \frac{x}{L}\right) \quad 0 \le x \le L \tag{B.21}$$

(1) $t \le t_d$

$$\frac{\partial Q}{\partial x} = -p_0\left(1 - \frac{t}{t_d}\right) + m\ddot{y}_s + m(\ddot{y}_m - \ddot{y}_s)\left(1 - \frac{x}{L}\right) \tag{B.22}$$

Integrate with respect to x and consider the initial condition $Q = -Q_0$ at $x = L$ and $Q = 0$ at $x = 0$

$$Q = -p_0\left(1 - \frac{t}{t_d}\right)x + m\ddot{y}_s x + m(\ddot{y}_m - \ddot{y}_s)\left(x - \frac{x^2}{2L}\right) \tag{B.23}$$

since $\frac{\partial M}{\partial x} = Q$, $M = M_0$ at $x = 0$ and $M = 0$ at $x = L$

$$M = -p_0\left(1 - \frac{t}{t_d}\right)\frac{x^2}{2} + m\ddot{y}_s \frac{x^2}{2} + m(\ddot{y}_m - \ddot{y}_s)\left(\frac{x^2}{2} - \frac{x^3}{6L}\right) + M_0 \tag{B.24}$$

$$\begin{cases} -Q_0 = -p_0\left(1-\dfrac{t}{t_d}\right)L + m\ddot{y}_s L + m\left(\ddot{y}_m - \ddot{y}_s\right)\dfrac{L}{2} \\ 0 = -p_0\left(1-\dfrac{t}{t_d}\right)\dfrac{L^2}{2} + m\ddot{y}_s\dfrac{L^2}{2} + m\left(\ddot{y}_m - \ddot{y}_s\right)\dfrac{L^2}{3} + M_0 \end{cases} \tag{B.25}$$

Solve the above equations

$$\ddot{y}_m = \frac{p_0\left(1-\dfrac{t}{t_d}\right)}{m} - \frac{6M_0}{mL^2} + \frac{2Q_0}{mL} \tag{B.26}$$

$$\ddot{y}_s = \frac{p_0\left(1-\dfrac{t}{t_d}\right)}{m} + \frac{6M_0}{mL^2} - \frac{4Q_0}{mL} \tag{B.27}$$

Integrate with respect to time and consider the initial condition as $\dot{y}_m = \dot{y}_s = 0$ and

$y_m = y_s = 0$ at $t = 0$

$$\begin{aligned} \dot{y}_m &= \frac{p_0}{m}\left(t - \frac{t^2}{2t_d}\right) - \frac{6M_0}{mL^2}t + \frac{2Q_0}{mL}t \\ &= \frac{p_0}{m}\left(t - \frac{t^2}{2t_d}\right) + \frac{2M_0}{mL^2}(2\upsilon - 3)t \end{aligned} \tag{B.28}$$

$$\begin{aligned} \dot{y}_s &= \frac{p_0}{m}\left(t - \frac{t^2}{2t_d}\right) + \frac{6M_0}{mL^2}t - \frac{4Q_0}{mL}t \\ &= \frac{p_0}{m}\left(t - \frac{t^2}{2t_d}\right) + \frac{2M_0}{mL^2}(3 - 4\upsilon)t \end{aligned} \tag{B.29}$$

$$\begin{aligned} y_m &= \frac{p_0}{m}\left(\frac{t^2}{2} - \frac{t^3}{6t_d}\right) - \frac{6M_0}{mL^2}\frac{t^2}{2} + \frac{2Q_0}{mL}\frac{t^2}{2} \\ &= \frac{p_0}{m}\left(\frac{t^2}{2} - \frac{t^3}{6t_d}\right) + \frac{M_0}{mL^2}(2\upsilon - 3)t^2 \end{aligned} \tag{B.30}$$

$$
\begin{aligned}
y_s &= \frac{p_0}{m}\left(\frac{t^2}{2}-\frac{t^3}{6t_d}\right)+\frac{6M_0}{mL^2}\frac{t^2}{2}-\frac{4Q_0}{mL}\frac{t^2}{2} \\
&= \frac{p_0}{m}\left(\frac{t^2}{2}-\frac{t^3}{6t_d}\right)+\frac{M_0}{mL^2}(3-4\upsilon)t^2
\end{aligned}
\tag{B.31}
$$

To initiate the shear slide motion it requires $p_0 > \frac{2M_0}{L^2}(4\upsilon-3)$, otherwise it will keep still. At the end of this phase, the velocity and displacement will be

$$
\dot{y}_m = \frac{p_0}{m}\frac{t_d}{2}+\frac{2M_0}{mL^2}(2\upsilon-3)t_d \tag{B.32}
$$

$$
\dot{y}_s = \frac{p_0}{m}\frac{t_d}{2}+\frac{2M_0}{mL^2}(3-4\upsilon)t_d \tag{B.33}
$$

$$
y_m = \frac{p_0}{m}\frac{t_d^2}{3}+\frac{M_0}{mL^2}(2\upsilon-3)t_d^2 \tag{B.34}
$$

$$
y_s = \frac{p_0}{m}\frac{t_d^2}{3}+\frac{M_0}{mL^2}(3-4\upsilon)t_d^2 \tag{B.35}
$$

So if $\frac{4M_0}{L^2}(4\upsilon-3) \le p_0$ the shear slide will cease in the next phase.

(2) $t_d \le t \le t_s$

$$
\frac{\partial Q}{\partial x} = m\ddot{y}_s + m(\ddot{y}_m-\ddot{y}_s)\left(1-\frac{x}{L}\right) \tag{B.36}
$$

Integrate with respect to x and consider the initial condition $Q=0$ at $x=0$ and $M=M_0$ at $x=0$

$$
Q = m\ddot{y}_s x + m(\ddot{y}_m-\ddot{y}_s)\left(x-\frac{x^2}{2L}\right) \tag{B.37}
$$

$$
M = m\ddot{y}_s\frac{x^2}{2}+m(\ddot{y}_m-\ddot{y}_s)\left(\frac{x^2}{2}-\frac{x^3}{6L}\right)+M_0 \tag{B.38}
$$

since $Q = -Q_0$ at $x = L$ and $M = 0$ at $x = L$

$$\begin{cases} -Q_0 = m\ddot{y}_s L + m(\ddot{y}_m - \ddot{y}_s)\dfrac{L}{2} \\ 0 = m\ddot{y}_s \dfrac{L^2}{2} + m(\ddot{y}_m - \ddot{y}_s)\dfrac{L^2}{3} + M_0 \end{cases}$$

Solve the above equations

$$\begin{aligned} \ddot{y}_m &= -\frac{6M_0}{mL^2} + \frac{2Q_0}{mL} \\ &= \frac{2M_0}{mL^2}(2\upsilon - 3) \end{aligned} \tag{B.39}$$

$$\begin{aligned} \ddot{y}_s &= \frac{6M_0}{mL^2} - \frac{4Q_0}{mL} \\ &= \frac{2M_0}{mL^2}(3 - 4\upsilon) \end{aligned} \tag{B.40}$$

Integrate with respect to time and consider the initial condition as at $t = t_d$

$$\dot{y}_m = \frac{p_0}{m}\frac{t_d}{2} + \frac{2M_0}{mL^2}(2\upsilon - 3)t_d \tag{B.41}$$

$$\dot{y}_s = \frac{p_0}{m}\frac{t_d}{2} + \frac{2M_0}{mL^2}(3 - 4\upsilon)t_d \tag{B.42}$$

$$y_m = \frac{p_0}{m}\frac{t_d^2}{3} + \frac{M_0}{mL^2}(2\upsilon - 3)t_d^2 \tag{B.43}$$

$$y_s = \frac{p_0}{m}\frac{t_d^2}{3} + \frac{M_0}{mL^2}(3 - 4\upsilon)t_d^2 \tag{B.44}$$

The result is

$$\begin{aligned} \dot{y}_m &= \frac{2M_0}{mL^2}(2\upsilon - 3)(t - t_d) + \frac{p_0}{m}\frac{t_d}{2} + \frac{2M_0}{mL^2}(2\upsilon - 3)t_d \\ &= \frac{2M_0}{mL^2}(2\upsilon - 3)t + \frac{p_0}{m}\frac{t_d}{2} \end{aligned} \tag{B.45}$$

$$\begin{aligned}\dot{y}_s &= \frac{2M_0}{mL^2}(3-4\upsilon)(t-t_d)+\frac{p_0}{m}\frac{t_d}{2}+\frac{2M_0}{mL^2}(3-4\upsilon)t_d \\ &= \frac{2M_0}{mL^2}(3-4\upsilon)t+\frac{p_0}{m}\frac{t_d}{2}\end{aligned} \tag{B.46}$$

$$\begin{aligned}y_m &= \frac{M_0}{mL^2}(2\upsilon-3)(t-t_d)^2+\left[\frac{p_0}{m}\frac{t_d}{2}+\frac{2M_0}{mL^2}(2\upsilon-3)t_d\right](t-t_d)+\frac{p_0}{m}\frac{t_d^2}{3}+\frac{M_0}{mL^2}(2\upsilon-3)t_d^2 \\ &= \frac{M_0(2\upsilon-3)}{mL^2}t^2+\frac{p_0t_d}{6m}(3t-t_d)\end{aligned} \tag{B.47}$$

$$\begin{aligned}y_s &= \frac{M_0}{mL^2}(3-4\upsilon)(t-t_d)^2+\left[\frac{p_0}{m}\frac{t_d}{2}+\frac{2M_0}{mL^2}(3-4\upsilon)t_d\right](t-t_d)+\frac{p_0}{m}\frac{t_d^2}{3}+\frac{M_0}{mL^2}(3-4\upsilon)t_d^2 \\ &= \frac{M_0(3-4\upsilon)}{mL^2}t^2+\frac{p_0t_d}{6m}(3t-t_d)t_d\end{aligned} \tag{B.48}$$

It is evident that the transverse shear slide ceases at the supports when $\dot{\omega}_s = 0$

$$t_s = \frac{p_0 \cdot t_d \cdot L^2}{4(4\upsilon-3)M_0} \tag{B.49}$$

$$\dot{y}_m = \frac{3p_0t_d}{m}\cdot\frac{\upsilon-1}{4\upsilon-3} \tag{B.50}$$

Since $\upsilon > 1$, $\dot{y}_m > 0$. Thus the beam has kinetic energy which should be dissipated in the next phase of motion. So at the end

$$y_m = \frac{(10\upsilon-9)p_0^2t_d^2L^2}{16M_0m(4\upsilon-3)^2}-\frac{p_0}{6m}t_d^2 \tag{B.51}$$

$$y_s = \frac{p_0^2t_d^2L^2}{16M_0m(4\upsilon-3)^2}-\frac{p_0}{6m}t_d^2 \tag{B.52}$$

(3) $t_s \le t \le t_f$

$$\frac{\partial Q}{\partial x} = m\ddot{y}_m\left(1-\frac{x}{L}\right) \tag{B.53}$$

$\because Q = 0$ at $x = 0$

$$Q = m\ddot{y}_m\left(x-\frac{x^2}{2L}\right) \tag{B.54}$$

$\because \frac{\partial M}{\partial x} = Q$ and $M = M_0$ at $x = 0$

$$M = m\ddot{y}_m\left(\frac{x^2}{2}-\frac{x^3}{6L}\right)+M_0 \tag{B.55}$$

$\because M = 0$ at $x = L$

$$\ddot{y}_m = -\frac{3M_0}{mL^2} \tag{B.56}$$

When ensuring the continuity condition at $t = t_s$

$$\begin{aligned}\dot{y}_m &= -\frac{3M_0}{mL^2}\left(t-t_s\right)+\frac{3p_0t_d}{m}\cdot\frac{\upsilon-1}{4\upsilon-3}\\ &= -\frac{3M_0}{mL^2}t+\frac{3p_0t_d}{4m}\end{aligned} \tag{B.57}$$

$$\begin{aligned}y_m &= -\frac{3M_0}{2mL^2}\left(t-t_s\right)^2+\frac{3p_0t_d}{m}\cdot\frac{\upsilon-1}{4\upsilon-3}\cdot\left(t-t_s\right)+\frac{\left(10\upsilon-9\right)p_0^2t_d^2L^2}{16M_0m\left(4\upsilon-3\right)^2}-\frac{p_0}{6m}t_d^2\\ &= -\frac{3M_0t^2}{2mL^2}+\frac{p_0\left(9t-2t_d\right)t_d}{12m}-\frac{p_0^2t_d^2L^2}{32\left(4\upsilon-3\right)M_0m}\end{aligned} \tag{B.58}$$

So the motion finally ceased at

$$t_f = \frac{p_0\cdot t_d\cdot L^2}{4M_0} \tag{B.59}$$

The final transverse displacement is

$$y_f = \frac{(6\upsilon - 5)p_0^2 t_d^2 L^2}{16M_0 m(4\upsilon - 3)} - \frac{p_0}{6m} t_d^2 \tag{B.60}$$

The critical P-I diagram equation for shear failure is derived as

$$\frac{mh\gamma_v}{I^2} + \frac{2}{3p_0} = \frac{L\upsilon}{2Q_0(4\upsilon - 3)} \tag{B.61a}$$

The critical P-I diagram equation for bending failure is derived as

$$\frac{mL\beta}{I^2} + \frac{2}{3p_0} = \frac{(6\upsilon - 5)L^2}{4M_0(4\upsilon - 3)} \tag{B.61b}$$

Mode IV. When $1 \le \upsilon \le 1.25$ **and** $\frac{4M_0}{L^2} < p_0 < \frac{2M_0}{L^2}(4\upsilon - 3)$

or $1.25 \le \upsilon \le 1.5$ **and** $\frac{2M_0}{L^2}(4\upsilon - 3) < p_0 < \frac{4M_0}{L^2}(4\upsilon - 3)$

The shear slide will cease in the first phase.

(1) $t \le t_s \le t_d$

$$\frac{\partial Q}{\partial x} = -p_0\left(1 - \frac{t}{t_d}\right) + m\ddot{y}_s + m(\ddot{y}_m - \ddot{y}_s)\left(1 - \frac{x}{L}\right) \tag{B.62}$$

$\because t_s = 2t_d - \frac{4(4\upsilon - 3)M_0 t_d}{p_0 L^2} \le t_d$

$$\dot{y}_m = \frac{24(\upsilon - 1)M_0 t_d}{mp_0 L^4}\left[p_0 L^2 - 2(4\upsilon - 3)M_0\right] \tag{B.63}$$

$$y_m = \frac{2t_d^2}{3mp_0^2L^6}[\left(-1728+6048\upsilon-6912\upsilon^2+2560\upsilon^3\right)M_0^3+\left(-540+1152\upsilon-576\upsilon^2\right)L^2M_0^2p_0$$
$$+\left(-36+24\upsilon\right)L^4M_0p_0^2+L^6p_0^3]$$
$$=\frac{2t_d^2}{3mp_0^2L^6}\left[32\left(4\upsilon-3\right)^2\left(5\upsilon-6\right)M_0^3-36\left(4\upsilon-3\right)\left(4\upsilon-5\right)L^2M_0^2p_0+12\left(2\upsilon-3\right)L^4M_0p_0^2+L^6p_0^3\right]$$
$$=\frac{2t_d^2}{3mp_0^2L^6}\left[\left(6-8\upsilon\right)M_0+L^2p_0\right]^2\cdot\left[\left(28\upsilon-30\right)M_0+L^2p_0\right]$$
$$y_s=\frac{2t_d^2\left[\left(6-8\upsilon\right)M_0+L^2p_0\right]^3}{3mp_0^2L^6}$$

(2) $t_s \le t \le t_d$

$$\frac{\partial Q}{\partial x}=-p_0\left(1-\frac{t}{t_d}\right)+m\ddot{y}_m\left(1-\frac{x}{L}\right) \tag{B.64}$$

Integrate with respect to x and consider the initial condition $Q=0$ at $x=0$

$$Q=-p_0\left(1-\frac{t}{t_d}\right)x+m\ddot{y}_m\left(x-\frac{x^2}{2L}\right) \tag{B.65}$$

since $\frac{\partial M}{\partial x}=Q$, $M=M_0$ at $x=0$ and $M=0$ at $x=L$

$$M=-p_0\left(1-\frac{t}{t_d}\right)\frac{x^2}{2}+m\ddot{y}_m\left(\frac{x^2}{2}-\frac{x^3}{6L}\right)+M_0 \tag{B.66}$$

Solve Eq. (B.66) and integrate with respect to time

$$\ddot{y}_m=\frac{3p_0\left(1-\frac{t}{t_d}\right)}{2m}-\frac{3M_0}{mL^2} \tag{B.67}$$

$$\dot{y}_m=-\frac{3\left(L^2t^2p_0+4tM_0t_d-2L^2tp_0t_d\right)}{4mL^2t_d} \tag{B.68}$$

$$y_m = \frac{-1}{12L^6 m p_0^2 t_d}[32(4\upsilon-3)^3 M_0^3 t_d^3 + 48(4\upsilon-3)^2 M_0^2 p_0 L^2 t_d^3 + 6M_0 p_0^2 L^4 t_d (3t^2 + 12t_d^2 - 16\upsilon t_d^2) + p_0^3 L^6 (3t^3 - 9t^2 t_d + 4t_d^3)] \quad \text{(B.69)}$$

At the end of this phase, the velocity and displacement is

$$\dot{y}_m = \frac{3t_d}{4m}\left(p_0 - \frac{4M_0}{L^2}\right) \quad \text{(B.70)}$$

$$y_m = \frac{t_d^2}{6L^6 m p_0^2}\left[16(4\upsilon-3)^3 M_0^3 - 24(4\upsilon-3)^2 M_0^2 p_0 L^2 + 3M_0 p_0^2 L^4 (16\upsilon-15) + p_0^3 L^6\right] \quad \text{(B.71)}$$

So if $\frac{4M_0}{L^2} \le p_0 \le \frac{4M_0}{L^2}(4\upsilon-3)$, the motion will cease in the next phase.

(2) $t_d \le t \le t_f$

$$\frac{\partial Q}{\partial x} = m\ddot{y}_m\left(1 - \frac{x}{L}\right) \quad \text{(B.72)}$$

Integrate with respect to x and consider the initial condition $Q = 0$ at $x = 0$ and $M = M_0$ at $x = 0$

$$Q = m\ddot{y}_m\left(x - \frac{x^2}{2L}\right) \quad \text{(B.73)}$$

$$M = m\ddot{y}_m\left(\frac{x^2}{2} - \frac{x^3}{6L}\right) + M_0 \quad \text{(B.74)}$$

since $M = 0$ at $x = L$

$$0 = m\ddot{y}_m \frac{L^2}{3} + M_0$$

Solve the above equation

$$\ddot{y}_m = -\frac{3M_0}{mL^2} \tag{B.75}$$

Integrate with respect to time and consider the initial condition as at $t = t_d$

$$\dot{y}_m = \frac{3}{4mL^2}\left(p_0 t_d L^2 - 4M_0 t\right) \tag{B.76}$$

$$\begin{aligned} y_m = \frac{1}{12L^6 m p_0^2}[&p_0^3 L^6 t_d\left(9t - 7t_d\right) + 32\left(4\upsilon - 3\right)^3 M_0^3 t_d^2 - 48\left(4\upsilon - 3\right)^2 M_0^2 p_0 L^2 t_d^2 \\ &- 6M_0 p_0^2 L^4\left(3t^2 + 12t_d^2 - 16\upsilon t_d^2\right)] \end{aligned} \tag{B.77}$$

It is evident that the bending ceases at the supports when $\dot{\omega}_m = 0$

$$t_f = \frac{p_0 \cdot t_d \cdot L^2}{4M_0} \tag{B.78}$$

$$\begin{aligned} y_f = \frac{t_d^2}{96L^6 M_0 m p_0^2}[&256\left(4\upsilon - 3\right)^3 M_0^4 - 384\left(4\upsilon - 3\right)^2 M_0^3 p_0 L^2 + 192\left(4\upsilon - 3\right) M_0^2 p_0^2 L^4 \\ &- 56M_0 p_0^3 L^6 + 9L^8 p_0^4] \end{aligned} \tag{B.79}$$

Apply the failure criteria, the critical P-I diagram equation for shear failure is derived as

$$\left(\frac{3mp_0 h\gamma_v}{8I^2}\right)^{\frac{1}{3}} + \frac{\left(4\upsilon - 3\right)Q_0}{p_0 L\upsilon} = 1 \tag{B.80a}$$

For bending failure, the critical P-I diagram equation is derived as

$$\frac{12mL\beta}{I^2} + \frac{28}{p_0} = \frac{9L^2}{2M_0} + \frac{96\left(4\upsilon - 3\right)M_0}{p_0^2 L^2} - \frac{192\left(4\upsilon - 3\right)^2 M_0^2}{p_0^3 L^4} + \frac{128\left(4\upsilon - 3\right)^3 M_0^3}{p_0^4 L^6} \tag{B.80b}$$

Mode V. When $1 \le \upsilon \le 1.25$ **and** $\frac{2M_0}{L^2}\left(4\upsilon - 3\right) < p_0 < \frac{4M_0}{L^2}$

The whole deformation will cease in the first phase.

(1) $t \le t_s \le t_d$

$$\frac{\partial Q}{\partial x} = -p_0\left(1-\frac{t}{t_d}\right) + m\ddot{y}_s + m\left(\ddot{y}_m - \ddot{y}_s\right)\left(1-\frac{x}{L}\right) \tag{B.81}$$

$$t_s = 2t_d - \frac{4(4\upsilon-3)M_0 t_d}{p_0 L^2} \le t_d$$

$$\dot{y}_m = \frac{24(\upsilon-1)M_0 t_d}{m p_0 L^4}\left[p_0 L^2 - 2(4\upsilon-3)M_0\right] \tag{B.82}$$

$$y_m = \frac{2t_d^2}{3mp_0^2 L^6}\left[(6-8\upsilon)M_0 + L^2 p_0\right]^2 \cdot \left[(28\upsilon-30)M_0 + L^2 p_0\right] \tag{B.83}$$

(2) $t_s \le t \le t_f \le t_d$

$$\frac{\partial Q}{\partial x} = -p_0\left(1-\frac{t}{t_d}\right) + m\ddot{y}_m\left(1-\frac{x}{L}\right) \tag{B.84}$$

Integrate with respect to x and consider the initial condition $Q = 0$ at $x = 0$

$$Q = -p_0\left(1-\frac{t}{t_d}\right)x + m\ddot{y}_m\left(x-\frac{x^2}{2L}\right) \tag{B.85}$$

since $\frac{\partial M}{\partial x} = Q$, $M = M_0$ at $x = 0$ and $M = 0$ at $x = L$

$$M = -p_0\left(1-\frac{t}{t_d}\right)\frac{x^2}{2} + m\ddot{y}_m\left(\frac{x^2}{2}-\frac{x^3}{6L}\right) + M_0 \tag{B.86}$$

$$\ddot{y}_m = \frac{3p_0\left(1-\frac{t}{t_d}\right)}{2m} - \frac{3M_0}{mL^2} \tag{B.87}$$

$$\dot{y}_m = -\frac{3\left(L^2 t^2 p_0 + 4tM_0 t_d - 2L^2 t p_0 t_d\right)}{4mL^2 t_d} \tag{B.88}$$

$$y_m = \frac{-1}{12L^6 m p_0^2 t_d}[32(4\upsilon-3)^3 M_0^3 t_d^3 + 48(4\upsilon-3)^2 M_0^2 p_0 L^2 t_d^3 + 6M_0 p_0^2 L^4 t_d (3t^2 + 12t_d^2 - 16\upsilon t_d^2) + p_0^3 L^6 (3t^3 - 9t^2 t_d + 4t_d^3)] \quad \text{(B.89)}$$

So the motion will cease at

$$t_f = \left(1 - \frac{2M_0}{p_0 L^2}\right) \cdot 2t_d \le t_d \quad \text{(B.90)}$$

the final displacement is

$$y_f = \frac{2t_d^2}{3L^6 m p_0^2}[8(-15 + 54\upsilon - 72\upsilon^2 + 32\upsilon^3)M_0^3 - 12(3 - 12\upsilon + 8\upsilon^2)M_0^2 p_0 L^2 + 6(2\upsilon - 3)M_0 p_0^2 L^4 + L^6 p_0^3] \quad \text{(B.91)}$$

The critical P-I diagram equation for shear failure is derived as

$$\left(\frac{3mp_0 h\gamma_v}{8I^2}\right)^{\frac{1}{3}} + \frac{(4\upsilon-3)Q_0}{p_0 L\upsilon} = 1 \quad \text{(B.92a)}$$

The critical P-I diagram equation for bending failure is derived as

$$\frac{3mL\beta}{8I^2} - \frac{1}{p_0} = \frac{6(2\upsilon-3)M_0}{p_0^2 L^2} - \frac{12(8\upsilon^2 - 12\upsilon + 3)M_0^2}{p_0^3 L^4} + \frac{8(32\upsilon^3 - 72\upsilon^2 + 54\upsilon - 15)M_0^3}{p_0^4 L^6} \quad \text{[B]} \quad \text{(B.92b)}$$

Mode VI. When $1 \le \upsilon \le 1.25$ **and** $\frac{2M_0}{L^2} < p_0 < \frac{2M_0}{L^2}(4\upsilon - 3)$

or $1.25 \le \upsilon$ **and** $\frac{2M_0}{L^2} < p_0 < \frac{4M_0}{L^2}$

There will be no shear slide in the first phase and the whole motion will cease in one phase.

$$\dot{y} = \dot{y}_m\left(1-\frac{x}{L}\right) \quad 0 \le x \le L \tag{B.93}$$

(1) $t \le t_d \le t_f$

$$\frac{\partial Q}{\partial x} = -p_0\left(1-\frac{t}{t_d}\right) + m\ddot{y}_m\left(1-\frac{x}{L}\right) \tag{B.94}$$

Integrate with respect to x and consider the initial condition $Q = 0$ at $x = 0$

$$Q = -p_0\left(1-\frac{t}{t_d}\right)x + m\ddot{y}_m\left(x-\frac{x^2}{2L}\right) \tag{B.95}$$

since $\frac{\partial M}{\partial x} = Q$, $M = M_0$ at $x = 0$ and $M = 0$ at $x = L$

$$M = -p_0\left(1-\frac{t}{t_d}\right)\frac{x^2}{2} + m\ddot{y}_m\left(\frac{x^2}{2}-\frac{x^3}{6L}\right) + M_0 \tag{B.96}$$

$$\ddot{y}_m = \frac{3p_0\left(1-\frac{t}{t_d}\right)}{2m} - \frac{3M_0}{mL^2} \tag{B.97}$$

$$\dot{y}_m = \frac{3p_0}{2m}\left(t-\frac{t^2}{2t_d}\right) - \frac{3M_0}{mL^2}t \tag{B.98}$$

$$y_m = \frac{3p_0}{2m}\left(\frac{t^2}{2}-\frac{t^3}{6t_d}\right) - \frac{3M_0}{mL^2}\cdot\frac{t^2}{2} \tag{B.99}$$

at the end of this phase,

$$\begin{aligned}\dot{y}_m &= \frac{3p_0t_d}{4m} - \frac{3M_0}{mL^2}t_d \\ &= \frac{3t_d}{4m}\left(p_0 - \frac{4M_0}{L^2}\right)\end{aligned} \tag{B.100}$$

$$y_m = \frac{3p_0}{2m}\left(\frac{t^2}{2} - \frac{t^3}{6t_d}\right) - \frac{3M_0}{mL^2}\cdot\frac{t^2}{2}$$
$$= \frac{t_d^2}{2m}\left(p_0 - \frac{3M_0}{L^2}\right) \tag{B.101}$$

Since then $\dot{y}_m < 0$ and $y_m < 0$, the whole deformation will cease in this first phase.

$$t_f = \left(1 - \frac{2M_0}{p_0 L^2}\right)\cdot 2t_d \tag{B.102}$$

So the final displacement is

$$y_f = \frac{\left(p_0 - \frac{Q_0}{L\upsilon}\right)^3}{mp_0^2}\cdot t_d^2 \tag{B.103}$$

The critical P-I diagram equation for bending failure is derived as

$$\left(\frac{mp_0 L\beta}{4I^2}\right)^{\frac{1}{3}} + \frac{2M_0}{p_0 L^2} = 1 \tag{B.104}$$

Mode VII. When $1.25 \le \upsilon \le 1.5$ **and** $\frac{4M_0}{L^2} < p_0 < \frac{2M_0}{L^2}(4\upsilon - 3)$

There will be no shear slide in the first phase.

$$\dot{y} = \dot{y}_m\left(1 - \frac{x}{L}\right) \quad 0 \le x \le L \tag{B.105}$$

(1) $t \le t_d$

$$\frac{\partial Q}{\partial x} = -p_0\left(1 - \frac{t}{t_d}\right) + m\ddot{y}_m\left(1 - \frac{x}{L}\right) \tag{B.106}$$

Integrate with respect to x and consider the initial condition $Q = 0$ at $x = 0$

$$Q = -p_0\left(1-\frac{t}{t_d}\right)x + m\ddot{y}_m\left(x-\frac{x^2}{2L}\right) \tag{B.107}$$

Since $\frac{\partial M}{\partial x} = Q$, $M = M_0$ at $x = 0$ and $M = 0$ at $x = L$

$$M = -p_0\left(1-\frac{t}{t_d}\right)\frac{x^2}{2} + m\ddot{y}_m\left(\frac{x^2}{2}-\frac{x^3}{6L}\right) + M_0 \tag{B.108}$$

$$\ddot{y}_m = \frac{3p_0}{2m}\left(1-\frac{t}{t_d}\right) - \frac{3M_0}{mL^2} \tag{B.109}$$

$$\dot{y}_m = \left[\frac{3p_0}{2m}\left(1-\frac{t}{2t_d}\right) - \frac{3M_0}{mL^2}\right]\cdot t \tag{B.110}$$

$$y_m = \frac{3p_0}{2m}\cdot\left(\frac{t^2}{2}-\frac{t^3}{6t_d}\right) - \frac{3M_0}{mL^2}\cdot\frac{t^2}{2} \tag{B.111}$$

(2) $t_d \le t \le t_f$

$$\frac{\partial Q}{\partial x} = m\ddot{y}_m\left(1-\frac{x}{L}\right) \tag{B.112}$$

Integrate with respect to x and consider the initial condition $Q = 0$ at $x = 0$ and $M = M_0$ at $x = 0$

$$Q = m\ddot{y}_m\left(x-\frac{x^2}{2L}\right) \tag{B.113}$$

$$M = m\ddot{y}_m\left(\frac{x^2}{2}-\frac{x^3}{6L}\right) + M_0 \tag{B.114}$$

Since $M = 0$ at $x = L$

$$0 = m\ddot{y}_m\frac{L^2}{3} + M_0$$

Solve the above equations

$$\ddot{y}_m = -\frac{3M_0}{mL^2} \tag{B.115}$$

Integrate with respect to time and consider the initial condition as at $t = t_d$

$$\dot{y}_m = -\frac{3M_0}{mL^2}t + \frac{3p_0}{4m}t_d \tag{B.116}$$

$$y_m = -\frac{3M_0}{2mL^2}t^2 + \frac{3p_0}{4m}t \cdot t_d - \frac{p_0}{4m}t_d^2 \tag{B.117}$$

It is evident that the bending ceases at the supports when $\dot{y}_m = 0$

$$t_f = \frac{p_0 \cdot t_d \cdot L^2}{4M_0} \tag{B.118}$$

$$y_f = \frac{3p_0^2 t_d^2 L^2}{32M_0 m} - \frac{p_0}{4m}t_d^2 \tag{B.119}$$

The critical P-I diagram equation for bending failure is derived as

$$\frac{mL\beta}{I^2} + \frac{1}{p_0} = \frac{3L^2}{8M_0} \tag{B.120}$$

Mode VIII. When $1.5 \le \upsilon$ **and** $p_0 > \frac{16M_0}{3L^2}\upsilon^2$

There is not only shear slide at the support but also bending hinge area in the middle of the beam.

(1) $t \le t_d$

The transverse velocity field is like

$$\dot{y} = \begin{cases} \dot{y}_m & 0 \le x \le \xi_0 \\ \dot{y}_s + (\dot{y}_m - \dot{y}_s)\dfrac{L-x}{L-\xi_0} & \xi_0 \le x \le L \end{cases} \tag{B.121}$$

So when $0 \le x \le \xi_0$, $Q = 0$ and $M = M_0$

$$\because \frac{\partial Q}{\partial x} = -p_0\left(1 - \frac{t}{t_d}\right) + m\ddot{y}_m = 0$$

$$\therefore \ddot{y}_m = \frac{p_0}{m}\left(1 - \frac{t}{t_d}\right) \tag{B.122}$$

When $\xi_0 \le x \le L$

$$\frac{\partial Q}{\partial x} = -p_0\left(1 - \frac{t}{t_d}\right) + m\ddot{y}_s + m(\ddot{y}_m - \ddot{y}_s)\cdot\frac{L-x}{L-\xi_0} \tag{B.123}$$

$$Q = -p_0\left(1 - \frac{t}{t_d}\right)(x - \xi_0) - \frac{m(x-\xi_0)((-2L + x + \xi_0)\ddot{y}_m + (-x + \xi_0)\ddot{y}_s)}{2(L-\xi_0)} \tag{B.124}$$

Since $Q = 0$ at $x = \xi_0$.

$$M = \frac{L-x}{6(L-\xi_0)}[3p_0\left(1 - \frac{t}{t_d}\right)(L + x - 2\xi_0)(L-\xi_0) - m\ddot{y}_m(2L^2 + 2Lx - x^2 - 6L\xi_0 + 3\xi_0^2) - m\ddot{y}_s(L^2 + Lx + x^2 - 3L\xi_0 - 3x\xi_0 + 3\xi_0^2)] \tag{B.125}$$

since $M = 0$ at $x = L$.

Since $Q = -Q_0$ at $x = L$ and $M = M_0$ at $x = \xi_0$, solve the equations

$$\ddot{y}_m = \frac{p_0}{m}\left(1 - \frac{t}{t_d}\right) - \frac{6M_0}{m(L-\xi_0)^2} + \frac{2Q_0}{m(L-\xi_0)} \tag{B.126}$$

$$\ddot{y}_s = \frac{p_0}{m}\left(1 - \frac{t}{t_d}\right) + \frac{6M_0}{m(L-\xi_0)^2} - \frac{4Q_0}{m(L-\xi_0)} \tag{B.127}$$

$$\because \ddot{y}_m = \frac{p_0}{m}\left(1-\frac{t}{t_d}\right)$$

$$\therefore \xi_0 = \frac{2\upsilon-3}{2\upsilon}L \tag{B.128}$$

$$\ddot{y}_s = \frac{p_0}{m}\left(1-\frac{t}{t_d}\right)-\frac{4Q_0\upsilon}{3mL} = \frac{p_0}{m}\left(1-\frac{t}{t_d}\right)-\frac{8M_0\upsilon^2}{3mL^2} \tag{B.129}$$

$$Q = -\frac{(3L-2L\upsilon+2x\upsilon)^2}{9L^2}Q_0 \tag{B.130}$$

$$M = \frac{2\upsilon(L-x)\left[2Lx\upsilon(9-4\upsilon)+4x^2\upsilon^2+L^2(27-18\upsilon+4\upsilon^2)\right]}{27L^3}M_0 \tag{B.131}$$

To initiate the shear slide motion it requires $p_0 > \frac{8M_0}{3L^2}\upsilon^2$, otherwise it will keep still.

$$\dot{y}_m = \frac{p_0}{m}\left(t-\frac{t^2}{2t_d}\right) \tag{B.132}$$

$$y_m = \frac{p_0}{m}\left(\frac{t^2}{2}-\frac{t^3}{6t_d}\right) \tag{B.133}$$

$$\dot{y}_s = \frac{p_0}{m}\left(t-\frac{t^2}{2t_d}\right)-\frac{8M_0\upsilon^2}{3mL^2}t \tag{B.134}$$

$$y_s = \frac{p_0}{m}\left(\frac{t^2}{2}-\frac{t^3}{6t_d}\right)-\frac{8M_0\upsilon^2}{3mL^2}\cdot\frac{t^2}{2} \tag{B.135}$$

at the end of this phase

$$\dot{y}_m = \frac{p_0}{2m}t_d \tag{B.136}$$

$$y_m = \frac{p_0}{3m}t_d^2 \tag{B.137}$$

$$\dot{y}_s = \left(\frac{p_0}{2m} - \frac{8M_0\upsilon^2}{3mL^2} \right) t_d \tag{B.138}$$

$$y_s = \left(\frac{p_0}{3m} - \frac{4M_0\upsilon^2}{3mL^2} \right) t_d^2 \tag{B.139}$$

(2) $t_d \le t \le t_s$

When $0 \le x \le \xi_0$

$$\because Q = 0 \text{ and } M = M_0$$

$$\therefore \frac{\partial Q}{\partial x} = m\ddot{y}_m = 0 \;\Rightarrow\; \ddot{y}_m = 0$$

When $\xi_0 \le x \le L$

$$\frac{\partial Q}{\partial x} = m\ddot{y}_s \cdot \frac{x - \xi_0}{L - \xi_0} \tag{B.140}$$

since $Q = 0$ at $x = \xi_0$

$$Q = m\ddot{y}_s \cdot \frac{(x - \xi_0)^2}{2(L - \xi_0)} \tag{B.141}$$

since $Q = -Q_0$ at $x = L$

$$\ddot{y}_s = \frac{-2Q_0}{m(L - \xi_0)} \tag{B.142}$$

since $M = 0$ at $x = L$

$$M = -m\ddot{y}_s (L - x) \frac{x^2 + Lx + L^2 - 3L\xi_0 - 3x\xi_0 + 3\xi_0^2}{6(L - \xi_0)} \tag{B.143}$$

since $M = M_0$ at $x = \xi_0$

$\xi_0 = \dfrac{2\upsilon - 3}{2\upsilon} L$, which means that the plastic hinges region hasn't changed.

Thus,

$$\ddot{y}_s = \frac{-8\upsilon^2 M_0}{3mL^2} \tag{B.144}$$

$$\dot{y}_m = \frac{p_0}{2m} t_d \tag{B.145}$$

$$y_m = \frac{p_0}{2m} t_d t - \frac{p_0}{6m} t_d^2 \tag{B.146}$$

$$\dot{y}_s = \frac{p_0 \cdot t_d}{2m} - \frac{8M_0\upsilon^2}{3mL^2} \cdot t \tag{B.147}$$

$$y_s = -\frac{4M_0\upsilon^2 t^2}{3mL^2} + \frac{p_0 t_d t}{2m} - \frac{p_0 t_d^2}{6m} \tag{B.148}$$

So the motion will cease at $t_s = \frac{3L^2 p_0 \cdot t_d}{16M_0\upsilon^2}$ when

$$\dot{y}_m = \frac{p_0}{2m} t_d \tag{B.149}$$

$$y_m = \frac{\left(-16M_0\upsilon^2 + 9L^2 p_0\right) \cdot p_0 t_d^2}{96M_0 m\upsilon^2} \tag{B.150}$$

$$\dot{y}_s = 0 \tag{B.151}$$

$$y_s = -\frac{p_0 t_d^2}{6m} + \frac{3p_0^2 L^2 t_d^2}{64M_0 m\upsilon^2} \tag{B.152}$$

(3) $t_s \le t \le t_1$

Since at the end of last phase $\dot{y}_m \neq 0$, the beam has a kinetic energy that must be dissipated as plastic work.. In this phase the position of bending hinges begin to travels from $x = \xi_0$ to the mid span till t_1.

When $0 \le x \le \xi$

$$\dot{y}_m = \frac{p_0}{2m} t_d \tag{B.153}$$

$$y_m = \frac{p_0}{2m} t_d t - \frac{p_0}{6m} t_d^2 \tag{B.154}$$

When $\xi \le x \le L$

$$\dot{y} = \dot{y}_m \cdot \frac{L-x}{L-\xi} = \frac{p_0}{2m} t_d \cdot \frac{L-x}{L-\xi} \tag{B.155}$$

$$\because \ \ddot{y} = \frac{p_0}{2m} t_d \cdot \frac{L-x}{(L-\xi)^2} \cdot \dot{\xi}$$

$$Q = \frac{p_0 t_d}{2} \cdot \frac{\dot{\xi}}{(L-\xi)^2} \cdot (x-\xi) \cdot \left[L - \frac{x+\xi}{2} \right] \tag{B.156}$$

$$M = M_0 + \frac{p_0 t_d \dot{\xi} (x-\xi)^2 \left(\frac{L}{2} - \frac{x}{6} - \frac{\xi}{3} \right)}{2(L-\xi)^2} \tag{B.157}$$

Since $M = 0$ at $x = L$

$$\dot{\xi} = \frac{-6M_0}{p_0 t_d (L-\xi)} \tag{B.158}$$

Solve the above differential equation with the initial condition $t_s = \frac{3L^2 p_0 \cdot t_d}{16 M_0 \upsilon^2}$

$$\xi = \xi_0 = \frac{2\upsilon - 3}{2\upsilon} L \tag{B.159}$$

$$\xi = L - \frac{\sqrt{12 t M_0 p_0 t_d}}{p_0 t_d} \tag{B.160}$$

So $\xi = 0$, $t_1 = \frac{p_0 t_d L^2}{12 M_0}$ when

$$y_m = \frac{p_0^2 t_d^2 L^2}{24 M_0 m} - \frac{p_0}{6m} t_d^2 = \frac{p_0}{6m} t_d^2 \left(\frac{p_0 L^2}{4 M_0} - 1 \right) \tag{B.161}$$

(4) $t_1 \le t \le t_f$

The transverse velocity field is

$$\dot{y} = \dot{y}_m \cdot \left(1 - \frac{x}{L} \right) \qquad 0 \le x \le L \tag{B.162}$$

$$Q = m \ddot{y}_m \left(x - \frac{x^2}{2L} \right) \tag{B.163}$$

$$M = M_0 + m \ddot{y}_m \left(\frac{x^2}{2} - \frac{x^3}{6L} \right) \tag{B.164}$$

since $M = 0$ at $x = L$

$$\ddot{y}_m = \frac{-3M_0}{mL^2} \tag{B.165}$$

$$\dot{y}_m = \frac{-3M_0}{mL^2} (t - t_1) + \frac{p_0 t_d}{2m} \tag{B.166}$$

$$y_m = \frac{-3M_0}{mL^2} \frac{(t - t_1)^2}{2} + \frac{p_0 t_d}{2m} (t - t_1) + \frac{p_0}{6m} t_d^2 \left(\frac{p_0 L^2}{4 M_0} - 1 \right) \tag{B.167}$$

solve $\dot{y}_m = 0$

$$t_f = \frac{p_0 t_d L^2}{4 M_0} \tag{B.168}$$

which predicts the mid-span displacement

$$y_f = \frac{p_0^2 L^2 t_d^2}{12 M_0 m} - \frac{p_0}{6m} t_d^2 \tag{B.169}$$

Apply the failure criteria, the critical P-I diagram equation for shear failure is derived as

$$\frac{mh\gamma_v}{I^2}+\frac{2}{3p_0}=\frac{3L}{8Q_0\upsilon} \tag{B.170a}$$

The critical P-I diagram equation for bending failure is derived as

$$\frac{3mL\beta}{2I^2}+\frac{1}{p_0}=\frac{L^2}{2M_0} \tag{B.170b}$$

Mode VIIII. When $1.5\le\upsilon\le\sqrt{\frac{9}{2}}$ **and** $\frac{8M_0}{3L^2}\upsilon^2\le p_0\le\frac{12M_0}{L^2}\le\frac{16M_0}{3L^2}\upsilon^2$

The shear slide will stop in the first phase.

(1) $t\le t_s\le t_d$

$$\because\ \dot{y}_s=\frac{p_0}{m}\left(t-\frac{t^2}{2t_d}\right)-\frac{8M_0\upsilon^2}{3mL^2}t \tag{B.171}$$

$$\therefore\ t_s=2t_d\cdot\left(1-\frac{8M_0\upsilon^2}{3p_0L^2}\right) \tag{B.172}$$

According to assumption that $0\le t_s\le t_d$

When the shear slides stops,

$$\dot{y}_m=\frac{M_0\upsilon^2t_d}{9mL^2}\left(48-\frac{128M_0\upsilon^2}{p_0L^2}\right) \tag{B.173}$$

$$y_m=\frac{2t_d^2\left(8M_0\upsilon^2-3p_0L^2\right)^2\left(16M_0\upsilon^2+3p_0L^2\right)}{81mL^6p_0^2} \tag{B.174}$$

$$y_s=\frac{2t_d^2\left(3p_0L^2-8M_0\upsilon^2\right)^3}{81mL^6p_0^2} \tag{B.175}$$

(2) $t_s\le t_1\le t_d$

The district of the bending hinges tends to coalesce at the center of the beam.

When $0 \le x \le \xi$, $Q = 0$ and $M = M_0$

$$\ddot{y}_m = \frac{p_0}{m}\left(1 - \frac{t}{t_d}\right) \tag{B.176}$$

When $\xi_0 \le x \le L$

$$\dot{y} = \dot{y}_m \cdot \frac{L - x}{L - \xi_0} \tag{B.177}$$

$$\begin{aligned} \ddot{y} &= \ddot{y}_m \cdot \frac{L - x}{L - \xi} + \dot{y}_m \cdot \frac{L - x}{(L - \xi)^2}\dot{\xi} \\ &= \frac{p_0}{m}\left(1 - \frac{t}{t_d}\right) \cdot \frac{L - x}{L - \xi} + \frac{p_0}{m}\left(t - \frac{t^2}{2t_d}\right) \cdot \frac{L - x}{(L - \xi)^2}\dot{\xi} \end{aligned} \tag{B.178}$$

$$\frac{\partial Q}{\partial x} = -p_0\left(1 - \frac{t}{t_d}\right) + p_0\left(1 - \frac{t}{t_d}\right) \cdot \frac{L - x}{L - \xi} + p_0\left(t - \frac{t^2}{2t_d}\right) \cdot \frac{L - x}{(L - \xi)^2}\dot{\xi} \tag{B.179}$$

since $x = \xi$, $Q = 0$

$$Q = Q(\xi) \tag{B.180}$$

since $x = L$, $M = 0$

$$M = M[\xi] \tag{B.181}$$

since $x = \xi$, $M = M_0$

$$\dot{\xi} = \frac{p_0(L - \xi)^2(t - t_d) + 6M_0 t_d}{t(L - \xi)p_0(t - 2t_d)} \tag{B.182}$$

The initial condition is $\xi_0 = \frac{2\upsilon - 3}{2\upsilon}L$ at $t_s = 2t_d \cdot \left(1 - \frac{8M_0\upsilon^2}{3p_0L^2}\right)$.

$$\xi = L - \frac{\sqrt{\frac{12t^2M_0(2t_d - t)t_d}{p_0}}}{t(2t_d - t)} \tag{B.183}$$

When $t_s = 2t_d \cdot \left(1 - \frac{6M_0}{p_0 L^2}\right)$, $\xi = 0$

$\because \frac{8M_0}{3L^2}\upsilon^2 \le p_0 \le \frac{12M_0}{L^2}$ and $1.5 \le \upsilon \le \sqrt{\frac{9}{2}}$ $\therefore t_s \le t_1 \le t_d$

at the end of this phase

$$\dot{y}_m = \frac{12M_0\left(p_0 L^2 - 6M_0\right)t_d}{mp_0 L^4} \tag{B.184}$$

$$y_m = \frac{2t_d^2\left(p_0 L^2 - 6M_0\right)^2\left(12M_0 + p_0 L^2\right)}{3mL^6 p_0^2} \tag{B.185}$$

(3) $t_1 \le t \le t_d$

$$\dot{y} = \dot{y}_m\left(1 - \frac{x}{L}\right) \quad 0 \le x \le L$$

$$\frac{\partial Q}{\partial x} = -p_0\left(1 - \frac{t}{t_d}\right) + m\ddot{y}_m\left(1 - \frac{x}{L}\right) \tag{B.186}$$

Integrate with respect to x and consider the initial condition $Q = 0$ at $x = 0$

$$Q = -p_0\left(1 - \frac{t}{t_d}\right)x + m\ddot{y}_m\left(x - \frac{x^2}{2L}\right) \tag{B.187}$$

Since $\frac{\partial M}{\partial x} = Q$, $M = M_0$ at $x = 0$ and $M = 0$ at $x = L$

$$M = -p_0\left(1 - \frac{t}{t_d}\right)\frac{x^2}{2} + m\ddot{y}_m\left(\frac{x^2}{2} - \frac{x^3}{6L}\right) + M_0 \tag{B.188}$$

$$\ddot{y}_m = \frac{3p_0}{2m}\left(1 - \frac{t}{t_d}\right) - \frac{3M_0}{mL^2} \tag{B.189}$$

Solve with the ICs by the former phase, at the end of this phase

$$\dot{y}_m = \frac{\left(3p_0L^2 - 12M_0\right)t_d}{4mL^2} \tag{B.190}$$

$$y_m = \frac{432M_0^3 - 216L^2M_0^2p_0 + 27L^4M_0p_0^2 + L^6p_0^3}{6mL^6p_0^2} \cdot t_d^2 \tag{B.191}$$

(4) $t_d \le t \le t_f$

$$\frac{\partial Q}{\partial x} = m\ddot{y}_m\left(1 - \frac{x}{L}\right) \tag{B.192}$$

Integrate with respect to x and consider the initial condition $Q = 0$ at $x = 0$ and $M = M_0$ at $x = 0$

$$Q = m\ddot{y}_m\left(x - \frac{x^2}{2L}\right) \tag{B.193}$$

$$M = m\ddot{y}_m\left(\frac{x^2}{2} - \frac{x^3}{6L}\right) + M_0 \tag{B.194}$$

Since $M = 0$ at $x = L$

$$0 = m\ddot{y}_m\frac{L^2}{3} + M_0$$

Solve the above equations

$$\ddot{y}_m = -\frac{3M_0}{mL^2} \tag{B.195}$$

Integrate with respect to time and consider the initial condition as at $t = t_d$

$$\dot{y}_m = -\frac{3M_0}{mL^2}t + \frac{3p_0}{4m}t_d \tag{B.196}$$

$$y_m = -\frac{3M_0}{2mL^2}\left(t^2 - 4t_d^2\right) + \frac{3p_0}{12m}\left(9t - 7t_d\right)\cdot t_d + \frac{72M_0^3t_d^2}{p_0^2mL^6} - \frac{36M_0^2}{p_0mL^4}t_d^2 \tag{B.197}$$

It is evident that the bending ceases at the supports when $\dot{y}_m = 0$

$$t_f = \frac{p_0 \cdot t_d \cdot L^2}{4M_0} \tag{B.198}$$

$$y_f = \frac{\left(6912M_0^4 - 3456M_0^3 p_0 L^2 + 576M_0^2 p_0^2 L^4 - 56M_0 p_0^3 L^6 + 9p_0^4 L^8\right)}{96L^6 M_0 m p_0^2} \cdot t_d^2 \tag{B.199}$$

Thus , the critical P-I diagram equation for shear failure is derived as

$$\left(\frac{81mp_0 h\gamma_v}{8I^2}\right)^{\frac{1}{3}} + \frac{4Q_0\upsilon}{p_0 L} = 3 \tag{B.200a}$$

The critical P-I diagram equation for bending failure is derived as

$$\frac{mL\beta}{I^2} - \frac{288M_0^3}{p_0^4 L^6} + \frac{144M_0^2}{p_0^3 L^4} - \frac{24M_0}{p_0^2 L^2} + \frac{7}{3p_0} = \frac{3L^2}{8M_0} \tag{B.200b}$$

Mode IX. When $\sqrt{\frac{9}{2}} \le \upsilon$ **and** $\frac{12M_0}{L^2} \le p_0 \le \frac{16M_0}{3L^2}\upsilon^2$

The shear slide will stop in the first phase.

(1) $t \le t_s \le t_d$

$$\because \dot{y}_s = \frac{p_0}{m}\left(t - \frac{t^2}{2t_d}\right) - \frac{8M_0\upsilon^2}{3mL^2}t \tag{B.201}$$

$$\therefore t_s = 2t_d \cdot \left(1 - \frac{8M_0\upsilon^2}{3p_0 L^2}\right) \tag{B.202}$$

According to assumption that $0 \le t_s \le t_d$

When the shear slides stops,

$$\dot{y}_m = \frac{M_0\upsilon^2 t_d}{9mL^2}\left(48 - \frac{128M_0\upsilon^2}{p_0 L^2}\right) \tag{B.203}$$

$$y_m = \frac{2t_d^2\left(8M_0\upsilon^2 - 3p_0L^2\right)^2\left(16M_0\upsilon^2 + 3p_0L^2\right)}{81mL^6p_0^2} \tag{B.204}$$

$$y_s = \frac{2t_d^2\left(3p_0L^2 - 8M_0\upsilon^2\right)^3}{81mL^6p_0^2} \tag{B.205}$$

(2) $t_s \le t \le t_d$

The district of the bending hinges tends to shrink to the center of the beam.

When $0 \le x \le \xi$, $Q = 0$ and $M = M_0$

$$\ddot{y}_m = \frac{p_0}{m}\left(1 - \frac{t}{t_d}\right) \tag{B.206}$$

When $\xi_0 \le x \le L$

$$\dot{y} = \dot{y}_m \cdot \frac{L - x}{L - \xi_0} \tag{B.207}$$

$$\begin{aligned} \ddot{y} &= \ddot{y}_m \cdot \frac{L - x}{L - \xi} + \dot{y}_m \cdot \frac{L - x}{(L - \xi)^2}\dot{\xi} \\ &= \frac{p_0}{m}\left(1 - \frac{t}{t_d}\right) \cdot \frac{L - x}{L - \xi} + \frac{p_0}{m}\left(t - \frac{t^2}{2t_d}\right) \cdot \frac{L - x}{(L - \xi)^2}\dot{\xi} \end{aligned} \tag{B.208}$$

$$\frac{\partial Q}{\partial x} = -p_0\left(1 - \frac{t}{t_d}\right) + p_0\left(1 - \frac{t}{t_d}\right) \cdot \frac{L - x}{L - \xi} + p_0\left(t - \frac{t^2}{2t_d}\right) \cdot \frac{L - x}{(L - \xi)^2}\dot{\xi} \tag{B.209}$$

since $x = \xi$, $Q = 0$

$$Q = Q(\xi) \tag{B.210}$$

since $x = L$, $M = 0$

$$M = M[\xi] \tag{B.211}$$

since $x = \xi$, $M = M_0$

$$\dot{\xi} = \frac{p_0(L-\xi)^2(t-t_d)+6M_0t_d}{t(L-\xi)p_0(t-2t_d)} \tag{B.212}$$

The initial condition is $\xi_0 = \frac{2\upsilon-3}{2\upsilon}L$ at $t_s = 2t_d \cdot \left(1-\frac{8M_0\upsilon^2}{3p_0L^2}\right)$.

$$\xi = L - \frac{\sqrt{\frac{12t^2M_0(2t_d-t)t_d}{p_0}}}{t(2t_d-t)} \tag{B.213}$$

When $t_1 = 2t_d \cdot \left(1-\frac{6M_0}{p_0L^2}\right)$, $\xi = 0$

$\because \frac{8M_0}{3L^2}\upsilon^2 \le p_0 \le \frac{12M_0}{L^2}$ and $1.5 \le \upsilon \le \sqrt{\frac{9}{2}}$ $\therefore t_s \le t_d \le t_1$

$\therefore$ the coalesce will be continued in the next phase.

at the end of this phase

$$\dot{\xi} = -\frac{6M_0}{(L-\xi)p_0t_d} \tag{B.214}$$

$$\xi = L - \sqrt{\frac{12M_0}{p_0}} \tag{B.215}$$

$$\dot{y}_m = \frac{p_0}{2m}t_d \tag{B.216}$$

$$y_m = \frac{p_0}{3m}t_d^2 \tag{B.217}$$

(3) $t_d \le t \le t_1$

The transverse velocity field is like

$$\dot{y} = \begin{cases} \dot{y}_m & 0 \le x \le \xi_0 \\ \dot{y}_m \dfrac{L-x}{L-\xi_0} & \xi_0 \le x \le L \end{cases} \tag{B.218}$$

So when $0 \le x \le \xi_0$, $Q = 0$ and $M = M_0$

$$\because \frac{\partial Q}{\partial x} = m\ddot{y}_m = 0$$

$$\therefore \ddot{y}_m = 0$$

$$\dot{y}_m = \frac{p_0}{2m} t_d$$

$$y_m = \frac{p_0}{2m} t_d \left(t - t_d\right)$$

When $\xi_0 \le x \le L$

$$\dot{y} = \dot{y}_m \cdot \frac{L - x}{L - \xi_0} \tag{B.219}$$

$$\begin{aligned} \ddot{y} &= \ddot{y}_m \cdot \frac{L - x}{L - \xi} + \dot{y}_m \cdot \frac{L - x}{\left(L - \xi\right)^2} \dot{\xi} \\ &= \frac{p_0 t_d}{2m} \cdot \frac{L - x}{\left(L - \xi\right)^2} \dot{\xi} \end{aligned} \tag{B.220}$$

$$\frac{\partial Q}{\partial x} = \frac{p_0 t_d}{2} \cdot \frac{L - x}{\left(L - \xi\right)^2} \dot{\xi} \tag{B.221}$$

since $x = \xi$, $Q = 0$

$$Q = \frac{2Lx - x^2 \xi - 2L\xi\dot{\xi} + \xi^2 \dot{\xi}}{4\left(L - \xi\right)^2} \cdot p_0 t_d \tag{B.222}$$

since $x = L$, $M = 0$

$$M = M\left[\xi\right] \tag{B.223}$$

since $x = \xi$, $M = M_0$

$$\dot{\xi} = -\frac{6M_0}{\left(L - \xi\right) p_0 t_d} \tag{B.224}$$

Use the initial conditions as $\xi_1 = L - \sqrt{\frac{12M_0}{p_0}}$ at $t = t_d$,

$$\xi = L - \frac{\sqrt{12M_0 t p_0 t_d}}{p_0} \tag{B.225}$$

So the coalesce will cease at

$$t_1 = \frac{p_0 L^2 t_d}{12M_0} \tag{B.226}$$

At the end of this phase

$$\dot{y}_m = \frac{p_0}{2m} t_d \tag{B.227}$$

$$y_m = \frac{p_0}{2m} t_d^2 \left(\frac{p_0 L^2}{12M_0} - \frac{1}{3} \right) \tag{B.228}$$

(4) $t_1 \le t \le t_f$

$$\frac{\partial Q}{\partial x} = m\ddot{y}_m \left(1 - \frac{x}{L} \right) \tag{B.229}$$

Integrate with respect to x and consider the initial condition $Q = 0$ at $x = 0$ and $M = M_0$ at $x = 0$

$$Q = m\ddot{y}_m \left(x - \frac{x^2}{2L} \right) \tag{B.230}$$

$$M = m\ddot{y}_m \left(\frac{x^2}{2} - \frac{x^3}{6L} \right) + M_0 \tag{B.231}$$

Since $M = 0$ at $x = L$

$$0 = m\ddot{y}_m \frac{L^2}{3} + M_0$$

Solve the above equations

$$\ddot{y}_m = -\frac{3M_0}{mL^2} \tag{B.232}$$

Integrate with respect to time and consider the initial condition at $t = t_d$

It is evident that the bending ceases at the supports when $\dot{y}_m = 0$

$$t_f = \frac{p_0 \cdot t_d \cdot L^2}{4M_0} \tag{B.233}$$

$$y_f = \frac{\left(-2M_0 + p_0 L^2\right)}{12M_0 m} \cdot p_0 t_d^2 \tag{B.234}$$

Thus, the critical P-I diagram equation for shear failure is derived as

$$\left(\frac{81mp_0 h\gamma_v}{8I^2}\right)^{\frac{1}{3}} + \frac{4Q_0\upsilon}{p_0 L} = 3 \tag{B.235a}$$

The critical P-I diagram equation for bending failure is derived as

$$\frac{mL\beta}{I^2} + \frac{2}{3p_0} = \frac{L^2}{3M_0} \tag{B.235b}$$

Mode X. When $1.5 \le \upsilon$ **and** $\frac{12M_0}{L^2} \le p_0 \le \frac{8M_0}{3L^2}\upsilon^2$

Velocity field is same as mode VI. There will be no transverse shear slide at the support.

(1) $t \le t_d$

The transverse velocity field is like

$$\dot{y} = \begin{cases} \dot{y}_m & 0 \le x \le \xi_0 \\ \dot{y}_m \dfrac{L-x}{L-\xi_0} & \xi_0 \le x \le L \end{cases} \tag{B.236}$$

So when $0 \le x \le \xi_0$, $Q = 0$ and $M = M_0$

$$\because \frac{\partial Q}{\partial x} = -p_0\left(1 - \frac{t}{t_d}\right) + m\ddot{y}_m = 0$$

$$\therefore \ddot{y}_m = \frac{p_0}{m}\left(1 - \frac{t}{t_d}\right)$$

$$\dot{y}_m = \frac{p_0}{m}\left(t - \frac{t^2}{2t_d}\right)$$

$$y_m = \frac{p_0}{m}\left(\frac{t^2}{2} - \frac{t^3}{6t_d}\right)$$

When $\xi_0 \le x \le L$

$$\dot{y} = \dot{y}_m \cdot \frac{L - x}{L - \xi_0} \tag{B.237}$$

$$\begin{aligned} \ddot{y} &= \ddot{y}_m \cdot \frac{L - x}{L - \xi} + \dot{y}_m \cdot \frac{L - x}{(L - \xi)^2}\dot{\xi} \\ &= \frac{p_0}{m}\left(1 - \frac{t}{t_d}\right) \cdot \frac{L - x}{L - \xi} + \frac{p_0}{m}\left(t - \frac{t^2}{2t_d}\right) \cdot \frac{L - x}{(L - \xi)^2}\dot{\xi} \end{aligned} \tag{B.238}$$

$$\frac{\partial Q}{\partial x} = -p_0\left(1 - \frac{t}{t_d}\right) + p_0\left(1 - \frac{t}{t_d}\right) \cdot \frac{L - x}{L - \xi} + p_0\left(t - \frac{t^2}{2t_d}\right) \cdot \frac{L - x}{(L - \xi)^2}\dot{\xi} \tag{B.239}$$

since $x = \xi$, $Q = 0$

$$Q = Q(\xi) \tag{B.240}$$

since $x = L$, $M = 0$

$$M = M[\xi] \tag{B.241}$$

since $x = \xi$, $M = M_0$

$$\dot{\xi} = \frac{(L-\xi)^2 p_0 (t - t_d) + 6M_0 t_d}{t(L-\xi) p_0 (t - 2t_d)} \tag{B.242}$$

Use the ICs as $\xi_0 = L - \sqrt{\frac{6M_0}{p_0}}$ at $t = 0$,

$$\xi = L - \sqrt{\frac{12M_0 t_d}{p_0 (2t_d - t)}} \tag{B.243}$$

$$\xi_1 = L - \sqrt{\frac{12M_0}{p_0}} \text{ at } t = t_d$$

$$\because \frac{12M_0}{L^2} \le p_0 \therefore L - \sqrt{\frac{12M_0}{p_0}} \ge 0$$

At the end of this phase

$$\dot{y}_m = \frac{p_0}{2m} t_d \tag{B.244}$$

$$y_m = \frac{p_0}{3m} t_d^2 \tag{B.245}$$

(2) $t_d \le t \le t_1$

In this phase the position of bending hinges begin to travels from $x = \xi_1$ to the mid span till t_1. When $0 \le x \le \xi$

$$\dot{y}_m = \frac{p_0}{2m} t_d \tag{B.246}$$

$$y_m = \frac{p_0}{2m} t_d t - \frac{p_0}{6m} t_d^2 \tag{B.247}$$

When $\xi \le x \le L$

$$\dot{y} = \dot{y}_m \cdot \frac{L-x}{L-\xi} = \frac{p_0}{2m} t_d \cdot \frac{L-x}{L-\xi} \tag{B.248}$$

$$\because\ \ddot{y} = \frac{p_0}{2m} t_d \cdot \frac{L-x}{(L-\xi)^2} \cdot \dot{\xi}$$

$$Q = \frac{p_0 t_d}{2} \cdot \frac{\dot{\xi}}{(L-\xi)^2} \cdot (x-\xi) \cdot \left[L - \frac{x+\xi}{2} \right] \tag{B.249}$$

$$M = M_0 + \frac{p_0 t_d \dot{\xi} (x-\xi)^2 \left(\frac{L}{2} - \frac{x}{6} - \frac{\xi}{3} \right)}{2(L-\xi)^2} \tag{B.250}$$

Since $M = 0$ at $x = L$

$$\dot{\xi} = \frac{-6M_0}{p_0 t_d (L-\xi)} \tag{B.251}$$

Solve the above differential equation with the initial condition $t = t_d$,

$$\xi = \xi_0 = L - \sqrt{\frac{12M_0}{p_0}} \tag{B.252}$$

$$\xi = L - \frac{\sqrt{12tM_0 p_0 t_d}}{p_0 t_d} \tag{B.253}$$

So $\xi = 0$, $t_1 = \frac{p_0 t_d L^2}{12M_0}$ when

$$\dot{y}_m = \frac{p_0}{2m} t_d$$

$$y_m = \frac{p_0^2 t_d^2 L^2}{24M_0 m} - \frac{p_0}{6m} t_d^2 = \frac{p_0}{6m} t_d^2 \left(\frac{p_0 L^2}{4M_0} - 1 \right) \tag{B.254}$$

(3) $t_1 \le t \le t_f$

The transverse velocity field is

$$\dot{y} = \dot{y}_m \cdot \left(1 - \frac{x}{L} \right) \qquad 0 \le x \le L$$

$$\therefore Q = m\ddot{y}_m\left(x - \frac{x^2}{2L}\right) \tag{B.255}$$

$$M = M_0 + m\ddot{y}_m\left(\frac{x^2}{2} - \frac{x^3}{6L}\right) \tag{B.256}$$

since $M = 0$ at $x = L$

$$\ddot{y}_m = \frac{-3M_0}{mL^2} \tag{B.257}$$

$$\dot{y}_m = \frac{-3M_0}{mL^2}(t - t_1) + \frac{p_0 t_d}{2m} \tag{B.258}$$

$$y_m = \frac{-3M_0}{mL^2}\frac{(t-t_1)^2}{2} + \frac{p_0 t_d}{2m}(t - t_1) + \frac{p_0}{6m}t_d^2\left(\frac{p_0 L^2}{4M_0} - 1\right) \tag{B.259}$$

solve $\dot{y}_m = 0$

$$t_f = \frac{p_0 t_d L^2}{4M_0} \tag{B.260}$$

which predicts the mid-span displacement

$$y_f = \frac{p_0^2 L^2 t_d^2}{12M_0 m} - \frac{p_0}{6m}t_d^2 \tag{B.261}$$

Applying the failure criteria, the critical P-I diagram equation for bending failure is derived as

$$\frac{mL\beta}{I^2} + \frac{2}{3p_0} = \frac{L^2}{3M_0} \tag{B.262}$$

Mode XI. When $1.5 \le \upsilon$ **and** $\frac{6M_0}{L^2} \le p_0 \le \frac{12M_0}{L^2}$

Velocity field is same as mode VI. There will be no transverse shear slide at the support.

(1) $t \le t_1 \le t_d$

The transverse velocity field is like

$$\dot{y} = \begin{cases} \dot{y}_m & 0 \le x \le \xi_0 \\ \dot{y}_m \dfrac{L-x}{L-\xi_0} & \xi_0 \le x \le L \end{cases} \tag{B.263}$$

So when $0 \le x \le \xi_0$, $Q = 0$ and $M = M_0$

$$\because \frac{\partial Q}{\partial x} = -p_0\left(1 - \frac{t}{t_d}\right) + m\ddot{y}_m = 0$$

$$\therefore \ddot{y}_m = \frac{p_0}{m}\left(1 - \frac{t}{t_d}\right)$$

$$\dot{y}_m = \frac{p_0}{m}\left(t - \frac{t^2}{2t_d}\right)$$

$$y_m = \frac{p_0}{m}\left(\frac{t^2}{2} - \frac{t^3}{6t_d}\right)$$

When $\xi_0 \le x \le L$

$$\dot{y} = \dot{y}_m \cdot \frac{L-x}{L-\xi_0} \tag{B.264}$$

$$\begin{aligned} \ddot{y} &= \ddot{y}_m \cdot \frac{L-x}{L-\xi} + \dot{y}_m \cdot \frac{L-x}{(L-\xi)^2}\dot{\xi} \\ &= \frac{p_0}{m}\left(1 - \frac{t}{t_d}\right) \cdot \frac{L-x}{L-\xi} + \frac{p_0}{m}\left(t - \frac{t^2}{2t_d}\right) \cdot \frac{L-x}{(L-\xi)^2}\dot{\xi} \end{aligned} \tag{B.265}$$

$$\frac{\partial Q}{\partial x} = -p_0\left(1 - \frac{t}{t_d}\right) + p_0\left(1 - \frac{t}{t_d}\right) \cdot \frac{L-x}{L-\xi} + p_0\left(t - \frac{t^2}{2t_d}\right) \cdot \frac{L-x}{(L-\xi)^2}\dot{\xi} \tag{B.266}$$

since $x = \xi$, $Q = 0$

$$Q = Q(\xi) \tag{B.267}$$

since $x = L$, $M = 0$

$$M = M[\xi] \tag{B.268}$$

since $x = \xi$, $M = M_0$

$$\dot{\xi} = \frac{(L-\xi)^2 p_0(t-t_d) + 6M_0 t_d}{t(L-\xi)p_0(t-2t_d)} \tag{B.269}$$

Use the ICs as $\xi_0 = L - \sqrt{\frac{6M_0}{p_0}}$ at $t = 0$,

$$\xi = L - \sqrt{\frac{12M_0 t_d}{p_0(2t_d - t)}} \tag{B.270}$$

$$t_1 = 2t_d \cdot \left(1 - \frac{6M_0}{p_0 L^2}\right) \tag{B.271}$$

$$\because \frac{6M_0}{L^2} \le p_0 \le \frac{12M_0}{L^2} \therefore 0 \le t_1 \le t_d$$

at the end of this phase

$$\dot{y}_m = \frac{12M_0(p_0L^2 - 6M_0)t_d}{mp_0L^4} \tag{B.272}$$

$$y_m = \frac{2t_d^2(p_0L^2 - 6M_0)^2(12M_0 + p_0L^2)}{3mL^6 p_0^2} \tag{B.273}$$

(3) $t_1 \le t \le t_d$

$$\frac{\partial Q}{\partial x} = -p_0\left(1 - \frac{t}{t_d}\right) + m\ddot{y}_m\left(1 - \frac{x}{L}\right) \tag{B.274}$$

Integrate with respect to x and consider the initial condition $Q = 0$ at $x = 0$

$$Q = -p_0\left(1 - \frac{t}{t_d}\right)x + m\ddot{y}_m\left(x - \frac{x^2}{2L}\right) \tag{B.275}$$

Since $\frac{\partial M}{\partial x} = Q$, $M = M_0$ at $x = 0$ and $M = 0$ at $x = L$

$$M = -p_0\left(1 - \frac{t}{t_d}\right)\frac{x^2}{2} + m\ddot{y}_m\left(\frac{x^2}{2} - \frac{x^3}{6L}\right) + M_0 \tag{B.276}$$

$$\ddot{y}_m = \frac{3p_0}{2m}\left(1 - \frac{t}{t_d}\right) - \frac{3M_0}{mL^2} \tag{B.277}$$

$$\dot{y}_m = \left[\frac{3p_0}{2m}\left(1 - \frac{t}{2t_d}\right) - \frac{3M_0}{mL^2}\right]\cdot t \tag{B.278}$$

$$y_m = \frac{3p_0}{2m}\cdot\left(\frac{t^2}{2} - \frac{t^3}{6t_d}\right) - \frac{3M_0}{mL^2}\cdot\frac{t^2}{2} \tag{B.279}$$

Solve with the ICs by the former phase, at the end of this phase

$$\dot{y}_m = \frac{\left(3p_0L^2 - 12M_0\right)t_d}{4mL^2} \tag{B.280}$$

$$y_m = \frac{432M_0^3 - 216L^2M_0^2p_0 + 27L^4M_0p_0^2 + L^6p_0^3}{6mL^6p_0^2}\cdot t_d^2 \tag{B.281}$$

(4) $t_d \le t \le t_f$

$$\frac{\partial Q}{\partial x} = m\ddot{y}_m\left(1 - \frac{x}{L}\right) \tag{B.282}$$

Integrate with respect to x and consider the initial condition $Q = 0$ at $x = 0$ and $M = M_0$ at $x = 0$

$$Q = m\ddot{y}_m\left(x - \frac{x^2}{2L}\right) \tag{B.283}$$

$$M = m\ddot{y}_m\left(\frac{x^2}{2} - \frac{x^3}{6L}\right) + M_0 \tag{B.284}$$

Since $M = 0$ at $x = L$

$$0 = m\ddot{y}_m \frac{L^2}{3} + M_0$$

Solve the above equations

$$\ddot{y}_m = -\frac{3M_0}{mL^2} \tag{B.285}$$

Integrate with respect to time and consider the initial condition as at $t = t_d$

$$\dot{y}_m = -\frac{3M_0}{mL^2} t + \frac{3p_0}{4m} t_d \tag{B.286}$$

$$y_m = -\frac{3M_0}{2mL^2}\left(t^2 - 4t_d^2\right) + \frac{3p_0}{12m}\left(9t - 7t_d\right)\cdot t_d + \frac{72M_0^3 t_d^2}{p_0^2 mL^6} - \frac{36M_0^2}{p_0 mL^4} t_d^2 \tag{B.287}$$

It is evident that the bending ceases at the supports when $\dot{y}_m = 0$

$$t_f = \frac{p_0 \cdot t_d \cdot L^2}{4M_0} \tag{B.288}$$

$$y_f = \frac{\left(6912M_0^4 - 3456M_0^3 p_0 L^2 + 576M_0^2 p_0^2 L^4 - 56M_0 p_0^3 L^6 + 9p_0^4 L^8\right)}{96L^6 M_0 m p_0^2} \cdot t_d^2 \tag{B.289}$$

Thus, the critical P-I diagram equation for bending failure is derived as

$$\frac{mL\beta}{I^2} - \frac{18M_0^3}{p_0^4 L^6} + \frac{9M_0^2}{p_0^3 L^4} - \frac{3M_0}{2p_0^2 L^2} + \frac{7}{48p_0} = \frac{3L^2}{128M_0} \tag{B.290}$$

Using the normalization criteria (Eqs. (6.92) and (6.93)), the results can be summarized in Table B.1.

Table B.1 Normalized P-I equations for triangular loads

Mode	Shear failure parameter				Bending failure parameters			
	$\varphi_1(p_e)$	λ_1	k_1	$f_1(\upsilon)$	$\varphi_2(p_e)$	λ_2	k_2	$f_2(\upsilon)$
I	1	1	$\frac{4}{3}$	1	N/A	N/A	N/A	N/A
II	$\frac{3}{16}p_e$	$\frac{1}{3}$	1	1	N/A	N/A	N/A	N/A
III	$\frac{1}{2}$	1	$\frac{2}{3}$	$\frac{\upsilon}{2(4\upsilon-3)}$	$\frac{1}{2}$	1	$\frac{2}{3}$	$\frac{(6\upsilon-5)\upsilon}{2(4\upsilon-3)}$
IV	$\frac{3}{16}p_e$	$\frac{1}{3}$	$\frac{(4\upsilon-3)}{\upsilon}$	1	3	1	14	(1)
V	$\frac{3}{16}p_e$	$\frac{1}{3}$	$\frac{(4\upsilon-3)}{\upsilon}$	1	$\frac{2}{32}$	$-\frac{1}{2}$	$\frac{1}{2}$	(2)
VI	N/A	N/A	N/A	N/A	$\frac{1}{8}p_e$	$\frac{1}{3}$	$\frac{1}{\upsilon}$	1
VII	N/A	N/A	N/A	N/A	$\frac{1}{4}$	1	$\frac{1}{2}$	$\frac{3\upsilon}{8}$
VIII	$\frac{1}{2}$	1	$\frac{2}{3}$	$\frac{3}{8\upsilon}$	$\frac{3}{4}$	1	1	υ
IX	$\frac{81}{16}p_e$	$\frac{1}{3}$	4υ	3	$\frac{1}{4}$	1	$\frac{1}{3}$	$\frac{\upsilon}{3}$
X	N/A	N/A	N/A	N/A	$\frac{1}{4}$	1	$\frac{1}{3}$	$\frac{\upsilon}{3}$
XI	$\frac{81}{16}p_e$	$\frac{1}{3}$	4υ	3	$\frac{1}{4}$	1	$\frac{7}{6}$	(3)
XII	N/A	N/A	N/A	N/A	$\frac{1}{4}$	1	$\frac{7}{6}$	(3)

$$\left(\frac{\varphi_1(p_e)\cdot\alpha}{i_e^2}\right)^{\lambda_1}+\frac{k_1}{p_e}=f_1(\upsilon) \text{ for shear failure}$$

$$\left(\frac{\varphi_2(p_e)\cdot\beta}{i_e^2}\right)^{\lambda_2}+\frac{k_2}{p_e}=f_2(\upsilon) \text{ for bending failure}$$

(1) $\frac{9\upsilon}{2}+\frac{24(4\upsilon-3)}{p_e^2\upsilon}-\frac{24(4\upsilon-3)^2}{p_e^3\upsilon^2}+\frac{8(4\upsilon-3)^3}{p_e^4\upsilon^3}$

(2) $\frac{3(2\upsilon-3)}{2p_e^2\upsilon}-\frac{3(8\upsilon^2-12\upsilon+3)}{2p_e^3\upsilon^2}+\frac{32\upsilon^3-72\upsilon^2+54\upsilon-15}{2p_e^4\upsilon^3}$

(3) $\frac{18}{p_e^4\upsilon^3}-\frac{18}{p_e^3\upsilon^2}+\frac{6}{p_e^2\upsilon}$

VITA

Haijian Shi was born in Nantong, China. He earned his Bachelor's degree in structural engineering in Southeast University of China in 1999. He returned to Southeast University as a graduate student in structural engineering in 2000 and received his Master's degree in 2003. He attended the Ph.D program in Nanyang Technological University in 2003. He transferred to University of Missouri-Columbia in 2005 and received his doctoral degree in 2007.